SPATIAL VARIABILITY OF SLAB STABILITY AND FRACTURE PROPERTIES IN AVALANCHE START ZONES

CAM CAMPBELL

UNIVERSITY OF CALGARY

Spatial variability of slab stability and fracture properties in avalanche start zones

by

Cameron Patrick Campbell

A THESIS

SUBMITTED TO THE FACULTY OF GRADUATE STUDIES

IN PARTIAL FULFILMENT OF THE REQUIREMENTS FOR THE

DEGREE OF MASTER OF SCIENCE

DEPARTMENT OF CIVIL ENGINEERING

CALGARY, ALBERTA

SEPTEMBER, 2004

Abstract

During the winters of 2003 and 2004, 705 rutschblock tests in 29 separate arrays, and 930 prototype fracture propagation tests in 23 separate arrays were performed. Slopes with sources of variability typical of avalanche start zones were selected for the array sites. Fracture properties such as propagation energy, fracture character and release type, for rutschblock tests, were found to be less variable than stability. Correlation analysis with snowpack and terrain variables measured for each rutschblock test revealed that varying slab thickness and slope angle are major causes of spatial variability of point stability. Correlation analysis with snowpack and terrain variables measured for each propagation test revealed that varying weak layer thickness and depth is a major cause of variability of propagation energy. Ultimately, spatial variability is influenced by a combination of various causal processes with different scales and is, therefore, difficult to assess with current methods.

Acknowledgements

First and foremost I would like to thank my wife Ashley for her encouragement and understanding. Next I would like to express my gratitude to Dr. Bruce Jamieson for conducting the early work on spatial variability and for his brilliant guidance. I would like to acknowledge Kyle Stewart for effectively “testing the water” for the current spatial variability research conducted at the University of Calgary. I would like to thank Karl Birkeland for his original ideas on spatial variability. I would like to acknowledge Kalle Kronholm for new ideas on the effects of variability on avalanche formation, and for creating a benchmark thesis. I would also like to acknowledge Chris Landry for providing a practical point of view.

For their tireless efforts in the field, I would like to thank Alec van Herwijnen, Antonia Zeidler, Paul Langevin, Ryan Gallagher and Ken Matheson. I would also like to thank the Parks Canada avalanche control crew in Rogers Pass. For proofreading this thesis, I would like to thank Alec van Herwijnen, Antonia Zeidler, Ian Campbell, Kevin Irish and Andrew Kovats. I would like to acknowledge Dr. Larry Bentley and Dr. Lynne Cowe Falls for reviewing this thesis as members of my defense committee. Finally I would like to thank my parents, John and Pat Campbell for their support.

Table of contents

List of tables

Tables of the results from testing for normality can be found in chronological order in Appendix C.

List of figures

Diagrams for all rutschblock test and fracture propagation test arrays can be found in chronological order in Appendix A.

Results from the manual snow profiles performed for every array can be found in chronological order in Appendix B.

List of symbols

○	clear sky (sky cover)
◔	a few clouds (sky cover)
◑	scattered clouds (sky cover)
◍	broken clouds (sky cover)
⊕	overcast (sky cover)
⊗	obscured (sky cover)
1F, ╳	one-finger (hand hardness)
4F, ╲	four-finger (hand hardness)
Asp	aspect (°)
B	break (fracture character)
Col	array column number
CV	coefficient of variation
D	Kolmogorov-Smirnov test statistic
DF, ／	decomposing and fragmented crystals
DH	drop height (cm)
DH, Λ	depth hoar
DHE	drop hammer energy (J/m^2)

E	grain size (mm)
E	edge of block (release type)
Emax	maximum grain size (mm)
Emin	minimum grain size (mm)
F	grain form
F	fist (hand hardness)
FC mx, ∩	mixed form faceted crystals
FC, □	faceted crystals
g	acceleration due to gravity (m/s^2)
GNP	Glacier National Park
gp, ⛬	graupel
H, Depth	slab thickness (cm)
HS	snowpack depth (cm)
I, ▬	ice (hand hardness)
IQR	interquartile range
K, ⨳	knife (hand hardness)
KHMR	Kicking Horse Mountain Resort
K-S	Kolmogorov-Smirnov
l	horizontal length of test column (m)

M	most of block (release type)
mass	mass of hammer used for propagation test (kg)
Med	median
mfc, ◎	melt-freeze crust
N	number of data
P, //	pencil (hand hardness)
p	significance level
PC	progressive compression (fracture character)
PP, +	precipitation particles (new snow)
Q_1	first quartile
Q_3	third quartile
QCV	quartile coefficient of variation
R	hand hardness
R^2	coefficient of multiple determination
RB	rutschblock
RG mx, ◒	mixed form rounded grains
RG, ●	rounded grains
Row	array row number
R_P	Pearson linear correlation coefficient

RP	resistant planar (fracture character)
R_S	Spearman rank order correlation coefficient
RT	release type
SC	sudden collapse (fracture character)
SH, **V**	surface hoar
SIQR	semi-interquartile range
Slope, Ψ	slope angle (°)
SP	sudden planar (fracture character)
Thick	weak layer thickness (cm)
W	whole block (release type)
w	width of test column
ξ	correlation length
ρ	density (kg/m^3)

1 Introduction

1.1 Relevance

The winter of 2003 was the deadliest in history for recreationists in western Canada with 29 avalanche related deaths. This follows a consistent increase in the number of recreational avalanche accidents in recent years, probably as a result of an increase in winter backcountry use as indicated by a marked increase in public bulletin users (Beernick, 2003). Since there were over 750 000 requests (mostly website “hits”) for the Canadian Avalanche Association’s public avalanche bulletin during the winter of 2003, the ability to accurately predict avalanches for these bulletins is paramount.

This thesis aims to aid avalanche forecasters with the interpretation of snowpack tests by:

- identifying sources of spatial variability
- outlining the role spatial variability plays in avalanche formation
- identifying the spatial variability associated with different fracture property observations

A better understanding of the sources of spatial variability of stability and fracture properties within avalanche start zones can help forecasters with site selection for snowpack tests. A better understanding of how the spatial variability of

stability within an avalanche start zone relates to avalanche formation can help avalanche forecasters incorporate variability information into their hazard assessments and plan accordingly. A better understanding of the spatial variability of fracture property observations within avalanche start zones, and how to incorporate these observations into forecasts, can help reduce the uncertainty associated with the spatial variability of stability.

Jamieson and Geldsetzer (1996) analyzed avalanche accidents that occurred in Canada between 1984 and 1996. They found that the majority (60%) of avalanche accidents involved backcountry recreation such as skiing, hiking and mountaineering. Very few (3%) of the accidents did not involve some form of winter recreation. Most (59%) of the accidents were caused by avalanches that were triggered by people on the slope (skier-triggered), and few (14%) were caused by naturally occurring avalanches. Jamieson and Johnston (1998) report that 99% of fatal avalanches in Canada between 1972 and 1991 involved slab avalanches. For these reason the focus of this thesis will be on stability and fracture properties with respect to skier-triggered slab avalanches. Furthermore, since dry snow conditions prevail during the winter in western Canada, the focus of this study will be on dry slab avalanches.

1.2 Slab avalanche formation and release

1.2.1 Slab avalanches

Figures 1.1 and 1.2b outline the nomenclature associated with slab avalanches. A snow slab is a cohesive layer of snow on top of a weak layer (McClung and Schaerer, 1993, p. 75). The presence of a weak layer is a necessary, but not a singularly causal, condition for slab avalanche formation (Bader and Salm, 1990). The bed surface is defined as the surface over which the slab slides, and can be the ground or older snow. It is the layer underneath the weak layer. The breakaway wall of the top periphery of the slab is called the crown. It is formed by a fracture in tension and is usually perpendicular to the bed surface. The flanks are the left and right sides of the slab. The flanks are usually smooth surfaces, as is the crown, formed by either shear fractures, tension fractures or a combination of both. The lowest down-slope fracture surface is termed the stauchwall.

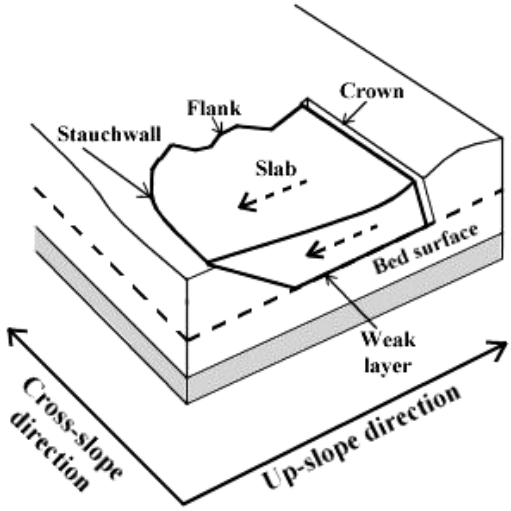

Figure 1.1 – Nomenclature associated with slab avalanches: crown, flank, stauchwall, weak layer and bed surface. A slab with varying thickness is shown.

Large avalanche paths have three distinct parts (Figure 1.2a). The start zone is where the avalanche initiates. The slope angle there is usually between 30˚ and 50˚. The runout zone is where large avalanches decelerate and debris is deposited. The track connects the start zone with the runout zone. Large avalanches will initiate and accelerate in the start zone, travel at a relatively constant speed through the track and come to a stop in the runout zone. It is possible for smaller avalanches to stop in the start zone or the track. For smaller avalanche paths (Figure 1.2b), the distinct zones are not always as obvious. The majority of the field observations for this study were made in the start zones of smaller avalanche paths.

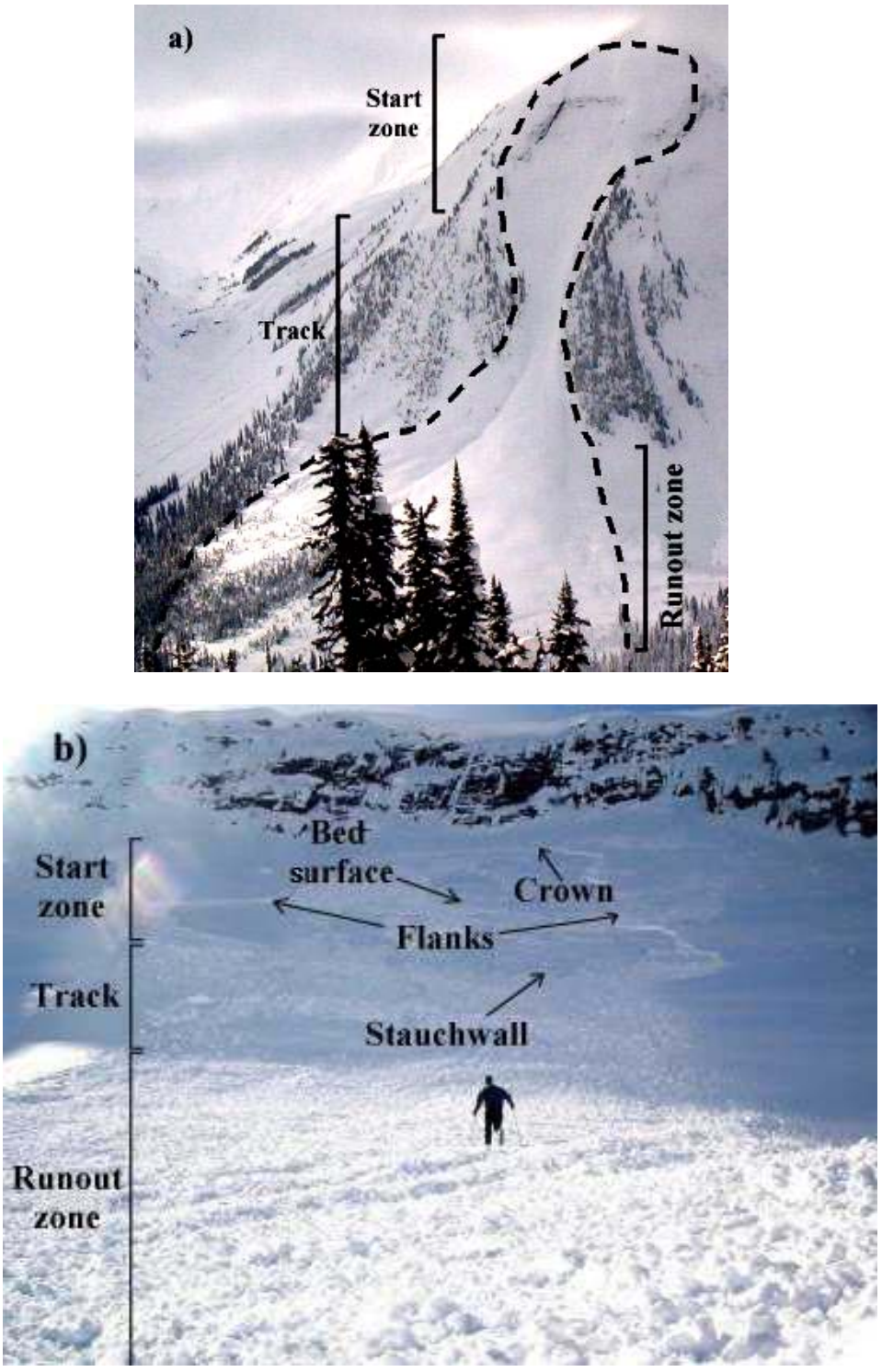

Figure 1.2 – Parts of an avalanche path: start zone, track and runout zone for a) a large avalanche path and b) a small avalanche path. Nomenclature associated with slab avalanches is labeled for the avalanche shown in b).

1.2.2 Formation of snowpack layers

Snow crystals form in the atmosphere either by sublimation of water vapor onto small particles (i.e. condensation nuclei) or by accretion of super cooled water droplets. Different crystal shapes result from variations in temperature and supersaturation in the atmosphere (McClung and Schaerer, 1993, p. 40). Snowfall from multiple storms throughout a winter produces a layered snowpack. On the ground, the properties of snow crystals change over time, starting immediately with the disappearance of branches. This initial metamorphic process produces decomposed and fragmented crystals which continue to metamorphose into either rounded or faceted crystals depending on the temperature gradient. These two main metamorphic processes occur in dry snow, with temperatures at or below 0˚C. They change the microstructure of dry snow, and thus the mechanical properties of dry layers. Snowpack metamorphism occurs faster at warmer temperatures and differences are often visible over several days.

Decomposed and fragmented crystals will become rounded grains if there is no strong temperature gradient within the snowpack. This process, called rounding or equilibrium metamorphism, is associated with bonding between grains and the gain of strength (Perla and Sommerfeld, 1987). Rounded grains form a cohesive layer (slab) which is a necessary component for slab avalanche formation. Faceting metamorphism, or kinetic growth, usually occurs when there

is a temperature gradient of greater than about 10˚C/m (Akitaya, 1974). Faceting does not promote bonding and is therefore often associated with a slow gain of strength. Because of this, faceted crystals often form weak layers for slab avalanches. Depth hoar crystals are fully developed cup-shaped faceted crystals often found at the base of the snowpack.

Another important process is the formation of surface hoar crystals, or the solid equivalent of dew. When buried by subsequent snowfalls, layers of surface hoar metamorphose very slowly and can remain weak for an extended period of time. Because of this they are considered persistent weak layers (Jamieson, 1995). Surface hoar crystals are relatively large crystals that form on the snow surface during cold and clear nights. The snow surface experiences radiant cooling causing water vapor from the air to be deposited on the snow surface. Light winds are favourable for surface hoar formation because the air circulation ensures a sufficient amount of water vapor by replenishing the supply available for deposition (McClung and Schaerer, 1993, p. 44). If the winds are too strong, however, the fragile surface hoar crystals can be easily destroyed.

1.2.3 Stability

An index of stability can be defined by the ratio of the shear strength of a weak layer to the applied stress from the static weight of the slab and artificial dynamic stresses such as skiers (Conway and Abrahamson, 1984, 1988; Föhn,

1989; Landry, 2002; Landry and others, 2004). If the ratio is less than one, than the stress exceeds the strength and avalanches are likely to occur. A five level stability rating, which ranges from very poor to very good, is commonly used to describe stability, partly by the magnitude of the dynamic trigger required to release an avalanche (CAA, 2002). Skiers will usually trigger avalanches on most slopes when the stability is rated as poor or very poor.

1.2.4 Slab release processes

The manner in which snow behaves during failure depends on the temperature and the strain rate (Schweizer and others, 2003). At a lower strain rate ($< 10^{-3}$ s^{-1} for warmer snow or $< 10^{-4}$ s^{-1} for colder snow) ductile failure occurs, which involves the breaking of grain bonds and the rearrangement of grains. Ductile failure can result in fracture (higher strain rates or colder snow), strain softening (weakening) or densification (lower strain rates or warmer snow). Snow behaves as a brittle material when strain rates exceed 10^{-3} s^{-1} for warmer snow or 10^{-4} s^{-1} for colder snow. In the mountain snowpack, strain rates of this magnitude can be achieved by the dynamic stresses such as skiers or falling cornices.

The usual convention is that slab avalanche release starts with a shear fracture in the weak layer initiated by a triggering mechanism such as skiers, falling cornices or the overburden of weight from new snowfall. If the initial

fracture exceeds a critical length, it will become a self-propagating brittle fracture until the slope parallel stress caused by the weight of the unsupported slab overcomes the peripheral strength of the slab (Schweizer and others, 2003). The critical length for fractures to become self-propagating has been estimated to be between 10 cm (rapid loading) and 10 m (slow loading) (Schweizer, 1999). Secondary fractures at the crown (tensile), flanks (tensile and shear) and stauchwall (shear) then release the slab from the slope. If a fracture propagates outwards from the trigger location, but does not release an avalanche, it is called a “whumpf” (Johnson and others, 2000). Whumpfs often produce a distinctive sound and downward displacement of the snow surface is sometimes noticeable. They usually occur on low angled terrain.

Once a self-propagating fracture is initiated, it will propagate as long as the driving energy exceeds the fracture resistance of the weak layer. A fracture can propagate several kilometers as long as the weak layer and slab are continuous and the fracture resistance of the weak layer is sufficiently low. If a propagating fracture encounters an area of sufficiently high fracture resistance, it would stop and, depending on the slope angle, produce a fracture through the slab.

1.2.5 Sources of spatial variability within a slope

Figure 1.3 is a conceptual flow diagram outlining the stages of slab avalanche formation where variability can be introduced. The sources of variability in stability can be divided into two main categories: the sources of variability in shear strength of the weak layer; and the sources of variability in applied stress (Figure 1.3). Any variations in the slab and ground cover can cause variations in applied stress and any variations in the weak layer can cause variations in the shear strength of the weak layer.

McKay and Gray (1981) suggest that spatial variability exists in virtually all properties of snow. Birkeland (2003, pers. comm.) notes that there is less variability in snowpack structure (e.g. presence of a crust, fracture character, etc), which is often only qualitative, than in stability (e.g. stability test scores). Processes which can cause variability in snowpack properties can cause variability in stability, because shear strength is dictated by snowpack structure. Such processes that can act on the snowpack at different degrees within a slope can cause slope-scale variability. These processes include wind, humidity, solar radiation absorption and longwave radiation emission (Figure 1.3). Processes such as precipitation and air temperature are considered to be constant at this scale.

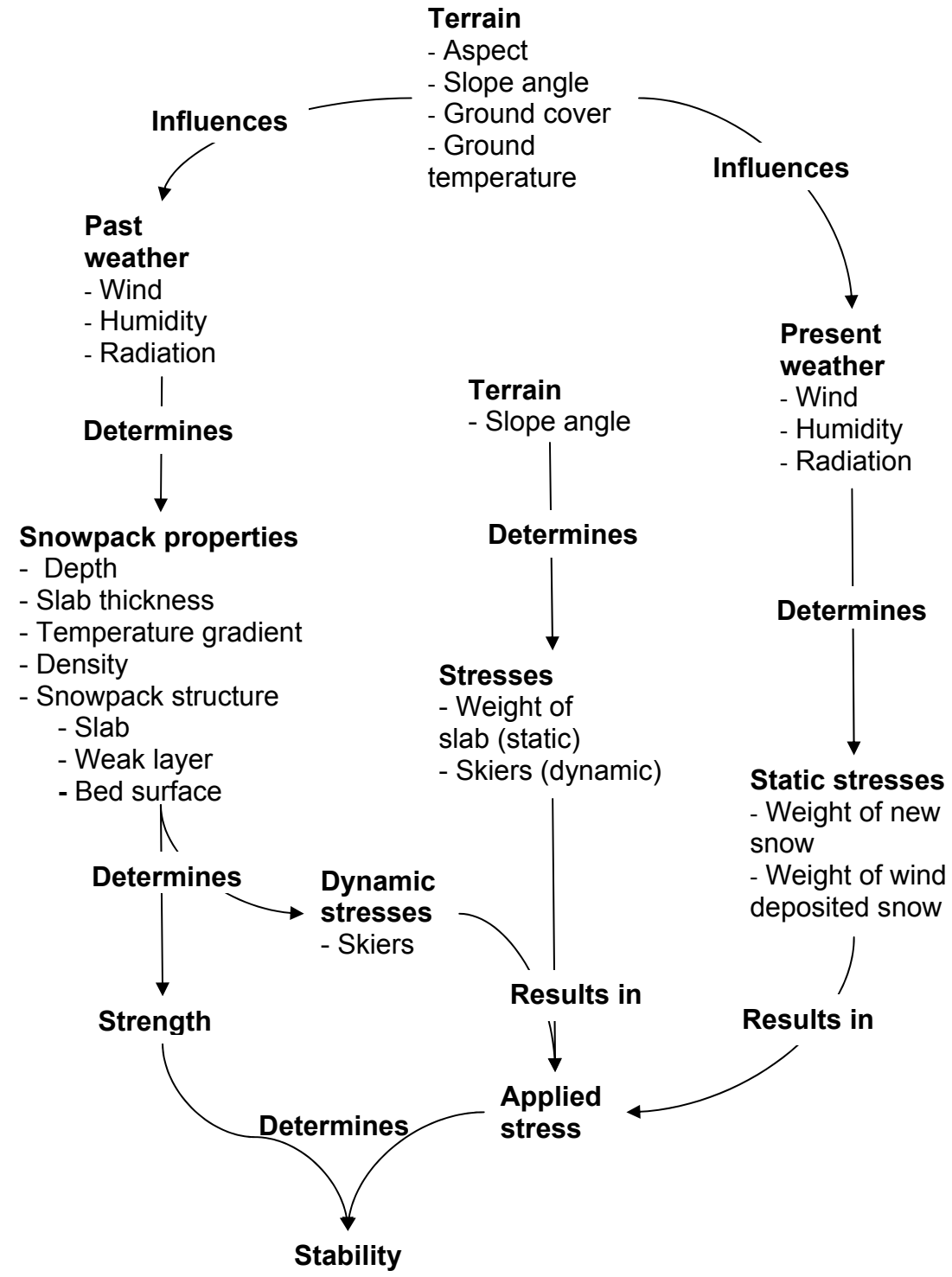

Figure 1.3 – Conceptual diagram showing how several terrain and meteorological variables interact to determine stability with respect to skier triggering (after Birkeland, 1997, p. 4). Terrain and weather parameters that can act as sources of variability of stability within a slope, and their influences, are shown.

Uneven deposition of wind transported snow, due to turbulent wind eddies on lee slopes near ridge tops (Doorschot and others, 2001) or cross-loading (McClung and Schaerer, 1993, p. 92) is a major cause of slope-scale variability in snowpack and slab depth. Figure 1.4 shows an example of wind drifts on the leeward side of trees. Since the stress from a skier dissipates in the snowpack (Camponovo and Schweizer, 1997), it follows that shallower weak layers are subject to greater dynamic stresses and are therefore more prone to skier-triggering. Variations in slab thickness, and therefore weight of the overlying slab, can also result in variations in static shear stress at the weak layer. Increased faceting for areas of locally shallow snow depth is possible since the temperature gradient would be greater than in adjacent areas with greater snow depth.

Figure 1.4 – Wind drifts (pillows) on the leeward (uphill) side of trees near the top of a ridge (Applied Snow and Avalanche Research, University of Calgary (ASARC) photo).

Any variations in the level of the snow surface can cause some areas of the slope to be exposed to wind while other areas are sheltered. Furthermore, turbulent wind eddies (e.g. small vortex or the snow equivalent to a “dust-devil”) can form on slopes with a relatively uniform snow surface. Variations in slab density across a slope can be caused by the compacting of snow in areas where wind transported snow is blowing into the slope. Keeler and Weeks (1968) found that shear strength can depend on density and hardness, with higher density and harder snow being stronger. Since density (Chernouss, 1995) and hardness (Birkeland and others, 1995), can vary across a slope, it is likely that these snow pack properties are sources of slope-scale variability in stability and fracture properties.

Variations in exposure to wind can also cause variability in buried surface hoar layers because wind can destroy surface hoar crystals when they are on the snow surface. Local variations in humidity can alter growth conditions for surface hoar resulting in larger surface hoar crystals where humidity is high (Feick and others, 2004). Surface hoar formation can be inhibited or prevented in concave areas on the snow surface by longwave radiation interception at the opposite wall in the concavity (McClung and Schaerer, 1993, p. 44).

Local variations in the aspect, or the orientation, can cause variations in the amount of intercepted solar radiation resulting in sun-crusts with variable

thickness and hardness. Figure 1.5 is an example of a slope with local changes in aspect and variations in exposure to solar radiation within the slope as indicated by the sunny and shaded areas. It is also conceivable that different grain types could have different amounts of variability since Keeler and Weeks (1968) found that strength is different for different grain types. Furthermore, Sommerfeld and others (1976) found that the shear strength of lower density layers, such as layers of faceted crystals, tend to be less variable.

Figure 1.5 – An example of a slope with local changes in aspect due to buried boulders and avalanche debris. Different parts of the slope are exposed to different amounts of solar radiation (as seen by the sunny and shaded areas) because of these changes in aspect (ASARC photo).

The fact that stability in avalanche start zones, with uneven ground cover, is more variable than on uniform slopes (Jamieson and Johnston, 2001) implies that ground cover can affect stability. This can be partly attributed to the effect

that ground cover has on the processes explained above (e.g. local changes in aspect of the snow surface causing variable exposure to wind and solar radiation). But local changes in ground cover can have effects on other snowpack processes, as well as the applied static and dynamic stresses. Deep week layers, such as depth hoar, are often triggered from areas above boulders where the slab is locally thin. Stewart (2002, p. 9-11) and Jamieson (2003b) provide case studies of this situation. This can be attributed to the increased faceting due to large temperature gradients around the boulder. The local vertical and horizontal temperature gradients are influenced by the snowpack depth and by the presence of boulders or rock outcrops, which absorb more solar radiation than the surrounding ground cover when exposed (Logan, 1993). Boulders and rock outcrops that bulge into the snowpack, once they are buried, act as a heat source for faceting. This is because rock has a greater conductivity than other types of ground cover.

Jamieson and Johnston (1993) found that a 10˚ increase in slope angle alone tended to cause a decrease in stability of one rutschblock load step (Sections 1.4.1 and 3.2.1). This is probably because the shear stress in the weak layer caused by skiers (dynamic) and gravity (static) is greater on steeper slopes. Ground cover can also cause variations in applied load by anchoring parts of the snowpack. Schaerer (1975) suggests that as soon as the ground cover is buried by at least 0.30 m, it is no longer anchoring the slab or interrupting the continuity of the weak layer. Trees can be very effective anchors, especially evergreen

trees when the branches penetrate the snow surface (Gubler and Rychetnik, 1991). Gubler and Rychetnik (1991) also note that intercepted snow collected in tree branches can be deposited unevenly, causing variations in slab thickness and snowpack depth. Furthermore, this intercepted snow is often deposited as hard clumps (tree bombs) that can destroy surface layers and break up continuous weak layers.

1.2.6 The effect of the magnitude of variability on avalanche formation

Figure 1.6 shows four hypothetical stability patterns for a slope transect. In situation (a), there are small areas of the slope susceptible to skier-triggering so a fracture would be initiated if these areas are stressed by a skier. Whether an avalanche releases depends on the fracture propagation propensity of the slab and weak layer. Situation (b) has the same average stability, but this time the variability is low so the slope has no areas susceptible to skier-triggering and avalanche release is unlikely. In situation (c) there are large areas of the slope susceptible to skier-triggering, but since the stability is highly variable there are small areas with good stability, which could resist fracture propagation. In this situation, small avalanches could release or the slope could whumpf if the fracture does not propagate far enough to release a slab. Situation (d) shows a slope with poor stability and low variability where skiers are likely to start fractures and release an avalanche.

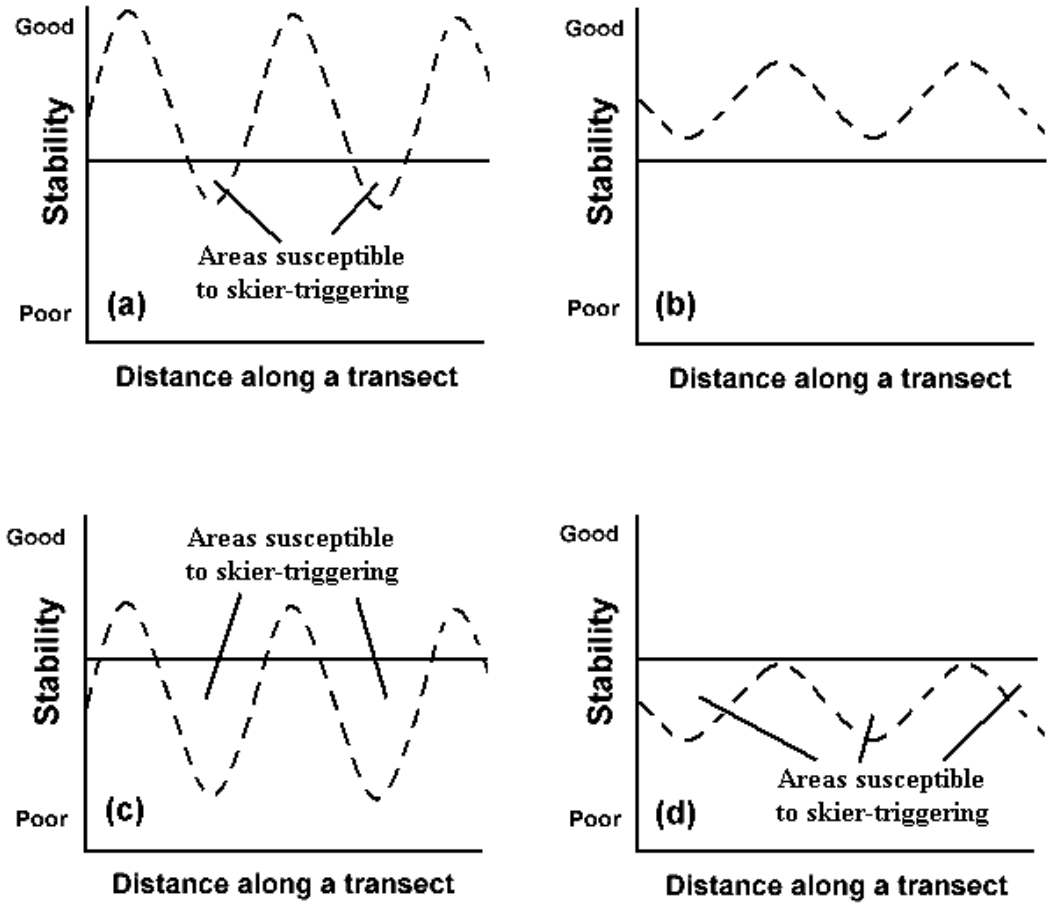

Figure 1.6 - Schematic of hypothetical cross-slope or up-slope sinusoidal stability patterns (after Kronholm and Schweizer, 2003). Four different situations are shown have (a) good median stability and high variability, (b) good median stability and low variability, (c) poor median stability and high variability and (d) poor median stability and low variability. The hypothetical threshold stability level for skier-triggering is also shown.

1.3 Spatial scales and correlation lengths of variability

Hägeli and McClung (2000) define scale as a characteristic length or time of a process, observation or model. Spatial variability of stability and other snowpack properties exists on many different scales ranging from grain-scale (0.1 to 1 mm) to mountain-range scale (10 to 100 km). Slope-scale (5 to 100 m) includes the size of typical avalanche slopes and is the scale of focus for this study. When making point stability measurements, there are three important scale attributes (Blöschl and Sivapalan, 1995; Hägeli and McClung, 2000). These include the size of the test (support), the spacing between the tests (spacing) and the overall coverage of the measurements (extent). It is these scale issues that force studies of slope-scale variability into the field. The importance of these scale issues limits the problems that can be solved in a laboratory. The large area (support) stability tests, such as the rutschbloch test (Section 1.4.1) can capture fracture initiation as well as fracture propagation information. The smaller area (support) stability tests, such as the compression test (Section 1.4.2) are better for capturing variability at small lag distances and hence, more promising for determining the correlation length (range) with variogram analysis.

The scale of snowpack structural parameters such as continuity of layers, hardness and fracture character is likely to be greater than point stability tests (K. Birkeland, 2004, pers. comm.). Landry (2002) found a particular weak layer of faceted crystals present at the same stratigraphic location with the snowpack

throughout the Bridger Mountain Range. This layer displayed different stability patterns at the three study sites sampled on 2001-02-18, which suggests that the scale of continuity of the weak layer is much larger than the scale of variability of stability.

The variability in measured properties of snow, including stability, is due to a combination of various processes that act on the snowpack with various correlation lengths (ξ). Causal processes are influenced by factors such as buried rocks (assumed ξ ~ 1 m), wind drifting (assumed ξ ~ 2 to 10 m), slope angle (assumed ξ ~ 2 to > 50 m) and surface hoar formation (assumed ξ ~ 1 to > 50 m). However, relating the spatial variability of stability within avalanche start zones to causal processes can be difficult with current methods (Kronholm, 2004). Variograms are geostatistical tools that have been used to estimate the correlation lengths (range) of slope-scale stability variations (Isaaks and Srivastava, 1989; Stewart, 2002; Kronholm, 2004). Variograms were used in this study and are introduced in Section 3.3.4.

Knowing the correlation length of stability for a particular slope would be valuable to avalanche forecasters when evaluating stability. Kronholm and Schweizer (2003) show that for a given median stability, slopes with variability at a small correlation length will have more but smaller areas susceptible to triggering than on slopes with larger correlation lengths. This is illustrated in Figure 1.7, which shows two hypothetical stability patterns for a slope transect

that have the same median and level of variability (spread) but different correlation lengths. Figure 1.7 (a) shows a slope with a relatively small correlation length that has several small areas susceptible to skier-triggering. In situation (b) the correlation length is much larger and the slope has one large area susceptible to skier-triggering. In both situations the slopes are prone to triggering, but in situation (b) larger avalanches can be expected.

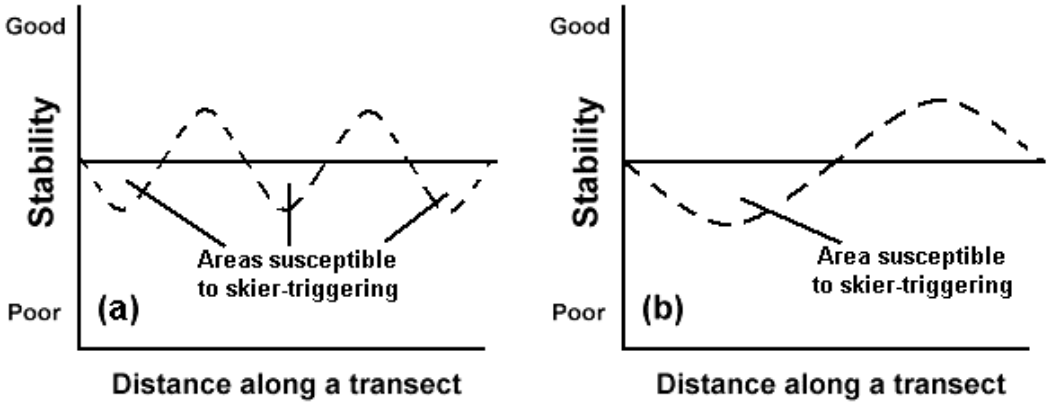

Figure 1.7 - Schematic of cross-slope or up-slope sinusoidal stability patterns (after Kronholm and Schweizer, 2003). Two situations are shown where median stability and variability (spread) are equal. Situation (a) has a small correlation length and situation (b) has a large correlation length of stability variation. The hypothetical threshold stability level for skier-triggering is also shown.

1.4 Stability tests

1.4.1 Rutschblock test

The rutschblock test is a slope stability test first used by the Swiss army to find weak snow layers (Föhn, 1987). The procedures can be found in Section

3.2.1. The effectiveness of the rutschblock test as an evaluation of snowpack stability has been widely documented (Föhn, 1987, 1989; Jamieson, 1995; Jamieson and Johnson, 1992, 1993). Low test scores are associated with poor stability and correlate well with a high probability of skier-triggered avalanches. Jamieson and Johnston (1992, 1993) found that on uniform slopes, 97% of independent rutschblock tests fall within one score of the slope median. This suggests that there is intrinsic variability associated with rutschblock tests on uniform slopes, but does not separate the variability in the test technique from the variability on uniform slopes

Since the dimensions of the rutschblock test (2 m x 1.5 m) are likely to be greater than the critical length for self-propagating brittle fractures, it follows that the rutschblock test can provide measures of fracture initiation as well as fracture propagation propensity. Schweizer and Wiesinger (2001) suggested incorporating release type observations, in terms of the proportion of the block that slides, in order to indicate fracture propagation propensity. Similar observations were used in this study and are outlined in Section 3.2.1.

1.4.2 Compression test

The compression test was developed by Parks Canada wardens in the 1970's (Jamieson, 1999). A 30 x 30 cm isolated column of snow is loaded by tapping on a shovel blade placed on top of the column until a fracture occurs

(CAA, 2002). The force applied with each tap is increased every ten taps, to a maximum of 30 taps, resulting in three load ranges: easy, moderate and hard. Jamieson (1999) found that as Rutschblock scores increase from 2 to 7, adjacent compression test scores increase from easy/moderate to hard, indicating a significant positive correlation. Variations of the compression test include the rammrutsch (Schweizer and others, 1995), drop hammer (Stewart, 2002), stuffblock (Birkeland and Johnson, 1999) and quantified loaded column test (QCLT) (Landry and others, 2001). Rammrutsch, drop hammer, stuffblock and QCLT test procedures are summarized in Chapter 2. The drop hammer test equipment was used for part of this study and is introduced in Section 3.2.2.1.

If the critical length for self-propagating brittle fractures is 10 cm (rapid loading) then the dimensions of the compression test (30 x 30 cm) should be large enough to capture fracture propagation information. In an attempt to improve the interpretation of compression test results by incorporating propagation information, avalanche researchers at the University of Calgary have been incorporating fracture character observations into stability tests since the winter of 1997. These visual fracture descriptors (outlined in Section 3.2.1), similar to shear quality observations used by Johnson and Birkeland (2002), can qualify the propagation propensity of a weak layer. Both fracture character and shear quality are based on less systematic observations of fractures, which have been used by avalanche field workers for decades. Van Herwijnen and Jamieson

(2003) show that by incorporating fracture character observations, the predictive merit of compression test results for skier-triggering are improved.

1.5 Research objectives

- Identify sources of spatial variability of point stability tests and fracture properties in avalanche start zones and relate to scale.
- Investigate whether a given location displays similar stability and fracture patterns on a year-to-year basis.
- Determine the spatial variability of fracture propagation energy with a prototype field test method.
- Determine the spatial variability of fracture character and release type observations.
- Offer strategies to reduce the risk associated with the uncertainty in stability evaluations caused by spatial variability.

2 Literature review

2.1 Introduction

The existence of large variations in shear strength and stability over short distances has been confirmed by many field studies (e.g. Keeler and Weeks, 1968; Conway and Abrahamson, 1984, 1988; Föhn, 1989; Jamieson, 1995; Jamieson and Johnston, 1992, 1993, 2001; Stewart, 2002; Landry, 2002; Landry and others, 2004; Krohnholm, 2004). Early analytical treatments of spatial variability were by Conway and Abrahamson (1984, 1988) who related shear strength measurements across a slope to snowpack and terrain variables, and by Jamieson (1989) who modeled the variability of slab tensile strength across a slope with a linear model.

This literature review covers studies of spatial variability of slab stability and fracture properties of weak layers. Studies of the spatial variability of other snowpack properties such as hardness and density (e.g. Jamieson, 1989; Birkeland and others, 1995; Chernouss, 1995; Takeuchi and others, 1998; Harper and Bradford, 2003; and Birkeland and others, in press) are not reviewed. Studies at spatial scales larger than the slope-scale (e.g. variability across a mountain range) are included because many of the processes that contribute to spatial variability can span more than one scale. Relatively few field studies have

looked at the spatial variability of fracture properties such as fracture character (Landry, 2002; Kronholm, 2004). Since no field studies have looked at the spatial variability of tests for fracture propagation, studies such as Faillettaz and others' (2002) report on field tests for fracture toughness are not reviewed.

Section 2.2 reviews the studies of spatial variability of stability and fracture properties at the slope-scale. Section 2.3 reviews the studies of spatial variability of stability at larger scales. Section 2.4 summarizes all of the studies reviewed.

2.2 Slope-scale spatial variability of stability and fracture properties

During the winters of 2001 to 2003, in the eastern Swiss Alps, Kronholm (2004) performed arrays of stuffblock and rammrutsch stability tests on 21 different weak layers. Array slopes were in the alpine with homogeneous snow depth and no large rocks. In each array, 12 pairs of tests were arranged in an 18 x 18 m regular grid pattern, separated by 6 m in the up-slope and cross-slope directions. Test pairs spanned the entire grid except for the four corners, resulting in an array shaped like an even-armed cross. Each 30 x 30 cm test column in a pair was separated by 1 m in the cross-slope direction. The tests were loaded until fracture with a stuff sack full of snow (stuffblock) or a rammrutsch, which is similar to the drop hammer tester used by Stewart (2002) and for this thesis. Additionally, six different visual descriptors, similar to the

fracture character classification scheme used by van Herwijnen and Jamieson (2003) and for this study, were used to characterize each fracture.

Kronholm (2004) found seven layers that showed significant array spanning linear trends in either the cross-slope or up-slope directions, or both. The variance explained by the all the regressions was generally low, with an average R^2 value of 0.36. Variograms, or plots of semi-variance versus lag distance, were used to analyze the spatial structure of the data. Semi-variance of the residual stability values, after linear trends were removed, was found to increase with increasing lag distances for approximately 22% of the arrays. However no variograms reached a sill equal to the underlying variability within the confines of the arrays. Variogram analysis of closely spaced penetration resistance measurements in the same arrays showed sills within a range of 2 to more than 10 m for 67% of the arrays.

Kronholm (2004) found that the variability in stability can be partly explained by slab thickness but had few correlations significant at the $p < 0.05$ level with slope angle. Overall, when estimated from the quartile coefficient of variation (QCV), Kronholm (2004) found the coefficient of variation (CV) of stability to be between 27% and 107%, with a median of 50%. The median CV is reduced to 33% when the array-spanning trends based on a linear regression were removed. In Kronholm's (2004) study, 91% of all fractures were planar; with the remainder being collapses, resistant planars or breaks.

During the winters of 2001 and 2002, in the Columbia Mountains of British Columbia, Stewart (2002) performed 39 spatial arrays of drop hammer stability tests. Array slopes were selected based on varying snowpack and ground conditions typical of avalanche start zones. Up to 126 test columns were arranged in a regularly spaced rectangular grid pattern, separated by 30 cm in the up-slope and cross-slope directions. Each 30 x 30 cm test column was loaded with a drop hammer tester until fracture occurred in at least one weak layer.

Stewart (2002) found that 16 arrays had correlations significant at the $p < 0.05$ level between stability and slab thickness. However, eight correlations were positive and eight were negative. Correlation analysis on the combined data from all arrays showed slab thickness as the most important source of variability, with a general trend of lower stability where slabs were thin. Eight arrays had significant correlations between stability and total snow depth. However, once again, four were positive and four were negative. Stewart (2002) found two significant correlations between stability and slope angle within the arrays, one positive and one negative. Stewart also found a tendency for slopes with higher median stability to have greater variability. This finding is supported by Keeler and Weeks (1968) who found similar results for closely spaced shear strength measurements.

Array-spanning linear trends in either the cross-slope or up-slope directions, or both, were found for 15 arrays. Clusters of low and high stability were found in most arrays (Stewart, 2002). A cluster consisted of four or more adjacent tests that had distinctly higher or lower stability than the tests that bound the cluster. Three different slopes, each tested in two consecutive winters, showed no year-to-year repeatability of stability patterns over the two winters. Variogram analysis of the stability measurements revealed no array wide correlation length and the spatial structure of the de-trended data was not analyzed. Overall, Stewart (2002) found the CV of stability to be between 10% and 82%, with an average of 50% for slopes with variability typical of avalanche start zones.

During the winters of 2001 and 2002, in the Bridger and Madison Ranges of southwestern Montana, Landry (2002) performed 11 arrays of quantified loaded column tests (QLCT) on uniform slopes. Each 30 x 30 m array consisted of five evenly spaced “snowpits” of 10 closely spaced tests. The top of 0.04 or 0.08 m^2 test columns were loaded downwards with a mechanical force gauge until fracture occurred in at least one weak layer (Landry and others, 2001). Fractures were classified as Q1, Q2 or Q3 planar fractures or collapses, based on Birkeland and Johnson’s (1999) shear quality classification scheme. Tests which produced very rough (Q3) planar fractures were rejected.

Landry (2002) suggested existence of slope-scale stability trends through visual analysis, but did not attempt quantitative spatial analysis. Slope angle and slab thickness were not investigated as causes of variability in stability. Overall, Landry (2002) found the CV of shear strength, calculated from the QLCT results, to be between 10% and 50% with an average of 24%. A similar range of values was found for the variability of a calculated stability index based on a ratio of shear strength to shear stress. Further analysis by Landry and others (2004) showed that the stability index for 39% of the snowpits were statistically or empirically unrepresentative of their respective site's stability index. Spatially homogeneous shear quality was observed in at least six of the arrays, which all had entirely Q1 fractures.

During the winters of 1990 to 1992 in the Cariboo and Monashee Mountains of British Columbia, Jamieson and Johnston (1993) and Jamieson (1995) performed several arrays of rutschblock tests. Each array consisted of 20 to 81 closely spaced tests arranged in a regular rectangular grid pattern. Arrays were carried out on uniform slopes as well as on slopes with trees, buried rocks, drifts and variations in slab thickness and slope angle.

Jamieson and Johnston (1993) analyzed six of the arrays which were on more uniform slopes and found that 97% of the rutschblock scores were within one rutschblock score (Section 3.2.2) of the slope median. Jamieson and Johnston (1993) analysed 24 arrays where slope inclination varied by more than

8° and found a tendency for rutschblock scores to increase by one step for each 10° decrease in slope angle. This was significant at the $p < 0.05$ level for 10 of the 24 arrays.

Jamieson (1995) analyzed nine of the arrays which were on uniform and non-uniform slopes. Slab thickness was identified as a source of variability in at least one array where thinner slabs produced lower rutschblock scores. Slope angle was also identified as a source of variability in at least one array where steeper slopes produced lower rutschblock scores. Furthermore, Jamieson (1995) found that sites near the top of slopes, near trees and on pillows of wind-deposited snow often had higher rutschblock scores and were more variable.

Föhn (1989) analyzed five spatial arrays of rutschblock tests, on alpine slopes of up to 300 x 200 m. Arrays of 18 to 54 tests, which were separated by 10 to 20 m, were performed by several operators on explosive-tested slopes. In addition, stability index calculations were made from shear frame measurements at regular intervals within each array. Föhn (1989) found stability index variations of 15 to 30%, with outliers removed, which was on the same order of magnitude as other snowpack parameters. When the outliers are included, the maximum CV increased to 38% (50% for a skier stability index). Föhn (1989) suggested that variability depends mainly on aspect, ground cover, terrain geometry. Furthermore, slab thickness in areas of very poor stability was 30% to 40% lower than the slab thickness values for adjacent areas. On one cross-loaded array,

where large scale cross-slope fluctuations corresponded with slab thickness, lower shear strength was found in areas with thinner slabs.

During the winters of 1981 and 1982, in the New Zealand Alps, Conway and Abrahamson (1984) performed 26 spatial arrays of 30 x 30 cm test columns spaced 0.5 to 10 m apart. Test slopes were in the alpine, in an area noted for considerable wind speeds. Because the test method involved pulling slope parallel on the top of the columns with large shear frames, it is possible that a bending mode of failure was introduced in the weak layer resulting in lower shear strength measurements and hence in the stability index. Conway and Abrahamson (1984) also identified an inconsistent loading rate as a source of error.

Nonetheless, Conway and Abrahamson (1984) found that unstable start zones, parts of which had released prior to testing, tended to be less variable than stable slopes. However, they used an index with a minimum of zero so the distribution of sets with low means was truncated and likely skewed. In 1998, Conway and Abrahamson (1998) analyzed the same data with an index which was not truncated, but did not compare the variability of slopes which had released avalanches to the variability of those which had not. Slab thickness was also found to affect the stability index in at least one array that had signs of drifting. They found that these arrays had shear strength patterns consistent with wind drift wavelengths (often < 5 m). Furthermore, weak layer thickness was

found to have an effect on shear strength; however the direction is unclear. Overall, the CV of shear strength was found to be between 65% and 82%.

2.3 Spatial variability of stability at larger scales

Armstrong and Armstrong (1987) analyzed weather data, from Westwide Data Network, and fatal accident data for the western United States. Five mountain weather observation sites were used in each of the three climatic zones: maritime, intermountain (transitional) and continental. Continental climates were found to have colder mean seasonal air temperatures and lower total snowfall and new snow density, than maritime climates.

Armstrong and Armstrong (1987) found that the continental snowpack had generally lower bulk strength than the maritime snowpack. This is supported by Gruber and others (in press) who found that the Coast Mountains in British Columbia (maritime snow climate) had a higher winter average stability rating than the Columbia Mountains (transitional snow climate) and the Rocky Mountains (continental snow climate). Furthermore, the difference between the stability ratings at different elevation bands (alpine, treeline and below treeline) was found to be larger for continental snow climates than for transitional or maritime snow climates (Gruber and others, in press). This implicates elevation as a source of variability.

Armstrong and Armstrong (1987) found continental climates to have better conditions for surface hoar formation, due to efficient radiation cooling, and for faceting, due to stronger temperature gradients. Consequently, continental climates tended to have more avalanches associated with persistent weak layers, whereas maritime climates tended to have more direct action new snow avalanches. It was qualitatively concluded that skier-triggered avalanches, during non-storm periods, were more likely in a continental climate. The CV for total snow depth was found to be 51% across the entire mountain range for the maritime climatic zone, 36% for the intermountain climatic zone and 24% for the continental climatic zone.

Hägeli (2004) examined avalanche activity for a facet-crust combination that was observed across the entire study area, spanning the three mountain ranges (the Coast Mountains, the Columbia Mountains and the Rocky Mountains) in western Canada, in November 2001. Avalanche activity associated with this layer was found to be more spatially variable in the Columbia Mountains (activity concentrated in the central part of the range) than in the Coast (basically absent activity) or Rocky Mountains (widespread activity).

Hägeli and McClung (2003) analyzed five years of avalanche activity observations, from 11 different Canadian Mountain Holidays helicopter skiing operations, covering a total area of approximately 20,000 km^2. Weather station data were used in conjunction with these avalanche observations in an attempt to

classify the “avalanche climate” of the Columbia Mountains in British Columbia. Hägeli and McClung (2003) found that the Columbia Mountains were characterized by a transitional snow climate with a heavy maritime influence. The percentage of natural avalanche activity that was associated with persistent weak layers ranged from 0% during a maritime winter, to 40% during a continental winter. This high annual variability of persistent weak layer avalanche activity was found to be typical for transitional snow climates.

Analysis of the same data by Hägeli (2004) showed that there is a strong east-west pattern in snow climates in the Columbia Mountains. The central part of the range was found to have a more maritime snow climate than the western side. This was attributed to the increased precipitation caused by the additional lift experienced by air masses approaching the main crest of the range.

Hägeli and McClung (2003) found facet-crust combinations and buried surface hoar to be the most important, in terms of number of avalanches, weak layers in the Columbia Mountains. Significant weak layers tended to cover large areas and most of these layers that were associated with considerable avalanche activity were observed across the entire mountain range. There was no evidence of a north-south or east-west variation in the frequency of early season facet layers or buried surface hoar layers. However, Hägeli and McClung (2003) noted a depth hoar layer that was observed across the entire Columbia Mountain range during November 2000, with the majority of the avalanche activity associated

with this weak layer limited to northerly and easterly aspects in the central part of the range. It was also suggested that during clear weather periods in late winter, surface hoar can form on northerly aspects while sun crusts form on southerly aspects. This implicates aspect as a potential source of spatial variability.

Stoffel and others (1998) analyzed 14 years of avalanche activity data from the Engadine Valley in the eastern Swiss Alps. The valley was characterized by a continental snow climate with most avalanche start zones having northwesterly and southeasterly aspects. Stoffel and others (1998) observed more faceting and depth hoar formation on the northerly aspects and consequently more avalanches. This was explained, in theory, by increased faceting due to stronger vertical temperature gradients within the snowpack, caused by colder snow surface temperatures on the shady northerly aspects.

On 1997-02-06 and 1997-04-02, Birkeland (1997) collected snowpack data from more than 70 sites each day. These sites spanned tens of kilometers and were located throughout the entire Bridger Range in southwestern Montana. The north-south running mountain range was characterized by a transitional snow climate. Rutschblock and stuffblock stability tests were performed at all observation sites which were distributed across the entire range, except for the windward (western) side of the range due to high stability variations.

On the first day, Birkeland (1997) found near surface faceting to be associated with surface crusts on southerly aspects, but not on easterly or northerly aspects. Better links between stability and terrain variables were found on the second sampling day. Spatial patterns found in stability and slab thickness were thought to be due to wind exposure. Birkeland (1997) found lower stability at higher elevations, which was possibly due to thinner slabs from local wind scouring. Lower stability was also found on northerly aspects, possibly due to better conditions for weak layer persistence because of colder snowpack temperatures. Multiple regression analysis showed that it was most unstable on northerly aspects at higher elevations with deep, cold snowpacks that had weaker surface snow.

During the winter of 2003, Feick and others (2004) focused on the basin-scale spatial variability of surface hoar layers in the Swiss Alps. Observations of surface hoar formation and destruction, while on the surface, were related to micro-meteorological conditions and topography. Variations in humidity, caused by local winds, were identified as a major source of variability due to the effect of humidity on growth conditions (i.e. lower humidity is less favorable for surface hoar growth). Variations in topography, such as aspect, were also found to be a source of variability (Feick and others, 2004) because aspect can affect incoming solar radiation and wind exposure at the basin scale (McClung and Schaerer, 1993, p. 92). Cold and relatively calm conditions favor surface hoar formation

(McClung and Schaerer, 1993, p. 44) and destruction was mainly due to melting, caused by solar radiation, and wind erosion (Feick and others, 2004).

2.4 Summary

- The CV of slope-scale spatial variability of point stability can range between 10% and 107% but is typically between 25% and 50%.
- Spatial variability of stability is generally lower for more uniform slopes.
- Slope-scale spatial variability of stability is due to various causes.
- Slab thickness can influence stability at all scales.
- Thinner slabs are typically more unstable.
- Steeper slopes tend to result in lower rutschblock scores.
- Slope-scale variability of stability has spatial structure and can sometimes be modeled as a slope-spanning linear trend plus residuals.
- Variograms rarely reveal a correlation length, perhaps due to insufficient sample sizes, excessive spacing between tests or lack of spatial structure other than the linear trends.
- It is common for fracture characteristics to be spatially homogeneous at the slope-scale.

The knowledge gaps that will be addressed in the remaining sections of this thesis include:

- The spatial variability of fracture properties such as fracture propagation energy and character observations.
- The relationships between array-spanning linear trends in stability and fracture properties and array-spanning linear trends in snowpack and terrain variables.
- The combined effect of multiple snowpack and terrain variables on stability and fracture properties.

3 Methods

3.1 Study areas

Field research for this thesis was carried out by graduate students and research technicians based out of two separate field stations in the Columbia Mountain Range of British Columbia (Figure 3.1). The Rogers Pass field station, located in the Selkirk Mountains, is operated in cooperation with Glacier National Park (Parks Canada). The Blue River field station, located in the Cariboo and Monashee Mountains, is operated in cooperation with Mike Wiegele Helicopter Skiing. Two arrays sites (Rudy's Bowl and Toilet Bowl) were located in the Purcell Mountains in cooperation with Kicking Horse Mountain Resort.

Several array sites were located on Mount St. Anne near Blue River or on Fidelity Mountain near Rogers Pass. Array sites on Mount St. Anne included Monashee View, Robson View, and Langevin Cutblock. Array sites on Fidelity Mountain include the Poetry Slopes and South Run areas as well as the Squirrel Slope, Schuss Creek and Christiania Ridge. Specific locations of all array sites can be found in Appendix B.

The Columbia Mountains are characterized by a transitional climate with a heavy maritime influence (Hägeli and McClung, 2003). The snowpack at treeline

is usually deeper than 2 m throughout the winter and persistent weak layers are often buried surface hoar or faceted crystals (Jamieson, 1995).

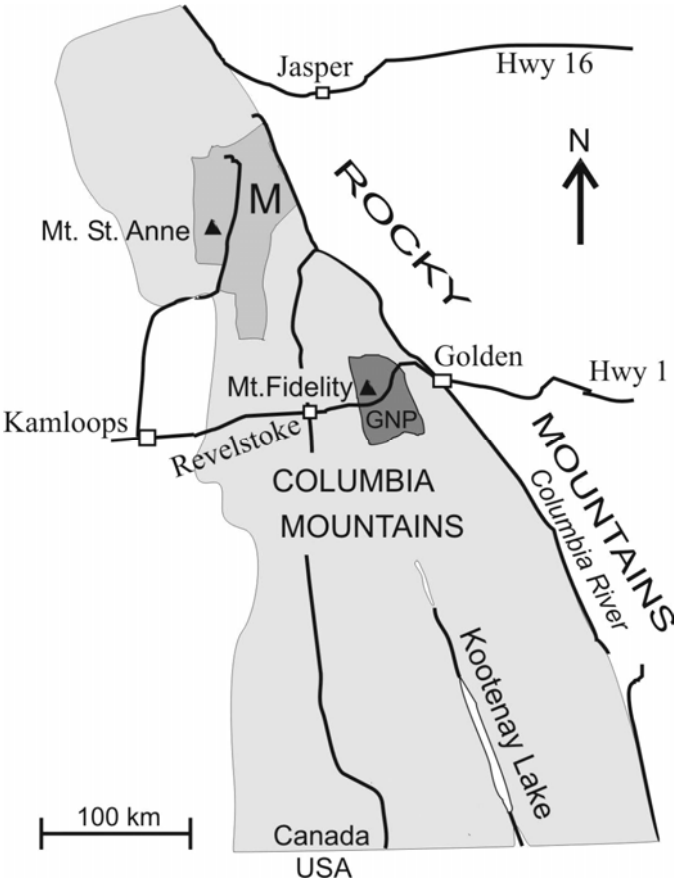

Figure3.1 – Map of the Columbia Mountains showing the area used by Mike Wiegele Helicopter Skiing (M) where the Blue River field station is located and Glacier National Park (GNP) where the Rogers Pass field station is located. Kicking Horse Mountain Resort is approximately 10 km west of Golden.

3.2 Field methods

3.2.1 Manual profiles

Manual snow profiles were performed for each array according to the Canadian avalanche Association's Observation Guidelines and Recording Standards (CAA, 2002). This included depth, hand hardness, density and grain form and size for all layers, thickness of all weak layers measured to the nearest millimeter as well as a vertical snowpack temperature profile. Hand hardness (R) for each layer was classified as fist (F), four-finger (4F), one-finger (1F), pencil (P), knife (K) or ice (I) based on the object that can be pushed into the snow with moderate effort. Site attributes, including aspect, slope angle, elevation, vegetation zone, total snowpack depth, air temperature, wind, precipitation and sky conditions, were also observed. Furthermore, three compression tests (CAA, 2002) were performed to assess the stability and to identify any layers that might have been overlooked. Each profile was deep enough to accurately assess the layer below the target weak layer for propagation tests or the deepest suspected failure plane for rutschblock tests.

3.2.2 Rutschblock test

Rutschblock tests were performed according to the Canadian Avalanche Association's Observation Guidelines and Recording Standards (CAA, 2002).

After all potential failure planes are identified, a block of snow is isolated by digging and, for this study, by cutting with a 1.2 m long saw. Figure 3.2 shows the slope parallel dimensions of the rutschblock test. The height of each block is sufficient to test all failure planes likely to be skier triggered (typically 0.6 to 1.2 m). First the vertical lower wall (2.1 m wide) is isolated and smoothed with the edge of the shovel blade. Then the two vertical side walls (1.5 m up-slope) are cut with the saw such that they taper to 1.9 m apart at the back wall. The vertical back wall (1.9 m wide) is then cut with the saw. This tapered block ensures that it is free to slide without binding on the sides.

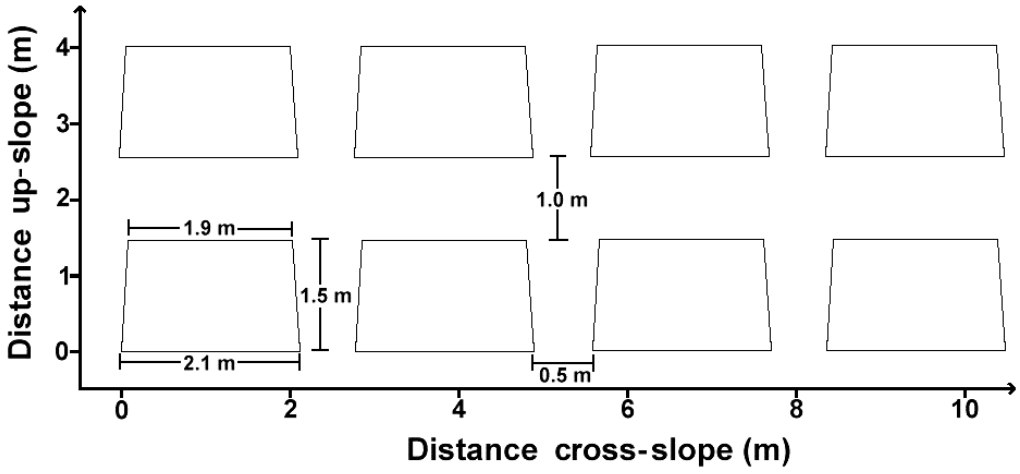

Figure 3.2 – Slope parallel dimensions of the rutschblock test, according to CAA (2002), when using a saw to cut the side and back walls. The height of the block is dictated by the depth of the deepest failure plane that a skier might trigger. The grid layout for spatial arrays is also shown.

Table 3.1 – Loading steps and rutschblock scores (CAA, 2002).

RB score	Loading step that produces a clean failure across the entire block
1	The block slides during digging or cutting.
2	The skier approaches the block from above and gently steps down onto the upper part of the block (within 35 cm of the upper wall).
3	Without lifting the heels, the skier drops from a straight leg to a bent knee position, pushing downwards and compacting the surface layers.
4	The skier jumps up and lands in the same compacted spot.
5	The skier jumps again onto the same compacted spot.
6	• For hard or deep slabs, remove skis and jump on the same spot. • For soft or thin slabs where jumping without skis might penetrate through the slab, keep the skis on, step down another 35 cm, almost to mid-block and push once then jump three times.
7	None of the loading steps produced a smooth slope-parallel failure.

Once isolated, the block is loaded according to Table 3.1. For each test, fracture character (van Herwijnen and Jamieson, 2003) and release type observations were recorded. Table 3.2 lists the fracture character types used. The release type was recorded as the whole block (W), most of the block (M) or only an edge of the block (E), as per Schweizer and Wiesinger (2001).

Table 3.2 – Fracture character types and descriptions from van Herwijnen and Jamieson (2003).

Fracture character	Description of fracture
Sudden Planar (SP)	Planar fracture suddenly crosses column in one loading step and the block slides easily* on the weak layer.
Resistant Planar (RP)	Planar fracture requires more than one loading step to cross column and/or the block does not slide easily on the weak layer.
Sudden Collapse (SC)	Fracture suddenly crosses column with single loading step and causes noticeable slope normal displacement.
Progressive Compression (PC)	Fracture usually crosses column with one loading step, followed by gradual compression of the layer with subsequent loading steps.
Non-planar Break (B)	Irregular fracture.

* Block slides off column on steep slopes. On low angle slopes, hold sides of block and note resistance to sliding.

Unfortunately there was some inconsistency amongst field workers with respect to the first loading step. When cutting the back wall with the saw, it is necessary to approach the block from above, which can disturb the snow. Occasionally the rutschblock would fail during the cutting process (RB score = 1) although it was triggered by operator disturbance during the approach (RB score = 2).

At the Blue River field station any test that failed while cutting from above when the operator was not moving or disturbing the snow was assigned a RB score of 1. If the operator was moving, it was given a RB score of 2. At the Rogers Pass field station, all tests that failed during the isolation process,

regardless of whether the operator was moving and disturbing the snow, were incorrectly assigned a RB score of 1. This inconsistency affected nine tests in three arrays at Roger Pass. These tests were changed to a RB score of 2 before the data were analyzed. In doing this, all rutschblock tests are performed according to Canadian standards (CAA, 2002), although some tests that actually failed on the first load step may have been incorrectly changed. An analysis of the uncorrected data shows some stronger correlations with terrain and snowpack variables, as indicated by the correlation coefficient, but the number of correlations significant at the $p < 0.05$ level remained unchanged.

Camponovo and Schweizer (1997) used buried load cells to measure the impact force associated with each rutschblock load step. They found that the impact increased strongly with each load step and the relationship is not linear. Furthermore, there can be substantial variability in the impact force delivered during each load step (Camponovo and Schweizer, 1997). Toft and Wakeling (2002) found that a 20 kg difference in the weight of operators can affect the RB score by up to two steps, although factors such as the height of the jumps were not considered. In order to minimize such sources of error in this study, the same operator was used for all tests in a rutschblock array.

3.2.3 Fracture propagation test

3.2.3.1 Equipment

For research purposes, a drop hammer tester (Stewart, 2002) was used to load the test column, but tapping as per compression tests would be more practical for avalanche workers or recreationists. The drop hammer tester (Figure 3.3) consists of a 30 x 30 cm base plate, with a vertical guide rod mounted in the center, and 300 g and 1 kg hammers used for loading.

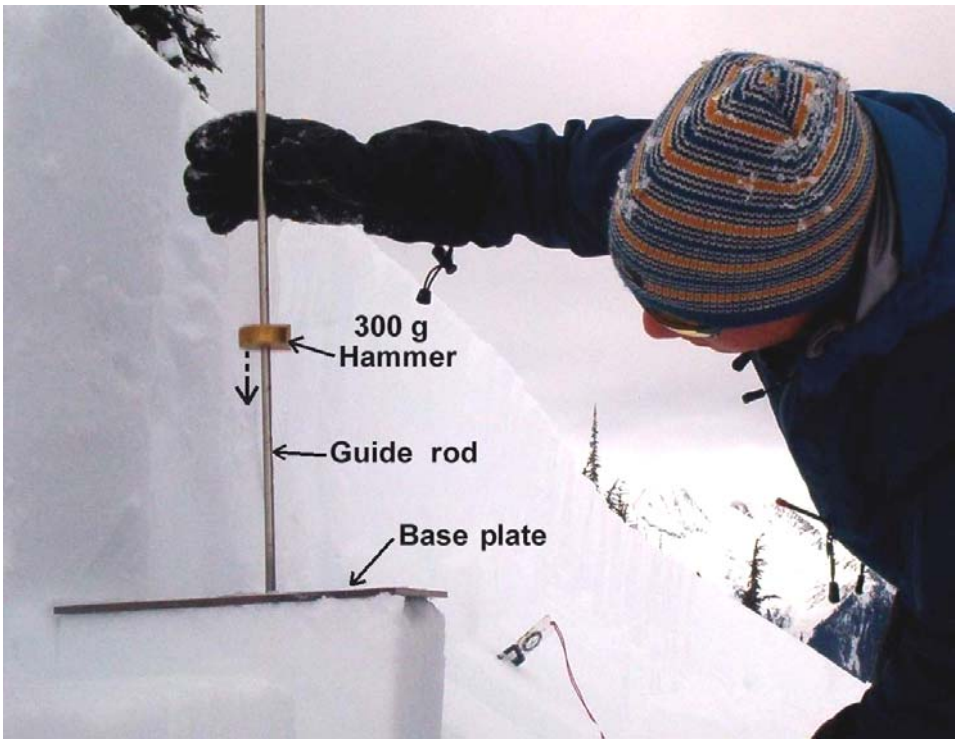

Figure 3.3 – The drop hammer tester being used on a fracture propagation test (ASARC photo).

Stewart (2002) was the first to use the drop hammer tester for extensive field research, although the design was based on the existing rammrutsch tester. The advantages of the drop hammer tester include: operator independence, fast (40-120 tests can be performed in 4-5 hours), relatively lightweight and portable, inexpensive equipment and the ability to quantify the stress applied to the snowpack surface. Some of the disadvantages include: weak layers can fracture during placement of the tester on the column and it is ineffective for testing shallow weak layer because the top of the column needs to be levelled (Stewart, 2002). Stewart (2002) found a significant positive correlation between drop heights for the drop hammer tester and compression test taps.

3.2.3.2 Test procedures

The fracture propagation test is a prototype field test designed to measure the fracture propagation energy of a specific weak layer, although a correlation with fracture frequency or distance has not been established yet. Figure 3.4 shows the dimensions of the test column and the test preparation procedures. Like the compression and shovel shear tests, the propagation test uses a 30 x 30 cm isolated snow column. However, in order to accommodate the base plate of the drop hammer tester (Stewart, 2002), the 30 cm for the side walls is measured horizontally instead of parallel to the slope.

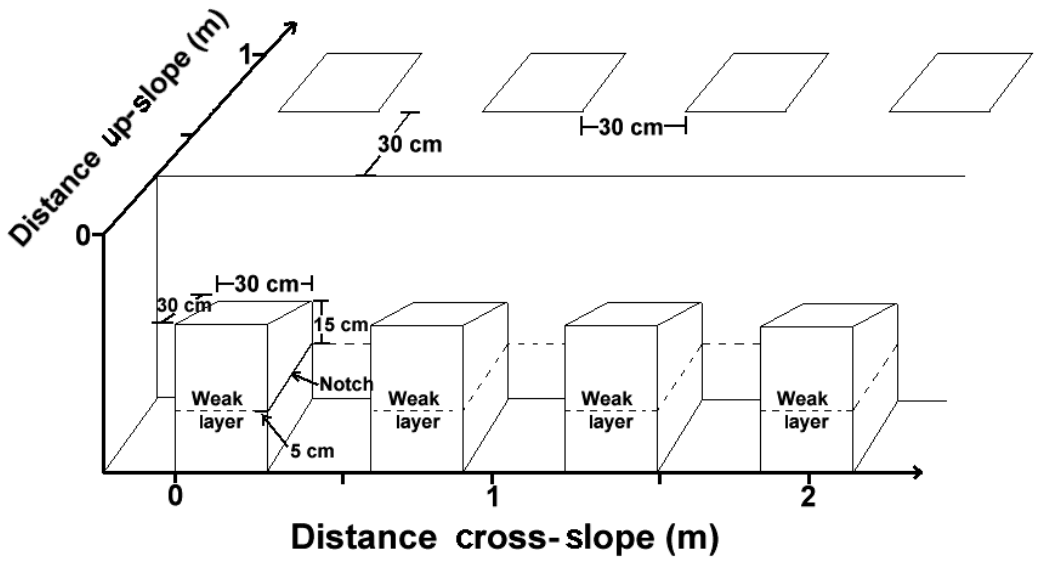

Figure 3.4 – The test column dimensions and preparation steps (notch and leveling) for the fracture propagation test. The grid layout for the arrays is also shown.

Once a target weak layer is identified, the test column is leveled such that all but 15 cm (measured at the back wall) of snow above the weak layer is removed. In order to ensure that no applied energy is lost, and/or the test column is not ruined, the remaining 15 cm of damping snow on top of the weak layer should be unlikely to crush during testing. Damping snow of at least one-finger (1F) hardness is usually adequate. This is important for the validity of the assumption that all the energy applied with the drop hammer tester reaches the weak layer. The weak layer is then notched 5 cm on the right side of the column with a snow saw to simulate a crack in the weak layer with the idea that sufficient additional applied energy causes the crack to propagate.

An appropriate hammer weight is chosen based on practice test results and mounted on the guide rod. The hammer is then dropped from successive 5 cm height increments, starting from 5 cm, until the fracture propagates across the entire test column. The drop height (DH) which caused the fracture to propagate is then recorded. If the fracture propagates when the tester is gently placed on the column, before the hammer is dropped, a DH of 0.1 is assigned to that test. If the fracture does not propagate after the highest DH is reached (120 cm) then a DH of 150 is assigned to that test. Fracture character observations (Table 3.2) are also made for each test. If it appears as though the fracture did not propagate from the notch (through visual examination of the fracture surface) then the test is rejected. These tests differ from Stewart's (2002) drop hammer stability tests in that the amount of damping snow is fixed and the weak layer is notched.

3.2.3.3 Conversion to drop hammer energy (DHE)

For analysis, the drop height (DH) recorded for each test was converted to energy applied to the weak layer, dubbed drop hammer energy (DHE) by Stewart (2002), using the following equation:

$$DHE = \frac{DH \times g \times mass}{w \times (l/\cos\Psi)} \qquad (J/m^2) \tag{3.1}$$

where *g* is the acceleration due to gravity, *mass* is the mass of the hammer used, *w* is the width of the test column, *l* is the length of the test column measured horizontally and Ψ is the slope angle. The assumption that all the energy from the drop hammer tester reaches the weak layer is required for this equation. This assumption is valid if all the compressible snow is removed during test column preparation. Furthermore all individual tests with visible crushing of the overlying snow and/or fractures in layers other than the target weak layer were rejected. Arrays were discontinued if these problems persisted.

3.2.3.4 Assessment of test variables

Development the fracture propagation test included analyzing the effects of the notch and the damping snow in study plots throughout the winter of 2004. This was done by eliminating and varying the thickness of the notch, and by varying the hardness and amount of damping snow for tests performed next to standard propagation tests. The Wilcoxon matched-pairs signed-ranks test (Walpole and others, 2002, p. 605) was used to assess the difference between the paired tests, and the difference was considered significant when $p < 0.05$.

In order to assess the effect of the notch, standard propagation tests were performed beside 25 x 30 cm test columns without notches and hence the same fracture area. The median DHE for the standard propagation test was significantly lower ($p < 10^{-3}$, 19 pairs) which suggests that the notch has a

significant effect. The thickness of the notch (which may affect the notch radius and hence the stress concentration at the crack tip) was tested with side-by-side tests notched with either a crystal screen (~ 1 mm) or a snow saw (~ 3 mm). The difference was also significant (p = 0.01, 48 pairs) with more energy required to propagate fractures initiated from thicker notches. A snow saw was used to notch the propagation tests since it was easier to cut a notch of consistent depth (5 cm) because the blade of a Life-Link saw is approximately 5 cm wide. These trials showed that the propagation test has some characteristics expected for a test of propagation energy, but the correlation with propagation frequency or distance is beyond the scope of this thesis.

In order to assess the effect of different amounts and hardness of damping snow, standard propagation tests (15 cm of damping snow) were performed beside tests with 30 cm or more damping snow. These trials were carried out for both pencil (P) and one-finger (1F) hardness slabs. The amount of damping snow had a significant effect on DHE for harder (P) slabs (p = 0.01, 21 pairs) but not for softer (1F) slabs (p = 0.10, 15 pairs). For P hardness slabs, the median DHE for tests with 30 cm or more damping snow was significantly higher than median DHE for adjacent standard propagation tests. Furthermore, when both P and 1F slabs are considered, tests with 30 cm or more damping snow consistently required more energy to propagate fractures from the notch (p = 0.04, 36 pairs).

A small propagation test array was performed in a uniform study plot in order to assess the intrinsic variability associated with the fracture propagation test. This array consisted of 32 tests with a median DHE of 15.6 J/m^2, a quartile coefficient of variation (QCV) of 10% which corresponds to a coefficient of variation (CV) of 15%. The conversion used for CV can be found in Section 3.3.1 (Equation 3.4).

3.2.4 Spatial arrays

3.2.4.1 Array sites

Spatial array sites were chosen based on characteristics of avalanche start zones. According to McClung and Schaerer (1993) this includes an open slope that is steeper than 25˚. A source of variability, such as variable slope angle, aspect or slab thickness, was also sought out when choosing array sites, as per Stewart (2002) and Jamieson (1995). Furthermore, sites had to be undisturbed by skiers, previous avalanches, over-snow vehicles, etc. Nevertheless, the primary concern when choosing array sites was the safety of the field workers. If conditions rendered a particular slope unsafe, another safer, and often smaller and/or less steep, slope was chosen.

The size of the slope and available time dictated the number of tests in each array. Tests were performed in a series of rows extending across the slope

starting at the bottom left or right corner. Subsequent rows were above the previous row and tests positioned directly above one another defined a grid column. Rows and columns were numbered starting with row = 1 and column = 1 at the bottom, left (when looking up-slope or “climber’s”) corner of the array. The position of each test in an array was then identified by the grid row number (Row) and column number (Col). The dimensions of the arrays were such that the sources of variability were captured. However, most arrays have more tests in the cross-slope direction than in the up-slope direction because it is easier to extend an array in the cross-slope direction.

In order to minimize the effect of temporal variability on test results all arrays were performed as quickly as possible. Usually they were performed within one day, but some of the larger arrays took two days. Nonetheless, any source of temporal variability (e.g. marked warming, heavy snowfall or increased solar radiation) during the course of an array was noted and if deemed necessary (i.e. the assumption of no temporal variability becomes invalid) the array was abandoned. Both Stewart (2002) and Jamieson (1995) found no significant correlation between test results and the sequence number for each array and, therefore, considered the assumption of no temporal variability to be valid for arrays performed within one day. Furthermore persistent weak layers such as buried surface hoar and faceted crystals are less likely to have a substantial change in mechanical properties than non-persistent weak layers during an array, and 47 (90%) of the 52 arrays were performed on persistent weak layers.

In addition to the manual snow profile, various snowpack and terrain variables, which characterized a source of variability for that particular array, were measured for each test. These variables included total snowpack depth (HS), weak layer depth also known as slab thickness (H), weak layer thickness (Thick), slope angle (Ψ), aspect (Asp) and weak layer crystal size (E). Slope angle was measured for all propagation tests for the calculation of DHE. The ground cover was also surveyed, during the summer, for three different array sites.

3.2.4.2 Rutschblock test arrays

Figure 3.2 in Section 3.2.2 shows the grid layout of the rutschblock arrays. The rutschblock tests were arranged in a regular grid pattern separated by 0.5 m in the cross-slope direction and 1 m (measured slope parallel) in the up-slope direction. The distance between the centre of one rutschblock test and the adjacent test in the cross or up-slope direction was 2.5 m.

3.2.4.3 Propagation test arrays

Figure 3.4 in Section 3.2.3.3 shows the grid layout of the propagation test arrays. The fracture propagation tests were arranged in a regular grid pattern separated by 0.3 m in both the cross-slope direction and the up-slope direction

(measured slope parallel). The distance between the centre of one propagation test and the adjacent test in the cross or up-slope direction was 0.6 m.

3.3 Analysis

3.3.1 Summary statistics

The Kolmogorov-Smirnov and Lilliefors tests were used to test the hypothesis of normality for all datasets. The Lilliefors test provides a corrected Kolmogorov-Smirnov p-value specifically for testing for normality when the mean and variance are unknown. The hypothesis of normality was rejected if the Lilliefors test was significant at the $p < 0.05$ level. The results from this normality testing can be found in Appendix C. For most of the individual arrays, the assumption of normality was rejected, so robust non-parametric statistics were used to describe the data. Furthermore, since rutschblock scores are ordinal and based on ranks, non-parametric statistics are more appropriate for the rutschblock test array data.

The central tendency of each array was described by the median and the first (Q_1) and third (Q_3) quartiles, where 25% of the data are less than Q_1 and 25% of the data are greater than Q_3. The spread of the data was described by

the semi-interquartile range (SIQR) as follows (Spiegel and Stephens, 1999, p. 90):

$$SIQR = \frac{Q_3 - Q_1}{2} \tag{3.2}$$

The semi-interquartile range is half the range of the middle 50% of the data and similar to the parametric standard deviation descriptor (e.g. 50% of the data fall within ± 1 SIQR).

The relative spread was described by the quartile coefficient of variation (QCV) as follows (Spiegel and Stephens, 1999, p. 108):

$$QCV = \frac{Q_3 - Q_1}{Q_3 + Q_1} \tag{3.3}$$

The quartile coefficient of variation is a measure of variability similar to the parametric coefficient of variation (CV). The coefficient of variation can be estimated from the QCV, as per Kronholm (2004), by the following equation:

$$CV \approx \frac{3}{2} QCV \tag{3.4}$$

3.3.2 Multivariate linear regression

Data from the individual rutschblock and fracture propagation test arrays were modeled as the sum of array spanning linear trends (V_{trend}) and corresponding residual values (V_{res}) as follows:

$$V = V_{trend} + V_{res} \tag{3.5}$$

Multivariate least-squares linear regression was used determine the significance of the coefficients *a* and *b* for variable *V* such that:

$$V_{trend} = a\,Col + b\,Row + c \tag{3.6}$$

where *Col* is the cross-slope position as defined by the grid column number and *Row* is the up-slope position as defined by the grid row number. With positive *Col* being from a climber's left to right across the slope and positive *Row* being up the slope.

Multivariate least-squares linear regression was also used to assess the combined affect of multiple terrain and snowpack variables on stability and propagation energy for large arrays and for the combined dataset. All regression coefficients were considered significant at the $p < 0.05$ level. This means that

there is a 5% chance of a type II error where a regression coefficient is considered to be significant when in fact it is not.

In order for least-squares linear regression to be valid, the assumption that the residual values are normally distributed must be fulfilled. A summary of the results from Kolmogorov-Smirnov and Lilliefors tests for normality of the residuals can be found in Sections 4.3 and 5.3. Complete results can be found in Appendix C.

3.3.3 Correlation analysis

Correlation analyses between RB score or DHE and terrain and snowpack variables were used to identify potential sources of variability. Four different datasets, for both rutschblock and propagation test arrays, were constructed.

The first dataset contained the raw data from each individual array. This included RB score or DHE and all of the terrain and snowpack variables measured for that array.

The second dataset contained the slope medians of RB score or DHE and medians of all of the terrain and snowpack variables from every array. The SIQR and QCV for RB score or DHE was also included in this dataset. Even though correlations between slope medians look at variability at a scale larger than

slope-scale, it can indicate potential sources of slope-scale variability. It also makes it possible to include data from the manual snow profiles performed for every array.

Manual snow profile data used in the second dataset included weak layer grain size (E) and hand hardness (R) as well as the difference in E and R between the weak layer and the adjacent layer. These variables were chosen because Schweizer and Jamieson (2002, 2003) identified them as significant predictors for skier-triggered avalanches. As per Schweizer and Jamieson (2002, 2003), hand hardness for individual layers were indexed from 1 to 6 for F, 4F, 1F, P, K and I respectively, with 0.5 increments for intermediate hardness values (e.g. 1F+ or P- = 3.5). The adjacent layer was defined as the harder of the two layers that bound the weak layer (above or below) or if there is no difference, it was defined as the layer below (Schweizer and Jamieson, 2002, 2003).

The third dataset consisted of the estimated and residual values from significant array-spanning linear trends.

The fourth dataset was a combination of the “normalized” data from all arrays. The data were normalized based on a non-parametric version of the parametric z-transformation such that:

$$V_{norm} = \frac{V - Med_V}{SIQR_V} \tag{3.7}$$

where V is a raw data value from an individual array, Med_V is the slope median of V and $SIQR_V$ is the semi-interquartile range of variable V.

Robust Spearman rank order correlations (Walpole and others, 2002, p. 620) were used to describe the associations between data that were not normally distributed. This included data from the individual arrays, the array medians as well as the normalized data from the combined dataset. Pearson product-moment linear correlations (Walpole and others, 2002, p. 392) were used to describe the associations between the data that were assumed normal. This included the array-spanning linear trends and the resulting residuals. All correlation coefficients are considered significant at the $p < 0.05$ level. This means that there is a 5% chance of a Type II error where a correlation coefficient is considered to be significant when in fact it is not.

3.3.4 Spatial statistics

Many earth science datasets exhibit spatial continuity, where two data points close to each other are more likely to have similar values than two data that are far apart (Isaaks and Srivastava, 1989, p. 50-51). A variogram is the most traditionally chosen method to describe spatial continuity or how the

autocorrelation (similarity) between two data points changes as a function of separation distance and direction (Isaaks and Srivastava, 1989, p. 143). Autocorrelation between two points separated by a specified distance (lag) is quantified with semi-variance. Ideally, as distance increases the autocorrelation decreases (the semi-variance increases) until the underlying variance in the dataset is reached (Figure 3.5).

The ideal variogram shown in Figure 3.5 has distinct features that are commonly used to describe variograms. A sill is reached when an increase in separation distance no longer causes an increase in semi-variance, or when there is no longer any spatial continuity. The value of the sill is equal to the underlying variance of the data. The range is the distance at which the sill is reached. The nugget reflects the variability at extremely small separation distances and is usually due to factors such as sampling error and small-scale variability (Isaaks and Srivastava, 1989, p. 143).

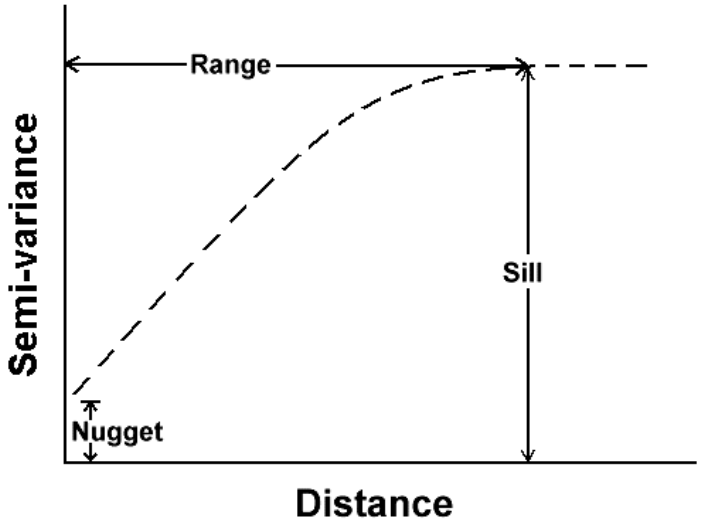

Figure 3.5 – Ideal variogram showing a distinct sill, range and nugget.

In order to produce variograms, distance and angular search parameters, as well as tolerances, must be specified. The usual convention is to define the lag distance as the distance between observation points and the lag tolerance as half that distance. Omnidirectional variograms, which are not restricted to a specified direction, serve as a useful starting point for variogram analysis (Isaaks and Srivastava, 1989, p.144). If linear trends exist in the data, it is common practice to analyze the spatial structure of the residual values with variograms.

4 Stability results

4.1 Introduction

During the winters of 2003 and 2004, 29 spatial arrays of rutschblock tests were performed consisting of a total of 705 tests. Diagrams for every array can be found in Appendix A. Eighteen of these arrays had buried surface hoar layers as the failure layer, with the remaining failing on either faceted crystals (six arrays), precipitation particles (two arrays) or on multiple weak layers (three arrays). Manual snow profile results for every array can be found in Appendix B.

This chapter starts with a summary of the rutschblock data in Section 4.2. The results from the use of multivariate linear regression to identify array-spanning linear trends are presented in Section 4.3. Correlation analysis results between point stability (rutschblock scores) and other snowpack and terrain variables are summarized in Section 4.4. Variogram analysis results are briefly summarized in Section 4.5; however, variograms did not prove to be a particularly useful tool for identifying spatial patterns in stability test arrays. In Section 4.6, selected rutschblock arrays are presented to highlight some of the concepts introduced with respect to causes of spatial variability.

4.2 Summary statistics

Table 4.1 shows that a wide range of stability conditions were targeted for these arrays. The median RB score for the individual arrays ranges from 2 to 7 with a median of 4. The QCV for the individual arrays ranged from 0% to 33% with a median of 14%, and the SIQR ranged from 0 to 1.5 with a median of 0.5. The most variability was found for the array performed on the Abbott Headwall on 2004-03-06/07, where RB scores ranged from 2 to 7. Several arrays showed very little variability, including the largest (Monashee View on 2004-02-27). The number of tests in each array ranged from 8 to 65 with a median of 20 tests, and all but three arrays were performed in a single day.

Table 4.1 – Summary statistics for the spatial variability of point stability as defined by the rutschblock test.

Location	Date	N	Rutschblock scores						
			Min	Q_1	Med	Q_3	Max	SIQR	QCV (%)
South Run	2002-12-17	16	2	3.0	3.5	4.0	6	0.5	14
Bear's Den	2003-01-03	21	2	3.0	3.0	4.0	4	0.5	14
South Run	2003-01-03	22	2	2.0	2.0	3.0	4	0.5	20
Poetry Slopes	2003-01-07	22	3	4.0	4.0	4.8	7	0.4	9
Robson View	2003-01-16	11	5	7.0	7.0	7.0	7	0.0	0
Cheops Bench	2003-01-20	20	4	4.0	5.0	6.3	7	1.1	22
South Run	2003-01-30	14	4	4.0	4.0	5.0	7	0.5	11
Fidelity	2003-02-21	20	2	2.0	2.0	2.0	3	0.0	0
Grizzly Shoulder	2003-02-25	12	3	3.0	3.0	3.3	4	0.1	4
Abbott Headwall	2003-02-27/28	63	2	3.0	4.0	5.0	6	1.0	25
Poetry Slopes	2003-03-05a	8	3	4.0	4.0	5.0	6	0.5	11
Poetry Slopes	2003-03-05b	9	2	2.0	2.0	2.0	3	0.0	0
Robson View	2003-03-05	29	5	6.0	7.0	7.0	7	0.5	8
Waikiki	2003-03-12	18	4	4.0	4.5	6.0	7	1.0	20
Toilet Bowl	2004-01-17	18	2	4.0	4.0	6.0	7	1.0	20
Poetry Slopes	2004-02-02	13	4	4.0	6.0	7.0	7	1.5	27
Langevin Cutblock	2004-02-12	34	2	4.0	4.0	4.0	6	0.0	0
Robson View	2004-02-25	43	2	2.0	3.0	3.0	4	0.5	20
Monashee View	2004-02-27	65	1	2.0	2.0	2.0	6	0.0	0
Poetry Slopes	2004-02-28	30	2	3.0	3.0	3.0	5	0.0	0

Table 4.1 (continued)

Location	Date	N	Rutschblock scores						
			Min	Q_1	Med	Q_3	Max	SIQR	QCV (%)
Squirrel Slope	2004-03-03	24	3	3.0	4.0	4.0	6	0.5	14
Abbott Headwall	2004-03-06/07	64	2	2.0	4.0	4.0	7	1.0	33
Mt. St. Anne	2004-03-10	33	1	2.0	3.0	3.0	3	0.5	20
Bear's Den	2004-03-11a	6	4	4.0	5.0	6.0	7	1.0	20
Bear's Den	2004-03-11b	9	6	6.0	6.0	7.0	7	0.5	8
Abbott	2004-03-11/12	26	3	4.0	4.0	5.0	7	0.5	11
South Run	2004-03-18	23	2	3.0	4.0	4.0	6	0.5	14
Schuss Cr.	2004-03-21a	13	4	4.0	5.0	5.0	7	0.5	11
Schuss Cr.	2004-03-21b	19	4	4.0	5.0	5.5	6	0.8	16
Median		20.0	3.0	4.0	4.0	4.8	6.0	0.5	14.0

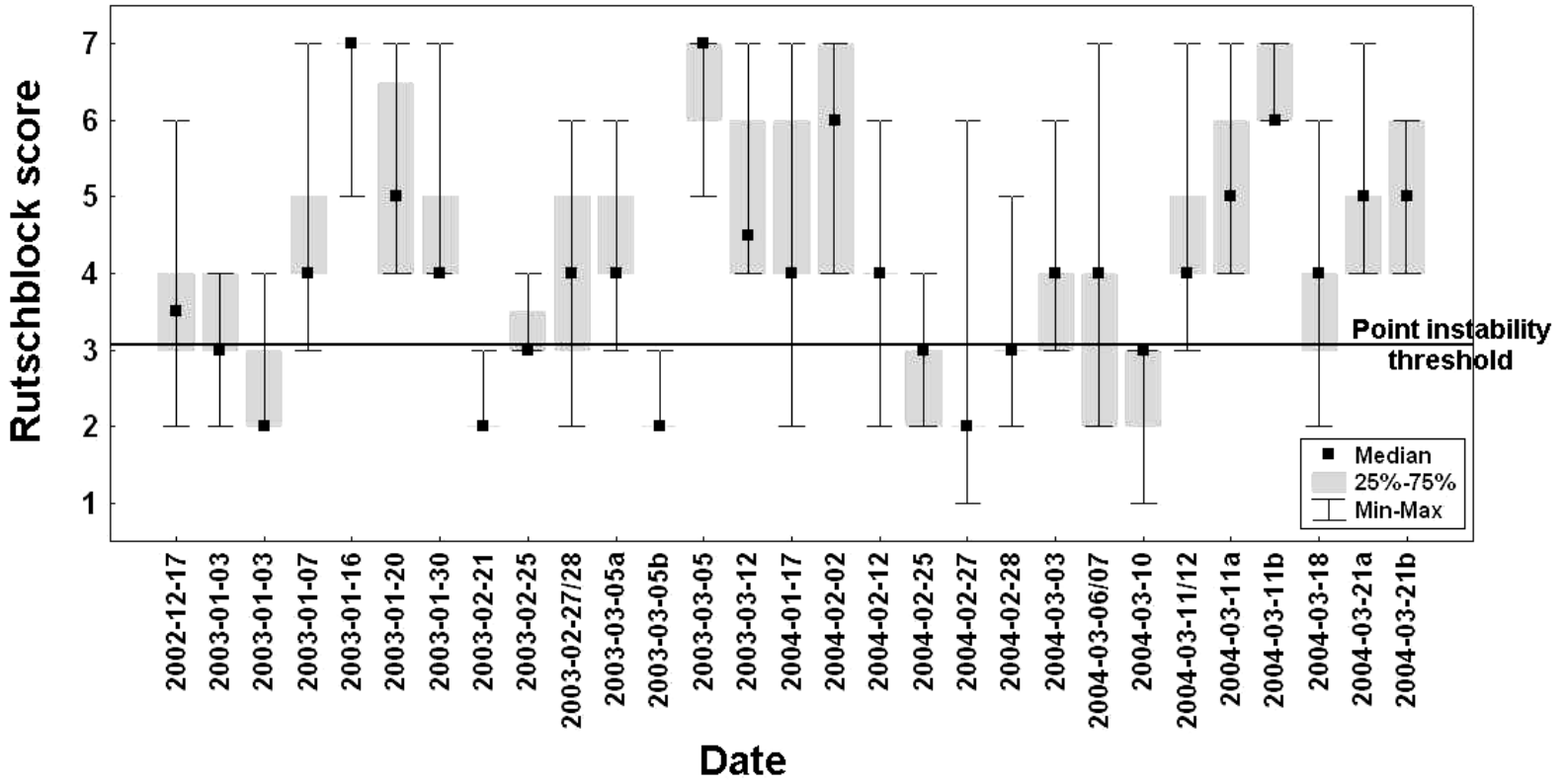

Figure 4.1 – Box and whisker plots of rutschblock arrays showing the median, IQR, minimum and maximum RB score for each array. The assumed threshold rutschblock score of point instability is also shown.

As can be seen in Figure 4.1, there is a tendency for variability (QCV) to decrease as slope median RB score decreases (R_S = 0.39, p = 0.04, N = 27 for 2 ≤ median RB ≤ 6), which is consistent with Keeler and Weeks' (1968) results for weak layer strength, and Conway and Abrahamson's (1984) and Stewart's (2002) results for point stability. The two arrays with a median RB score of 7 are not included because of truncated variability. This increased variability could be intrinsic to the snowpack. However, it could also be due to the truncated distribution of rutschblock load steps (i.e. arrays with low medians have low variability because the lowest RB score is 1) or the possibility of increased operator error associated with higher rutschblock loading steps. Regardless, it seems that a single rutschblock test can better indicate the overall slope stability when the median RB score is low.

The threshold RB score for skier-triggering was assumed to be 3 based on the CAA's (2002) interpretation that for RB scores of 1, 2 or 3, skier-triggering is likely. When the portion of the slope below this assumed threshold for point instability (RB score ≤ 3) is considered, slopes with higher median stability can have the same portion that is susceptible to skier-triggering, as slopes with lower overall stability. Such is the case for the array performed on 2003-02-27/28 (median RB = 4) when compared to the array performed 2002-12-17 (median RB = 3.5) with the same portion (25% of the area of the slope) susceptible to skier-triggering (below the threshold).

Figure 4.2 shows that 84% of randomly sampled rutschblock tests in avalanche start zones are within ±1 RB score of the slope median. For uniform slopes in the Columbia Mountains, Jamieson and Johnston (1993) found that 97% of tests are within ± 1 RB score of the slope median. This confirms Stewart's (2002) conclusion that the stability of start zones is substantially more variable than the stability of study plots (uniform slopes).

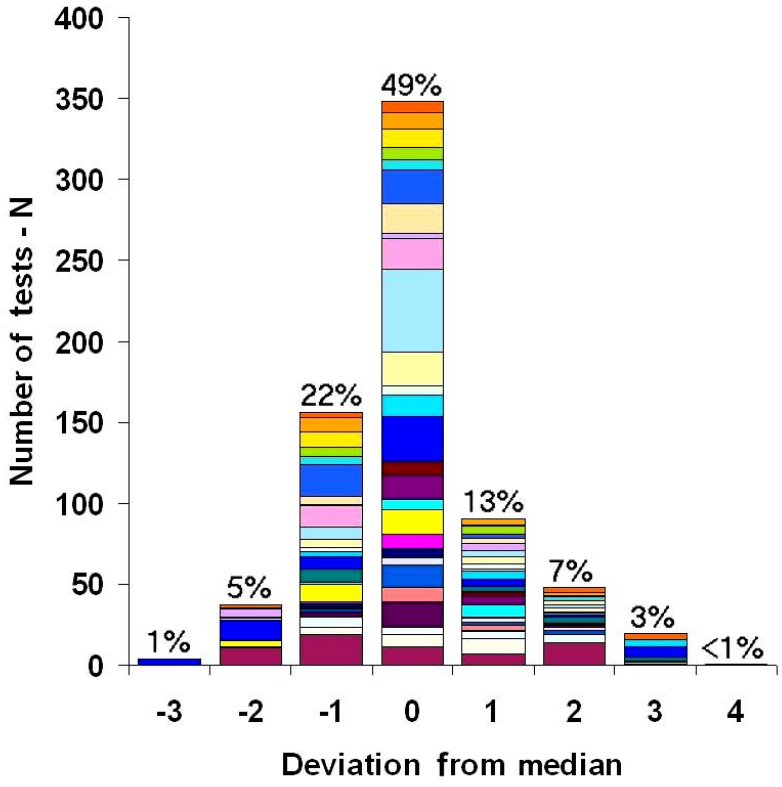

Figure 4.2 – Histogram showing the combined distribution of the deviations from the median for the 29 rutschblock arrays summarized in Table 5.1. Each bar in the columns represents one array (N = 705).

4.3 Array spanning linear trends

In Table 4.2, eight of the 29 arrays have significant linear trends in either the up-slope or cross-slope directions. The assumption of normality of the residuals was found to be valid for 20 of the 29 arrays (Appendix C), suggesting that least-squares linear regression is appropriate for assessing the linear trends in RB score.

Table 4.2 – Summary of the linear regression results based on the equation: RB = aCol + bRow + c, Col is the cross-slope position based on the array column number and Row is the up-slope position based on the array row number. The positive Col direction is from a climber's left to right across the slope and the positive Row direction is up the slope. The regression coefficients that are significant at the p < 0.05 level, are marked in bold. RB_{res} is the residual rutschblock score after trend removal.

Location Date	Max Col	Max Row	Valid *N*	a *p*	b *p*	c *p*	R^2	SIQR of RB_{res}
South Run 2002-12-17	8	2	16	-0.09 0.32	**-0.88** **0.04**	**4.47** **< 10^{-3}**	0.31	0.2
Bear's Den 2003-01-03	11	2	21	0.10 0.06	0.25 0.45	**3.54** **< 10^{-3}**	0.19	0.5
South Run 2003-01-03	6	6	22	$4x10^{-4}$ 0.99	-0.15 0.07	**2.94** **< 10^{-3}**	0.17	0.3
Poetry 2003-01-07	11	2	22	-0.08 0.22	-0.64 0.14	**4.87** **< 10^{-3}**	0.17	0.4
Robson View 2003-01-16	11	1	11	-0.08 0.20	-	**6.24** **< 10^{-3}**	0.18	0.2
Cheops Bench 2003-01-20	5	4	20	0.12 0.54	0.18 0.49	**5.27** **< 10^{-3}**	0.05	1.0
South Run 2003-01-30	4	4	14	-0.44 0.06	0.15 0.52	**3.18** **0.003**	0.29	0.3
Fidelity 2003-02-21	5	5	20	-0.04 0.25	0.02 0.53	**2.10** **< 10^{-3}**	0.10	0.2
Grizzly Shoulder 2003-02-25	4	3	12	**-0.23** **0.04**	-0.13 0.38	**2.92** **< 10^{-3}**	0.42	0.2

Location Date	Max Col	Max Row	Valid *N*	a *p*	b *p*	c *p*	R^2	SIQR of RB_{res}
Abbott Headwall 2003-02-27/28	16	4	63	-0.03 0.39	-0.11 0.50	**3.88** **< 10^{-3}**	0.02	1.1
Poetry Slopes 2003-03-05a	4	2	8	0.25 0.47	-0.25 0.74	**5.38** **0.01**	0.13	0.7
Poetry Slopes 2003-03-05b	5	2	9	-0.07 0.49	-0.23 0.37	**2.63** **10^{-3}**	0.17	0.2
Robson View 2003-03-05	10	3	29	-0.06 0.16	**0.39** **0.01**	**5.34** **< 10^{-3}**	0.28	0.4
Waikiki 2003-03-12	7	3	18	0.09 0.57	0.03 0.93	**5.21** **< 10^{-3}**	0.02	0.9
Toilet Bowl 2004-01-17	8	3	18	**0.51** **10^{-3}**	0.37 0.39	**6.34** **< 10^{-3}**	0.54	1.0
Poetry Slopes 2004-02-02	5	3	13	-0.26 0.36	-0.39 0.40	**5.48** **10^{-3}**	0.14	1.1
Langevin Cutblock 2004-02-12	9	4	34	0.07 0.25	0.05 0.70	**3.58** **< 10^{-3}**	0.05	0.3
Robson View 2004-02-25	9	5	43	0.01 0.68	-0.06 0.39	**2.82** **< 10^{-3}**	0.02	0.5
Monashee View 2004-02-27	12	8	65	-0.06 0.05	0.09 0.07	**1.51** **< 10^{-3}**	0.07	0.2
Poetry Slopes 2004-02-28	6	5	30	**0.19** **0.03**	-0.12 0.25	**2.86** **< 10^{-3}**	0.19	0.4
Squirrel Slope 2004-03-03	8	3	24	0.02 0.84	**-0.50** **0.03**	**4.99** **< 10^{-3}**	0.20	0.5
Abbott Headwall 2004-03-06/07	17	4	64	**-0.09** **0.03**	0.17 0.30	**4.08** **< 10^{-3}**	0.08	0.8
Mt. St. Anne 2004-03-10	6	7	33	**0.14** **0.01**	0.08 0.09	**1.77** **< 10^{-3}**	0.27	0.3
Bear's Den 2004-03-11a	4	2	6	0.73 0.35	0.03 0.99	7.07 0.18	0.79	0.4
Bear's Den 2004-03-11b	4	3	9	0.09 0.56	-0.55 0.09	**7.45** **< 10^{-3}**	0.54	0.2
Abbott 2004-03-11/12	9	3	26	0.01 0.94	0.39 0.21	**3.88** **< 10^{-3}**	0.07	0.3
South Run 2004-03-18	6	4	23	0.13 0.24	-0.07 0.65	**3.37** **< 10^{-3}**	0.07	0.4
Schuss Cr. 2004-03-21a	5	3	13	-0.04 0.86	-0.33 0.39	**5.44** **10^{-3}**	0.08	0.7
Schuss Cr. 2004-03-21b	7	3	19	-0.13 0.16	-0.04 0.87	**5.55** **< 10^{-3}**	0.13	0.6

The significant linear trends, or directions of the trends, do not seem to be limited to arrays with a particular number of rows (max Row), columns (max Col) or total tests (valid *N*). However, only two of the six arrays with $N > 30$ had significant linear trends. An explanation for this could be that the array spanning trends are in fact not linear (e.g. Abbott Headwall on 2003-02-27/28, Section 4.6.1). Furthermore, when only the middle array columns (Col = 5 to Col = 12) are considered for this array (Figure 4.5) a significant cross-slope linear trend emerges ($p < 10^{-3}$, $N = 32$). This suggests that the larger ($N > 30$) arrays could have linear trends at smaller scales which are masked by other larger scale trends.

The variability of stability decreases after the linear trends are removed, with a median SIQR for the residual RB score of 0.4. The variability explained by the linear trends is generally low, with a median R^2 of 0.17. No patterns in the up-slope trends were found that support Jamieson's (1995) observation that sites near the top of a slope generally have higher stability.

4.4 Correlation analysis

4.4.1 Introduction

Correlation analysis between RB scores and terrain and snowpack variables was performed on four different datasets. Section 4.4.2 reviews the

correlations of the raw data from each of the 29 individual arrays. Section 4.4.3 reviews the correlations associated with the medians of the individual arrays. Section 4.4.4 covers the correlations of the significant array-spanning linear trends, and the residuals, in stability and snowpack and terrain variables. Section 4.4.5 reviews the correlations associated with the normalized data from a combined dataset of all 29 arrays.

Since RB scores have ordinal properties, Spearman rank correlations were used to describe the associations of RB score with terrain and snowpack variables. However, the residuals from the array-spanning linear trends were found to be mostly normal; consequently Pearson correlations were used. Spearman rank correlations were used for the analysis of the normalized data from the combined dataset. Normality testing results can be found in Appendix C.

4.4.2 Correlation analysis of individual arrays

In Table 4.3, four of the 28 (14%) arrays have significant positive correlations between RB score and slab thickness, suggesting that some areas with thinner slabs are less stable. When the insignificant and significant correlations are considered, 18 of the 28 (64%) correlations with slab thickness are positive. Slope angle also emerged as a potential source of variability, with a general trend for steeper parts of the slope to have lower scores. Seventeen of the 29 (59%) arrays had negative correlations between slope angle and RB

score and two (7%) were significant. Furthermore, the array at Fidelity on 2003-02-21 (Figure A.8) had 14 tests that failed during the isolation process or with only one ski partially weighting the block. When these tests are assigned a RB score of 1.5, instead of 2, a significant correlation emerges with slope angle (R_S = -0.51, p = 0.02, N = 20).

Table 4.3 – Spearman rank correlation coefficients (R_S) from the correlations of rutschblock scores to snowpack and terrain variables. Correlations that are significant at the $p < 0.05$ level, are marked in bold. N can differ within any particular array because occasionally certain measurements were not made for all tests.

Location Date		Snowpack variables		Terrain variables	
		H (cm)	HS (cm)	Ψ (˚)	Asp (˚)
South Run 2002-12-17	R_S	0.14	-0.00	**-0.62**	
	p	0.61	0.99	**0.01**	-
	N	16	16	**16**	
Bear's Den 2003-01-03	R_S	**0.45**		-0.01	
	p	**0.04**	-	0.98	-
	N	**21**		21	
South Run 2003-01-03	R_S	0.19	-0.21	0.19	
	p	0.40	0.36	0.40	-
	N	22	22	22	
Poetry Slopes 2003-01-07	R_S	-0.31	-0.25	-0.26	-0.03
	p	0.16	0.25	0.23	0.94
	N	22	22	22	10
Robson View 2003-01-16	R_S		0.35	-0.01	
	p	-	0.30	0.98	-
	N		11	11	
Cheops Bench 2003-01-20	R_S	0.33	-0.36	0.08	
	p	0.16	0.12	0.73	-
	N	20	20	20	
South Run 2003-01-30	R_S	-0.33	0.13	-0.41	
	p	0.25	0.67	0.15	-
	N	14	14	14	
Fidelity 2003-02-21	R_S	0.24	0.36	-0.30	
	p	0.30	0.12	0.20	-
	N	20	20	20	
Grizzly	R_S	0.17	**-0.64**	-0.37	-

Table 4.3 (continued)

Location Date		Snowpack variables		Terrain variables	
		H (cm)	HS (cm)	Ψ (˚)	Asp (˚)
2003-02-25	***p***	0.59	**0.03**	0.24	
	N	12	**12**	12	
Abbott Headwall 2003-02-27/28	R_S	0.15	0.06	**-0.40**	
	p	0.25	0.63	**0.01**	-
	N	63	63	**45**	
Poetry Slopes 2003-03-05a	R_S	-0.31	-0.09	0.25	
	p	0.46	0.83	0.56	-
	N	8	8	8	
Poetry Slopes 2003-03-05b	R_S	0.42	0.27	-0.55	
	p	0.26	0.48	0.12	-
	N	9	9	9	
Robson View 2003-03-05	R_S	0.12	0.19	0.12	
	p	0.55	0.31	0.52	-
	N	29	29	29	
Waikiki 2003-03-12	R_S	-0.01	0.19	0.11	
	p	0.98	0.45	0.68	-
	N	18	18	18	
Toilet Bowl 2004-01-17	R_S	**0.60**	**0.55**	-0.24	
	p	**0.01**	**0.02**	0.33	-
	N	**18**	**18**	18	
Poetry Slopes 2004-02-02	R_S	0.32	-0.04	0.02	
	p	0.29	0.89	0.94	-
	N	13	13	13	
Langevin Cutblock 2004-02-12	R_S	-0.16	-0.09	-0.25	
	p	0.37	0.61	0.15	-
	N	34	34	34	
Robson View 2004-02-25	R_S	-0.03	-0.03	0.19	-0.02
	p	0.83	0.83	0.21	0.89
	N	43	43	43	43
Monashee View 2004-02-27	R_S	-0.10	**0.31**	0.18	0.21
	p	0.42	**0.01**	0.16	0.10
	N	65	**65**	65	65
Poetry Slopes 2004-02-28	R_S	-0.34	-0.26	-0.13	
	p	0.06	0.16	0.48	-
	N	30	30	30	
Squirrel Slope 2004-03-03	R_S	0.37	0.33	0.29	-0.25
	p	0.08	0.12	0.17	0.24
	N	24	24	24	24
Abbott Headwall 2004-03-06/07	R_S	0.18	**-0.30**	**0.29**	
	p	0.16	**0.02**	**0.02**	-
	N	62	**62**	**64**	
Mt. St. Anne 2004-03-10	R_S	-0.11	-0.13	-0.08	-
	p	0.54	0.47	0.64	

Table 4.3 (continued)

Location Date		Snowpack variables		Terrain variables	
		H (cm)	HS (cm)	Ψ (˚)	Asp (˚)
	N	33	33	33	
Bear's Den 2004-03-11a	R_S	**0.83**	-0.12	0.39	0.86
	p	**0.04**	0.82	0.44	0.06
	N	**6**	6	6	5
Bear's Den 2004-03-11b	R_S	0.28	0.00	-0.26	0.32
	p	0.47	1.00	0.54	0.44
	N	9	8	8	8
Abbott 2004-03-11/12	R_S	**0.45**	0.06	-0.06	
	p	**0.02**	0.77	0.78	-
	N	**26**	26	26	
South Run 2004-03-18	R_S	-0.01	0.05	-0.37	-0.35
	p	0.95	0.81	0.08	0.10
	N	23	23	23	23
Schuss Creek 2004-03-21a	R_S	0.13	0.19	0.11	-0.06
	p	0.68	0.54	0.73	0.84
	N	13	13	13	13
Schuss Creek 2004-03-21b	R_S	0.07	-0.21	-0.30	
	p	0.76	0.38	0.21	-
	N	19	19	19	

The proportion of arrays with significant correlations between RB score and H increases to 15% (3 of 20), when only the large arrays (N > 15) are considered. The proportion of arrays with significant correlations between RB score and slope angle also increases when only large (N > 15) arrays are considered (15% versus 10%, when the array at Fidelity on 2003-02-21 is included as significant). This suggests that there is a minimum sample size required to detect these sorts of effects.

Four arrays had significant correlations between RB score and HS; two positive and two negative. The general lack of association between stability and HS is not surprising considering variations in HS generally only affect the faceting

process, while most of these arrays had buried surface hoar weak layers. No arrays showed significant correlations between RB score and aspect, but aspect is identified as a source of variability in two of the arrays discussed in Section 4.6.

The array in Toilet Bowl on 2004-01-07 (Figure A.14) showed a significant positive correlation between RB score and HS (and H because the failure plane was at the bottom of the snowpack). Since the failure layer was depth hoar crystals that were on the ground, the variability could be caused by increased faceting and/or greater dynamic stress reaching the weak layer for tests with thinner slabs. Another possible source of variability in this array is differences in ground temperature across the slope resulting in variable conditions for faceting. This idea is supported by the observation of a thin crust within the weak layer for a group of five tests in close proximity. The presence of the crust suggests that the faceting process was progressing slower than for the surrounding tests, where no crust was found.

4.4.3 Correlation analysis of array medians

Median RB score as well as SIQR have significant positive correlations with weak layer hardness. This suggests that slopes with harder weak layers tend to have a higher median point stability, but are more variable. Both SIQR and QCV have significant positive correlations with median weak layer depth.

This suggests that the point stability of slopes with deeper weak layers tends to be more variable. Array median values of H, HS and slope angle did not correlate significantly with the array median RB score. Since 20 (69%) of the 29 rutschblock arrays had buried surface hoar as a weak layer (the remainder being precipitation particles, faceted crystals, rounded grains or multiple weak layer types), there were insufficient data to establish associations between variability and weak layer grain type.

Table 4.4 – Spearman rank correlation coefficients (R_S) from the comparison of array median rutschblock scores, the semi-interquartile range (SIQR) and the quartile coefficient of variation (QCV) to array median snowpack and terrain variables, weak layer grain size (E) and hardness (R) and the difference in E and R across the failure plane. The values for E and R are from the manual snow profiles.

RB score		Array median			Weak layer		Difference	
		H (cm)	HS (cm)	Ψ (˚)	E (mm)	R	E (mm)	R
Med	R_S	0.23	0.20	0.07	-0.34	**0.50**	-0.24	-0.21
	p	0.24	0.31	0.72	0.09	**0.01**	0.34	0.33
	N	29	28	29	26	**25**	18	25
SIQR	R_S	**0.49**	0.15	0.27	-0.24	**0.41**	-0.31	-0.37
	p	**0.01**	0.45	0.15	0.23	**0.04**	0.21	0.07
	N	**29**	28	29	26	**25**	18	25
QCV	R_S	**0.41**	0.07	0.21	-0.21	0.30	-0.31	-0.32
	p	**0.03**	0.74	0.28	0.30	0.14	0.21	0.12
	N	**29**	29	29	26	25	18	25

4.4.4 Correlation analysis of array-spanning linear trends

Table 4.5 lists the correlations between estimated RB scores and estimated snowpack and terrain variables. The data were estimated though

linear regression with position within the array (Section 3.3.2). Table 4.6 lists the correlations between the residual values of RB score and snowpack and terrain variables. Only data with significant ($p < 0.05$) array spanning linear trends were included in this analysis. Only correlations with trends in terrain variables that are significant at the $p < 0.05$ level in the same direction as the trend in rutschblock score were included.

From Tables 4.5 and 4.6, it is apparent that slope-scale trends in stability are often very similar to slope-scale trends in snowpack and terrain variables, but the residual stability appears to be independent of the residual terrain and snowpack variables. Once again, there is a tendency for areas of locally thin slab to be less stable, as indicated by the positive correlations with H. Furthermore, a tendency for steeper areas to be less stable is evident, when the arrays with significant correlations between trends in stability and trends in slope angle, that do not have other significant correlations, are considered (e.g. the arrays performed on Grizzly Shoulder on 2003-02-25 and Poetry Slopes on 2004-02-28).

Table 4.5 – Results from correlations between estimated rutschblock scores and estimated snowpack and terrain variables. Correlations that are significant at the p < 0.05 level, are marked in bold. Some results are omitted because the linear trends in the snowpack or terrain variables were either not significant or significant in a different direction than the linear trend in RB score.

Location Date		Estimated		
		H (cm)	HS (cm)	Ψ (˚)
South Run 2002-12-17	R_P	**0.99**		**-0.97**
	p	**< 10^{-3}**	-	**< 10^{-3}**
	N	**16**		**16**
Grizzly Shoulder 2003-02-25	R_P			**-0.99**
	p	-	-	**< 10^{-3}**
	N			**12**
Robson View 2003-03-05	R_P	0.06		**0.60**
	p	0.76	-	**10^{-3}**
	N	29		**29**
Toilet Bowl 2004-01-17	R_P	**0.90**	**0.89**	
	p	**< 10^{-3}**	**< 10^{-3}**	-
	N	**18**	**18**	
Poetry Slopes 2004-02-28	R_P			**-0.90**
	p	-	-	**< 10^{-3}**
	N			**30**
Squirrel Slope 2004-03-03	R_P	**0.68**		**0.83**
	p	**< 10^{-3}**	-	**< 10^{-3}**
	N	**24**		**24**
Abbott Headwall 2004-03-06/07	R_P		**-0.99**	**0.88**
	p	-	**< 10^{-3}**	**< 10^{-3}**
	N		**64**	**64**

Table 4.6 – Results from the correlations between residual rutschblock scores and residual snowpack and terrain variable values, after trend removal. Correlations that are significant at the p < 0.05 level, are marked in bold. Some results are omitted because the linear trends in the snowpack or terrain variables were either not significant or significant in a different direction than the linear trend in RB score.

Location Date		Residual		
		H (cm)	HS (cm)	Ψ (˚)
South Run 2002-12-17	R_P	-0.22		-0.21
	p	0.41	-	0.45
	N	16		16
Grizzly Shoulder 2003-02-25	R_P			0.24
	p	-	-	0.45
	N			12
Robson View 2003-03-05	R_P	-0.20		-0.09
	p	0.30	-	0.65
	N	29		29
Toilet Bowl 2004-01-17	R_P	0.38	0.39	
	p	0.12	0.11	-
	N	18	18	
Poetry Slopes 2004-02-28	R_P			0.08
	p	-	-	0.66
	N			30
Squirrel Slope 2004-03-03	R_P	0.13		-0.11
	p	0.54	-	0.62
	N	24		24
Abbott Headwall 2004-03-06/07	R_P	-0.07	**-0.29**	0.12
	p	0.59	**0.02**	0.37
	N	63	**64**	64

4.4.5 Correlation analysis of the combined dataset

Once again, slab thickness emerges as the dominant source of variability, when the normalized values from the combined dataset are considered (Table 4.8). Multivariate linear regression was used to assess the combined affect of

slab thickness and slope angle (the two most significant variables) on stability and derive the coefficients for the following equation:

$$RB_{norm} = 0.11H_{norm} - 0.08\Psi_{norm} + 0.05 \quad (4.1)$$

where RB_{norm}, H_{norm} *and* Ψ_{norm} are the normalized RB score, slab thickness and slope angle, respectively, from the combined dataset. Even though the hypothesis of normality was rejected for the residual RB_{norm} values (Lilliefors $p < 0.01$) least-squares linear regression was still used as a convenient way of assessing the significance of the effects.

Table 4.7 – Spearman rank correlation coefficients (R_S) from the comparison of normalized rutschblock scores to normalized snowpack and terrain variables, from the combined dataset. Variables are normalized with the median and SIQR. Correlations that are significant at the p < 0.05 level, are marked in bold.

		Normalized		
		H	**HS**	**Ψ**
RB_{norm}	***R_S***	**0.13**	-0.04	-0.05
	p	**0.003**	0.43	0.22
	N	**534**	512	515

The slab thickness (H) term, in Equation 4.1, is significant ($p = 0.006$, $N = 515$); however, the slope angle term is not ($p = 0.053$, $N = 515$), although it is almost significant. Furthermore, since the coefficient for the slab thickness term is more significant than the coefficient for the slope angle term, and shows up in more arrays, slab thickness can have a more dominant affect on point stability

than slope angle. The significance of the linear coefficients in Equation 4.1 suggests that variations in slab thickness and slope angle combine to cause variations in point stability (Figure 4.3). The positive coefficient for the slab thickness term suggests that areas in a start zone where slabs are thinner usually have lower point stability. The negative coefficient for the slope angle term suggests that steeper sections of the start zone are sometimes more unstable.

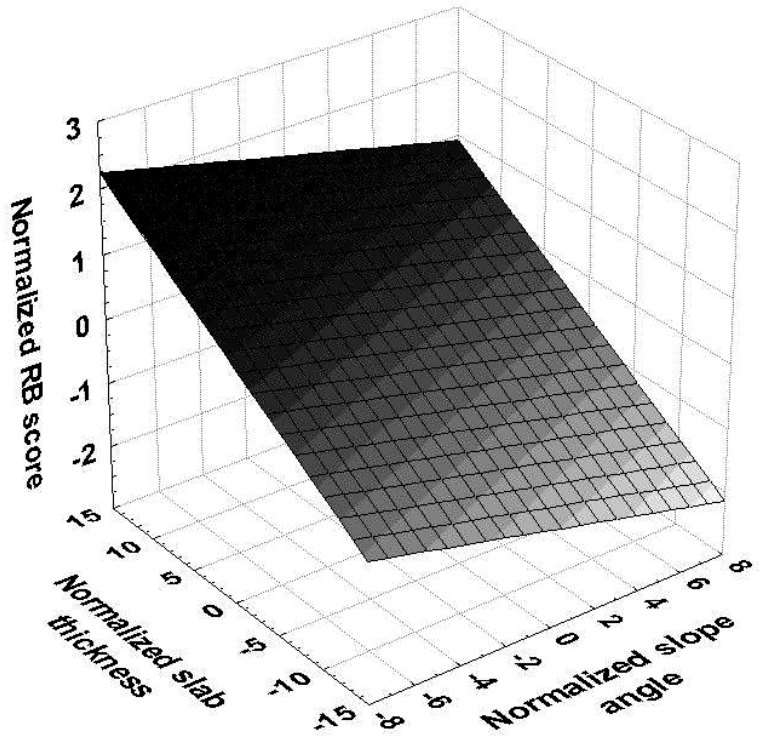

Figure 4.3 – Linear trend surface based on Equation 4.1. The surface is shaded based on normalized RB score.

Given the linear trend shown in Figure 4.3 and Equation 4.1, for an average start zone ($SIQR_{RB}$ = 0.5, $SIQR_H$ = 3.0, $SIQR_\Psi$ = 2.0) a 45 cm decrease

in slab thickness combined with a 16˚ increase in slope angle would result in a decrease in stability of one RB score from the slope median. However, the correlations in Table 4.3 suggest that much smaller variations slab thickness and slope angle can sometimes affect stability. Furthermore, Jamieson and Johnston (1993) found that a 10˚ increase in slope angle alone tended to cause a decrease in stability of one RB score. Based on this, and experience, the magnitude of the combined effect of slope angle and slab thickness on RB score is greatly underestimated by this linear trend. This inaccuracy is to be expected considering that the use of least-squares linear regression is invalid for this dataset.

4.4.6 Summary

Since a significance level of $p < 0.05$ was used, 5% of the already low proportion (14%) of arrays with significant positive correlations between RB score and slab thickness could be a result of Type II errors. Moreover, the same proportion of Type II errors is expected for the arrays with significant correlations between RB score and slope angle (7%). This undermines the ability to draw conclusions from these correlations. However, one reason for the low proportions of arrays with significant correlations with slab thickness or slope angle is that the sites for a limited number of arrays were selected with slab thickness or slope angle as the primary source of variability. Furthermore, the effect of slope angle

or slab thickness on stability was often masked by other sources of variability within the array.

Variations in slab thickness at the slope-scale can have significant effects on point stability. There is a considerable trend for areas of the slope with locally thin slabs to be less stable, which supports the results from previous studies (Föhn, 1989; Jamieson, 1995; Stewart, 2003; Kronholm, 2004). Variations in slope angle at the slope-scale can also have significant affects on point stability. The tendency for locally steep areas to be less stable is also supported by previous studies (Jamieson and Johnston, 1993; Jamieson 1995). HS and aspect have been shown to have an effect on point stability in arrays with faceted crystals as the primary failure plane. Aspect can also affect point stability for arrays performed on buried surface hoar weak layers that were exposed to wind or sun when on the snow surface.

4.5 Variogram analysis

As in previous studies (Stewart, 2002; Kronholm, 2004), variograms did not prove to be a useful tool for analyzing the spatial structure of variations in stability. Only two of the variograms (Figure 4.4 a and b) showed a distinct sill and range where the semi-variance of the residual RB scores reaches a sill within a distance of 7 to 14 m. Figure 4.4 (c) is an example of a typical variogram which immediately reaches a sill. Eighteen of the 29 (62%) variograms of

residual RB scores had properties similar to Figure 4.4 (c). These types of variograms can be modeled as pure nugget variograms, which suggests that there is a total absence of auto-correlation at separation distances of greater than 2.5 m. A sill at a semi-variance value of approximately 2.5 (Figure 4.4 c) suggests that adjacent tests can vary by more than one RB score. Since the linear trends tended to be relatively weak, the variograms of the raw rutschblock data are almost identical to the variograms of the residuals.

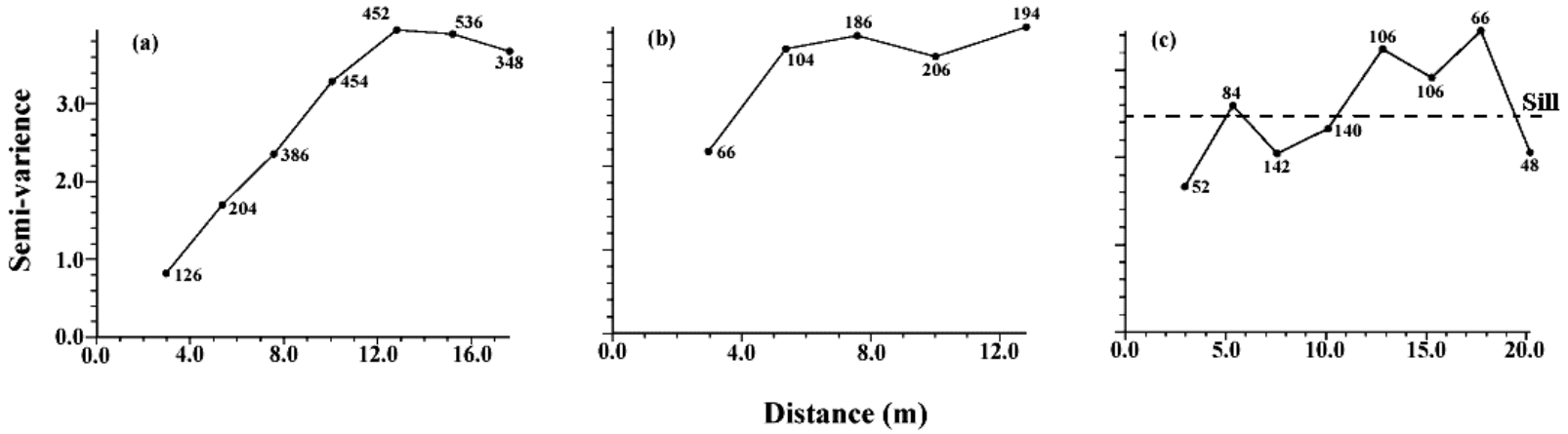

Figure 4.4 – Omnidirectional sample variograms of residual RB scores for the arrays performed on (a) Mt. Abbott on 2003-02-27/28, (b) Langevin Cutblock on 2004-02-12 and (c) Mt. Abbott on 2004-03-11/12. Lag distance is 2.5 ± 1.25 m. The number of pairs is also shown.

In the end, the infrequency of significant ranges in the variograms limits the application this approach. Perhaps this is because of insufficient size (support), spacing or number of tests (extent) to capture the complex variability of snow. This complexity likely requires more closely spaced tests over a greater extent to detect. The problem with identifying the correlation lengths of stability is that there are many processes at different scales affecting the variability of point stability.

4.6 Example arrays

4.6.1 Abbott Headwall – 2003-02-27/28 and 2004-03-06/07

Figures 4.5 to 4.8 show two rutschblock test arrays that demonstrate the effects of microscale weather phenomena and microscale terrain features on spatial variability. These arrays were performed on the same slope with similar snowpack conditions, each over two days in different winters. This slope is characterized by cross-slope undulations (~ 1 m) in terrain height, as can be seen in Figures 4.6 and 4.8. Cross-loading often occurs on this slope with the predominant wind direction being from the left hand side to the right hand side of the photographs.

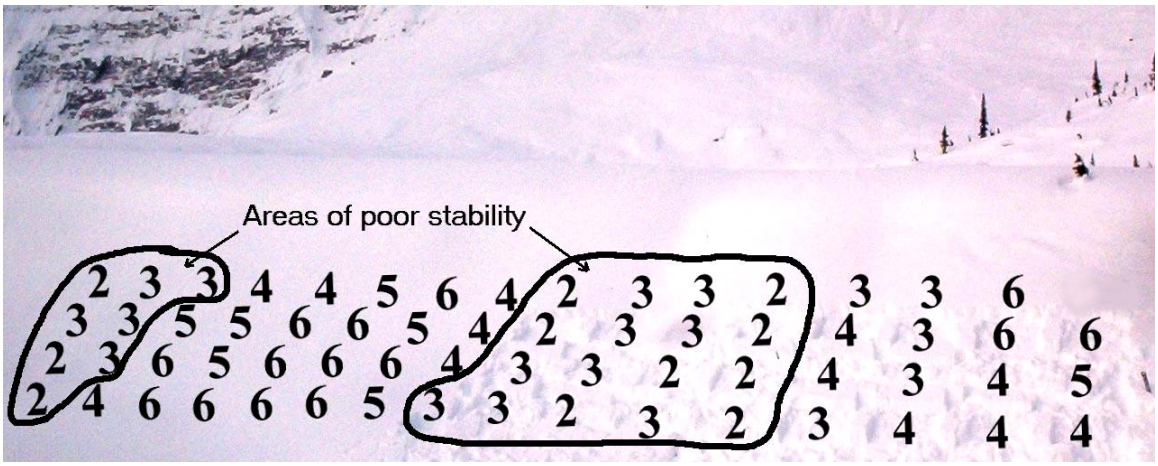

Figure 4.5 – Rutschblock test array performed on the headwall above the Abbott weather plot on 2003-02-27/28. All the tests failed on the 030215 surface hoar layer at an average depth of 52 cm. Areas of poor stability are circled. Average slope angle is 33˚.

Figure 4.6 – Terrain features of the Abbott Headwall in summer and the results from the rutschblock array performed on 2003-02-27/28.

*Figure 4.7 – Rutschblock test array performed on the headwall above the Abbott weather plot on 2004-03-06/07. Most (57) tests failed on the 040224 surface hoar layer, at an average depth of 82 cm, while the remainder (marked with *) failed on the 040214 surface hoar layer which was about 10 cm deeper. The tests marked 2- failed during isolation with the saw or during partial weighting with one ski. Average slope angle is 36˚.*

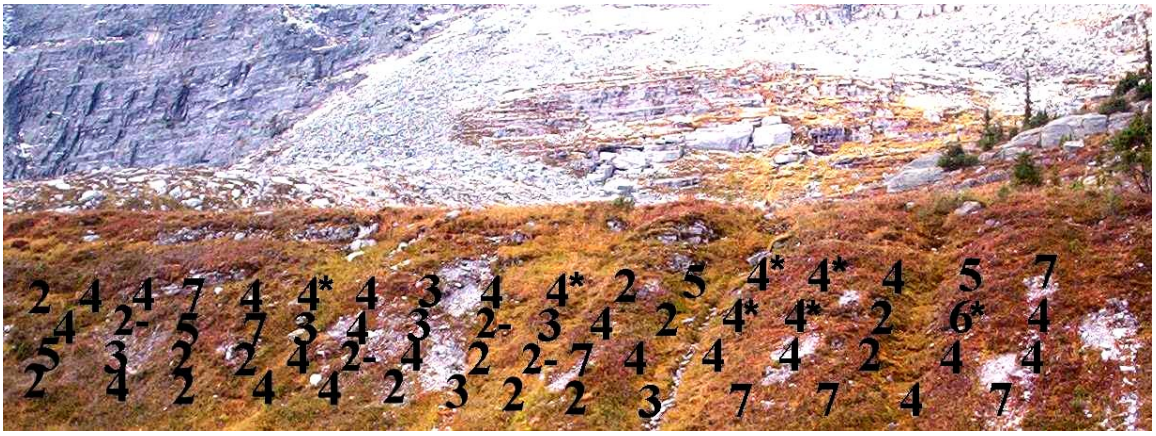

Figure 4.8 - Terrain features of the Abbott Headwall in summer and the results from the rutschblock array performed on 2004-03-06/07.

For the array performed on 2003-02-27/28, a depression in the snow surface can be seen just right of the centre of the array. This corresponded with an area of lower RB scores where the surface hoar layer was distinct and easy to

find, and the crystals looked to be well preserved. The group of high scores near the left side of the array was on higher ground where a distinct layer was hard to find. There were no signs of prior avalanching, or other disturbances such as skiers, snow falling from trees, cornice debris, etc., so the weak layer discontinuity may be due to wind when the surface hoar was on the surface (B. McMahon, 2004, pers. comm.).

When the cross-slope variability is considered, the spatial structure of stability for this array appears to be sinusoidal (Figure 4.9) with a wavelength of about 28 m. This stability pattern is consistent with the cross-slope undulations in terrain height seen in Figure 4.6. Based on this result, it is conceivable that the spatial scale of variability for this particular slope is about 14 m, or half the wavelength of the sinusoidal stability pattern, which is consistent with the variogram results (Figure 4.4 a). Even though this array had a median RB score of 4, over 30% of the slope was below the assumed threshold for skier-triggering (RB score ≤ 3) as can be seen in Figure 4.9.

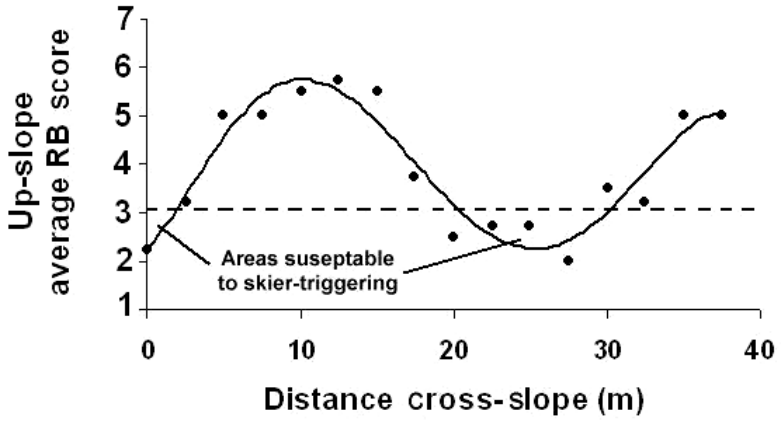

Figure 4.9 - Scatterplot of average RB score versus cross-slope distance (m) for the array performed on the headwall above the Abbott weather plot on 2003-02-27/28. The distribution is fitted with a sine curve based on Equation 4.2. The assumed threshold RB score for skier-triggering (RB score ≤ 3) is also shown (dashed line).

The average up-slope RB score was regressed on a sine function of cross-slope position yielding:

$$RB\ score = 1.8 \sin (0.21 X + 5.5) + 4.0 \qquad (4.2)$$

where *RB score* is the up-slope average and X is the cross-slope distance in metres.

A similar, although much more random, stability pattern was observed for the array performed on 2004-03-06/07. Once again, the RB scores corresponded very well with the condition of the surface hoar layer (RB score vs. Thick: R_S = -0.46, $p < 10^{-3}$, N = 62; RB score vs. E: R_S = -0.55, $p < 10^{-3}$, N = 63). However the areas of low and high scores were not nearly as consistent as for the array on

2003-02-27/28. One possible explanation involves a different wind pattern as indicated by the presence of a small cornice at the top of the slope that was not there the year before. The cornice indicates that the slope was leeward and subject to turbulent wind eddies while the surface hoar was on the surface, which can cause discontinuity in the weak layer.

The average up-slope RB score for the array performed on 2004-03-06/07 was regressed on a sine function of cross-slope position yielding:

$$RB\ score = 0.8 \sin (0.21 X + 4.2) + 3.5 \quad (4.3)$$

where *RB score* is the up-slope average and *X* is the cross-slope distance in metres. The wavelength for this regression is approximately 30 m (Figure 4.10). The sinusoidal cross-slope stability pattern found for this array has a similar wavelength to the array performed on 2003-02-27/28 (28 m), which again corresponds to the terrain undulations. The results from these two arrays suggest that slope-scale stability patterns can be repeatable given similar weather and snowpack conditions.

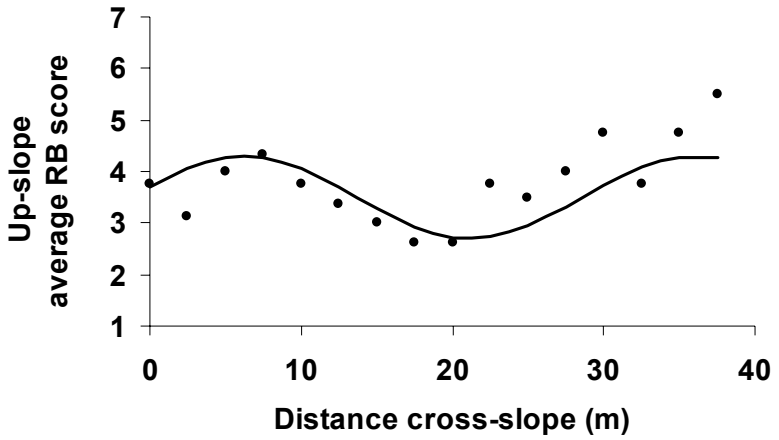

Figure 4.10 - Scatterplot of average RB score versus cross-slope distance (m) for the array performed on the headwall above the Abbott weather plot on 2004-03-06/07. The distribution is fitted with a sine curve (Equation 4.3).

4.6.2 Monashee View – 2004-02-27

The array shown in Figure 4.11 was performed on Mt. St. Anne in the Cariboo Mountains on a predominantly northeasterly aspect at treeline. All the tests failed on a buried surface hoar layer which was approximately 40 cm deep. When performing the array, it became apparent that size of the surface hoar crystals affected the rutschblock result, such that larger surface hoar crystals generally gave lower RB scores (RB score vs. E: R_S = -0.27, p = 0.04, N = 65). Another cause of variability in this array was the interruption of weak layer continuity by hard clumps of snow that had fallen off of tree branches, known as “tree bombs”. This resulted in higher RB scores for the two tests that were performed in the areas affected by the tree bombs (Figure 4.11).

When a RB score of 1.5 is assigned to every test that failed with only one ski partially weighting the block (2- in Figure 4.11), a significant correlation emerges between RB score and slope angle (R_S = 0.27, p = 0.03, N = 65). The positive correlation coefficient suggests that stability decreases for less steep areas of the slope. These types of terrain features have a better view of the open sky, which can result in increased radiant cooling of the snow surface and hence surface hoar growth. There is also a significant negative correlation between surface hoar crystal size and aspect (R_S = -0.30, p = 0.02, N = 65) implying that larger surface hoar crystals were found on more northerly aspects. This can be explained by longer diurnal growth periods on the more northerly aspects due to decreased exposure to solar radiation during the day. The stability patterns found for this array can, therefore, be explained by better conditions for surface hoar growth in areas with lower point stability. Also, the high scores where the weak layer was interrupted by tree bombs indicates the small scale stabilizing effect of tree bombs, as previously found by Schweizer and others (1995).

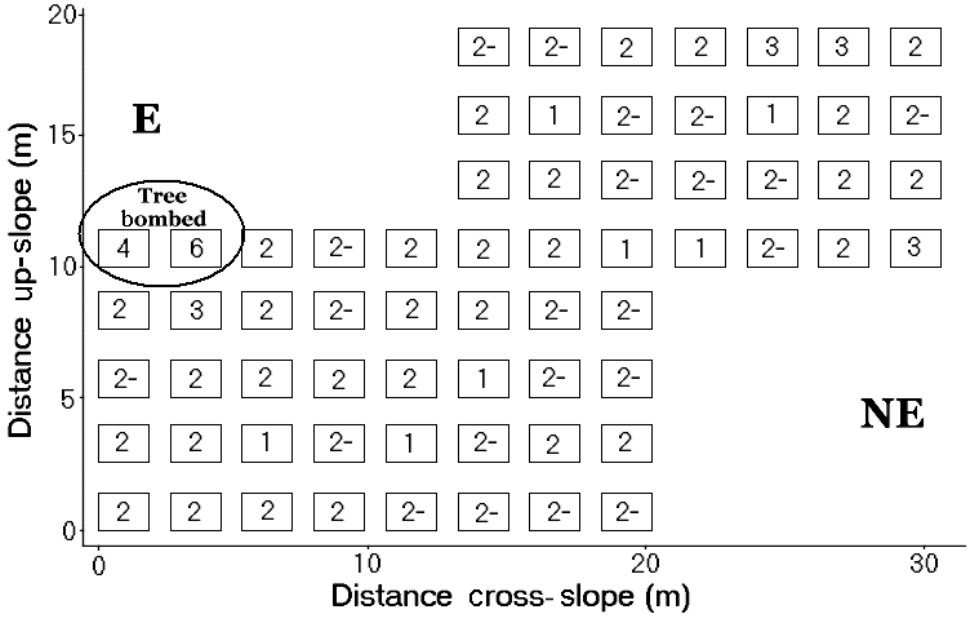

Figure 4.11 – Rutschblock test array performed at Monashee View on 2004-02-27. All the tests failed on the 040214 surface hoar layer with an average depth of 39 cm. Average slope angle is 34˚. For two tests on the left side of the array, the continuity of the weak layer was interrupted by hard chunks of snow that had fallen off of a tree, known as "tree bombs".

Multivariate linear regression was used to assess the combined affect of slope angle and aspect on stability (Figure 4.12) based on the following equation:

$$RB\ score = 0.054\ \Psi + 0.025\ Asp - 1.30 \tag{4.4}$$

where Ψ is the slope angle in degrees and *Asp* is the aspect in degrees from north. The aspect term in Equation 4.4 is significant (p = 0.001, N = 65), however the slope angle term is not (p = 0.061, N = 65), although it is almost significant. The regression with aspect includes the two tests that were affected by the tree bombs, and if these test are ignored the regression is no longer

significant. Furthermore, the assumption of normality of the residual values is rejected (Lilliefors $p < 0.01$), suggesting that least-squares linear regression is not suited to this dataset. Nonetheless, given the linear trend in Equation 4.4, a 10˚ decrease in slope angle combined with a 20˚ northerly change in aspect would result in a decrease in point stability of one RB score.

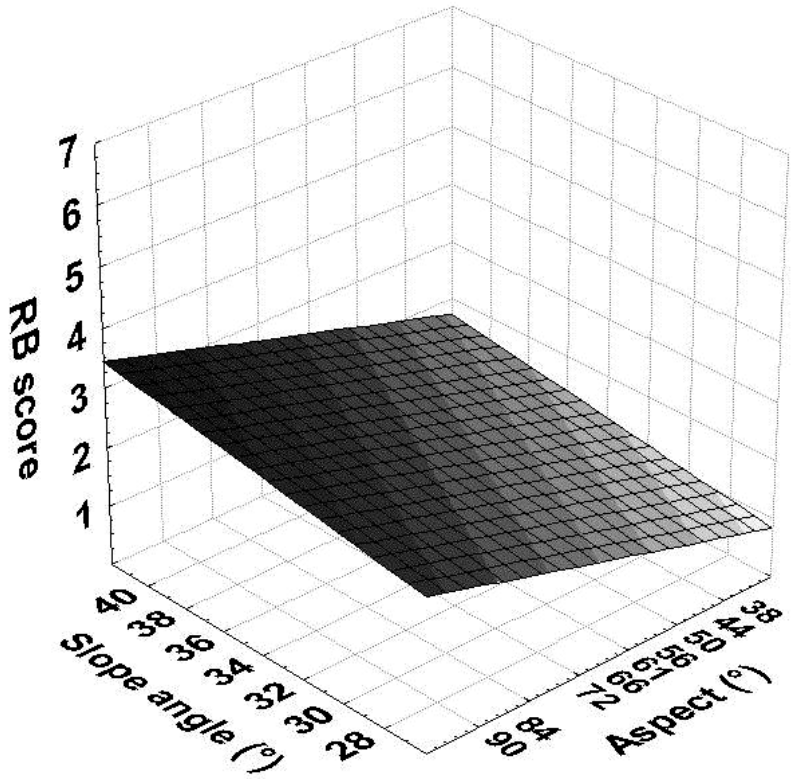

Figure 4.12 – Linear trend surface for the array at Monashee View on 2004-02-07 based on Equation 4.3. The surface is shaded based on RB score.

4.6.3 Abbott – 2004-03-11/12

The array in Figure 4.13 had a significant positive correlation between RB score and slab thickness, as shown in Table 4.3. In the upper left corner of the array there was a buried tree which caused a wind drift on the leeward side where the weak layer was found to be up to 108 cm deep. This corresponded with the three tests on the left side of the array with RB scores of 7. Furthermore, the entire upper slope whumpfed (i.e. a fracture audibly propagated along the weak layer without releasing an avalanche) when the rutschblock operator moved to the windward side of the buried tree, where the slab was found to be only 40 cm thick.

A similar event happened when performing the array on South Run on 2003-01-03 (Figure A.3). For this array, the undisturbed portion of the slope was triggered by the rutschblock operator from a locally thin area (H = 50 cm) when the average slab thickness for the rutschblock tests was 65 cm.

Figure 4.13 – Rutschblock test array performed on Mt. Abbott on 2004-03-11/12. All the tests failed in a 3 cm thick layer of faceted crystals, with an average depth of 70 cm. The weak layer was sandwiched between crusts on the right side of the slope (ESE aspect), in the middle of the slope a crust was only found below the weak layer and no crusts were found on the left side (E aspect). The entire upper part of the slope whumpfed when a field worker stepped above a buried tree where the slab was thin (marked with an X).

4.6.4 South Run – 2004-03-18

The array in Figure 4.14 shows how changing conditions for the growth of facets on a crust can affect stability. The array was performed on the side of a knoll where the aspect changes from easterly, on the left side of the slope, to northeasterly on the right side. The bed surface for the fractures was a buried crust which was formed from a melt-freeze process caused by direct solar radiation. When the bottom row of tests, which was influenced by varying slab thickness, is ignored, a significant correlation between RB score and aspect (R_S = -0.7, p = 0.002, N = 17) emerges. The crust on the easterly aspect was harder

and thicker, and had bigger and sharper facets on it, which resulted in lower stability than on the more northerly (shadier) aspect (RB score vs. E: R_S = -0.42, p = 0.04, N = 23).

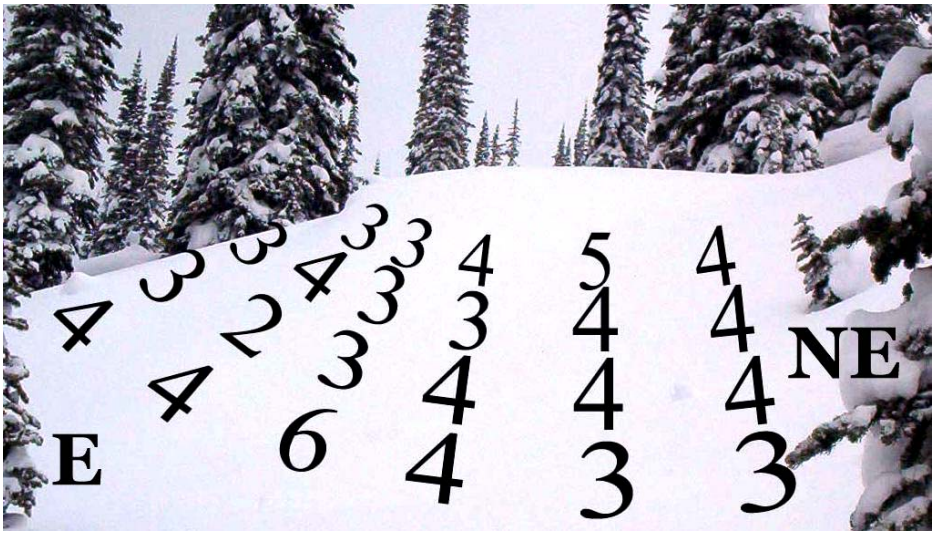

Figure 4.14 – Rutschblock test array performed on the upper slopes of South Run on Fidelity Mtn. All the tests failed on a thin layer of faceted crystals on top of a melt-freeze crust. Average slab thickness was 73 cm and average slope angle was 30˚.

4.7 Summary

Two winters of field work produced 29 arrays of 8 to 65 closely spaced rutschblock tests with array median RB scores ranging from 2 to 7. The coefficient of variation (CV) of stability for the individual arrays ranged from 0% to 50% with a median of 21%. This is lower than the range of values found in other

studies of variability in start zones (Stewart, 2002; Kronholm, 2004). Variability tends to be higher for slopes with higher overall stability.

When point stability data across a slope are modeled as a linear trend and residuals, the trends can usually be explained by similar trends in snowpack and terrain variables, while the residuals follow the geostatistical phenomenon of spatial continuity (Isaaks and Srivastava, 1989, p. 50-51). Variations in slab thickness, slope angle, aspect or terrain features were found to affect stability, either on their own or through interactions with microscale weather phenomena. The combined effect of slab thickness and slope angle showed that steeper areas with thinner slabs tend to be less stable. Furthermore, slab thickness had a more dominant affect on stability than slope angle.

Few ranges or sill were observed in the variograms because of the complex interaction between variables with different scales. More data, spaces closer and over larger extents, are required to interpret the effects and interactions of terrain and snowpack variables.

5 Results of fracture properties within arrays

5.1 Introduction

The fracture properties reviewed in this chapter are fracture character, release type from the rutschblock arrays and fracture propagation energy from the propagation test arrays. During the winters of 2003 and 2004, 23 spatial arrays of fracture propagation tests were performed consisting of a total of 930 tests. Diagrams for every array can be found in Appendix A. Eighteen of these arrays had buried surface hoar layers as the target failure layer for every test, while the remaining arrays targeted weak layers of either faceted crystals (two arrays), precipitation particles (one array) or multiple grain types (two arrays). Manual snow profile results for every array can be found in Appendix B.

This chapter is structured the same as Chapter 4, starting with summary statistics of the DHE data in Section 5.2. Sections 5.3, 5.4 and 5.5 cover the regression, correlation and variogram analysis results respectively. Once again, variograms analysis did not prove to be a particularly useful tool for identifying spatial patterns in fracture propagation energy. The homogeneity of the fracture character and rutschblock release type observations is covered in Section 5.6 and example fracture propagation test arrays are presented in Section 5.7.

5.2 Summary statistics

The size of the arrays in Table 5.1 ranged from 8 to 131 tests with a median of 35, and all but one array were performed in a single day. Table 5.1 shows that a wide range of conditions were targeted for these arrays. The median DHE for the individual arrays ranged from 6.7 to 56.6 J/m^2 with a median of 20.0 J/m^2. The QCV for the individual arrays ranged from 5% to 29% with a median of 18%, and the SIQR ranged from 0.7 to 10.4 J/m^2 with a median of 2.6 J/m^2. This is considerably lower than the variability that Stewart (2002) found for similar arrays of *stability* tests (QCV_{min} = 7%, QCV_{max} = 67%, QCV_{med} = 31%), showing that the DHE in these fracture propagation tests is less variable than the drop hammer energy in Stewart's (2002) stability tests. This is very likely because Stewart's (2002) tests had variability due to slab and weak layer properties, but the within-array variability in slab properties has largely been eliminated for the fracture propagation tests. The amount of energy required for fracture propagation is also considerably less than that required for fracture initiation and propagation as indicated by the medians in Stewart's (2002) stability test arrays which ranged from 10.9 to 147.2 J/m^2, with a mean of 55.2 J/m^2.

Unlike stability, the variability (QCV) of DHE did not increase with the median DHE (R_S = -0.28, p = 0.20, N = 23). There is, however, a tendency for SIQR to increase with array median DHE (R_S = 0.57, p = 0.004, N = 23) which

can be seen in Figure 5.1. Although, the possibility of greater operator induced error with higher drop heights could be an explanation for this.

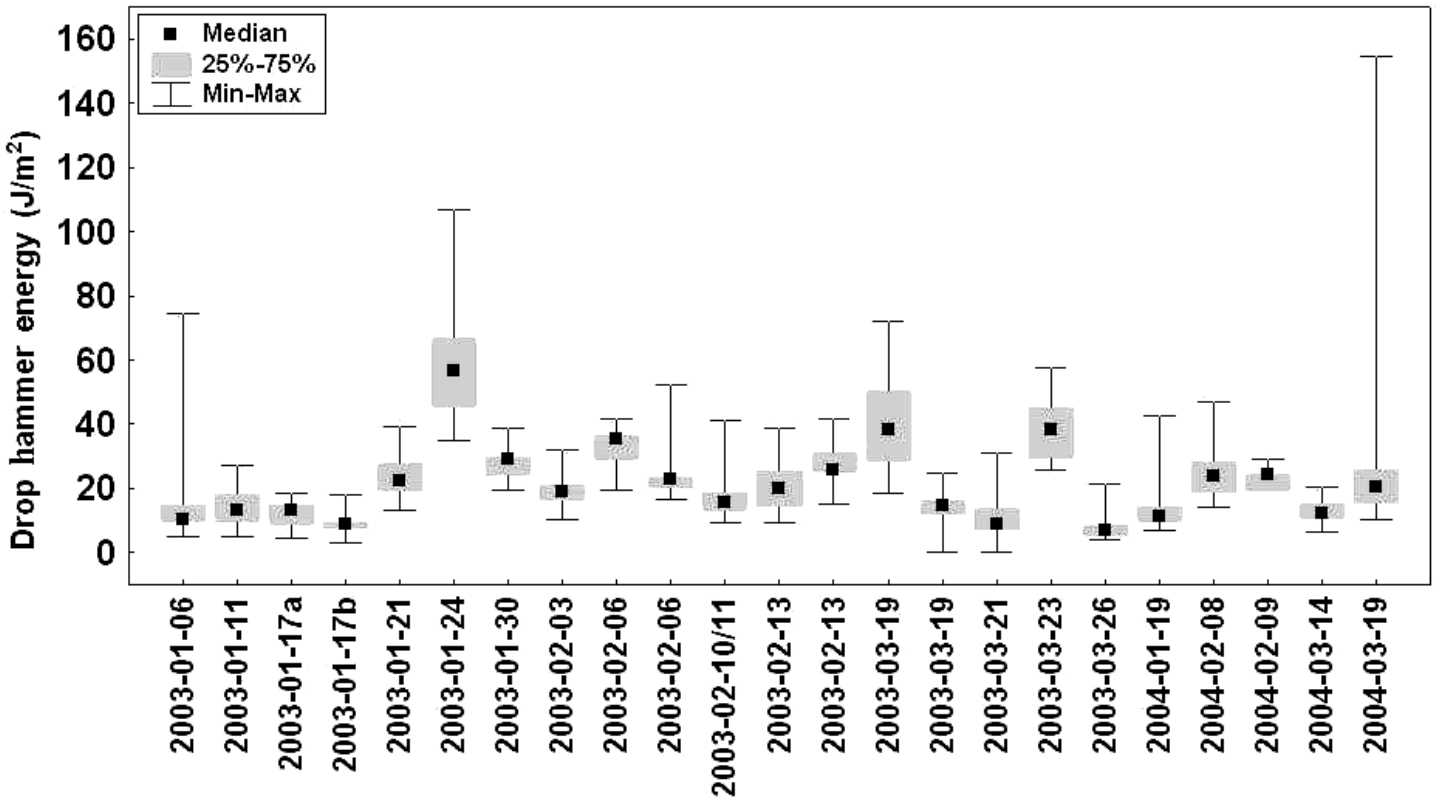

Figure 5.1 – Box and whisker plots of fracture resistance arrays showing the median, IQR, minimum and maximum DHE for each array.

Table 5.1 – Summary statistics for the spatial variability of DHE in arrays of fracture propagation tests.

Location	Date	N	Min (J/m^2)	Q_1 (J/m^2)	Med (J/m^2)	Q_3 (J/m^2)	Max (J/m^2)	SIQR (J/m^2)	QCV (%)
Poetry Slopes	2003-01-06	56	4.9	9.7	10.1	14.8	74.6	2.6	21
South Run	2003-01-11	43	4.9	9.4	12.7	14.4	24.7	2.5	21
NRC Gully	2003-01-17a	19	4.3	8.9	13.2	14.1	18.5	2.6	23
NRC Gully	2003-01-17b	24	3.2	8.1	8.9	9.5	17.8	0.7	8
Christiania Ridge	2003-01-21	29	13.4	19.4	22.6	27.9	39.1	4.2	18
Poetry Slopes	2003-01-24	39	34.8	45.9	56.6	66.7	106.7	10.4	19
Mt. St. Anne	2003-01-30	19	19.4	24.3	29.1	29.5	38.8	2.6	10
Poetry Slopes	2003-02-03	52	10.2	16.5	19.0	21.0	31.9	2.2	12
Mt. St. Anne	2003-02-06	13	19.5	29.4	35.3	36.2	41.7	3.4	10
Poetry Slopes	2003-02-06	41	16.7	20.2	22.8	23.6	52.2	1.7	8
Abbott Headwall	2003-02-10/11	131	9.2	13.4	15.9	18.5	41.1	2.6	20
Cheops	2003-02-13	35	9.1	15.2	20.0	23.8	38.6	4.3	22
Diamond Head	2003-02-13	28	15.1	25.4	26.0	30.9	41.9	2.8	10
Mt. St. Anne	2003-03-19	39	18.5	29.3	38.5	50.1	72.1	10.4	26
South Run	2003-03-19	43	0.3	12.4	14.4	16.2	24.9	1.9	13
Rudy's Bowl	2003-03-21	28	0.3	7.4	8.9	13.5	31.2	3.1	29
Cheops Bench	2003-03-24	8	25.7	31.9	38.3	44.2	57.7	6.2	16
Caribou Hideout	2003-03-26	35	4.1	5.4	6.7	8.3	21.4	1.4	21
Poetry Slopes	2004-01-19	56	6.8	9.8	11.4	13.9	49.0	2.1	17
Fortitude	2004-02-08	45	14.1	18.9	23.6	28.3	47.2	4.7	20
Slick Glades	2004-02-09	27	19.6	22.0	24.5	24.5	29.4	1.2	5
Cheops Bench	2004-03-14	33	8.9	10.7	12.2	15.2	20.3	2.3	17
Monashee View	2004-03-24	87	10.2	15.4	20.5	25.7	154.4	5.1	25
Median		35.0	9.2	15.4	20.0	23.6	39.1	2.6	18.0

5.3 Array-spanning linear trends

In Table 5.2, seven arrays have significant linear trends in either the up-slope or cross-slope directions or both. The hypothesis of normality of the residual DHE values could not be rejected for 13 of the 23 arrays (Appendix C), suggesting that least squares linear regression is reasonable for assessing linear trends in DHE. The variability of propagation energy decreases after the linear trends are removed, with a median SIQR for the residual DHE of 2.5 J/m^2. The variability explained by the linear trends is again generally low, with a median R^2 of 0.11. Furthermore, there are no patterns in trends in the up-slope direction based on the number of positive and negative coefficients for Row, in the arrays with significant trends in the up-slope direction.

Table 5.2 – Summary of the linear regression results based on the equation: DHE = aCol + bRow + c, where Col is the cross-slope position based on the grid column number and Row is the up-slope position based on the grid row number. The positive Col direction is from climber's left to climber's right across the slope and the positive Row direction is up the slope. The regression coefficients that are significant at the p < 0.05 level, are marked in bold. DHE_{res} is the residual DHE after trend removal.

Location Date	Max Col	Max Row	Valid *N*	a *p*	b *p*	c *p*	R^2	SIQR of DHE_{res} (J/m^2)
Poetry Slopes 2003-01-06	19	3	56	0.38 0.09	-0.46 0.75	**17.7** **< 10^{-3}**	0.06	1.5
South Run 2003-01-11	11	4	43	0.25 0.24	-1.20 0.05	**15.7** **< 10^{-3}**	0.13	2.7
NRC Gully	8	3	19	**-1.13**	-1.59	**10.1**	0.31	1.8

Location Date	Max Col	Max Row	Valid *N*	a *p*	b *p*	c *p*	R^2	SIQR of DHE_{res} (J/m^2)
2003-01-17a				**0.02**	0.14	**10^{-3}**		
NRC Gully 2003-01-17b	8	3	24	0.06 0.83	1.28 0.13	**6.86** **0.01**	0.11	1.6
Christiania Ridge 2003-01-21	16	2	29	0.43 0.08	4.19 0.07	**21.3** **< 10^{-3}**	0.14	3.1
Poetry Slopes 2003-01-24	13	3	39	-0.90 0.13	**9.48** **10^{-3}**	**32.5** **< 10^{-3}**	0.30	6.9
Mt. St. Anne 2003-01-30	20	1	19	0.31 0.21	-	**34.1** **< 10^{-3}**	0.09	2.8
Poetry Slopes 2003-02-03	13	4	52	0.26 0.05	0.73 0.10	**18.9** **< 10^{-3}**	0.12	2.3
Mt. St. Anne 2003-02-06	14	1	13	0.32 0.50	-	**35.5** **< 10^{-3}**	0.04	2.4
Poetry Slopes 2003-02-06	22	2	42	-0.33 0.11	-3.11 0.21	**24.7** **< 10^{-3}**	0.10	2.8
Abbott Headwall 2003-02-10/11	22	6	131	**-0.14** **0.03**	**-0.95** **< 10^{-3}**	**18.4** **< 10^{-3}**	0.14	2.4
Cheops 2003-02-13	5	7	35	0.09 0.91	0.51 0.40	**18.5** **< 10^{-3}**	0.02	3.5
Diamond Head 2003-02-13	9	2	28	-0.26 0.15	-2.86 0.25	**30.0** **< 10^{-3}**	0.21	2.5
Mt. St. Anne 2003-03-19	41	1	39	**0.80** **< 10^{-3}**	-	**57.7** **< 10^{-3}**	0.56	6.7
South Run 2003-03-19	12	4	43	0.05 0.84	-1.09 0.13	**17.3** **< 10^{-3}**	0.06	2.3
Rudy's Bowl 2003-03-21	15	2	28	-0.21 0.56	-1.90 0.54	**13.0** **0.03**	0.03	2.9
Cheops Bench 2003-03-24	2	5	8	-0.59 0.86	-0.37 0.97	38.3 0.08	0.01	7.0
Caribou Hideout 2003-03-26	6	6	35	0.01 0.97	**-0.92** **< 10^{-3}**	**10.7** **< 10^{-3}**	0.28	1.0
Poetry Slopes 2004-01-19	14	4	56	**0.52** **0.01**	0.37 0.60	**16.1** **< 10^{-3}**	0.13	2.0
Fortitude 2004-02-08	15	3	45	0.31 0.26	-0.79 0.58	**28.6** **< 10^{-3}**	0.04	4.9
Slick Glades 2004-02-09	14	2	27	0.07 0.87	1.23 0.73	**25.7** **0.01**	0.03	1.7
Cheops Bench 2004-03-14	7	5	33	**0.59** **0.02**	**0.81** **0.03**	**13.1** **< 10^{-3}**	0.28	2.0
Monashee View 2004-03-24	31	3	87	0.26 0.20	-1.31 0.54	**28.7** **< 10^{-3}**	0.02	4.8

5.4 Correlation analysis

5.4.1 Introduction

Correlation analysis of DHE with terrain and snowpack variables was performed on four different datasets. Section 5.4.2 reviews the correlations within each of the 23 individual arrays. Section 5.4.3 reviews the correlations associated with the medians of the individual arrays. Section 5.4.4 covers the correlations between significant array-spanning linear trends in DHE and snowpack and terrain variables. These correlations are used to assess whether the direction of significant trends in DHE is similar to the direction of the significant trends in snowpack and terrain variables for each array. Correlations of the residuals are also included to check for residual effects. Section 5.4.5 reviews the correlations associated with the normalized data from a combined dataset of all 23 arrays.

Since the individual array data were generally not normally distributed, Spearman rank correlations were used to describe the associations. However, the array-spanning linear trends were found to mostly normal; thus Pearson linear correlations were used. Spearman rank order correlations were used for the analysis of the normalized data from the combined dataset. The results of testing for normality can be found in Appendix C.

5.4.2 Correlation analysis of individual arrays

In Table 5.3, there is one significant positive correlation and one significant negative correlation between DHE and weak layer thickness. This implies that there is no consistent relationship between weak layer thickness and energy required for fracture propagation. The four significant positive correlations, versus one significant negative correlation between H and DHE, suggest that some deeper weak layers require more energy to propagate fractures. Assuming DHE and fracture toughness are related, this result is consistent with McClung's (2002a) conclusion that thicker slabs have increased fracture toughness, due to creep and bonding processes at the weak layer under the weight of the slab.

There are six significant correlations between DHE and HS, four positive and two negative. Three of these arrays also had significant correlations with H, and since H often correlates with HS, the variations in DHE could be caused by variations in H. There are nine significant negative correlations and no significant positive correlation between DHE and slope angle. Only one of the correlations remains significant when drop height (without dividing by fracture area) is used instead of DHE. This implies that the significantly lower DHE for tests on steeper slopes is likely due to larger fracture areas because DHE is inversely related to fracture area.

Table 5.3 – Results from the correlations between DHE and snowpack and terrain variables. Correlations that are significant at the $p < 0.05$ level, are marked in bold. Layer thickness (Thick) was only measured for some buried surface hoar weak layers. N can differ within any particular array because occasionally certain measurements were not made for all tests.

Location Date		Snowpack variables			Terrain variables	
		Thick (cm)	H (cm)	HS (cm)	Ψ (˚)	Asp (˚)
Poetry Slopes 2003-01-06	R_S	-0.22	**-0.39**	**-0.35**	**-0.63**	-0.07
	p	0.10	**0.003**	**0.01**	**$< 10^{-3}$**	0.84
	N	56	**56**	**56**	**56**	11
South Run 2003-01-11	R_S	-0.03*	0.24	**0.33**	0.26	-
	p	0.87	0.13	**0.03**	0.10	
	N	54	43	**43**	43	
NRC Gully 2003-01-17a	R_S	0.20	0.06	0.10	-0.28	-
	p	0.41	0.81	0.70	0.25	
	N	19	19	19	19	
NRC Gully 2003-01-17b	R_S	-0.22	0.11	-0.14	**-0.49**	-
	p	0.30	0.62	0.52	**0.02**	
	N	24	24	24	**24**	
Christiania Ridge 2003-01-21	R_S	-0.02	**0.61**	**0.70**	-0.31	-
	p	0.94	**$< 10^{-3}$**	**$< 10^{-3}$**	0.10	
	N	14	**29**	**29**	29	
Poetry Slopes 2003-01-24	R_S	-0.29	**0.46**	0.26	-0.27	-
	p	0.08	**0.003**	0.11	0.10	
	N	39	**39**	39	39	
Mt. St. Anne 2003-01-30	R_S	-	-	**-0.49**	-0.11	-
	p			**0.03**	0.65	
	N			**19**	19	
Poetry Slopes 2003-02-03	R_S	0.25	-0.10	0.06	-0.24	-
	p	0.07	0.47	0.65	0.08	
	N	52	52	52	52	
Mt. St. Anne 2003-02-06	R_S	-	-	0.22	**-0.55**	-
	p			0.47	**0.049**	
	N			13	**13**	
Poetry Slopes 2003-02-06	R_S	**-0.33**	0.06	0.14	-0.11	-
	p	**0.04**	0.70	0.40	0.49	
	N	**41**	41	41	41	
Abbott Headwall 2003-02-10/11	R_S	-0.02	**0.19**	-0.08	**-0.23**	-
	p	0.84	**0.03**	0.38	**0.01**	
	N	131	**131**	131	**131**	
Cheops 2003-02-13	R_S	-	0.15	-0.16	-0.09	-
	p		0.40	0.35	0.60	

Table 5.3 (continued)

Location Date		Snowpack variables			Terrain variables	
		Thick (cm)	H (cm)	HS (cm)	Ψ (˚)	Asp (˚)
	N		35	35	35	
Diamond Head 2003-02-13	R_S	-0.08*		-0.32	**-0.56**	-0.28
	p	0.68	-	0.10	**0.002**	0.145
	N	28		28	**28**	28
Mt. St. Anne 2003-03-19	R_S		**0.47**	**0.52**	**-0.57**	**-0.75**
	p	-	**0.002**	**10^{-3}**	**< 10^{-3}**	**< 10^{-3}**
	N		**39**	**39**	**39**	**39**
South Run 2003-03-19	R_S	-0.24	0.20	0.11	**-0.33**	
	p	0.13	0.19	0.50	**0.03**	-
	N	43	43	43	**43**	
Rudy's Bowl 2003-03-21	R_S	-0.28	0.14	-0.19	-0.21	0.89
	p	0.17	0.47	0.34	0.28	0.11
	N	26	28	28	28	4
Cheops Bench 2003-03-24	R_S	0.09	-0.61	-0.61	-0.43	
	p	0.83	0.11	0.11	0.29	-
	N	8	8	8	8	
Caribou Hideout 2003-03-26	R_S	**0.34**	0.05	-0.18	**-0.33**	
	p	**0.047**	0.76	0.30	**0.049**	-
	N	**34**	35	35	**35**	
Poetry Slopes 2004-01-19	R_S		0.15	**0.27**	0.03	
	p	-	0.27	**0.04**	0.84	-
	N		56	**56**	56	
Fortitude 2004-02-08	R_S		0.22	-0.08	-0.07	
	p	-	0.15	0.62	0.65	-
	N		45	45	45	
Slick Glades 2004-02-09	R_S		0.17	-0.11		-0.35
	p	-	0.41	0.57	-	0.40
	N		27	27		8
Cheops Bench 2004-03-14	R_S		0.15	0.14	**-0.39**	
	p	-	0.39	0.45	**0.03**	-
	N		33	33	**33**	
Monashee View 2004-03-24	R_S		0.05	0.02	-0.12	
	p	-	0.67	0.82	0.28	-
	N		87	83	87	

* maximum surface hoar grain size used instead of weak layer thickness because the crystal size was not measured for these arrays.

The array at Mt. St. Anne on 2003-03-19 had a significant correlation with aspect. However the thickness of the surface hoar layer, on which the tests were

performed, did not change with aspect. Since slope angle, in this array, has a stronger correlation (higher R_S) with aspect (R_S = 0.69, $p < 10^{-3}$, N = 39) than H (R_S = -0.66, $p < 10^{-3}$, N = 39) or HS (R_S = -0.52, $p < 10^{-3}$, N = 39), the variation in DHE is probably due to slope angle or H, or both. Multivariate linear regression was used to assess the combined affect of slope angle and H on DHE and only the slope angle term was significant (p = 0.021). This implies that variations in slope angle were more dominant than variations in slab thickness for this array. Furthermore, the correlation between slope angle and drop height (instead of DHE) is still significant (R_S = -0.50, p = 0.001, N = 39), which means that the decrease in DHE for steeper parts of the array is only partially due to larger fracture areas.

5.4.3 Correlation analysis of array medians

When the array medians are considered (Table 5.4), both weak layer thickness and slope angle have significant negative correlations with DHE. This suggests that variations in weak layer thickness and slope angle are potential sources of between-slope variations in propagation energy. Arrays with thicker buried surface hoar weak layers tend to require lower overall fracture propagation energy. It is probable that the significant effect of slope angle on DHE is mostly due to increased fracture area for tests on steeper slopes (Section 5.4.2).

The SIQR of DHE has a significant negative correlation with median slope angle and a significant positive correlation with the hardness change across the failure plane. This implies that steeper slopes and slopes with a smaller hardness change across the failure plane have less variable DHE. Twenty (87%) of the 23 propagation test arrays used buried surface hoar as the target weak layer while the others used either faceted crystals or rounded grains (Appendix B). There were, therefore, insufficient data to establish associations between variability and weak layer grain type.

Table 5.4 – Spearman rank correlation coefficients (R_S) from the comparison of array median DHE, semi-interquartile range (SIQR) and quartile coefficient of variation (QCV) to array median snowpack and terrain variables, weak layer crystal size (E) and hardness (R) and the difference in E and R across the failure plane. Weak layer and failure plane attributes are from the manual profiles. Correlations that are significant at the $p < 0.05$ level, are marked in bold.

DHE		Median				Weak layer		Difference	
		Thick (cm)	H (cm)	HS (cm)	Ψ (˚)	E (mm)	R	E (mm)	R
Median	R_S	**-0.51**	0.37	0.32	**-0.48**	0.11	-0.01	0.22	0.21
	p	**0.04**	0.11	0.13	**0.02**	0.64	0.98	0.34	0.37
	N	**16**	20	23	**23**	22	21	21	21
SIQR	R_S	-0.30	0.19	0.10	**-0.52**	0.25	-0.35	0.38	**0.45**
	p	0.26	0.43	0.65	**0.01**	0.27	0.12	0.09	**0.04**
	N	16	20	23	**23**	22	21	21	**21**
QCV	R_S	0.39	-0.18	-0.12	-0.06	0.28	-0.39	0.22	0.25
	p	0.13	0.46	0.59	0.80	0.20	0.08	0.35	0.27
	N	16	20	23	23	22	21	21	21

5.4.4 Correlation analysis of array-spanning linear trends

Table 5.5 lists the results from the correlations between estimated DHE and estimated snowpack and terrain variables. The data were estimated through linear regression with position within the array (Section 3.3.2). Table 5.6 lists the results from the correlations between the residual DHE and the residual snowpack and terrain variables, after the trends were removed. Only the estimated and residual data from significant ($p < 0.05$) array spanning linear trends are included in this analysis. Furthermore the significant trends in the terrain and snowpack variables had to be in the same direction (cross-slope and/or up-slope) as the significant trends in DHE.

Table 5.5 – Results from the correlations between estimated DHE and estimated snowpack and terrain variables. The data were estimated from significant array-spanning linear trends. Correlations that are significant at the p < 0.05 level, are marked in bold. Weak layer thickness (Thick) was not measured for the arrays performed on Cheops Bench on 2004-03-14 and at Caribou Hideout on 2003-03-26. Results for other arrays are omitted because the trends in the snowpack or terrain variables are either not significant or significant in a different direction than the trend in DHE.

Location Date		Estimated			
		Thick (cm)	H (cm)	HS (cm)	Ψ (˚)
NRC Gully 2003-01-17a	R_P	**0.81**			**-0.99**
	p	**$< 10^{-3}$**	-	-	**$< 10^{-3}$**
	N	**19**			**19**
Poetry Slopes 2003-01-24	R_P		**0.96**	**1.00**	
	p	-	**$< 10^{-3}$**	**$< 10^{-3}$**	-
	N		**39**	**39**	
Abbott Headwall 2003-02-10/11	R_P	**0.99**	**0.21**	**-0.55**	**-0.99**
	p	**$< 10^{-3}$**	**0.02**	**$< 10^{-3}$**	**$< 10^{-3}$**
	N	**131**	**131**	**131**	**131**
Mt. St. Anne 2003-03-19	R_P		**1.00**	**1.00**	**-1.00**
	p	-	**$< 10^{-3}$**	**$< 10^{-3}$**	**$< 10^{-3}$**
	N		**39**	**39**	**39**
Caribou Hideout 2003-03-26	R_P			**-0.60**	**-0.80**
	p	-	-	**$< 10^{-3}$**	**$< 10^{-3}$**
	N			**35**	**35**
Cheops Bench 2004-03-14	R_P			**0.35**	**-0.74**
	p	-	-	**0.046**	**$< 10^{-3}$**
	N			**33**	**33**

Table 5.6 – Results from the correlations between residual DHE and residual snowpack and terrain variables, after trend removal. Correlations that are significant at the p < 0.05 level, are marked in bold. Layer thickness (Thick) was not measured for the arrays performed on Cheops Bench on 2004-03-14 and at Caribou Hideout on 2003-03-26. Results for other arrays are omitted because the trends in the snowpack or terrain variables are either not significant or significant in a different direction than the trend in DHE.

Location Date		Residual			
		Thick (cm)	H (cm)	HS (cm)	Ψ (˚)
NRC Gully 2003-01-17a	R_P	-0.22			0.30
	p	0.37	-	-	0.21
	N	19			19
Poetry Slopes 2003-01-24	R_P		-0.08	-0.23	
	p	-	0.65	0.16	-
	N		39	39	
Abbott Headwall 2003-02-10/11	R_P	**-0.25**	**0.18**	0.03	0.03
	p	**0.004**	**0.04**	0.77	0.76
	N	**131**	**131**	131	131
Mt. St. Anne 2003-03-19	R_P		-0.13	0.20	0.05
	p	-	0.43	0.23	0.76
	N		39	39	39
Caribou Hideout 2003-03-26	R_P			0.25	-0.23
	p	-	-	0.15	0.19
	N			35	35
Cheops Bench 2004-03-14	R_P			0.04	-0.19
	p	-	-	0.83	0.29
	N			33	33

From Tables 5.5 and 5.6, it is apparent that slope-scale trends in DHE are often similar to slope-scale trends in snowpack and terrain variables; as expected the residual DHE values have no consistent correlation with measured terrain or snowpack variables. All three arrays with significant trends in DHE and H have significant positive linear correlations between these trends. Again, this implies that areas with locally thicker slabs require more energy to propagate fractures. The significant correlations with trends in HS are, again, likely to be mostly due to

significant correlations with trends in H. Furthermore, the significant negative correlations with trends in slope angle are probably due to increased fracture area for tests on steeper slopes. There are not enough correlations with trends in weak layer thickness for any conclusive results.

5.4.5 Correlation analysis of the combined dataset

When the normalized data from the combined dataset are considered, weak layer depth (H) and slope angle emerge as potential causes of variability in DHE (Table 5.7). The significant positive correlation between H and DHE confirms the dependence of fracture propagation energy on weak layer depth, where deeper weak layers require more energy for fracture propagation. The significant negative correlation between slope angle and DHE could, once again, suggest that steeper parts of a slope are more likely to propagate fractures. However the propagation tests on the steeper parts also have a greater weak layer area for the fractures to propagate across.

Table 5.7 – Results from the correlations between normalized DHE and normalized snowpack and terrain variables. The data from all propagation test arrays are normalized with the median and SIQR and then combined. Correlations that are significant at the p < 0.05 level, are marked in bold. Layer thickness (Thick) was only measured for some buried surface hoar weak layers (12 arrays).

		Normalized			
		Thick	**H**	**HS**	**Ψ**
DHE_{norm}	***R_S***	-0.09	**0.15**	0.05	**-0.21**
	p	0.09	**$< 10^{-3}$**	0.12	**$< 10^{-3}$**
	N	357	**883**	939	**764**

Figure 5.2 shows a general trend for fracture propagation energy to be lower and less variable for thicker buried surface hoar weak layers. One theory which explains the lower DHE for thicker surface hoar layers is that there is vertical displacement (collapse) of the slab when surface hoar fractures which causes a bending moment and wave in the slab as the fracture propagates across the slope (Johnson, 2000). The thicker the surface hoar layer, the further the slab collapses which provides more gravitational energy to drive the fracture across the slope, hence less energy is required for propagation.

The lower variability for thicker surface hoar layers suggests that fractures in thicker surface hoar weak layers are less likely to encounter areas that resist propagation. These data are highly skewed in that only 42 tests (in 2 different arrays) have a weak layer thickness > 1.0 cm. Furthermore, there is no significant correlation between median weak layer thickness and QCV of DHE when all arrays on buried surface hoar are considered (R_S = 0.40, p = 0.13, N =

16). Nonetheless, it is consistent with the requirement of a continuous weak layer for the formation slab avalanches. Thin weak layers are less likely to be spatially continuous and more likely to have areas that require high amounts of energy for fracture propagation.

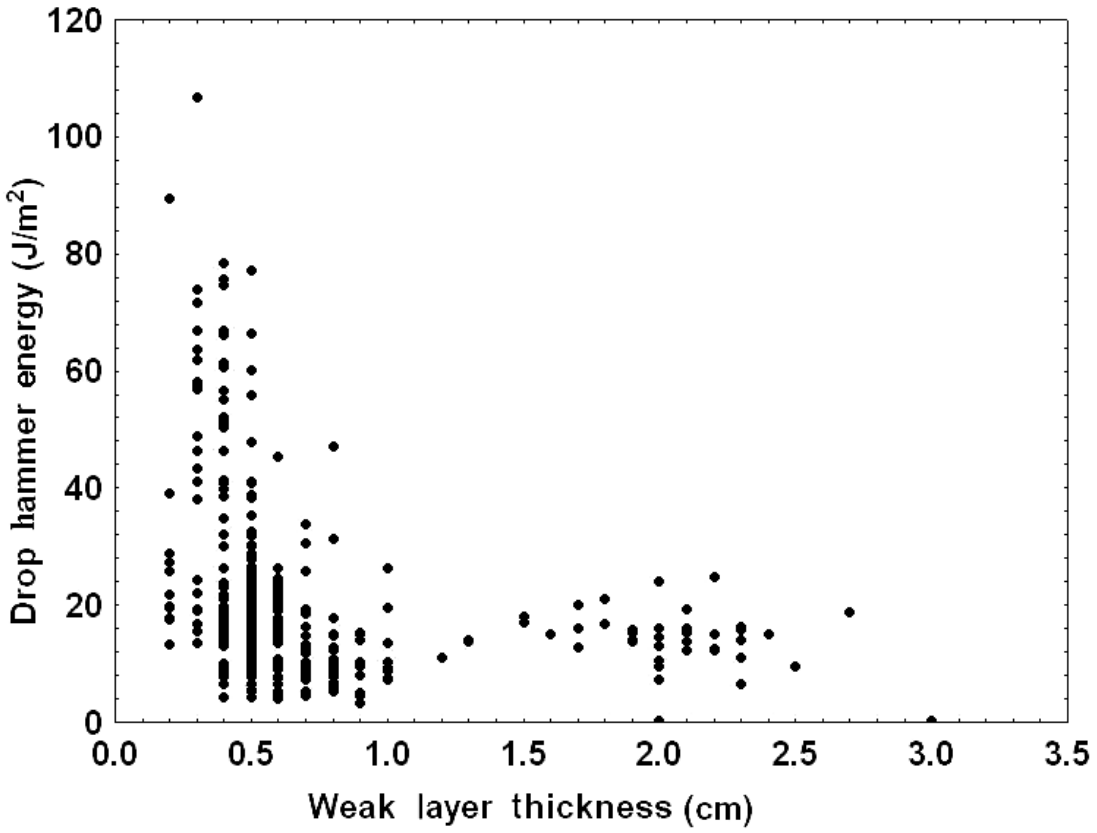

Figure 5.2 – Scatterplot of DHE versus Thick for buried surface hoar weak layers with varying thickness (R_S = -0.51, $p < 10^{-3}$, N = 399). Only arrays with varying weak layer thickness are included because weak layer thickness cannot be a source of variability in DHE unless it varies.

5.4.6 Summary

Since a significance level of $p < 0.05$ was used, 5% of the already low proportion (17%) of arrays with significant positive correlations between DHE and weak layer depth could be a result of type II errors. This undermines the ability to draw conclusions from these correlations. However, one reason for the low proportions of arrays with significant correlations with weak layer depth is that few arrays focused on weak layer depth as the only source of variability. Furthermore, the effect of weak layer depth on propagation energy was often masked by other sources of variability acting simultaneously.

Both slab thickness and buried surface hoar weak layer thickness emerge as sources of variability for fracture propagation energy. There is a tendency for thicker slabs to require more energy for propagation, which is consistent with previous studies of fracture toughness (McClung, 2002a). There is also a tendency for thinner surface hoar weak layers to have higher propagation energy, when the entire dataset is considered. The effect of HS is inconclusive in general terms as there are no obvious patterns in the correlations, and the influence of slab thickness also needs to be considered. Furthermore, there is no theory as to why HS should affect fracture propagation energy.

Stewart (2002) proposed that negative correlations between stability and HS were due to the increased energy transfer efficiency for the denser slabs that

are found deeper in the snowpack. Since the all the energy applied with the drop hammer tester is assumed to reach the weak layer for the propagation test, Stewart's (2002) explanation does not apply to this study.

5.5 Variogram analysis

As with the case for stability (RB score), variograms did not prove to be a particularly useful tool for analyzing the spatial structure of variations in fracture propagation energy. Only two arrays showed a distinct sill and range (Figure 5.3 a and b) where the semi-variance of the residual DHE reaches a sill within a distance of approximately 2 m. Figure 5.3 (c) is an example of an array that immediately reaches a sill. Eleven (48%) of the 23 arrays had similar variograms. These types of variograms can be modeled as pure nugget variograms, which suggests that there is a total absence of auto-correlation at separation distances of greater than 0.6 m. A sill at a semi-variance value of ~ 35 suggests that adjacent tests can vary by more than 10 J/m^2. Since the linear trends were relatively weak, the variograms of the raw propagation test data were similar to the variograms of the residuals.

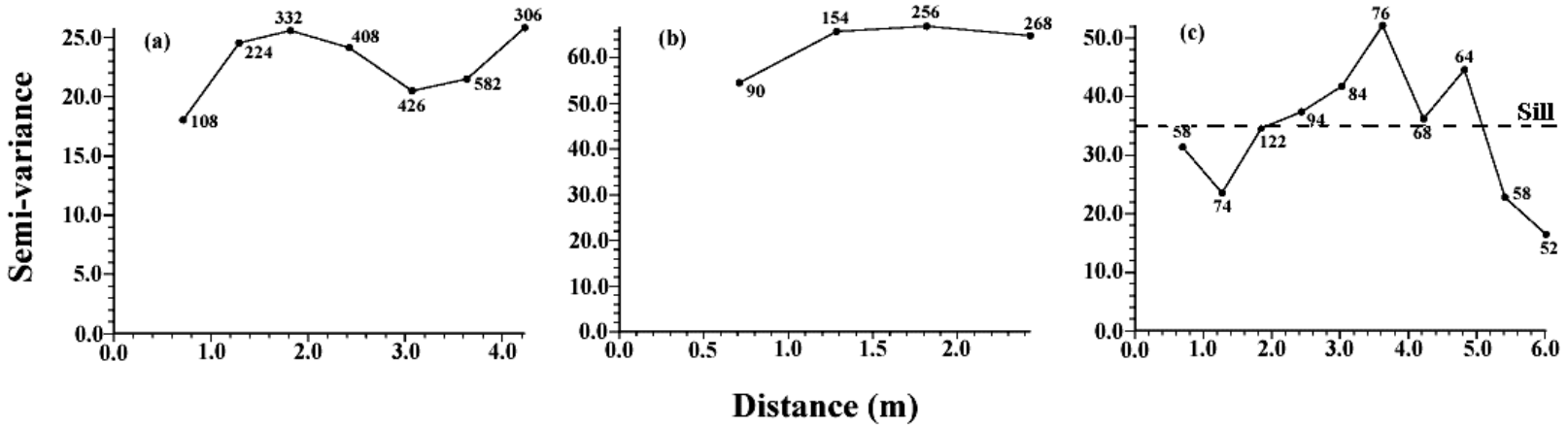

Figure 5.3 – Omnidirectional sample variograms for DHE_{res} for the arrays performed on (a) South Run on 2003-01-11, (b) Mt. Fortitude on 2004-02-08 and (c) Christiania Ridge on 2003-01-21. Lag distance is 0.6 ± 0.3 m. The number of pairs is also shown.

5.6 Fracture character and release type

Of the 939 fracture character observations (not including NF) made for propagation tests, 83% are SP, 12% are SC, 5% are B and less than 0.5% are RP or PC. Ninety-five percent of the 644 fracture character observations made for rutschblock tests are SP, 3% are RP, 1% are SC, 1% are B and < 0.5% are PC. These data are influenced by weak layer crystal type (van Herwijnen and Jamieson, 2003) in that the high proportion of SP fractures is probably due to the large number of arrays performed on buried surface hoar weak layers. Nonetheless, 16 (70%) of the 23 propagation test arrays have a single fracture character of either SP (15 arrays) or SC (1 array).

Twenty-two (76%) of the 29 rutschblock arrays have consistent SP fracture character, another array is over 95% SP fractures. Furthermore, fracture character seems to be independent of RB score and DHE as no relationship between fracture character and either RB score or DHE was apparent.

Of the 626 release type (RT) observations made for rutschblock tests, 76% are Whole-block (W), 22% are Most-of-block (M) and 2% are Only-an-edge (E). Only 8 (30%) of the 27 arrays where RT was observed have consistent RT (all W).

The proportion of either W or M release type observations (which ever is greatest) within an array was analyzed with respect to array median RB score. As shown in Figure 5.4, the homogeneity of RT depends on overall slope stability, that is, less stable slopes are more likely to have homogeneous RT. However, this relationship is affected by the truncated distribution of RB scores, in that few arrays have medians of one (non-existent) or seven (rare). Furthermore, as RB score increases, the proportion of the less frequent release types (M and E) increase.

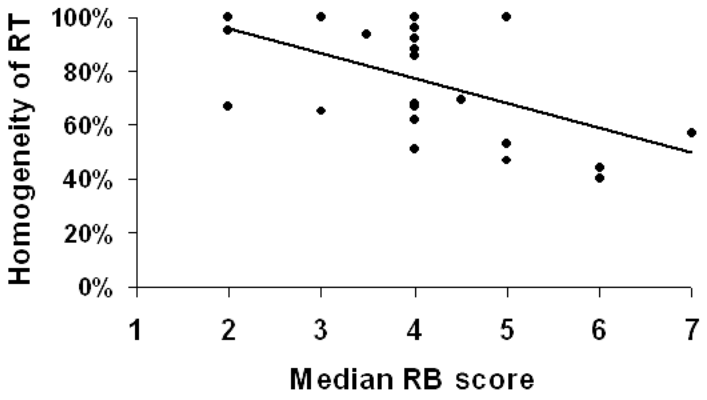

Figure 5.4 – Proportion of either W or M release type observations (which ever is greatest) as a function of slope median RB score (R_S = -0.53, p = 0.01, N = 27). Each point represents one rutschblock test array.

5.7 Example arrays

5.7.1 NRC Gully 2003-01-17

The example in Figure 5.5 demonstrates the effect of aspect on surface hoar formation and consequently fracture propagation energy. As can be seen in Figure 5.5, two arrays were performed on opposite sides of a gully with similar weak layer depths and slope angles. A manual profile on each side of the gully showed that the surface hoar crystals were smaller, and the layer was thinner, on the west-southwesterly aspect (Figure 5.5). This is probably due to shorter diurnal growth periods on the more southerly aspect because of increased exposure to solar radiation during the day (e.g. Jamieson and Schweizer, 2000). That is, there is more outgoing long wave radiation (negative energy balance) on the more northerly aspect, favouring surface hoar growth, than on the sunnier side of the gully.

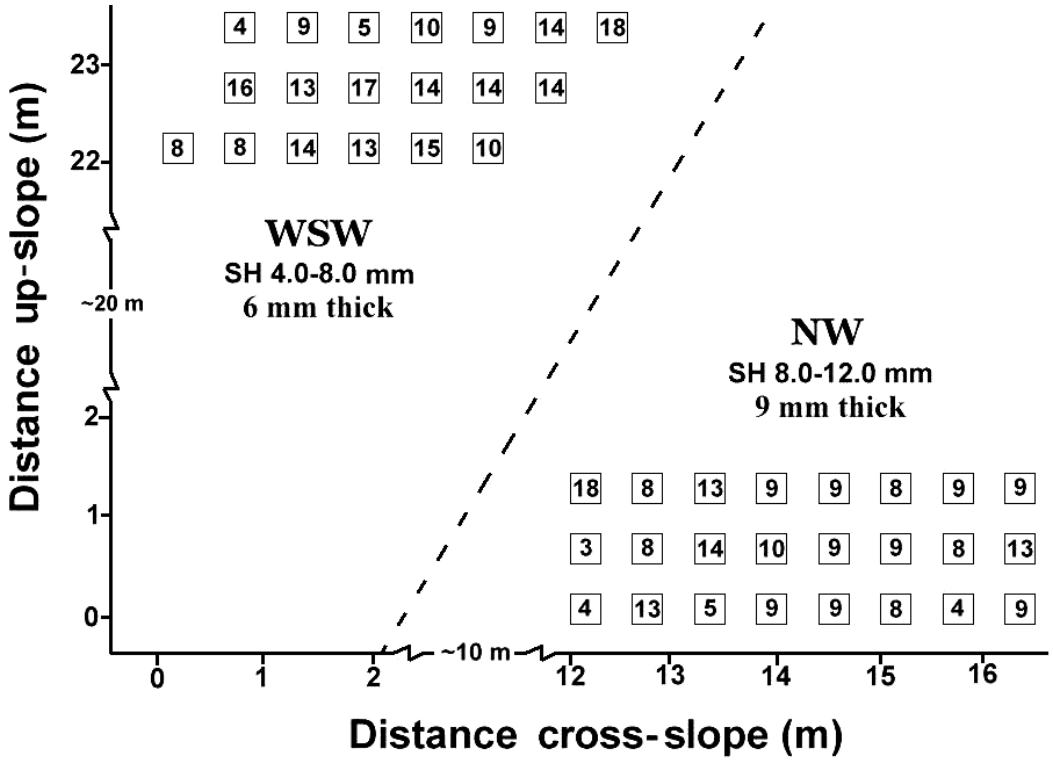

Figure 5.5 – Two propagation test arrays performed at treeline in NRC Gully on 2003-01-17. All the tests failed on the 021225 surface hoar layer. The upper array had an average weak layer depth of 56 cm and average slope angle of 36˚. The lower array had an average weak layer depth of 53 cm and average slope angle of 36˚. DHE (J/m^2) is shown within the boxes. Aspect, surface hoar (SH) crystal size, and weak layer thickness are shown for each array.

The Mann-Whitney U-test for difference of means between the two arrays is significant (p = 0.02), which means that the average DHE for the array on the west-southwesterly aspect is significantly higher than the average DHE for the array on the northwesterly aspect. This corresponded with surface hoar crystal size, in that the slope with the larger crystals (and thicker layer) tended to require less energy for fracture propagation.

5.7.2 Christiania Ridge 2003-01-21

Figure 5.6 shows an example of the effect of weak layer depth on DHE. The weak layer depth ranged from 65 to 106 cm due to a wind drift in the middle of the array. Weak layer depth (and HS) has a significant positive correlation with DHE (Table 5.3), indicating that the deeper area requires more energy for fracture propagation. This can be seen in Figure 5.6 by a region of higher DHE values in the middle of the array. This result is consistent with the results found in Sections 5.4.2 and 5.4.4.

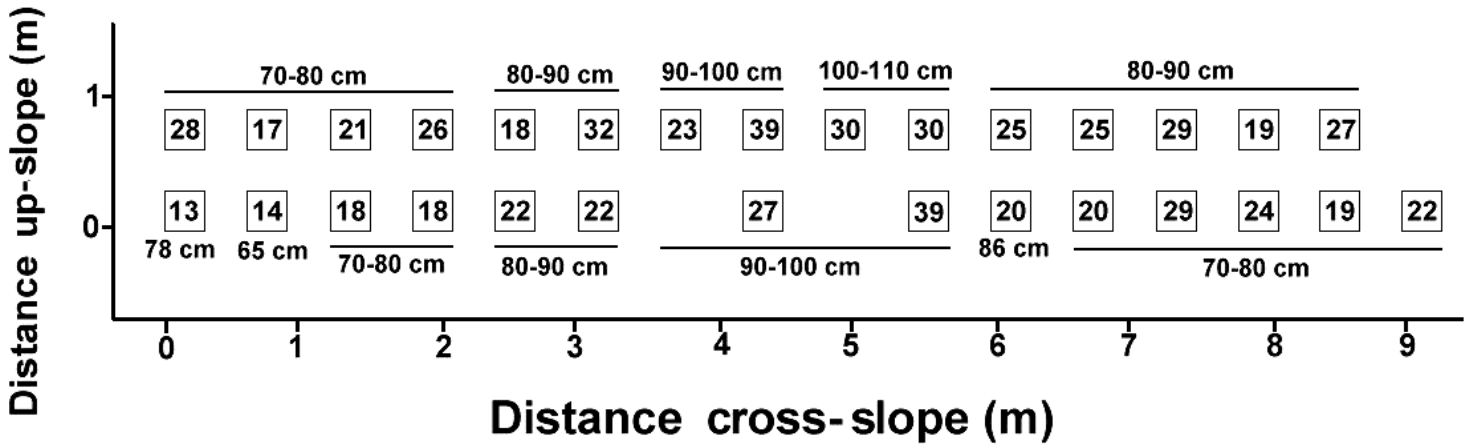

Figure 5.6 - Propagation test array performed at treeline on Christiania Ridge on 2003-01-21. All the tests failed on the 021225 surface hoar layer at an average depth of 82 cm. DHE (J/m^2) is shown in the boxes. The distribution of the weak layer depth across the array is also shown. Average slope angle is 32˚.

5.7.3 Slick Glades 2004-02-09

Figure 5.7 is an example of the effect of crystal type on the variability of fracture character. This is one of the rare arrays with variable fracture character. On the sides of the array, the target weak layer was composed of rounding faceted crystals (FC mx) and consistently produced SP fractures. In the middle on the array, only rounded grains (RG) with no signs of faceting was found, and the tests produced non-planar breaks (B). The crystal type of the weak layer (softer layer) changed across the slope likely due to a change in aspect. Furthermore, as can be seen in Figure 5.7 and Table 5.2, DHE does not substantially change across the array. This suggests that for this array fracture character is independent of DHE, which is consistent with other arrays with varying fracture character.

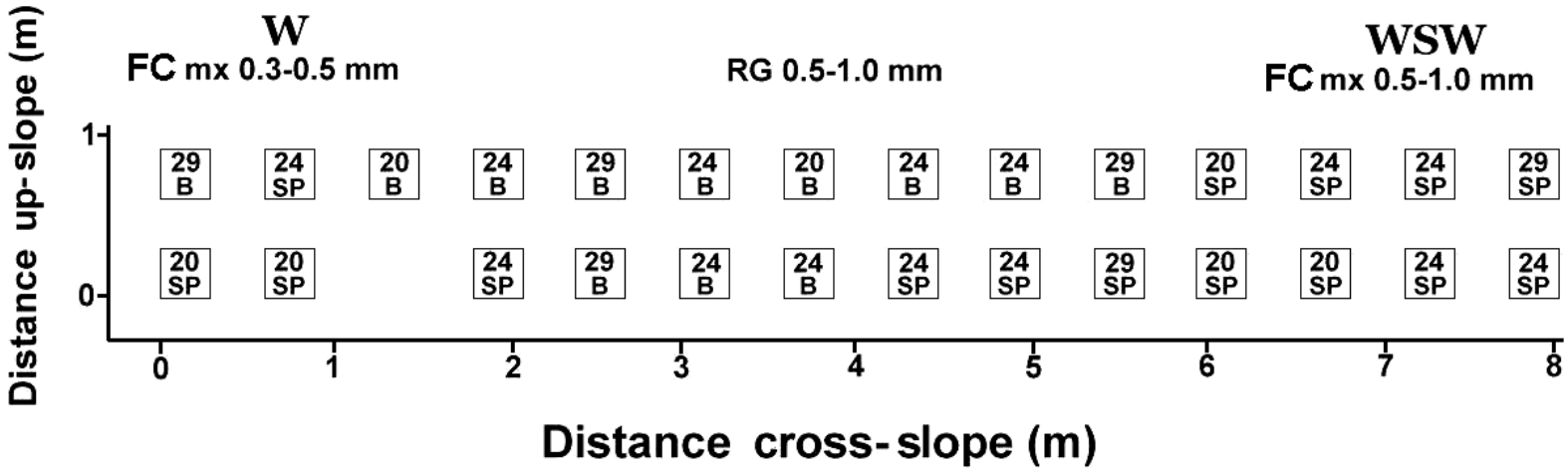

Figure 5.7 – Propagation test array performed at treeline in the glades on the west side of Mt. Slick. All tests failed at an interface where a distinct change in hardness (hard over soft) was found. The average depth of this interface is 75 cm and average slope angle is 26˚. DHE (J/m^2) and fracture character are shown in the boxes. The distributions of aspect and crystal type and size across the array are also shown.

5.8 Summary

Two winters of field work produced 23 arrays of 8 to 131 closely spaced prototype fracture propagation tests with a wide range of slope median DHE. The CV of DHE for individual arrays ranges from 3% to 45% with a median of 26%. When point propagation energy data across a slope are modeled as a linear trend and residuals, the significant trends can be mostly explained by similar trends in snowpack and terrain variables, while the residuals follow the geostatistical phenomenon of spatial continuity (Isaaks and Srivastava, 1989, p. 50-51).

Fracture properties (propagation energy, fracture character and release type) were found to be less variable than in similar arrays of stability tests. These results support the hypotheses of Johnson and Birkeland (2002) that shear quality (fracture character) is related to fracture propagation and should be less variable within slopes than point stability. Variations in weak layer thickness, H, HS, slope angle, aspect, as well as weak layer crystal type can affect fracture properties (DHE and fracture character). The most significant correlations with DHE were found to be H and weak layer thickness, where areas with deeper weak layers and/or thinner surface hoar weak layers tended to require more energy for propagation.

6 Discussion

6.1 Effects of slope scale spatial variability

An attempt was made to verify Kronholm and others' (2004) hypothesis that the probability of avalanching is a function of the mean point stability, the magnitude of variability of point stability and the scale of variability, as outlined in Section 1.2.6 and Section 1.3. Assuming a constant scale, the product of the median RB score and the QCV for each array were correlated with avalanche observations for the same day as the array measurements. The avalanche observations included both natural and artificially triggered avalanches from within a 100 km radius of Rogers Pass during the winter of 2004 and. No significant correlations were found for the number of tabulated avalanches (Spearman R = -0.12, p = 0.79, N = 7), nor for the sum of the avalanche sizes (Spearman R = -0.09, p = 0.85, N = 7).

Obvious signs of very poor stability (whumpfing, shooting cracks and avalanches) were experienced on slopes adjacent to the array sites on 2003-02-21 (Fidelity Mtn.), 2003-03-05 (Poetry Slopes) and on 2004-02-06/07 (Abbott Headwall). The Abbott Headwall array was the most variable of all 29 rutschblock arrays (QCV = 33%), whereas both the array at Fidelity and at the Poetry Slopes had a QCV of 0%. The median RB score for the arrays performed at Fidelity Mtn.

and the Poetry Slopes was low (Median RB score = 2 for both arrays). The median RB score for the Abbott Headwall array was relatively high (Median RB score = 4) as is expected for arrays with high variability.

If the increased variability found for slopes with higher median RB scores is not due to the truncated distribution of rutschblock load steps or increased error associated with higher RB scores, then it could reveal some important concepts for avalanche forecasting. Specifically, as a particular slab stabilizes over time, the variability of that layer would increase. When a large storm deposits snow on that slab the stability would temporarily decrease, because of the additional weight of new snow, and the variability would decrease accordingly, as proposed by Birkeland and Landry (2002).

6.2 Practical implications

First and foremost, it must be emphasized that extremely variable slopes were sought after for this thesis. The variability found is typical of avalanche start zones. Uniform study plots, from which point stability data is usually extrapolated, are less variable.

Conventional stability evaluation includes, as a minor factor, the extrapolation of point stability data to an entire slope or even larger areas. The uncertainty due to slope-scale spatial variability reduces the reliability of

extrapolating point stability data (Landry and others, 2004). Avalanche workers have been factoring this uncertainty into their stability evaluations for decades and have developed strategies for managing the risk associated with variable snowpacks. Jamieson (2003a) compiled these strategies and one suggestion was to attempt to detect slope-scale variability by manually probing (with ski poles or collapsible probe poles) the snowpack in several areas across the slope. By doing this, spatial patterns in HS, depths of significant layers, and continuity of crusts can be detected.

Once the level of variability is determined avalanche workers use a wider margin of safety when, and where, variability is high (Jamieson, 2003a). As shown in Section 1.3, the scale of variability can also have an affect on skier-triggered avalanche probability such that a wider margin of safety should also be used when the spatial scale of variability is high. Furthermore, route selection on slopes with a small spatial scale of variability would be more intuitive because areas of instability (e.g. steeper parts of the slope, concave areas where surface hoar is likely to be preserved, areas where wind drifting caused locally thin slabs, areas around rock outcrops or boulders, etc.) can be recognized and avoided. If the amount and scale of variability observed while skiing and probing was consistently reported, it could be incorporated into public avalanche bulletins, and hence contribute to safety.

McClung (2002b) suggests that targeted sampling for worst-case stability data can reduce the uncertainty associated with spatial variability. In this way, the overall stability level is more often underestimated and the number of high-consequence, false stable predictions are reduced. Furthermore, it is in these areas of relatively poor stability that skiers are most likely to trigger avalanches. McClung and Schaerer (1993, p. 126) recommend to collect an abundance of relevant information (e.g. avalanche observations, stability tests, snow profile data, etc.) in order to compensate for uncertainty associated with spatial variability. Results from fracture propagation tests and fracture character and release type observations can also be considered as relevant information for stability evaluation. Furthermore, this information can be effective at reducing the uncertainty associated with spatial variability because it is less variable than stability tests.

6.3 Experience with the propagation test

The fracture propagation test was modeled after a modified compression test that a ski guide was using in the mid 1990s to test deep weak layers (Jamieson, 2003b). Once finished with the compression test, the ski guide leveled the test column above a deep weak layer that had not fractured, and loaded it like a compression test (taps). For the fracture propagation test, the weak layer is notched, the amount of damping snow is fixed and a drop hammer is used for loading. If taps are used, instead of the drop hammer, this remains a

convenient test to perform on deep weak layers that did not fracture during a compression test.

The fact that the notch significantly reduces the energy required for propagation (Section 3.2.2.4) supports the hypothesis that this is a test for fracture propagation energy. The idea that the stress wave from the applied load concentrates at the notch tip is supported by observations of fractures (usually RP) starting at the notch and propagating to the other side of the test column. When fracture surfaces of tests that produced non-planar breaks are examined, a planar fracture surface that extends from the notch, and then becomes non-planar, is observed. Furthermore, the test was rejected if it appeared that that the fracture did not propagate from the notch, but such occurrences were very rare.

Fracture propagation tests were performed on several different weak layer crystal types. Performing this test on thin weak layers, such as surface hoar, was more straightforward than on thicker weak layers, such as depth hoar, because the correct location for cutting the notch was more evident in thin weak layers. When the target failure plane is visible or has a distinct hardness change across it, it generally requires less effort to find. Otherwise, it can be very difficult to locate the correct location to cut the notch.

7 Conclusions

Based on the data and ideas presented in this thesis, the following conclusions can be made:

- Varying slab thickness was found to be a source of spatial variability in stability for four arrays with areas of relatively thin slabs tending to have lower point stability.
- Varying slope angle was found to be a source of spatial variability in stability for two arrays with areas with relatively steep slope angles tending to have lower point stability.
- Most arrays do not show significant correlations between slab thickness or slope angle and RB score because slab thickness or slope angle did not vary sufficiently and/or the effect of slab thickness or slope angle on stability was obscured by variability caused by other parameters.
- The significant correlations between slab thickness or slope angle and RB score are consistent with snow mechanics and previous studies.
- Varying aspect across a slope was identified as a source of spatial variability in stability for two arrays.
- Spatial variability of stability within avalanche start zones can be caused by a combination of physical processes.

- The causes of spatial variability of stability within avalanche start zones can be difficult to assess with the methods and array sizes used in this thesis.
- Since the stability process must be a superposition (combination) of various causal processes with different scales, it would take many rutschblock tests, perhaps over 100+ m to identify correlation lengths.
- Varying weak layer depth was found to be a source of variability in fracture propagation energy for four arrays, with deeper weak layers tending to require more energy to propagate fractures.
- Most arrays do not show significant correlations between weak layer depth and DHE because weak layer depth did not vary and/or the effect of weak layer depth on DHE was obscured by variability caused by other parameters.
- Varying thickness of buried surface hoar weak layers was identified as a potential source of variability in fracture propagation energy within avalanche start zones, with thinner weak layers tending to require more energy to propagate fractures.
- Three rutschblock test arrays performed on buried surface hoar showed correlation lengths between 14 and 30 m.
- The correlation length of variability is difficult to estimate from the arrays used in this study because of insufficient resolution and extent.

- One pair of arrays performed on a slope with stability patterns that was governed by terrain features showed the potential for repeatability on a year-to-year basis.
- The slope-scale spatial variability of fracture propagation energy (as measured with the propagation test) is less than the slope-scale spatial variability of point stability.
- Fracture character and release type observations can be spatially homogeneous over 10 m.
- A wider margin of safety should be used when evaluating stability for slopes with high variability, large spatial scales of variability and, most obviously, low median point stability.

8 Recommendations for further research

Targeting a particular source of variability for array sites would be a more effective means of determining sources of variability if the arrays were categorized with respect to the terrain or snowpack variable being targeted. This way, the proportion of significant correlations with the targeted source would not be influenced by all the arrays for which that particular terrain or snowpack variable is constant. Principal component analysis could be used to assess the effects of snowpack and terrain variables. Further analysis could also include an analysis of the variance with ANOVA techniques.

In order to quantify the spatial scale of variability, high resolution arrays with a large number of tests are required. One solution is to utilize a resistance probe such as the SnowMicroPen (Kronholm, 2004) to perform arrays of vertical hardness profiles. This way, observations can be closely spaced and made quickly.

More development of the fracture propagation test is required before it can be reliably used as an avalanche forecasting tool. This could include correlations with large avalanches and remotely triggered avalanche activity and by comparing tests performed in areas of high and low fracture resistance along crowns.

Avalanche forecasters are often faced with the dilemma of evaluating the stability for a slope that had been previously skied. This can be difficult, since the long-term effect of skier compaction on weak layer or slab properties and hence stability is not known. Research into the effect of skier compaction on stability, and the spatial variability of stability, would help with this problem.

9 References

Akitaya, E. 1974. Studies on depth hoar. *Contributions from the Institute of Low Temperature Science*, Series A, 26, 1-67.

Armstrong, R. L. and B. R. Armstrong. 1987. Snow and avalanche climates of the western United States: A comparison of maritime, intermountain and continental conditions. *Avalanche Formation, Movement and Effects*, *Proceedings of the Davos Symposium*, IAHS Publ. No. 162, 281-294.

Bader, H.P. and B. Salm. 1990. On the mechanics of snow slab release. *Cold Regions Science and Technology*, 17, 287-300.

Beernick, T. 2003. Editor's view. *Avalanche News 66*, Canadian Avalanche Association, 4-5.

Birkeland, K. W., K. J. Hanson and R. L. Brown. 1995. The spatial variability of snow resistance on potential avalanche slopes. *Journal of Glaciology*, 41(137), 183–190.

Birkeland, K. W. 1997. Spatial and temporal variations in snow stability and snowpack conditions throughout the Bridger Mountains, Montana. Ph.D. Dissertation, Dept. of Geography, Arizona State University, Tempe, Arizona, USA, 205 pp.

Birkeland, K. 2003. Personal communication.

Birkeland, K. 2004. Personal communication on 2004-02-08.

Birkeland, K.W. and R.F. Johnson. 1999. The stuffblock snow stability test: comparability with the rutschblock, usefulness in different snow climates, and repeatability between observers. *Cold Regions Science and Technology*, 30(1-3), 115-123.

Birkeland, K.W. and C.C. Landry. 2002. Changes in spatial patterns of snow stability through time. *Proceedings of the 2002 International Snow Science Workshop*, Penticton, BC, Canada, 482-490.

Birkeland, K. W., K. Kronholm, M. Schneebeli and C. Pielmeier. In press. Changes in shear strength and micro-penetration hardness of a buried surface hoar layer. *Annals of Glaciology*, 38.

Blöschl, G. and M. Sivapalan. 1995. Scale issues in hydrological modeling – a review. *Hydrological Processes*, 9(3-4), 251-290.

Camponovo, C. and J. Schweizer. 1997. Measurements on skier triggering. *Proceedings of the 1996 International Snow Science Workshop,* Banff, Alberta, Canada, 100-103.

Canadian Avalanche Association (CAA). 2002. *Observation guidelines and recording standards for weather, snowpack and avalanches.* Canadian Avalanche Association, Revalstoke, BC, Canada, 77 pp.

Chernouss, P. A. 1995. Spatial and time variability of avalanche predictors and accuracy of their estimations. *Les apports de la recherche scientifique à la sécuritè neige, glace te avalanche*, Chamonix, France, 123-128.

Conway, H. and J. Abrahamson. 1984. Snow stability index. *Journal of Glaciology*. 30(126), 321-327.

Conway, H. and J. Abrahamson. 1988. Snow-slope stability – a probabilistic approach. *Journal of Glaciology*, 34(117), 170-177.

Doorschot, J., N. Raderschall and M. Lehning. 2001. Measurements and one-dimensional model calculations of snow transport over a mountain ridge. *Annals of Glaciology*, 32, 153-158.

Faillettaz, J., D. Daudon, D. Bonjean and F. Louchet. 2002. Snow toughness measurements and possible applications to avalanche triggering. *Proceedings of 2002 International Snow Science Workshop,* Penticton, British Columbia, Canada.

Feick, S., K. Kronholm and J. Schweizer. 2004. Spatial variability of surface hoar layers at the basin scale. *Geological Research Abstracts*, 6: 06265.

Föhn, P. M. B. 1987. The rutschblock as a practical tool for slope stability evaluation. *Avalanche Formation, Movement and Effects – Proceedings of the Davos Symposium*. September 1986, Davos, Switzerland, IAHS Publication No. 162, 195-211.

Föhn, P. M. B. 1989. Snowcover stability tests and the areal variability of snow strength. *Proceedings of the 1988 International Snow Science Workshop*, Whistler, British Columbia, Canada, 262-273.

Gruber, U., Hägeli, P., McClung, D.M. and Manner, E. In press. Large-scale snow instability patterns in Western Canada: First analysis of the CAA-InfoEx database 1991-2002. *Annals of Glaciology*, 38.

Gubler, H. and J. Rychetnik. 1991. Effects of forests near timberline on avalanche formation. *Proceedings of the 1990 International Snow Science Workshop*, Bigfork, Montana, USA, 73-92.

Hägeli, P. 2004. Scale analysis of avalanche activity on persistent snowpack weaknesses with respect to large-scale backcountry avalanche forecasting. PhD thesis, Atmospheric Science Program, University of British Columbia, Vancouver, British Columbia, Canada.

Hägeli, P. and D. M. McClung. 2000. A new perspective on computer-aided avalanche forecasting: scale and scale issues. *Proceedings of the 2000 International Snow Science Workshop*, Big Sky, Montana, USA.

Hägeli, P. and D. M. McClung. 2003. Avalanche characteristics of a transitional snow climate – Columbia Mountains, British Columbia, Canada. *Cold Regions Science and Technology*, 37, 255-276.

Harper, J. T. and J. H. Bradford. 2003. Snow stratigraphy over a uniform depositional surface: spatial variability and measurement tools. *Cold Regions Science and Technology*, 37, 289-298.

Isaaks, E. H. and R. M. Srivastava. 1989. *An Introduction to Applied Geostatistics.* Oxford University Press, Oxford, 561 pp.

Jamieson, J. B. 1989. In situ tensile strength of snow in relation to slab avalanches. M.Sc. thesis, Dept. of Civil Engineering, University of Calgary, Calgary, Alberta, Canada, 142 pp.

Jamieson, J. B. 1995. Avalanche prediction for persistent snow slabs. Ph.D. Dissertation, Dept. of Civil Engineering, University of Calgary, Calgary, Alberta, Canada, 255 pp.

Jamieson, B. 1999. The compression test - after 25 years. *The Avalanche Review,* 18(1), 10-12.

Jamieson, J. B. 2003a. Risk management for the spatial variable snowpack. *Avalanche News 66*, Canadian Avalanche Association, 30-31.

Jamieson, B. 2003b. Fracture propagation and resistance in weak snowpack layers. *Avalanche News 67*, Canadian Avalanche Association, 36-43.

Jamieson, J. B. and C. D. Johnston. 1992. Experience with Rutschblocks. *Proceedings of the 1992 International Snow Science Workshop*, 4-8 October 1992, Brekenridge, Colorado, USA, 150-159.

Jamieson, J. B. and C. D. Johnston. 1993. Rutschblock precision, technique, variations and limitations. *Journal of Glaciology*, 39(133), 666-674.

Jamieson, B. and T. Geldsetzer. 1996. Avalanche accidents in Canada, Volume 4: 1984 – 1996. *Canadian Avalanche Association,* Revelstoke, BC, Canada.

Jamieson, J.B. and C.D. Johnston. 1998. Snowpack characteristics for skier triggering. *Avalanche News 55*, Canadian Avalanche Association, 31-39.

Jamieson, J. B. and J. Schweizer. 2000. Texture and strength changes of buried surface-hoar layers with implications for dry snow-slab avalanche release. *Journal of Glaciology*, 46(152), 151-160.

Jamieson, J. B. and C. D. Johnston. 2001. Evaluation of the shear frame test for weak snowpack layers. *Annals of glaciology*, 32, 59-68.

Johnson, B.C. III. 2000. Remotely Triggered Slab Avalanches**.** MSc thesis. Dept. of Civil Engineering, University of Calgary, Calgary, Alberta, Canada, 98 pp.

Johnson, B.C., J.B. Jamieson and C.D. Johnston. 2000. Field data and theory for human triggered whumpfs and remote avalanches. *Proceedings of the 2000 International Snow Science Workshop*, Big Sky, Montana, USA.

Johnson, R. and K. Birkeland. 2002. Integrating shear quality into stability test results. *Proceedings of 2002 International Snow Science Workshop,* Penticton, British Columbia, Canada, 508-513.

Keeler, C. M. and W. F. Weeks. 1968. Investigations into the mechanical properties of alpine snow-packs. *Journal of Glaciology*, 7(50), 253-271.

Kronholm, K. 2004. Spatial variability of snow mechanical properties with regard to avalanche formation. Ph.D. Dissertation, Dept. of Geography, University of Zurich, Zurich, Switzerland, 187 pp.

Kronholm, K. and J. Schweizer. 2003. Snow stability variation on small slopes. *Cold Regions Science and Technology*, 37, 453-465.

Kronholm, K., J. Schweizer and M. Schneebeli. 2004. The effect of spatial variability on snow avalanche formation. *Geophysical Research Abstracts*, 6: 06272.

Landry, C. C. 2002. Spatial variations in snow stability on uniform slopes: implications for extrapolation to surrounding terrain. M.Sc. Thesis, Dept. of Earth Sciences, Montana State University, Bozeman, Montana, USA, 194 pp.

Landry, C. C., J. J. Borkowski and R. L. Brown. 2001. Quantified loaded column stability test: mechanics, methodology, and preliminary trials. *Proceedings of the 2000 International Snow Science Workshop,* Big Sky, Montana, USA, 230-237.

Landry, C., K. Birkeland, K. Hansen, J. Borkowski, R. Brown and R. Aspinall. 2004. Variations in snow strength and stability on uniform slopes. *Cold Regions Science and Technology*, 38, in press.

Logan, H. 1993. Snow temperature patterns and artificial release. *Proceedings of the 1992 International Snow Science Workshop*, Breckenridge, Colorado, USA, 37-46.

McClung, D. M. 2001. Characteristics of terrain, snow supply and forest cover for avalanche initiation caused by logging. *Annals of Glaciology,* 32, 223-229.

McClung, D. M. 2002a. Fracture toughness for dry slab avalanches. *Proceedings of 2002 International Snow Science Workshop,* Penticton, BC, Canada.

McClung, D. M. 2002b. The elements of applied avalanche forecasting Part 1: the human issues. *Natural Hazards*, 25, 111-119.

McClung, D. M., and P. A. Schaerer. 1993. *The Avalanche Handbook*. The Mountaineers, Seattle, Washington, USA, 271 pp.

McKay, G. A. and D. M. Gray. 1981. The Distribution of Snowcover. *Handbook of Snow – Principles, Processes, Management and Use*, Edited by Gray, D. M. and D. H. Male, Pergamon Press Canada Ltd. Toronto, Ontario, Canada, 153-190.

McMahon, B. 2004. Personal communication on 2004-04-28.

Perla, R. L., and R. A. Sommerfeld. 1987. On the metamorphism, morphology and microstructure of snow. *Proceedings of the International Snow Science Workshop*, Lake Tahoe, California, USA, 98-102.

Schaerer, P. A. 1975. Relation between the mass of avalanches and characteristics of terrain at Rogers Pass, B.C., Canada. *Avalanche Formation, Movement and Effects*, *Proceedings of the Symposium on Interdisciplinary Studies of Snow and Ice in Mountain Regions,* Moscow, Russia, August 1971, IAHS Publ. No. 104, 378 - 380.

Schweizer, J. 1999. Review of dry snow slab avalanche release. *Cold Regions Science and Technology*, 30(1-3), 43-57.

Schweizer, J., M. Schneebeli, M. Fierz, and P. M. B. Föhn. 1995. Snow mechanics and avalanche formation: Field experiments on the dynamic response of snow cover. *Surveys of Geophysics*, 16(5-6), 621-633.

Schweizer, J. and T. Wiesinger. 2001. Snow profile interpretation for stability evaluation. *Cold Regions Science and Technology*, 33, 179-188.

Schweizer, J. and J. B. Jamieson. 2002. Contrasting stable and unstable snow profiles with respect to skier loading. *Proceedings of 2002 International Snow Science Workshop,* Penticton, BC, Canada.

Schweizer, J. and J. B. Jamieson. 2003. Snowpack properties for snow profile analysis. *Cold Regions Science and Technology,* 37, 233-241.

Schweizer, J., J. B. Jamieson and M. Schneebeli. 2003. Snow avalanche formation. *Reviews of Geophysics*, 41, 4 / 1016 2003, 1-25.

Sommerfeld, R. A., R. M. King and F. Budding. 1976. A correction factor for Roch's stability index of slab avalanche release. *Journal of Glaciology*, 17(75), 145-147.

Spiegel, M. R., and L. J. Stephens. 1999. *Schaum's Outline of Theory and Problems of Statistics. Schaum's Outline Series.* McGraw-Hill, New York, New York, USA, 538 pp.

Stewart, W. K. 2002. Spatial variability of slab stability within avalanche starting zones. M.Sc. Thesis, Dept. of Geology and Geophysics, University of Calgary, Calgary, Alberta, Canada, 100 pp.

Stoffel, A., R. Meister and J. Schweizer. 1998. Spatial characteristics of avalanche activity in an alpine valley – a GIS approach. *Annals of glaciology*, 26, 329-336.

Takeuchi, Y., Y. Nohguchi, K. Kawashima and K. Izumi. 1998. Measurement of snow-hardness distribution. *Annals of Glaciology*, 26, 27-30.

Toft, M., and J. Wakeling. 2002. Re-evaluating the rutschblock. *ACC Safety Committee Technical Report*, not published.

van Herwijnen, A. F. G. and B. Jamieson. 2003. An update on fracture character in stability tests. *Avalanche News 66*, Canadian Avalanche Association, 26-28.

van Herwijnen, A. F. G. In prep. Ph. D. thesis, Dept. of Civil Engineering, University of Calgary, Calgary, Alberta, Canada.

Walpole, R. E., R. H. Myers, S. L. Myers and K. Ye. 2002. *Probability and Statistics for Engineers and Scientists, Seventh Edition*. Prentice Hall, Upper Saddle River, New Jersey, USA, 730 pp.

Appendix A - Arrays

A.1 Introduction

Sections A.2 and A.3 contain graphs of rutschblock test arrays and propagation test arrays respectively. Example arrays covered in Section 4.6 and Section 5.7 are not included in this appendix. RB score is plotted for the rutschblock tests arrays and DHE is plotted for the propagation test arrays. The primary failure planes for all arrays are marked on the profiles in Appendix B.

A.2 Rutschblock test arrays

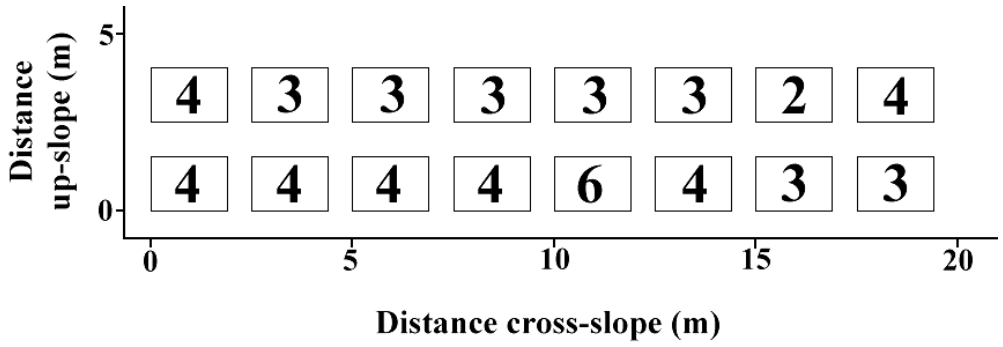

Figure A.1 – Rutschblock scores for the array performed at South Run on 2002-12-17.

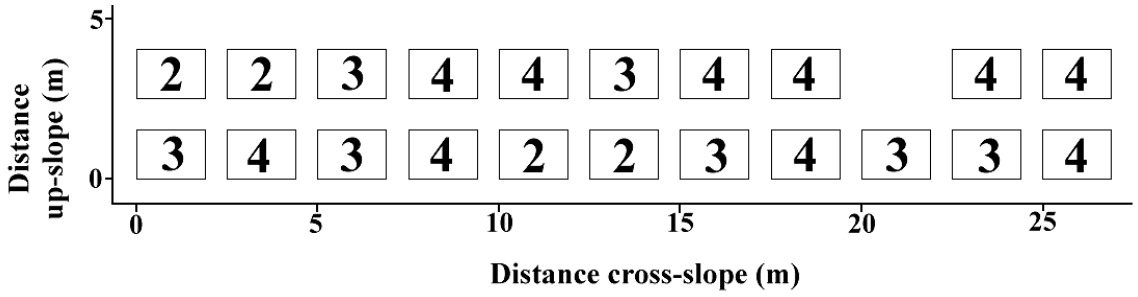

Figure A.2 – Rutschblock scores for the array performed at Bears Den on 2003-01-03.

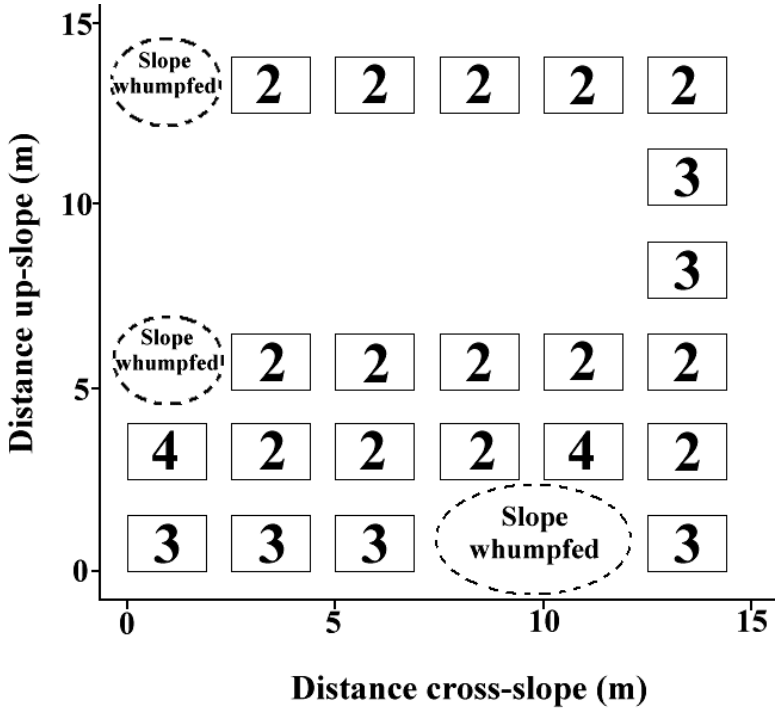

Figure A.3 – Rutschblock scores for the array performed at South Run on 2003-01-03.

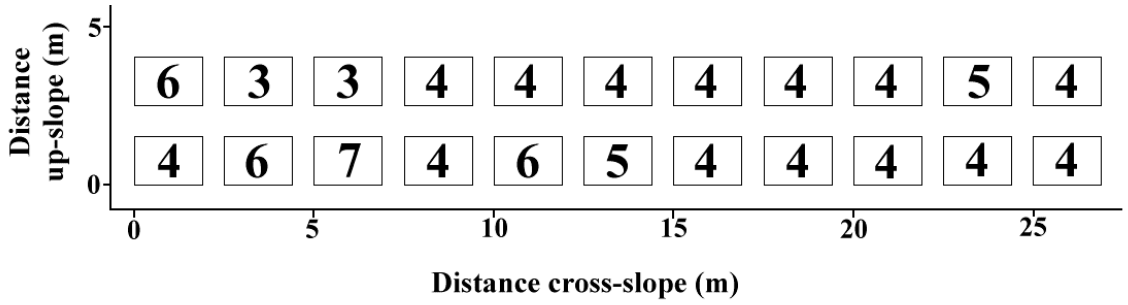

Figure A.4 – Rutschblock scores for the array performed at Poetry Slopes on 2003-01-07.

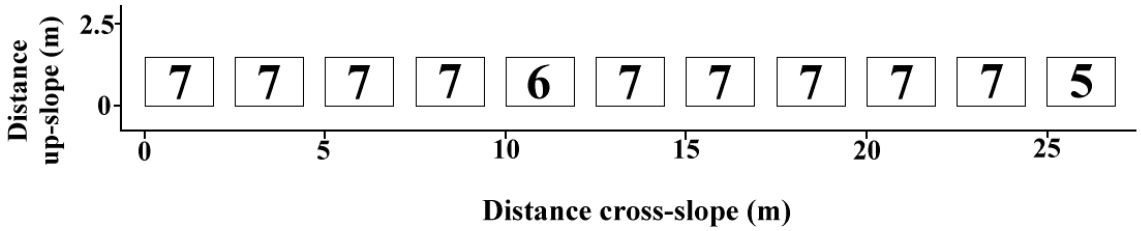

Figure A.5 – Rutschblock scores for the array performed at Robson View on 2003-01-16.

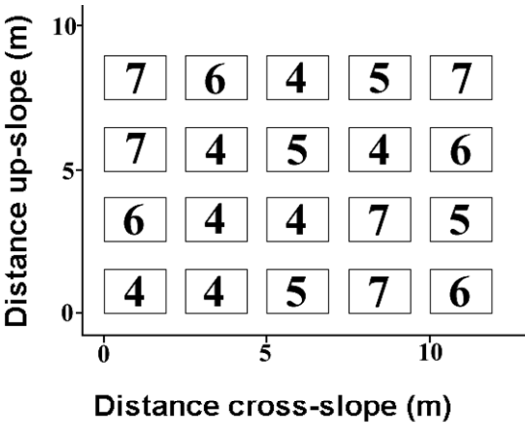

Figure A.6 – Rutschblock scores for the array performed at Cheops Bench on 2003-01-20.

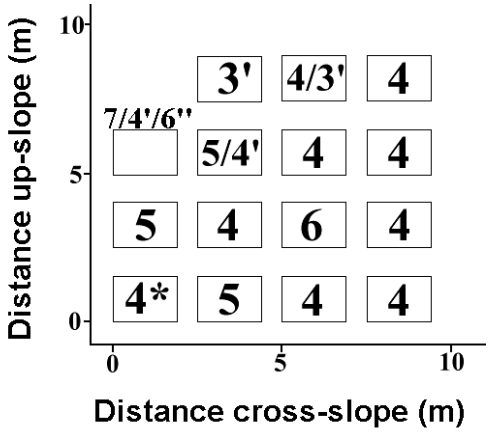

*Figure A.7 – Rutschblock scores for the array performed at South Run on 2003-01-30. Tests with secondary fractures down 30 cm (~ 15 cm in profile) are marked with '. Secondary fractures down 50 cm (~ 30 cm in profile) are marked with ". Secondary fractures down 75 cm are marked with *.*

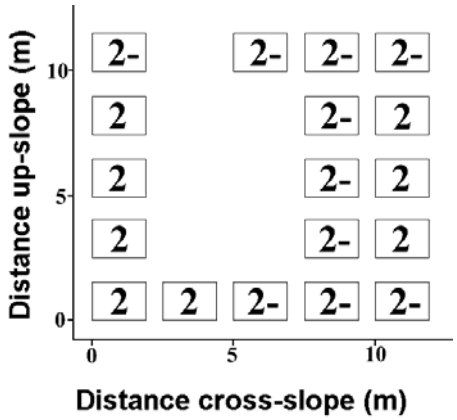

Figure A.8 – Rutschblock scores for the array performed at Fidelity on 2003-02-21. Tests marked with 2- failed when the skier was stepping onto the block with the first ski partially weighted.

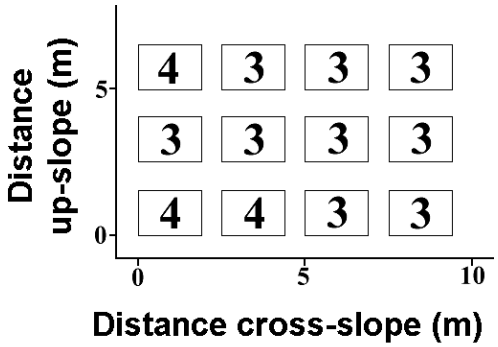

Figure A.9 – Rutschblock scores for the array performed at Grizzly Shoulder on 2003-02-25.

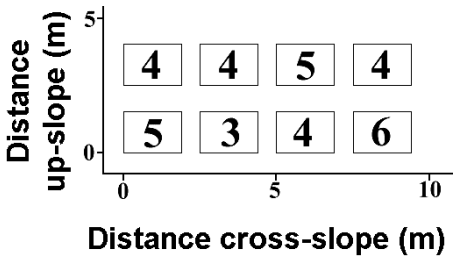

Figure A.10 – Rutschblock scores for the array performed at Poetry Slopes on 2003-03-05a.

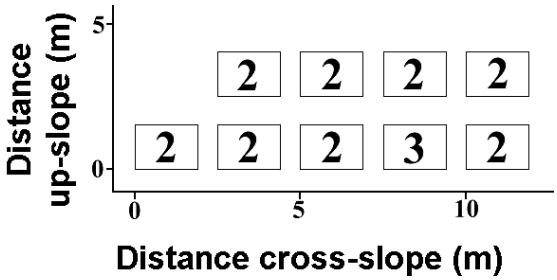

Figure A.11 – Rutschblock scores for the array performed at Poetry Slopes on 2003-03-05b.

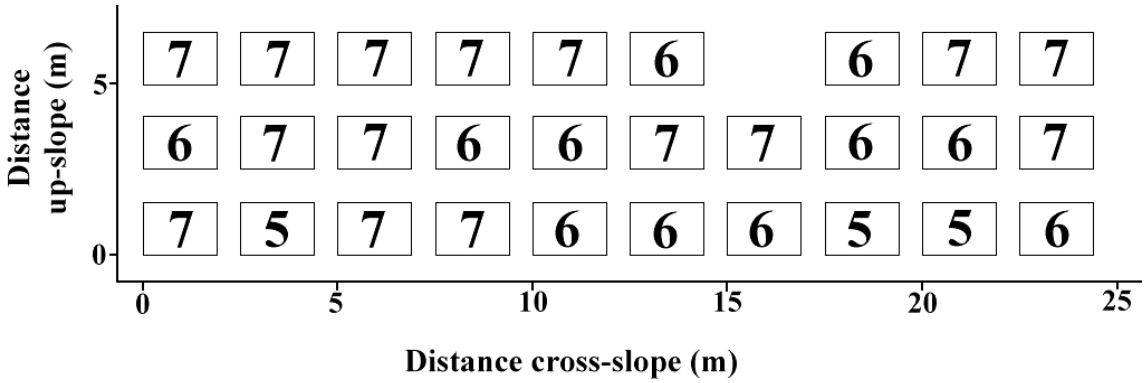

Figure A.12 – Rutschblock scores for the array performed at Robson View on 2003-03-05.

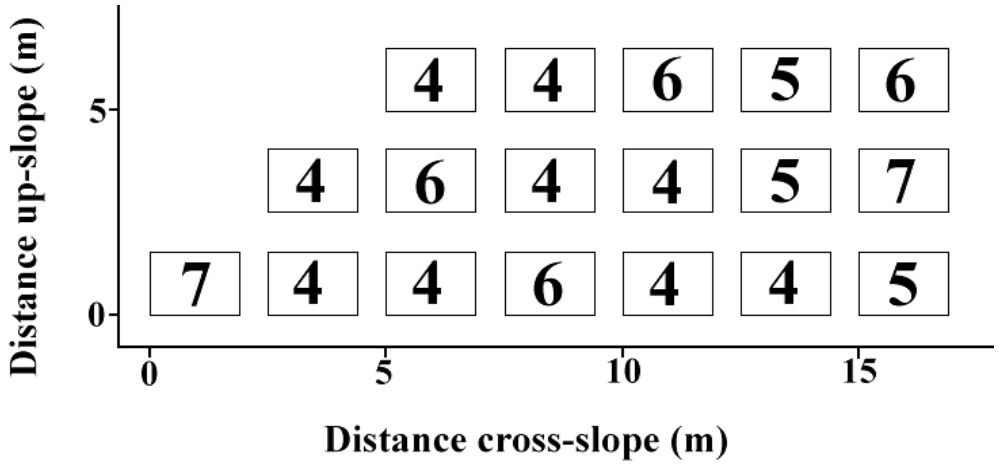

Figure A.13 – Rutschblock scores for the array performed at Waikiki on 2003-03-12.

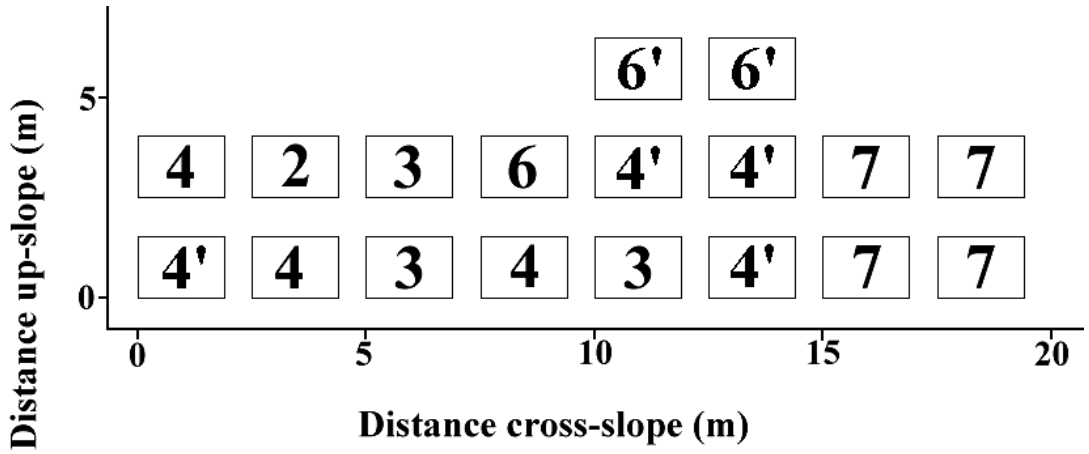

Figure A.14 – Rutschblock scores for the array performed at Toilet Bowl on 2004-01-17. A thin crust was found within the depth hoar weak layer for tests marked with '.

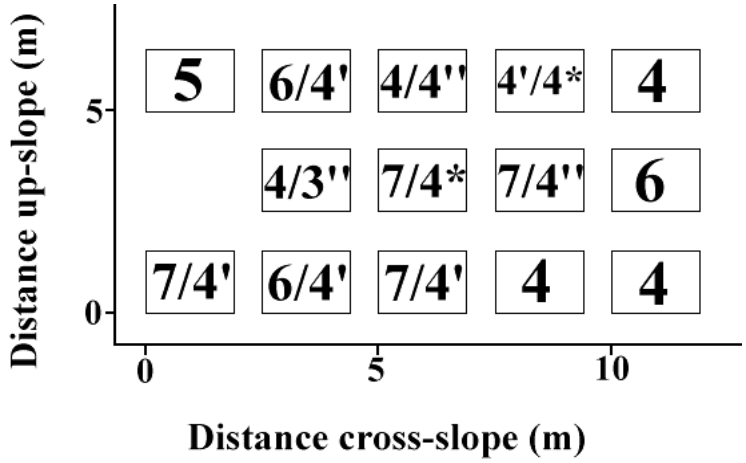

*Figure A.15 – Rutschblock scores for the array performed at Poetry Slopes on 2004-02-02. Tests with secondary fractures down 40 cm (~ 35 cm in profile) are marked with '. Secondary fractures down 54 cm (~ 60 cm in profile) are marked with ". Secondary fractures down 97 cm are marked with *.*

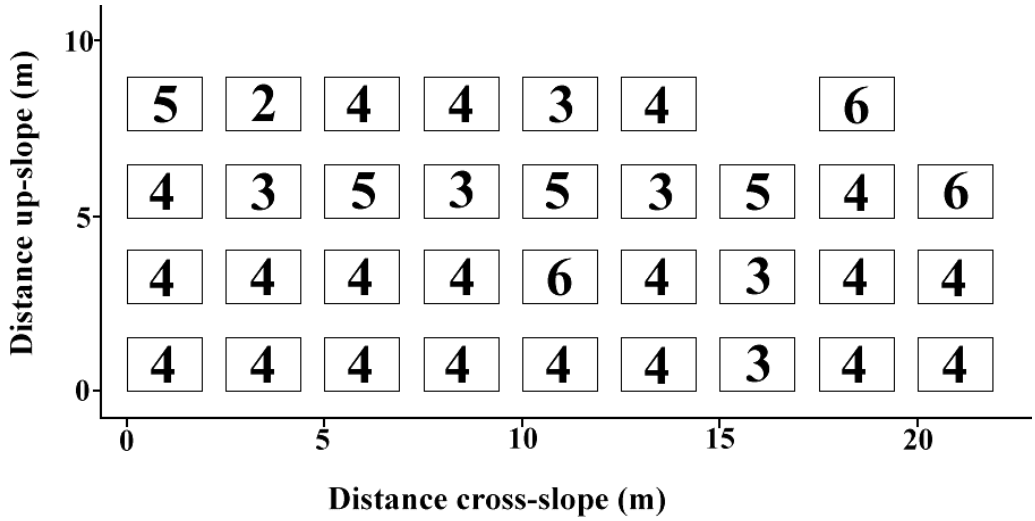

Figure A.16 – Rutschblock scores for the array performed at Langevin Cutblock on 2004-02-12.

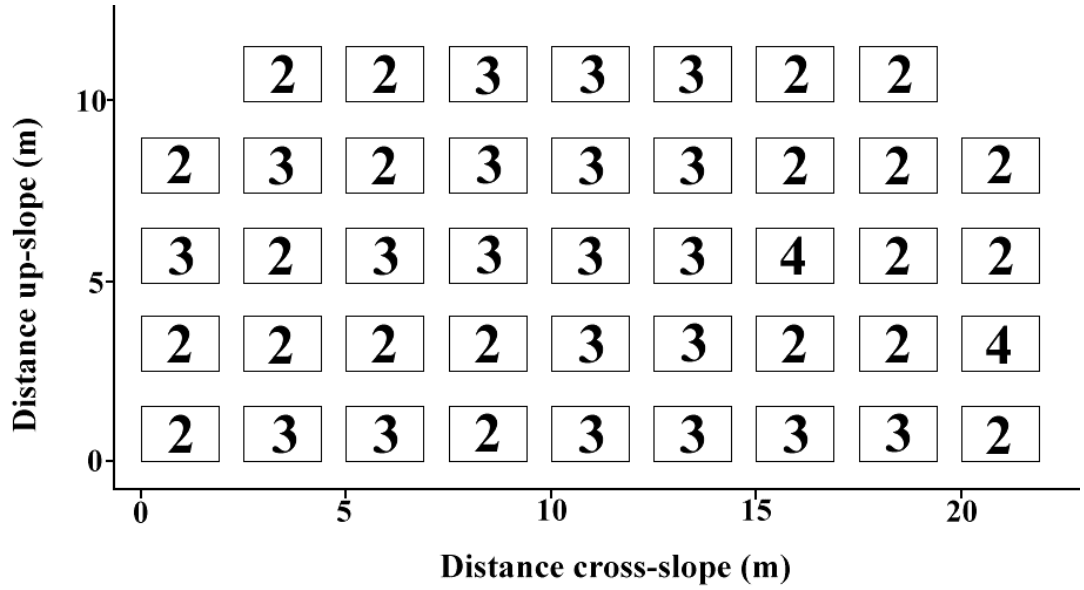

Figure A.17 – Rutschblock scores for the array performed at Robson View on 2004-02-25.

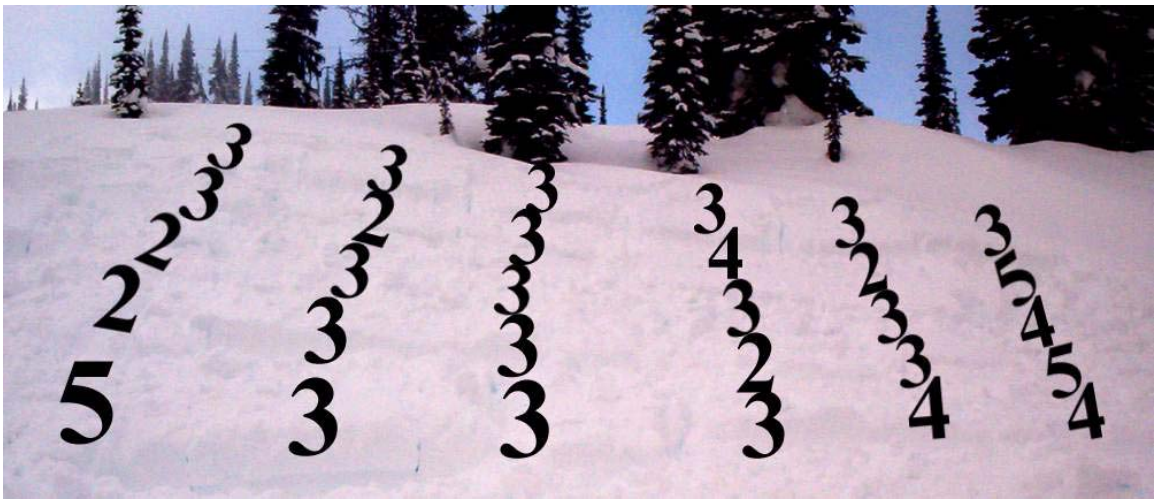

Figure A.18 – Rutschblock scores for the array performed at Poetry Slopes on 2004-02-28.

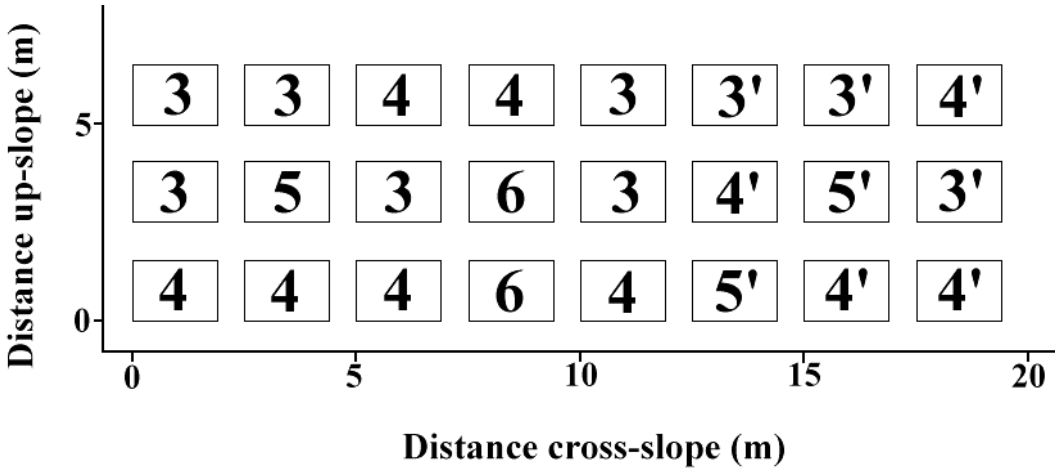

Figure A.19 – Rutschblock scores for the array performed at Squirrel Slope on 2004-03-03. A crust was found below the surface hoar weak layer for tests marked with '.

Figure A.20 – Rutschblock scores for the array performed at Mt. St. Anne on 2004-03-10.

Figure A.21 – Rutschblock scores for the arrays performed at Bears Den on 2004-03-11. Array (a) is on the right side and array (b) is on the left side.

Figure A.22 – Rutschblock scores for the arrays performed at Schuss Cr. on 2004-03-21. Array (a) is on the right side and array (b) is on the left side of gully.

A.3 Propagation test arrays

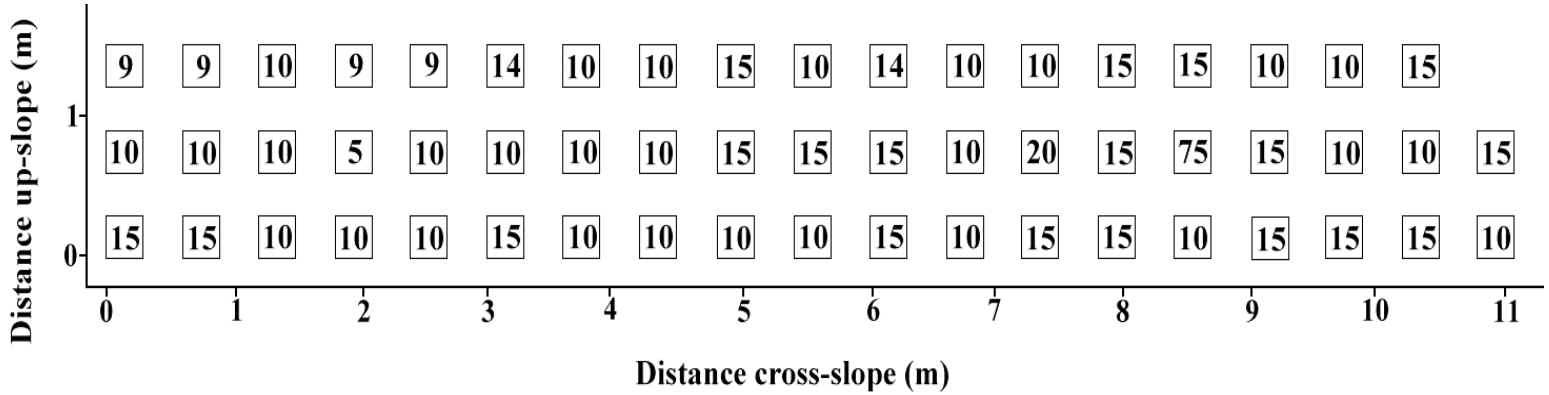

Figure A.23 – DHE for propagation test array performed at Poetry Slopes on 2003-01-06.

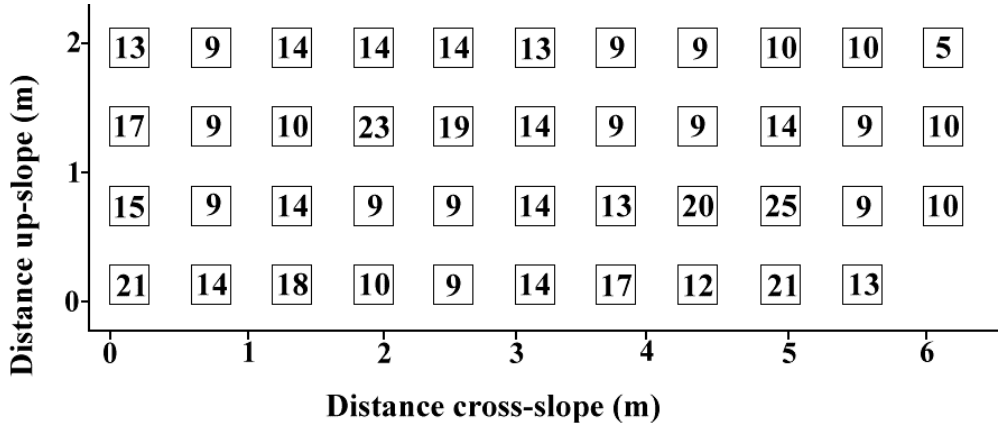

Figure A.24 – DHE for propagation test array performed at South Run on 2003-01-11.

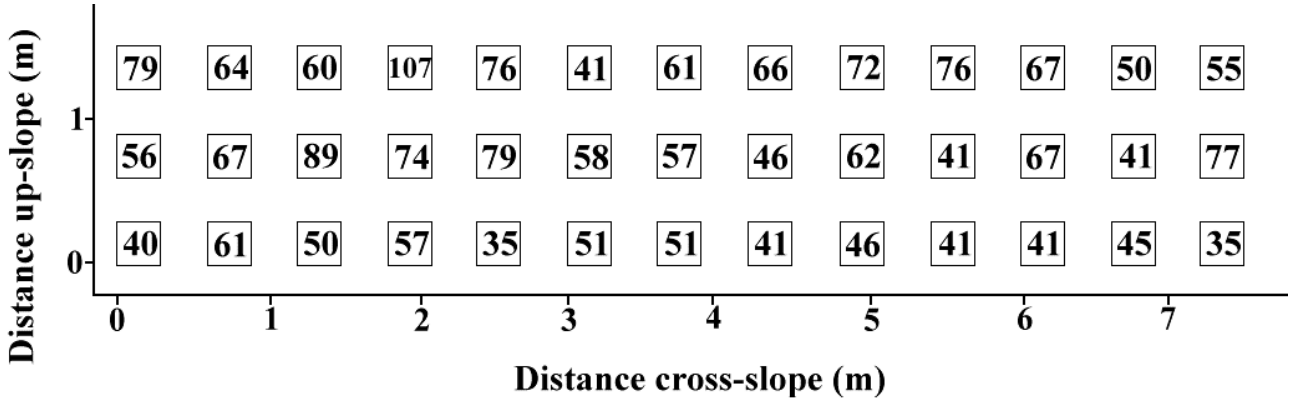

Figure A.25 – DHE for propagation test array performed at Poetry Slopes on 2003-01-24.

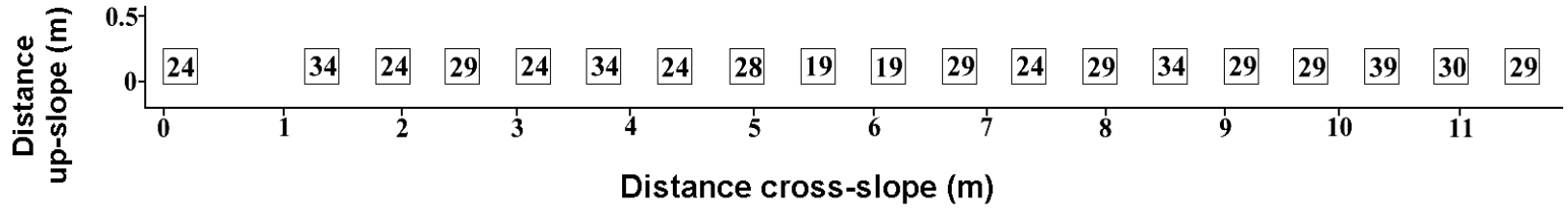

Figure A.26 – DHE for propagation test array performed at Mt. St. Anne on 2003-01-30.

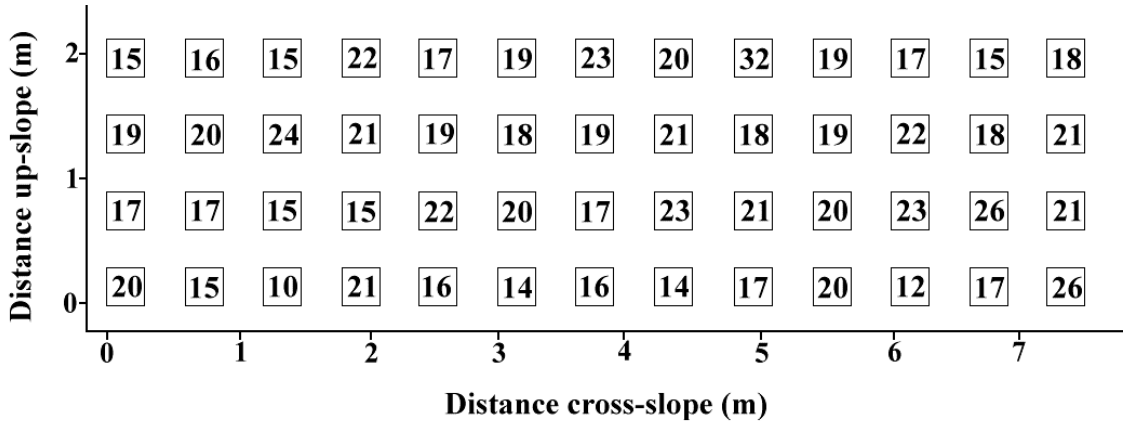

Figure A.27 – DHE for propagation test array performed at Poetry Slopes on 2003-02-03.

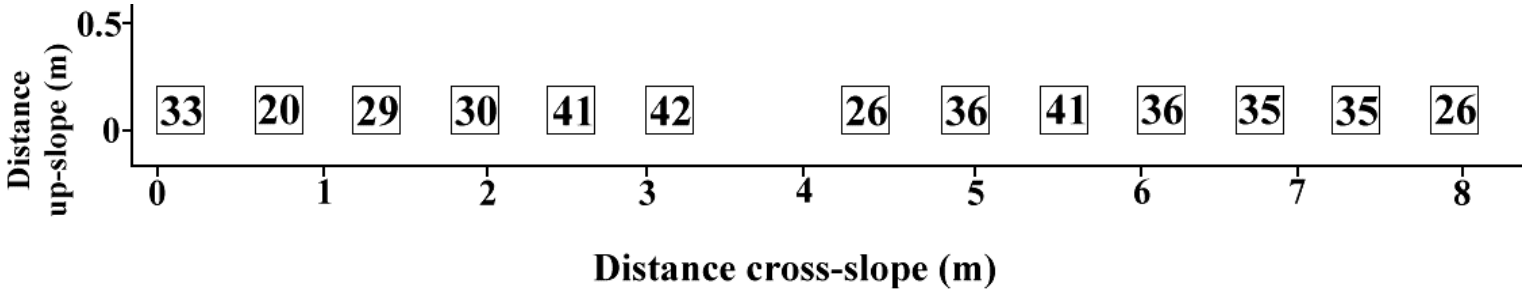

Figure A.28 – DHE for propagation test array performed at Mt. St. Anne on 2003-02-06.

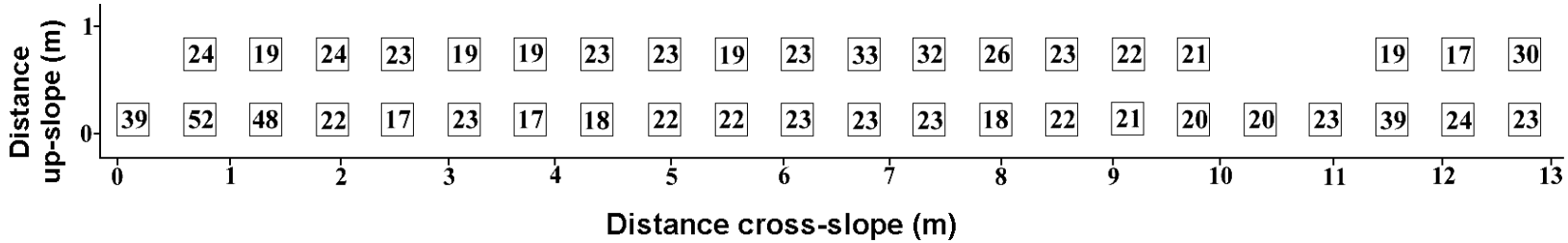

Figure A.29 – DHE for propagation test array performed at Poetry Slopes on 2003-02-06.

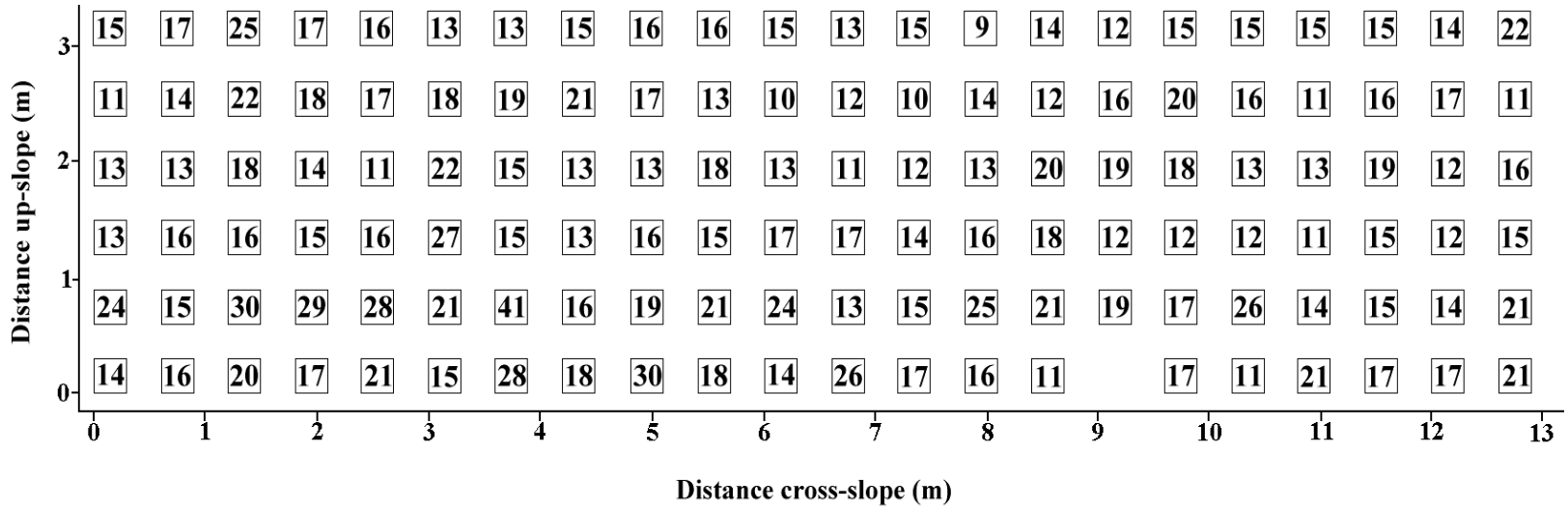

Figure A.30 – DHE for propagation test array performed at Abbott Headwall on 2003-02-10/11.

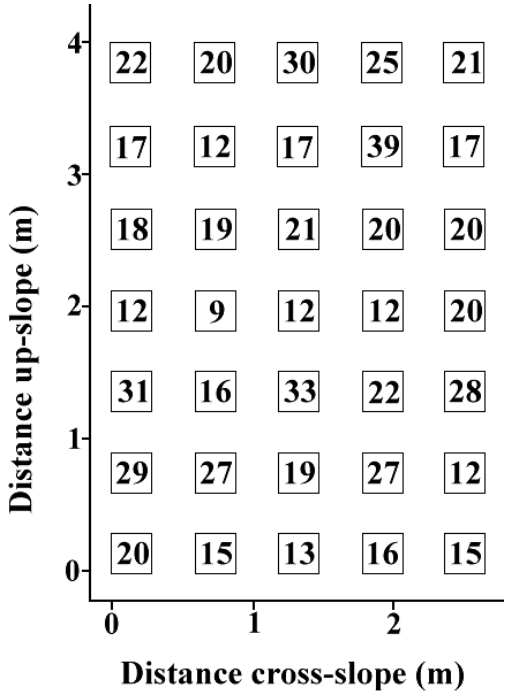

Figure A.31 – DHE for propagation test array performed at Cheops on 2003-02-13.

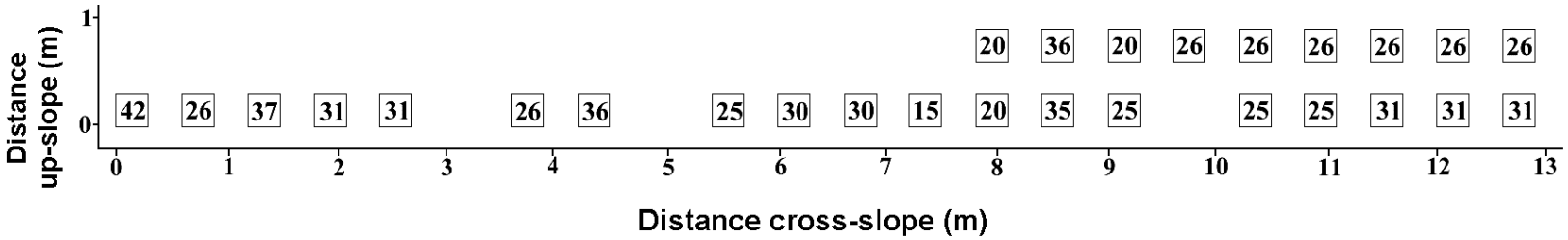

Figure A.32 – DHE for propagation test array performed at Diamond Head on 2003-02-13.

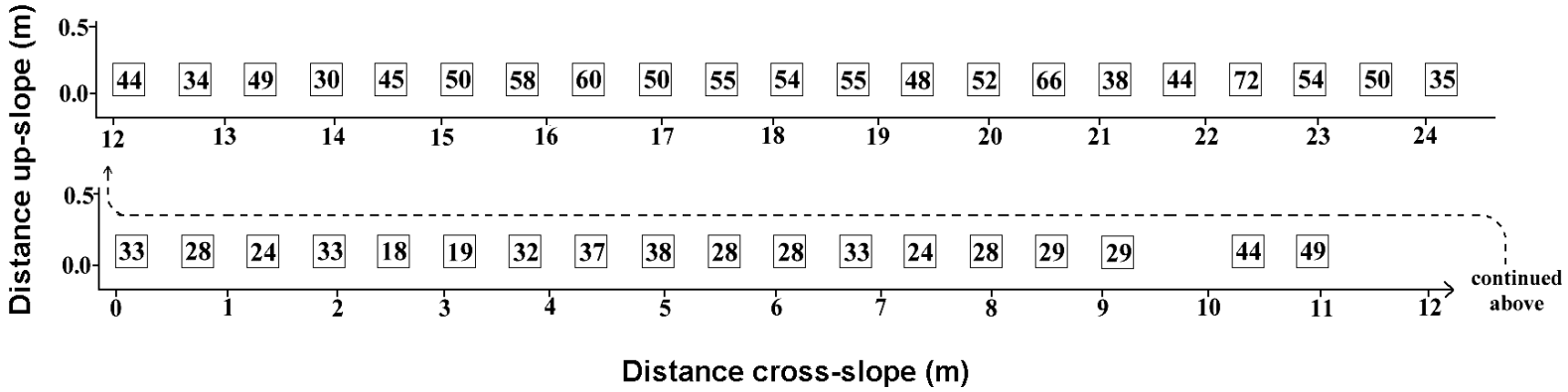

Figure A.33 – DHE for propagation test array performed at Mt. St. Anne on 2003-03-19.

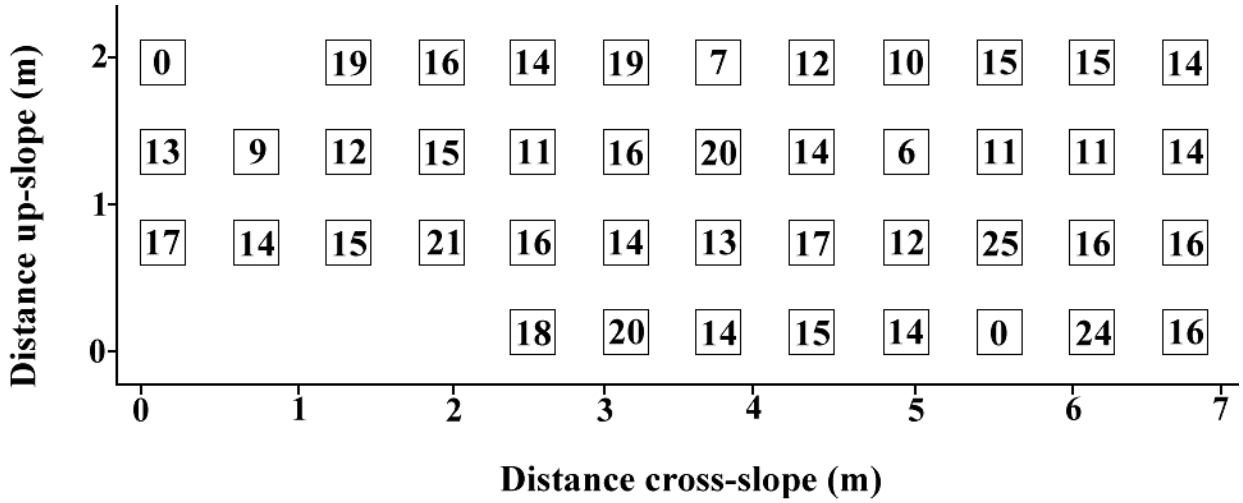

Figure A.34 – DHE for propagation test array performed at South Run on 2003-03-19.

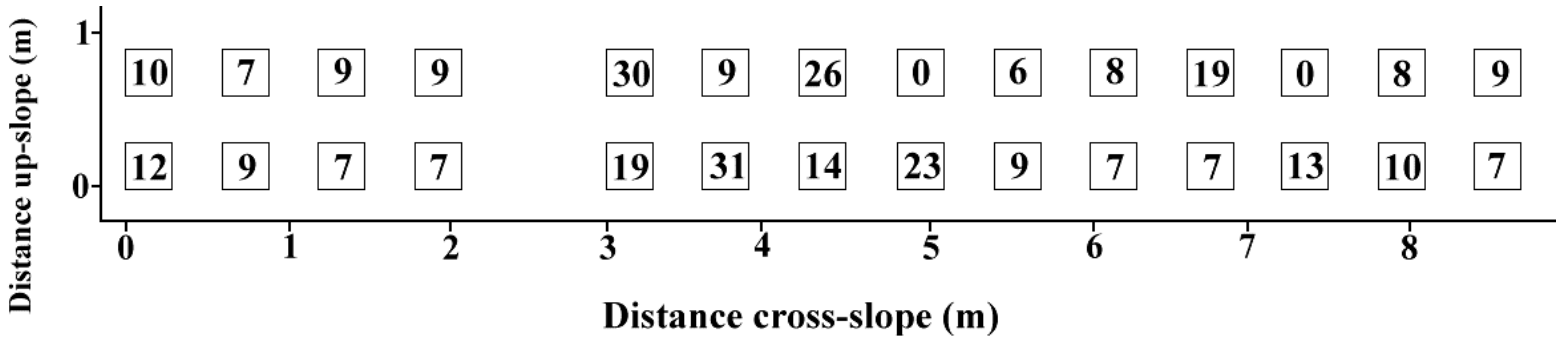

Figure A.35 – DHE for propagation test array performed at Rudy's Bowl on 2003-03-21.

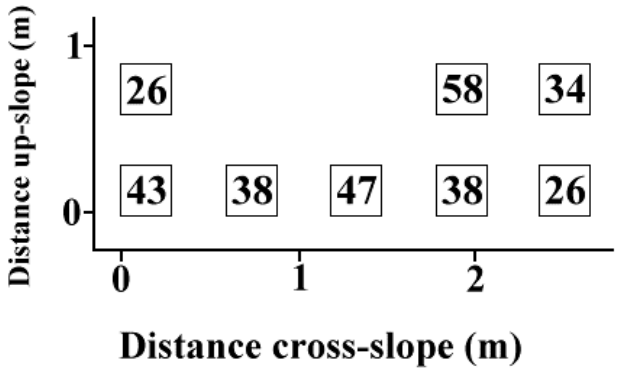

Figure A.36 – DHE for propagation test array performed at Cheops Bench on 2003-03-24.

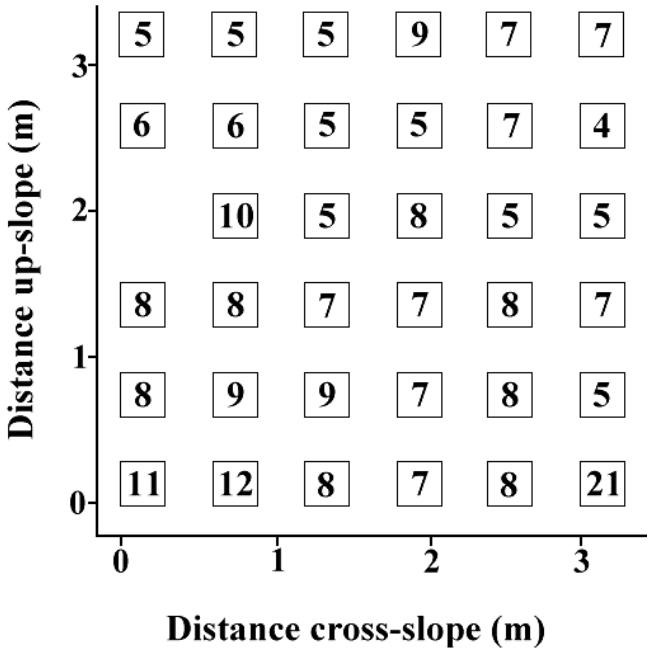

Figure A.37 – DHE for propagation test array performed at Caribou Hideout on 2003-03-26.

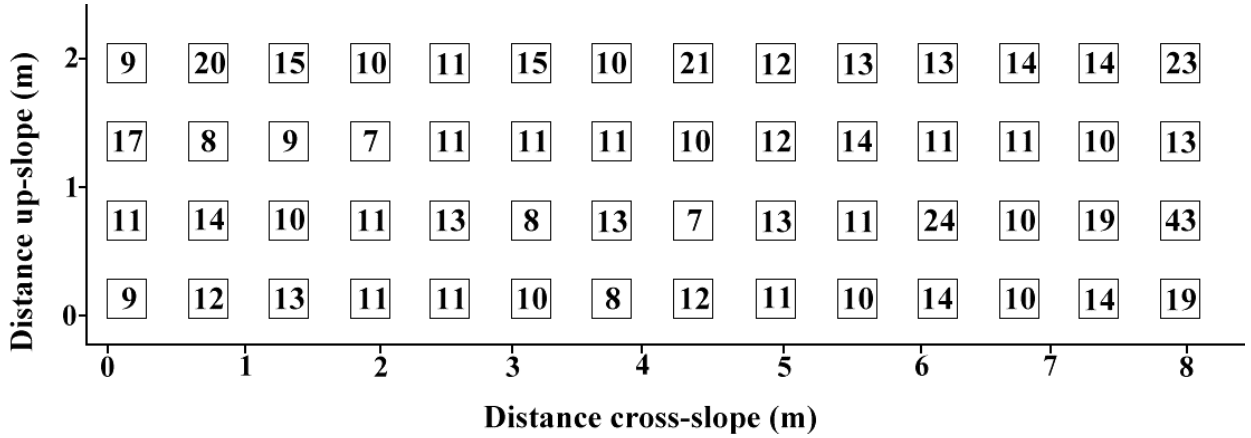

Figure A.38 – DHE for propagation test array performed at Poetry Slopes on 2004-01-19.

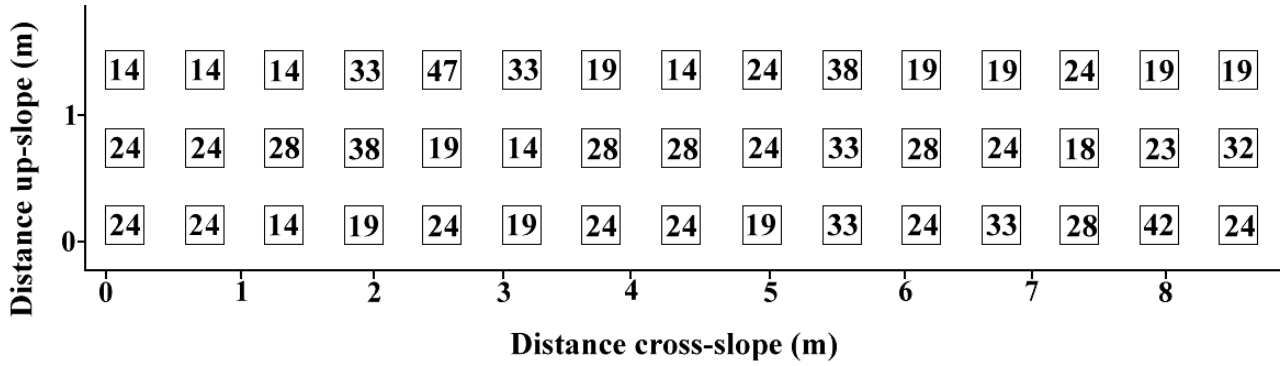

Figure A.39 – DHE for propagation test array performed at Fortitude on 2004-02-08.

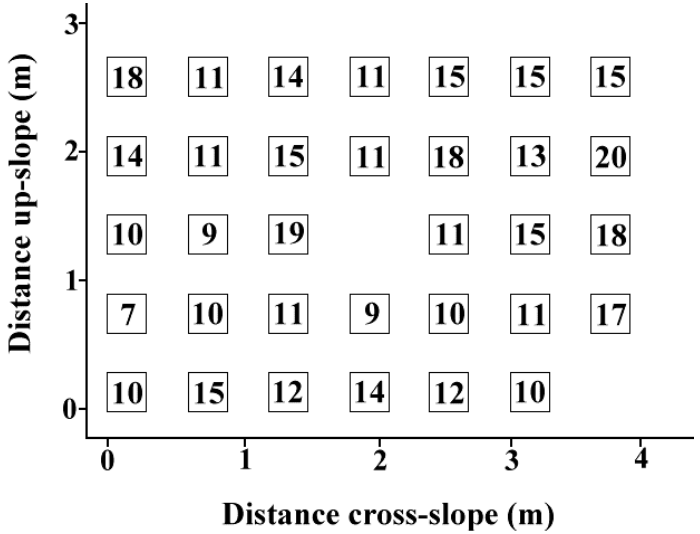

Figure A.40 – DHE for propagation test array performed at Cheops Bench on 2004-03-14.

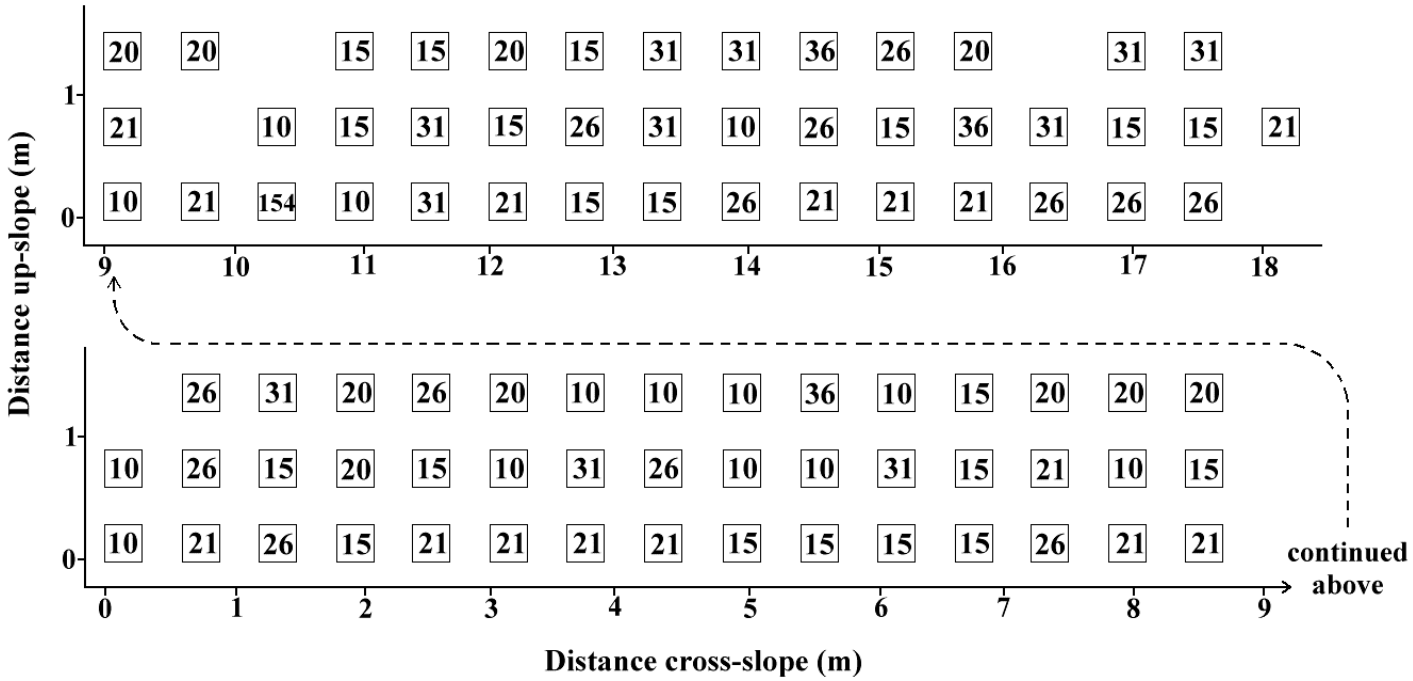

Figure A.41 – DHE for propagation test array performed at Monashee View on 2004-03-24.

Appendix B – Snow profiles

B.1 Introduction

A list of symbols used in the following profiles can be found at the beginning of this thesis. The primary failure layer for each array is marked with a large arrow pointing to the right. No snow observations were made for the rutschblock array performed at Robson View on Mount St. Anne near Blue River, on 2003-01-16 because of time constraints.

B.2 Rutschblock test arrays

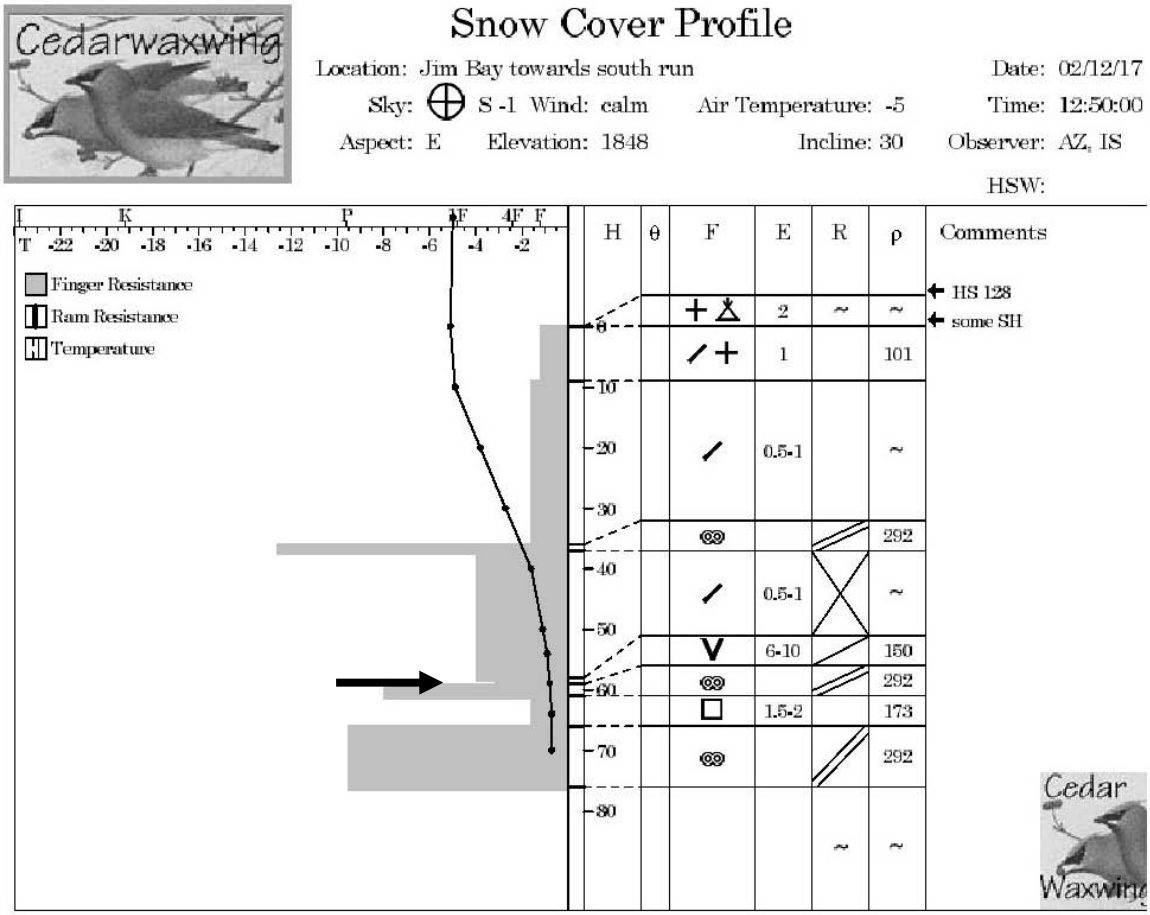

Figure B.1 – Manual snow profile for the rutschblock test array performed at South Run on Fidelity Mountain near Rogers Pass on 2002-12-17. The primary failure plane is indicated.

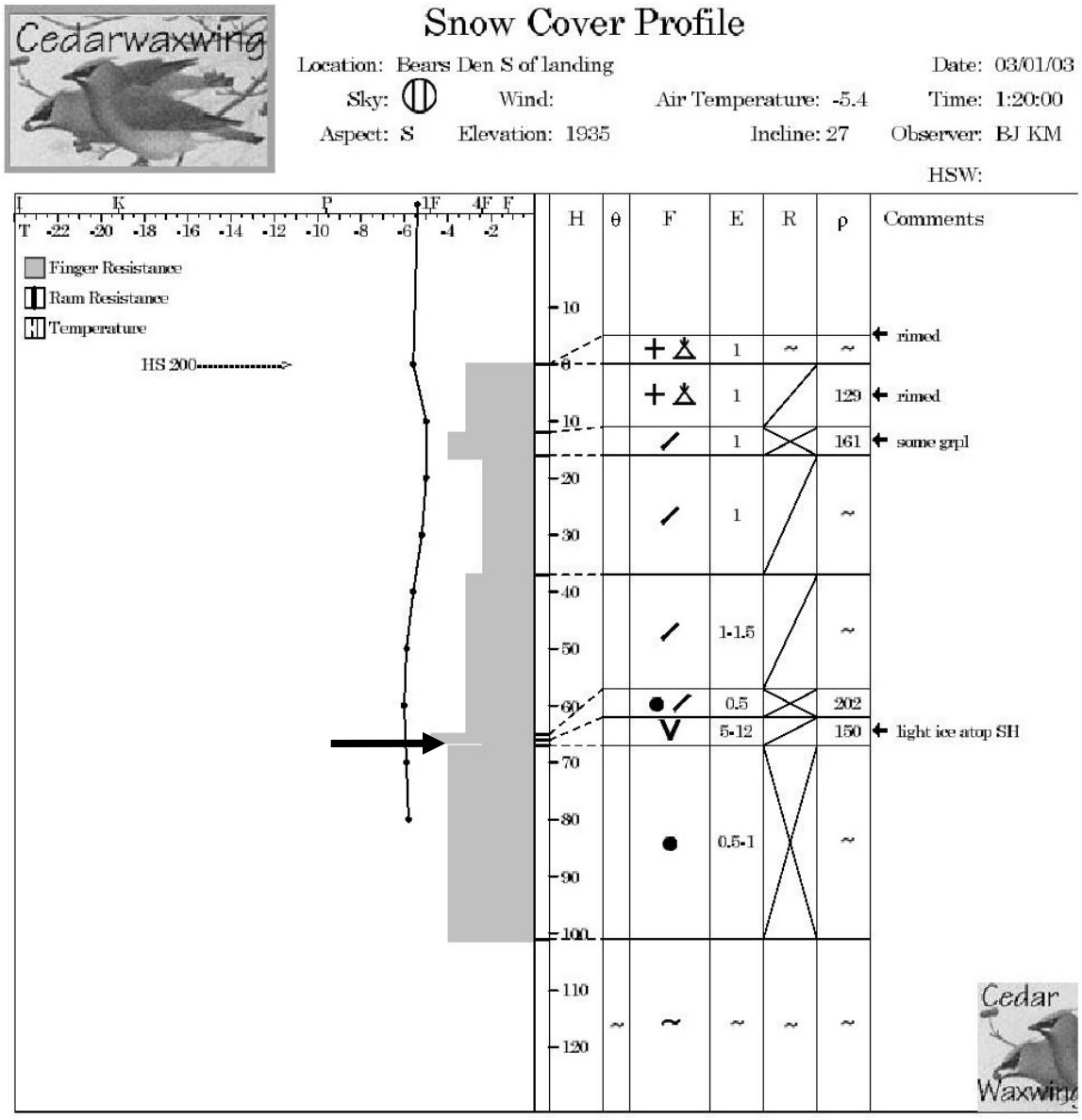

Figure B.2 – Manual snow profile for the rutschblock test array performed at Bear's Den near Blue River on 2003-01-03. The primary failure plane is indicated.

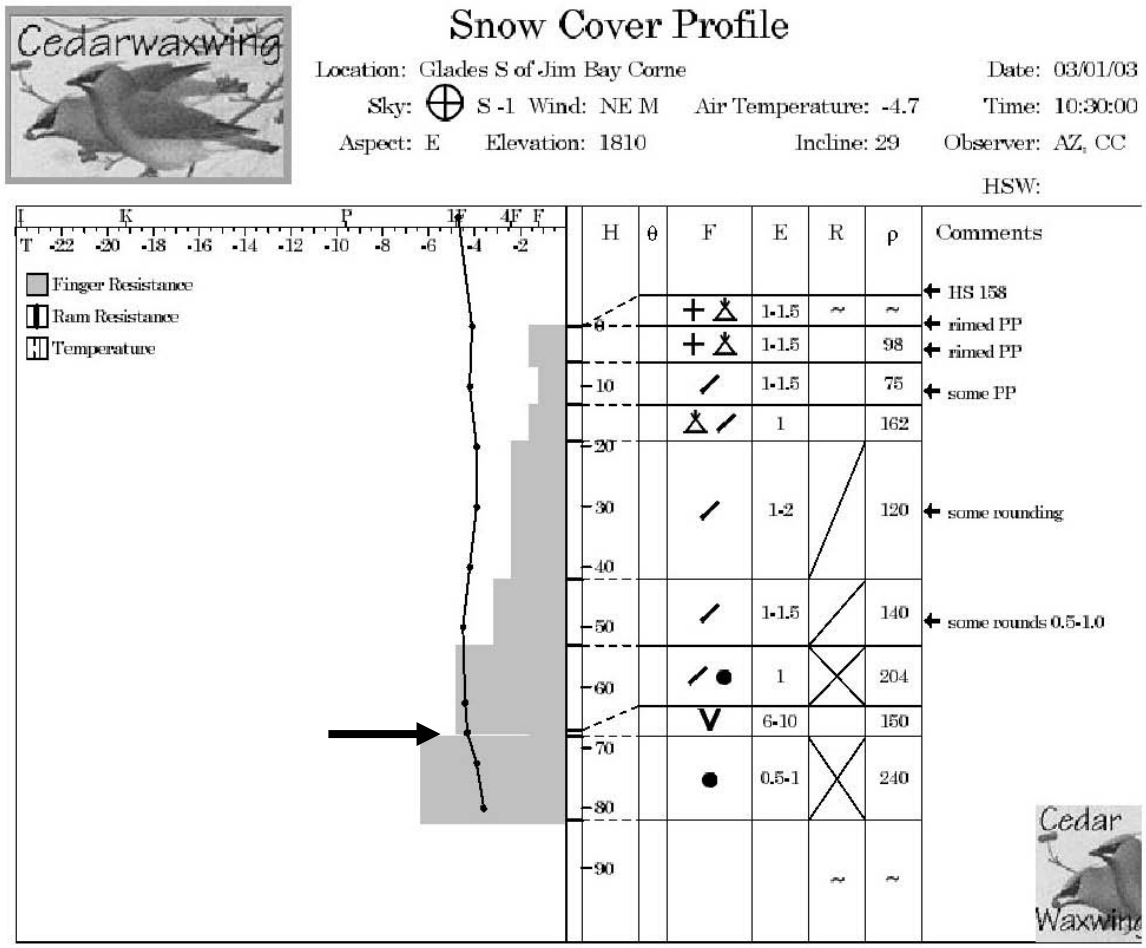

Figure B.3 – Manual snow profile for the rutschblock test array performed at South Run on Fidelity Mountain near Rogers Pass on 2003-01-03. The primary failure plane is indicated.

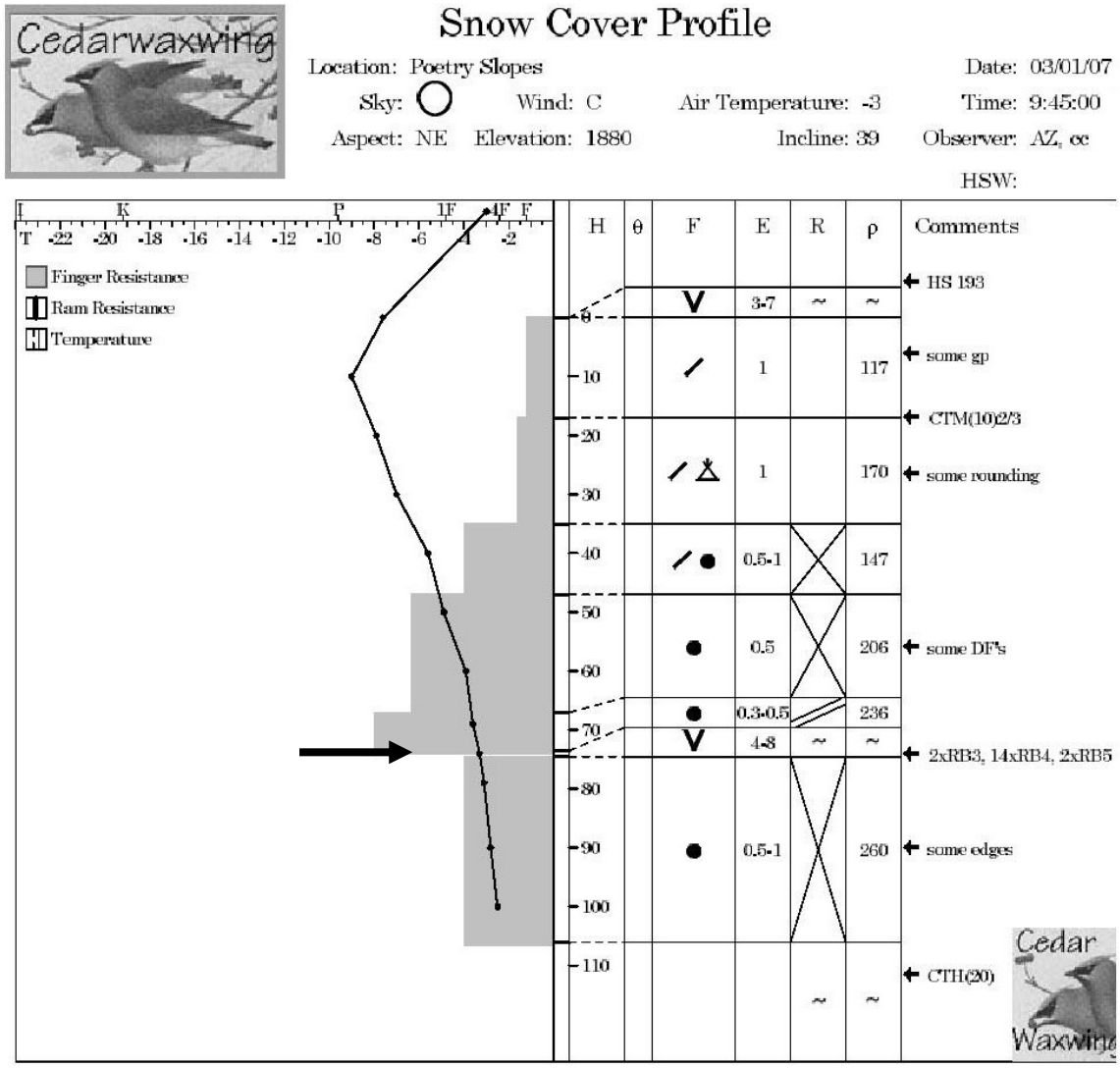

Figure B.4 – Manual snow profile for the rutschblock test array performed at the Poetry Slopes on Fidelity Mountain near Rogers Pass on 2003-01-07. The primary failure plane is indicated.

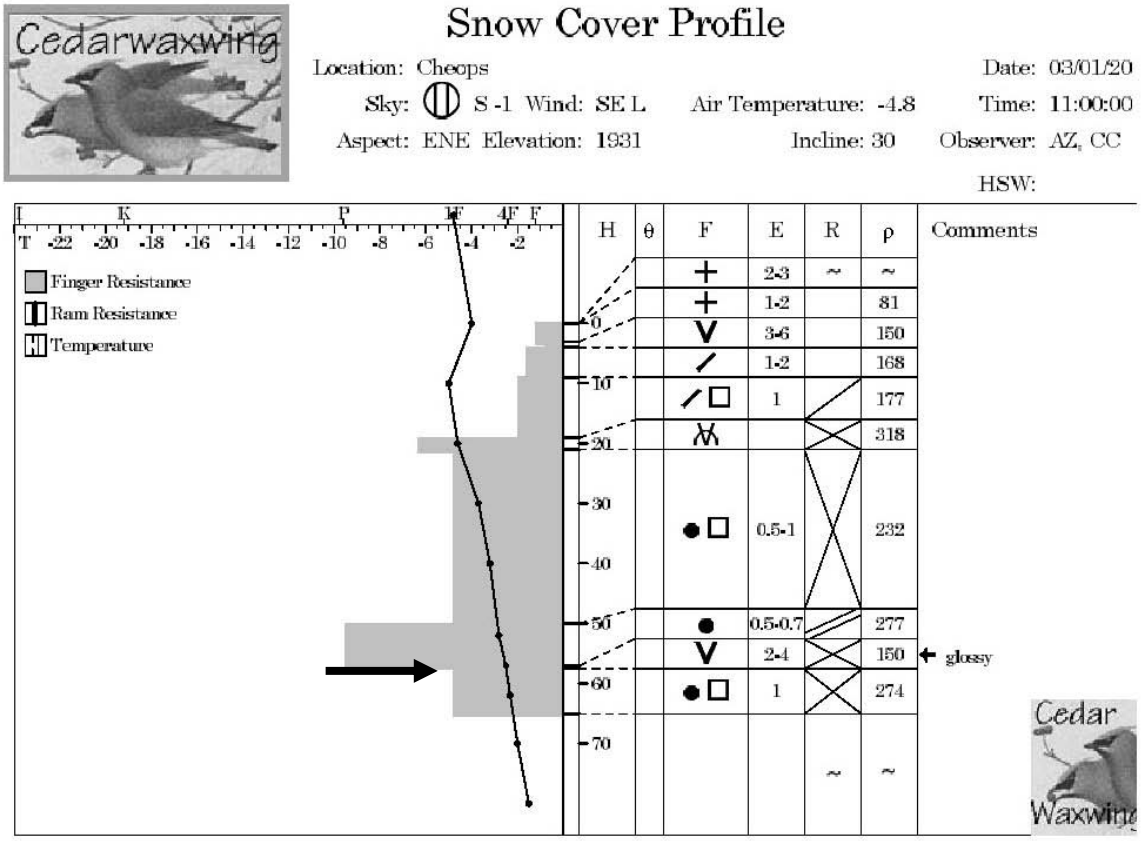

Figure B.5 – Manual snow profile for the rutschblock test array performed on Cheops Bench near Rogers Pass on 2003-01-20. The primary failure plane is indicated.

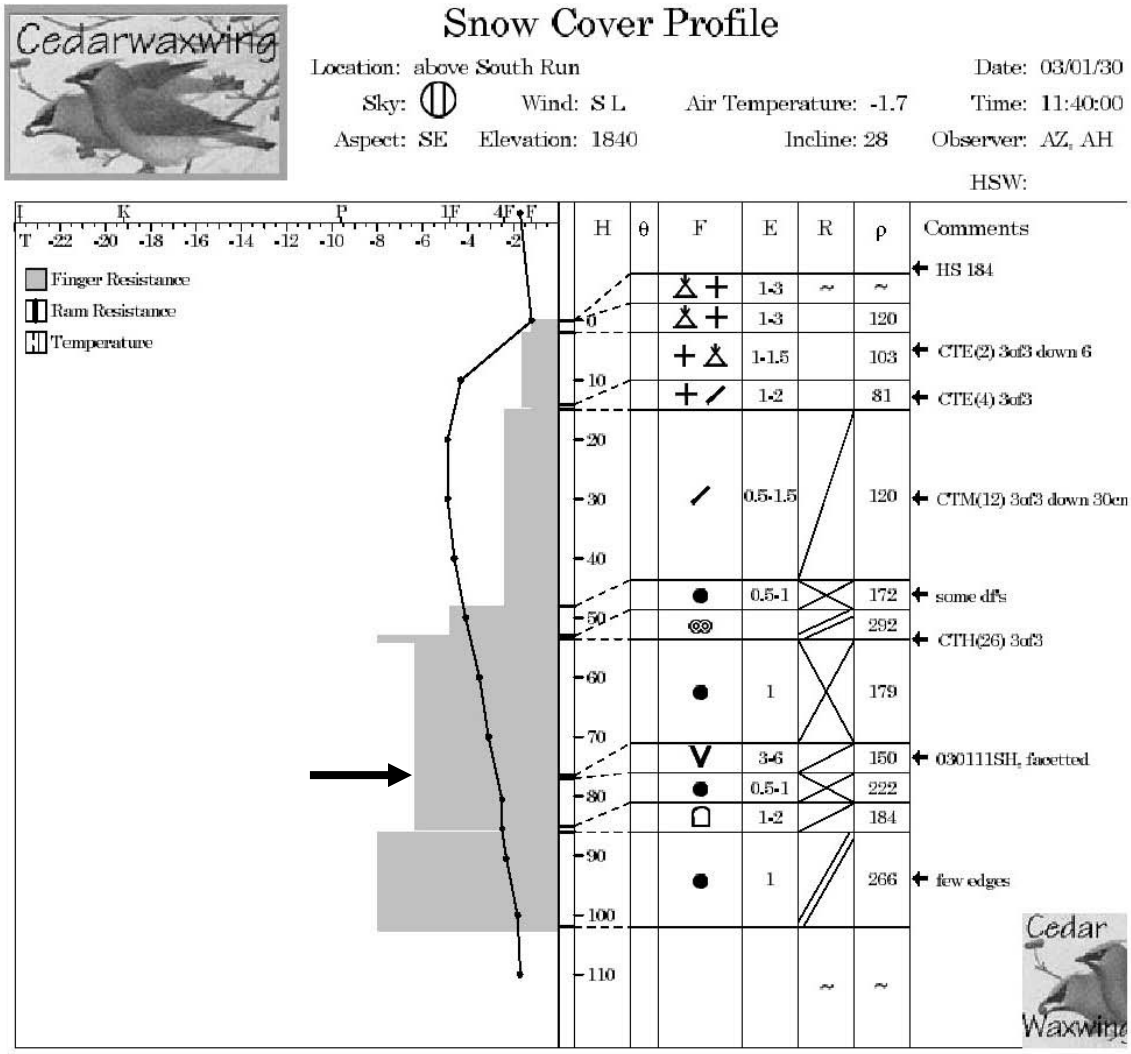

Figure B.6 – Manual snow profile for the rutschblock test array performed at South Run on Fidelity Mountain near Rogers Pass on 2003-01-30. The primary failure plane is indicated.

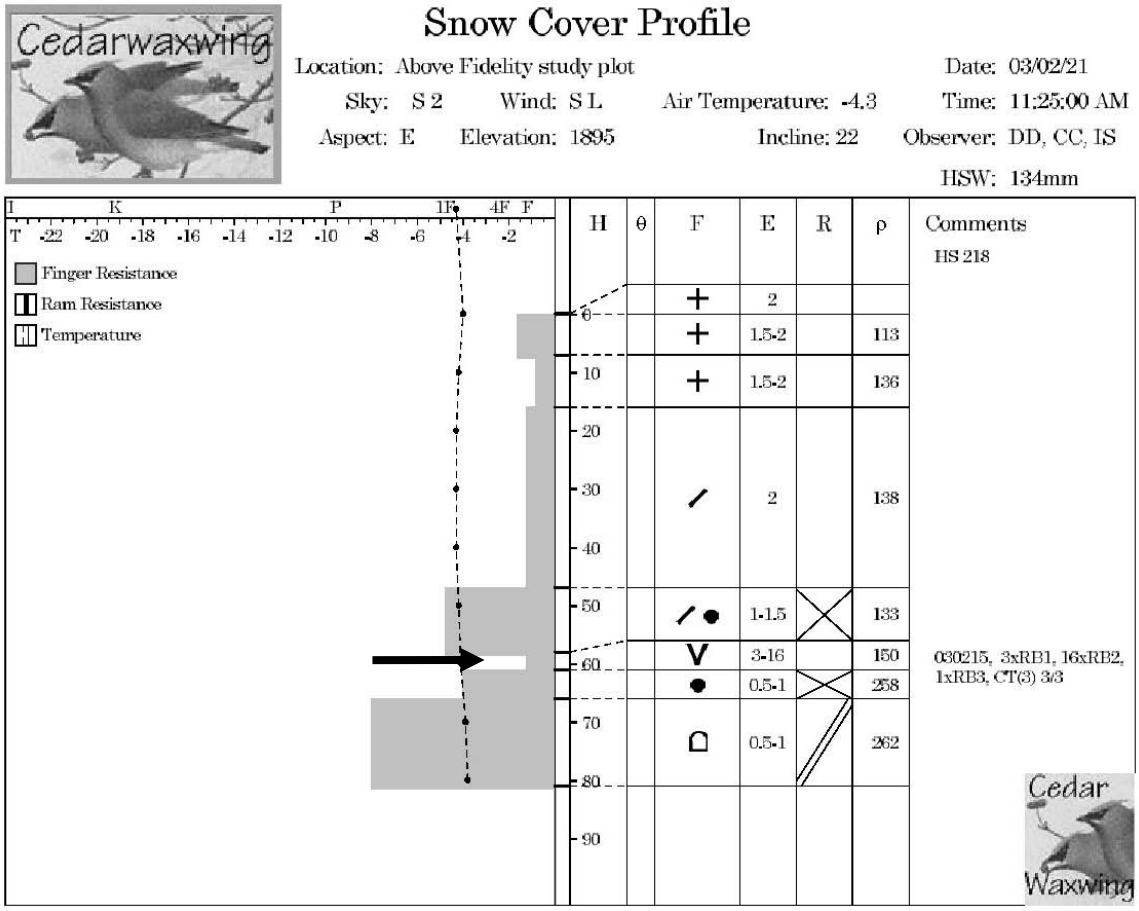

Figure B.7 – Manual snow profile for the rutschblock test array performed on Fidelity Mountain on 2003-02-21. The primary failure plane is indicated.

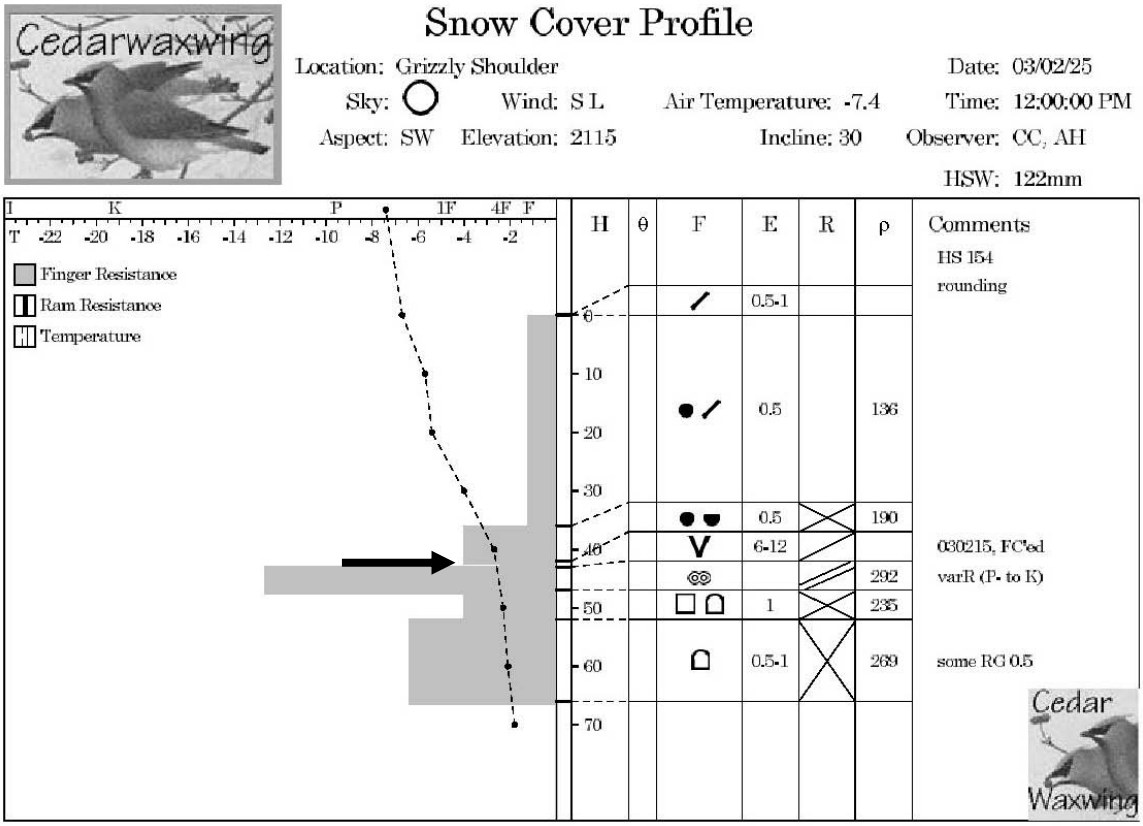

Figure B.8 – Manual snow profile for the rutschblock test array performed at Grizzly Shoulder on 2003-02-25. The primary failure plane is indicated.

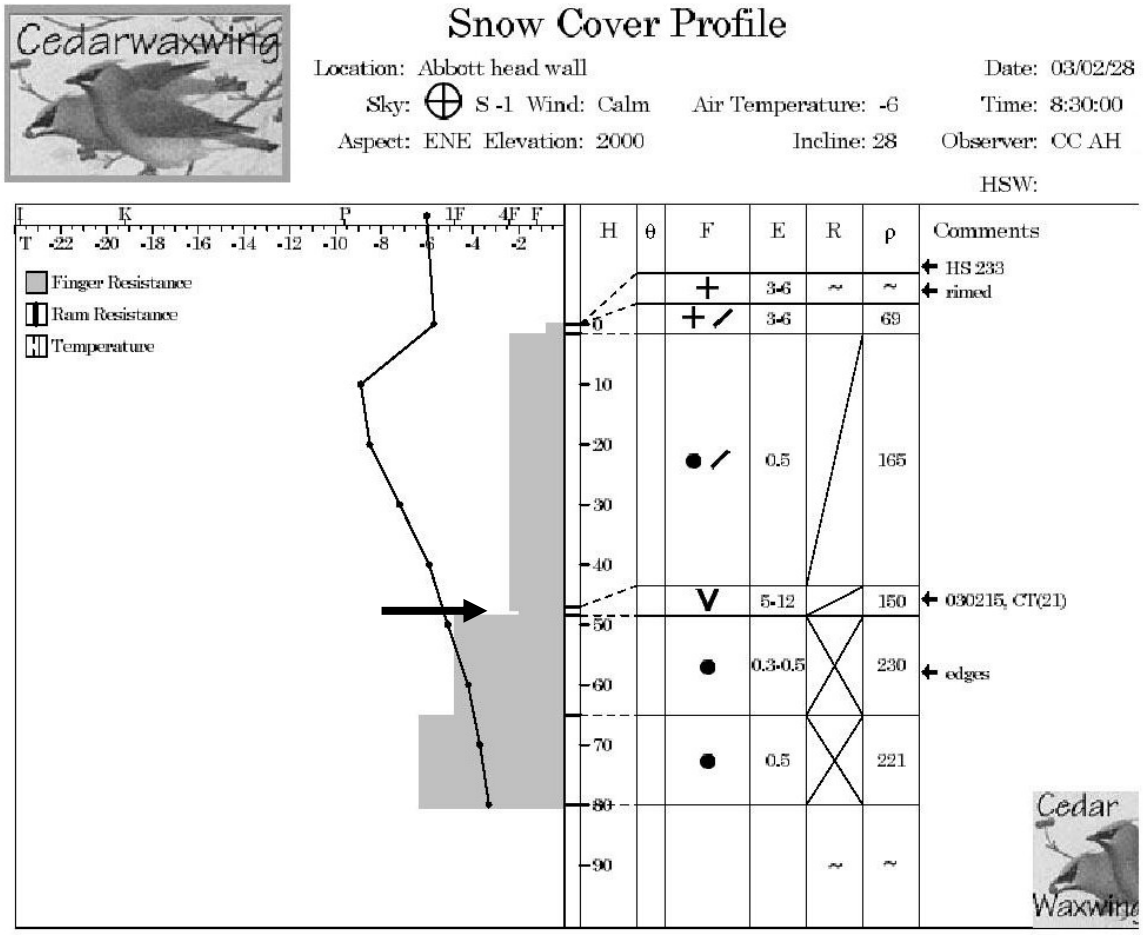

Figure B.9 – Manual snow profile for the rutschblock test array performed at the Abbott Headwall near Rogers Pass on 2003-02-27/28. The primary failure plane is indicated.

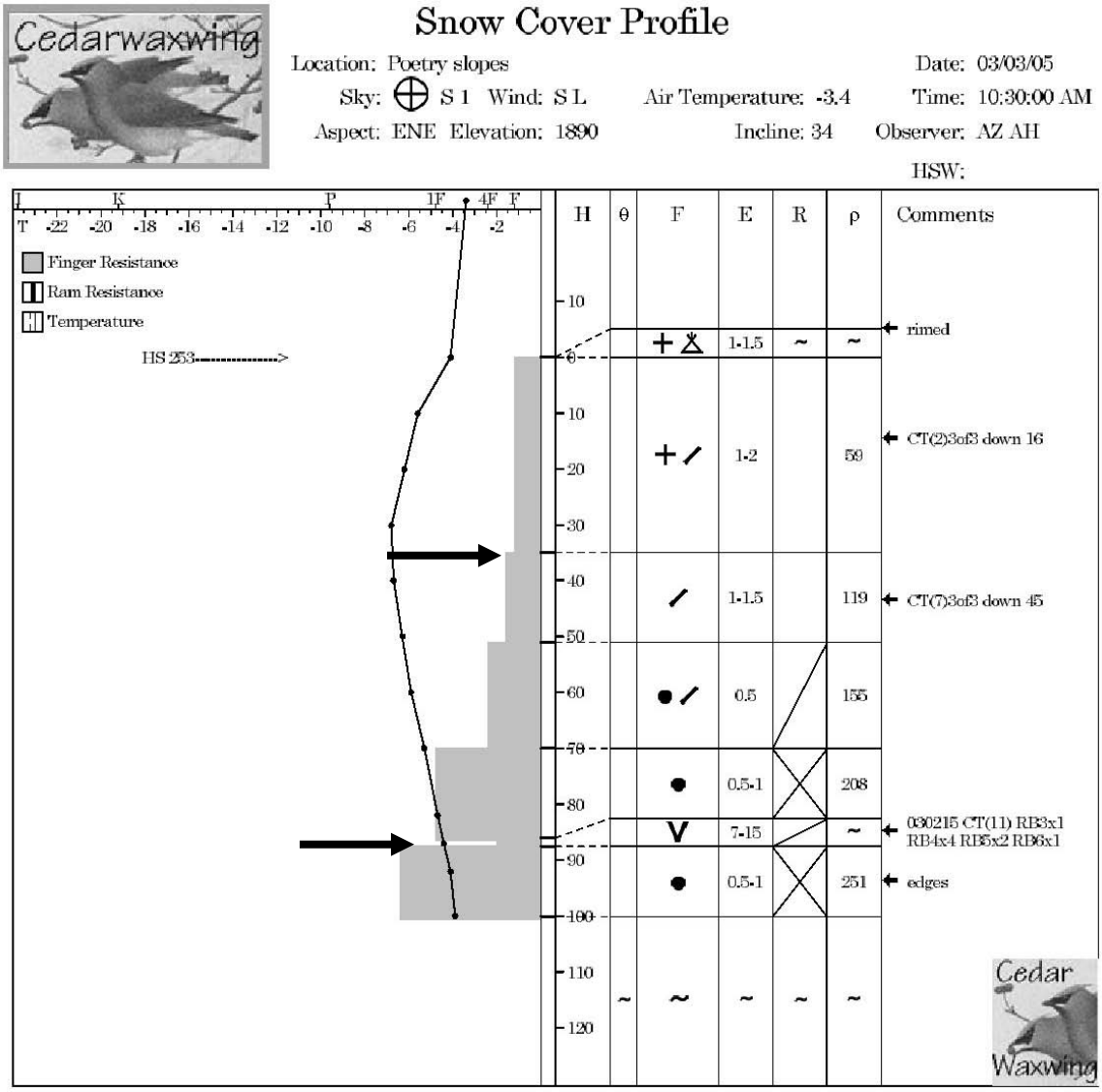

Figure B.10 – Manual snow profile for the rutschblock test array performed at the Poetry Slopes on Fidelity Mountain near Rogers Pass on 2003-03-05. Array (a) was performed on the lower failure plane and array (b) was performed on the upper failure plane.

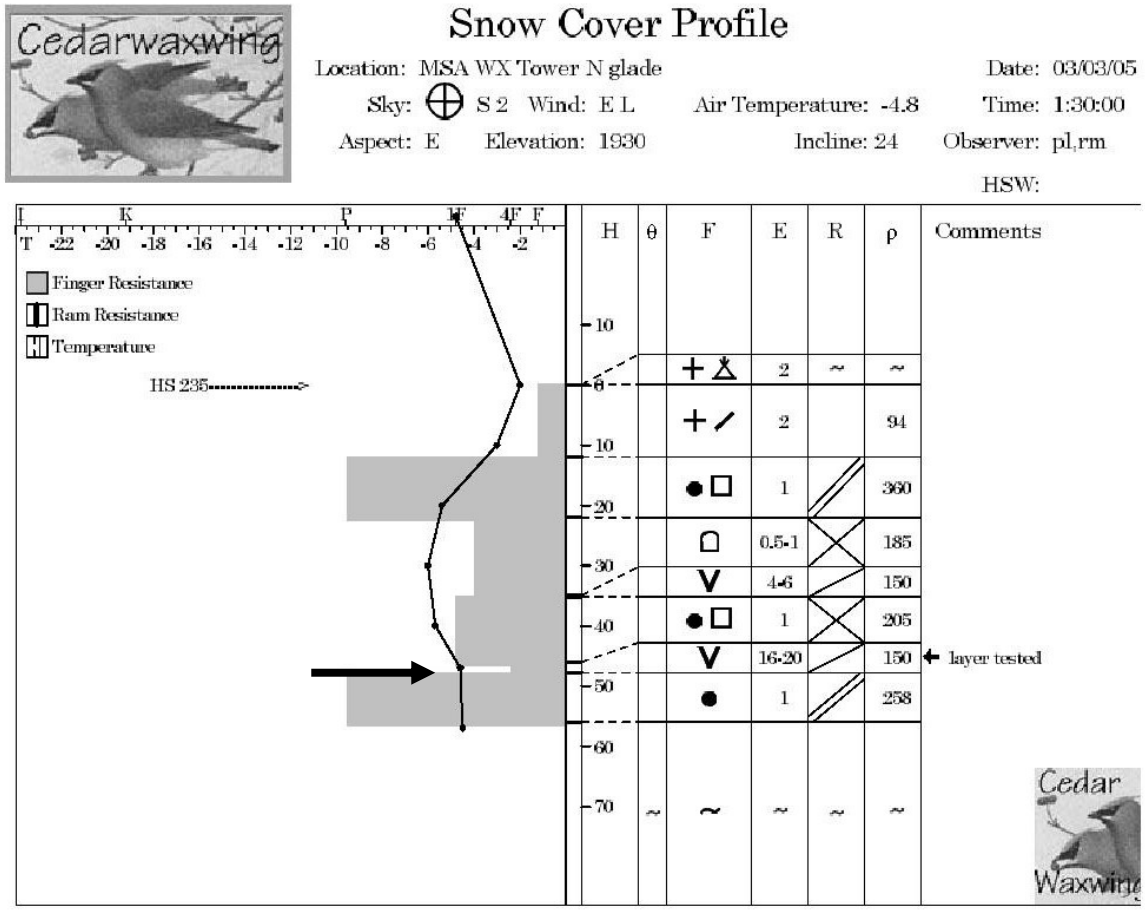

Figure B.11 – Manual snow profile for the rutschblock test array performed at Robson View on Mount St. Anne near Blue River on 2003-03-05. The primary failure plane is indicated.

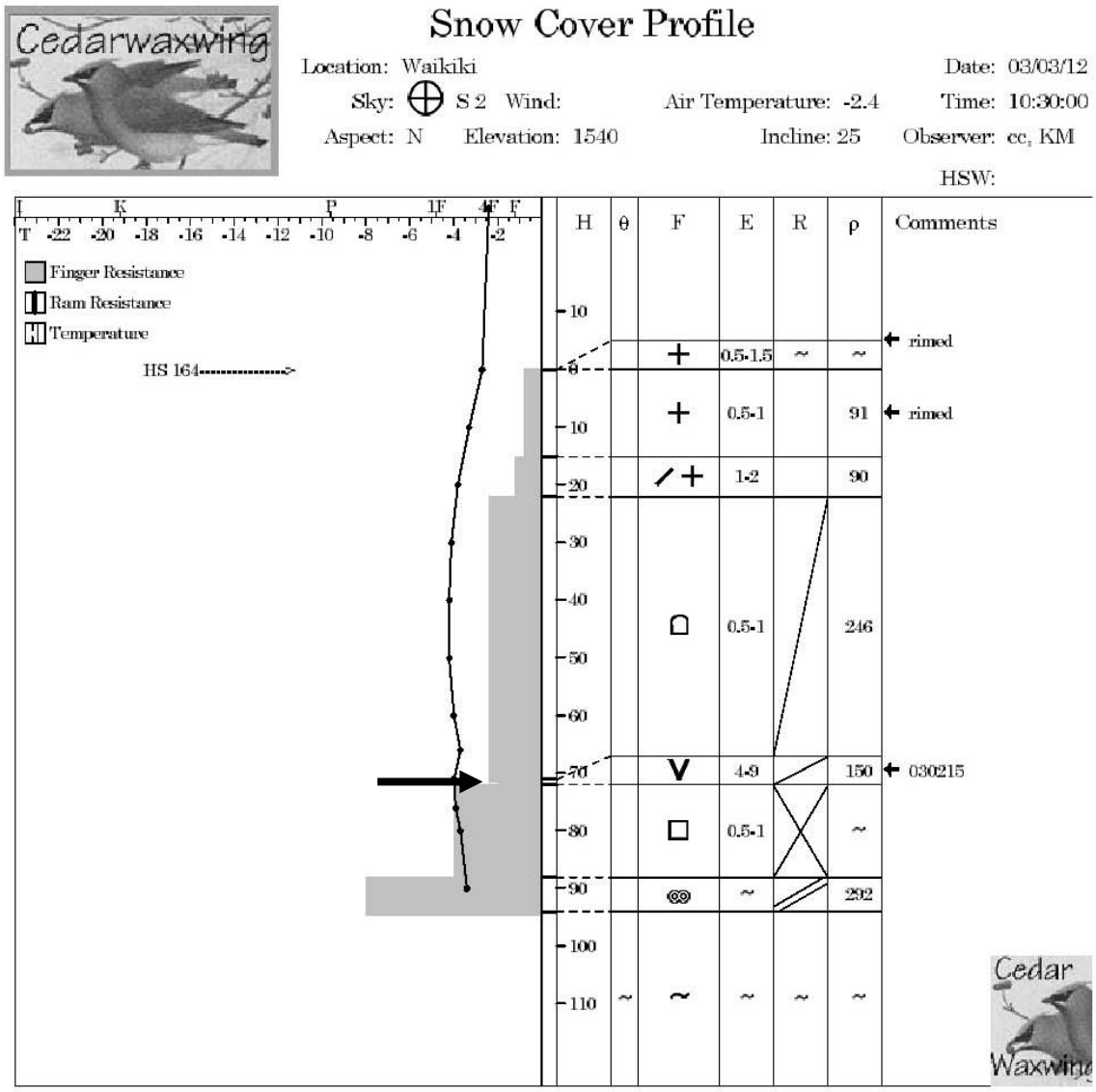

Figure B.12 – Manual snow profile for the rutschblock test array performed at Waikiki near Blue River on 2003-03-12. The primary failure plane is indicated.

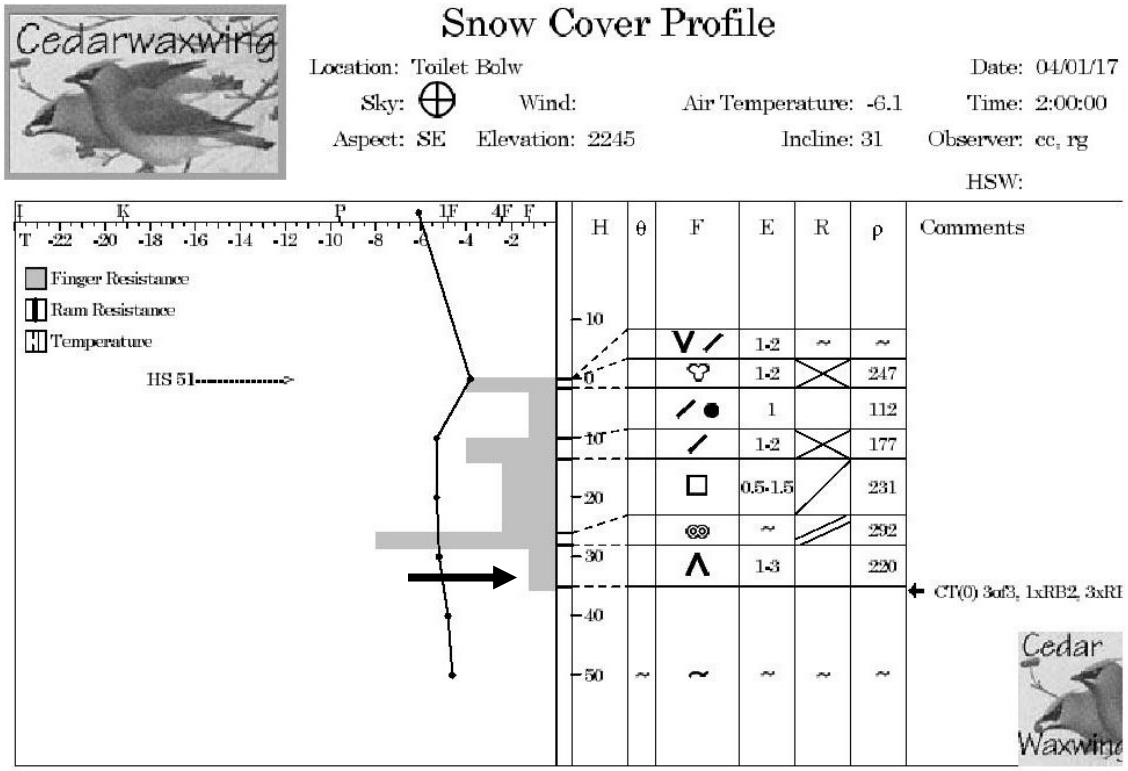

Figure B.13 – Manual snow profile for the rutschblock test array performed in the Toilet Bowl near Kicking Horse Mountain Resort on 2004-01-17. The primary failure plane is indicated.

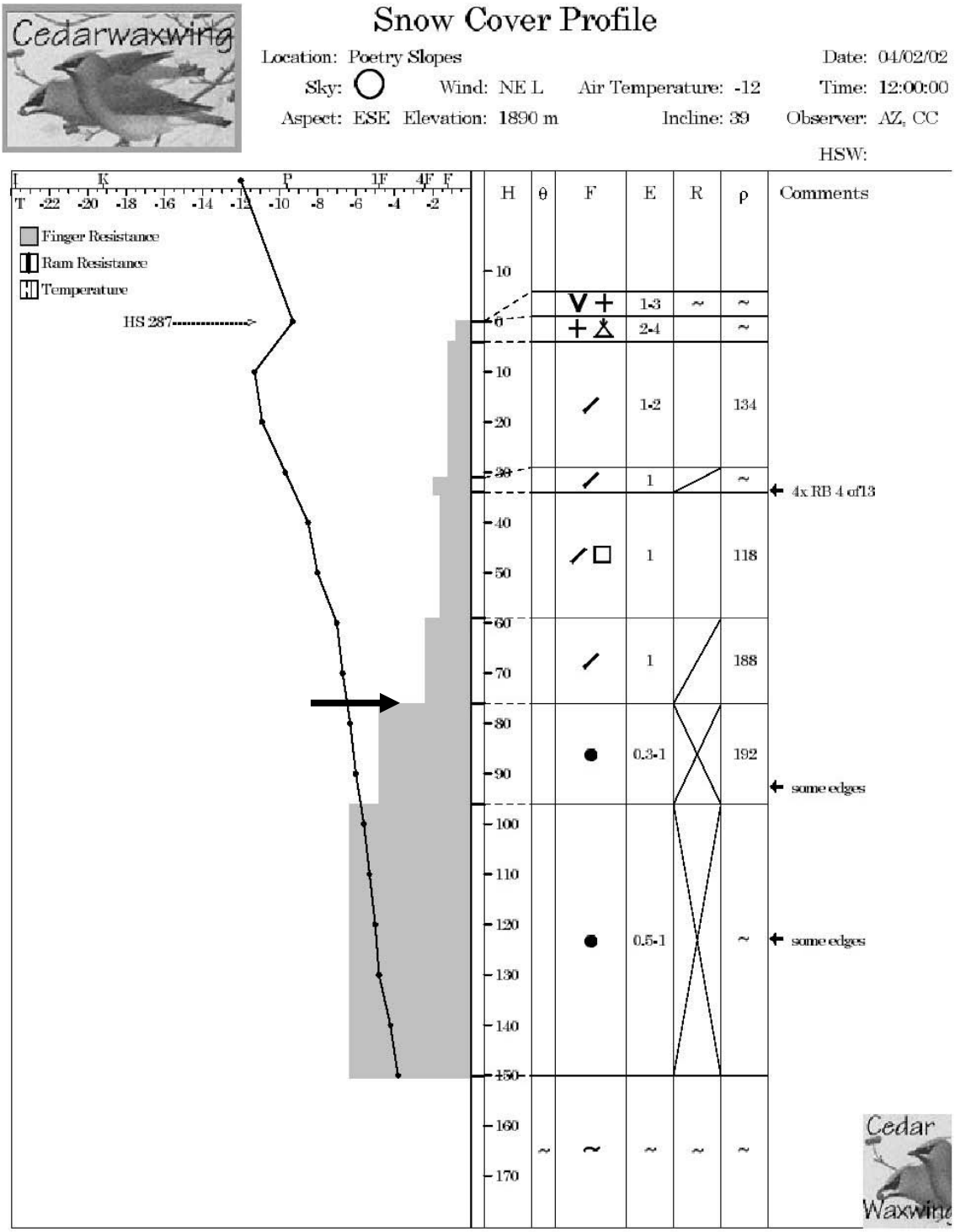

Figure B.14 – Manual snow profile for the rutschblock test array performed at the Poetry Slopes on Fidelity Mountain near Rogers Pass on 2004-02-02. The primary failure plane is indicated.

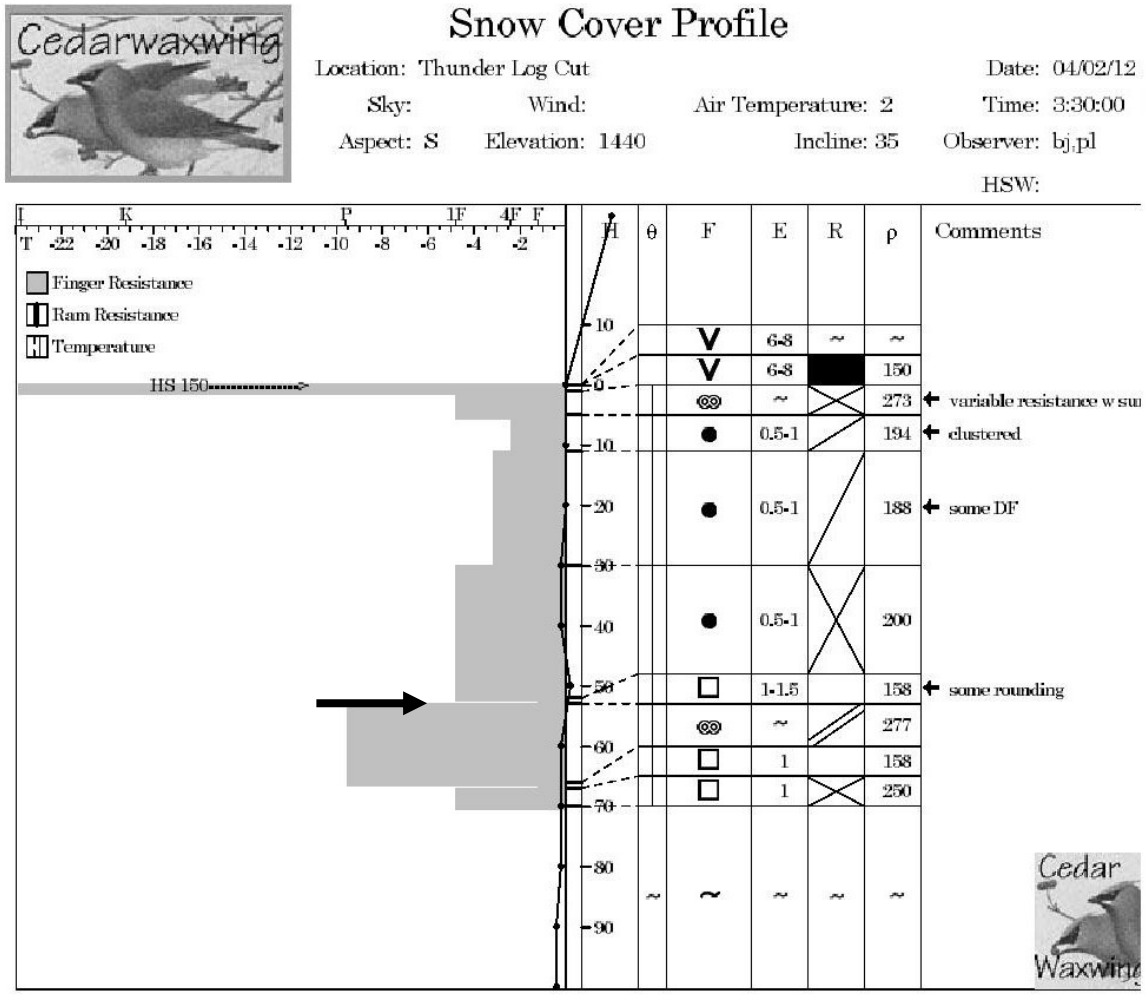

Figure B.15 – Manual snow profile for the rutschblock test array performed at Langevin Cutblock on Mount St. Anne near Blue River on 2004-02-12. The primary failure plane is indicated.

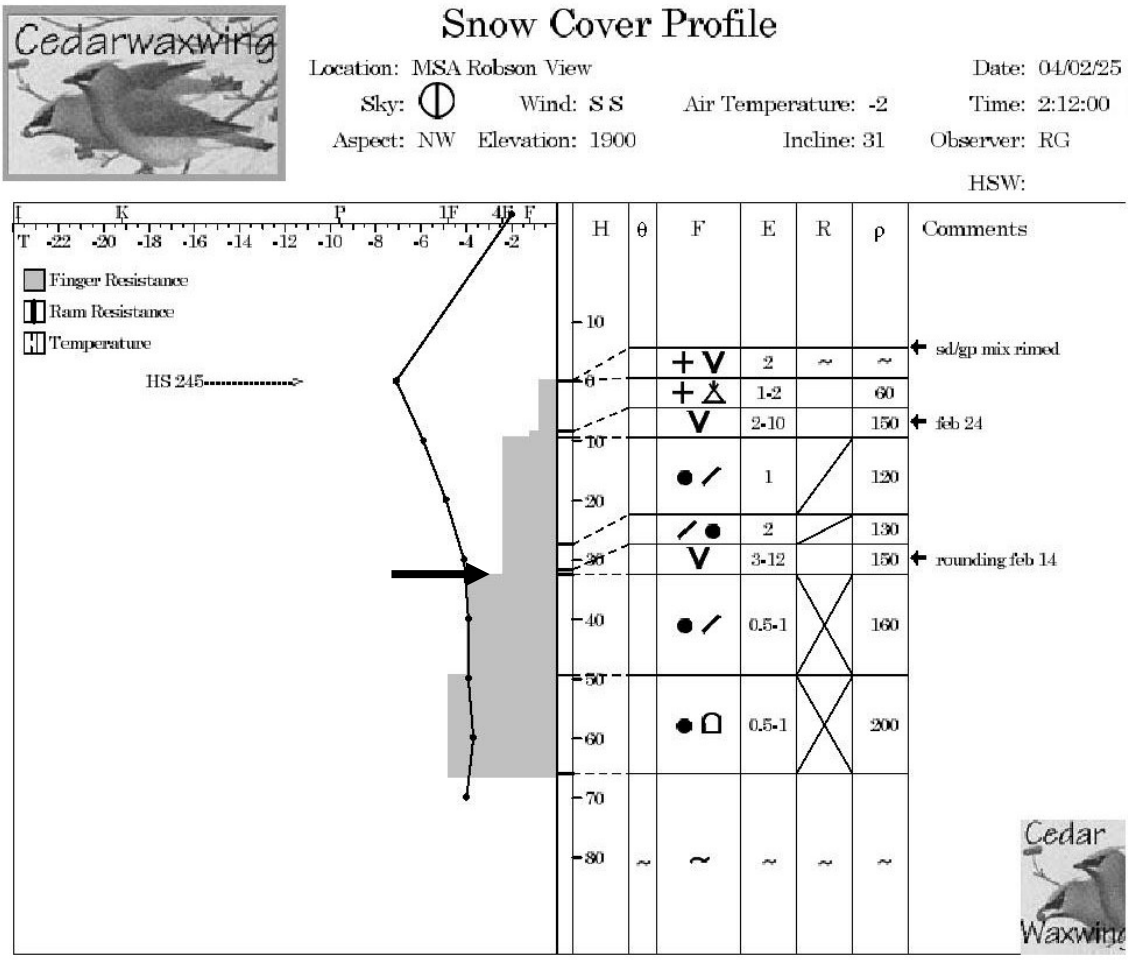

Figure B.16 – Manual snow profile for the rutschblock test array performed at Robson View on Mount St. Anne near Blue River on 2004-02-25. The primary failure plane is indicated.

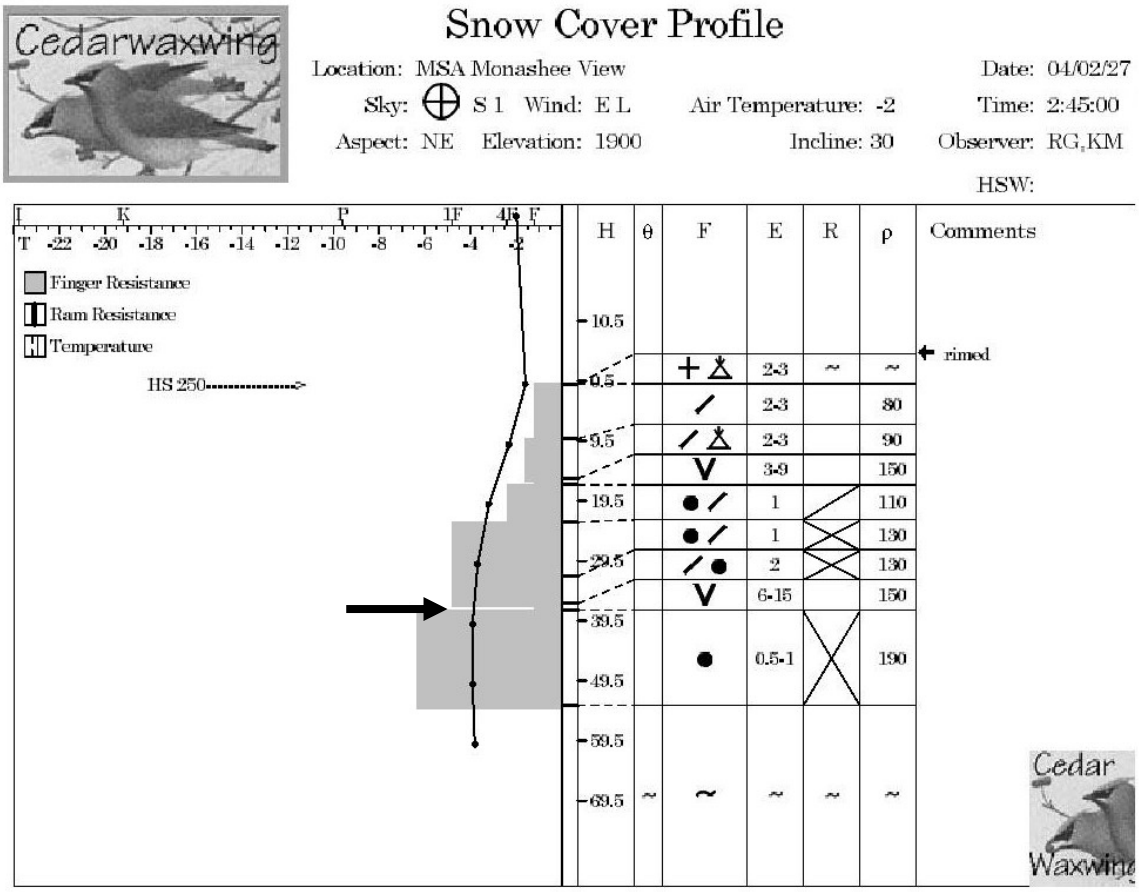

Figure B.17 – Manual snow profile for the rutschblock test array performed at Monashee View on Mount St. Anne near Blue River on 2004-02-27. The primary failure plane is indicated.

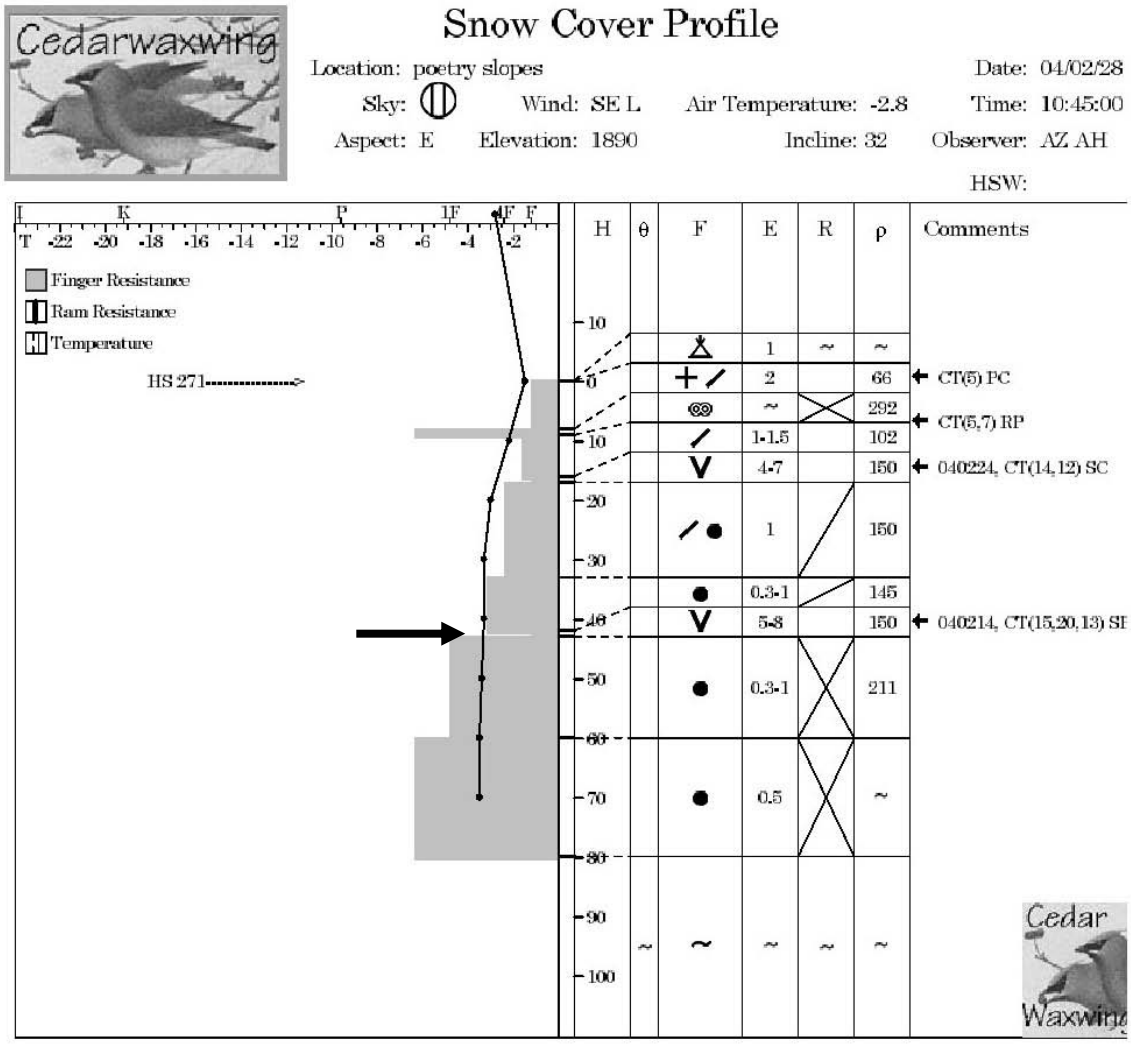

Figure B.18 – Manual snow profile for the rutschblock test array performed at the Poetry Slopes on Fidelity Mountain near Rogers Pass on 2004-02-28. The primary failure plane is indicated.

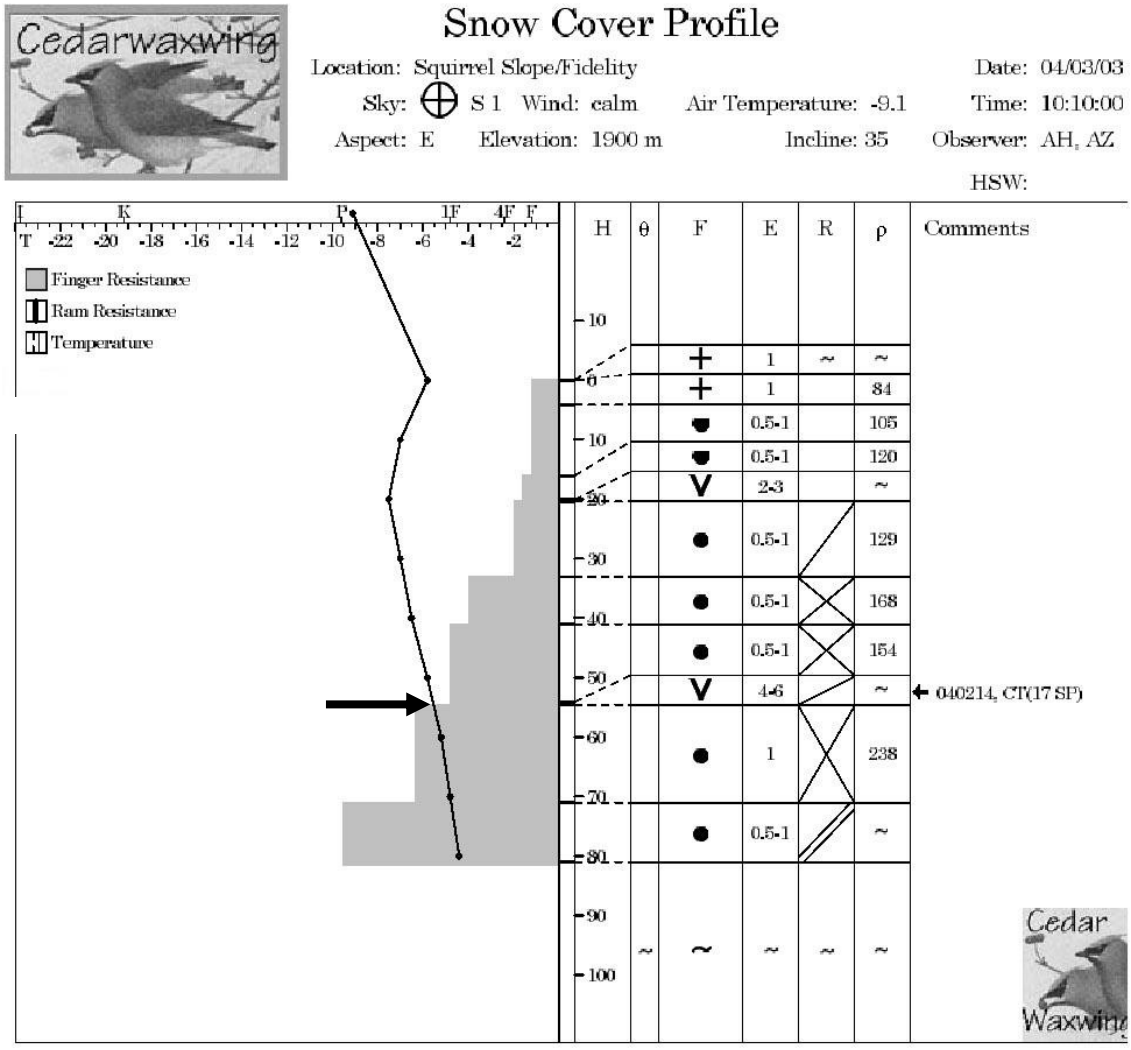

Figure B.19 – Manual snow profile for the rutschblock test array performed at Squirrel Slope on Fidelity Mountain near Rogers Pass on 2004-03-03. The primary failure plane is indicated.

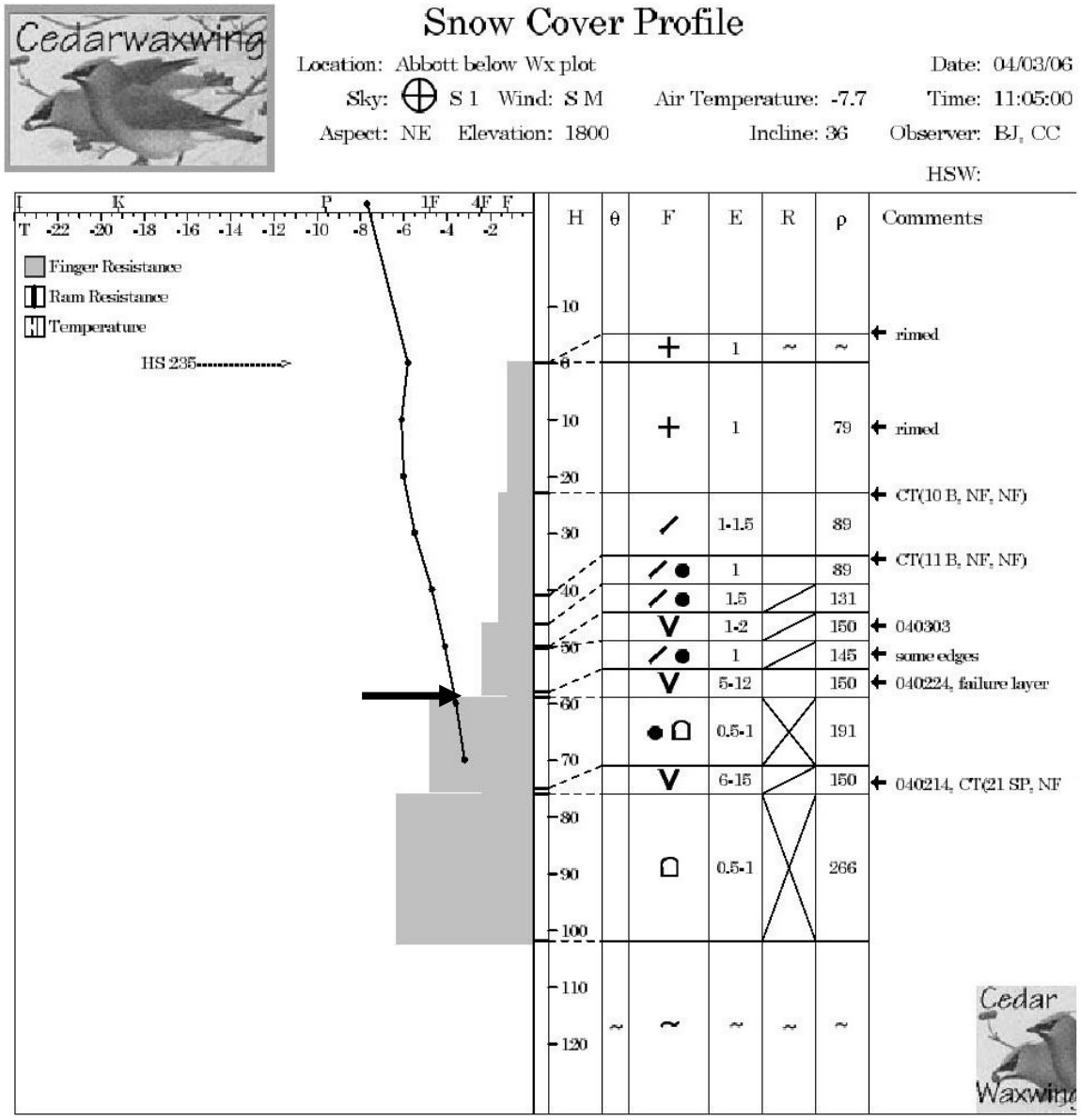

Figure B.20 – Manual snow profile for the rutschblock test array performed at the Abbott Headwall near Rogers Pass on 2004-03-06/07. The primary failure plane is indicated.

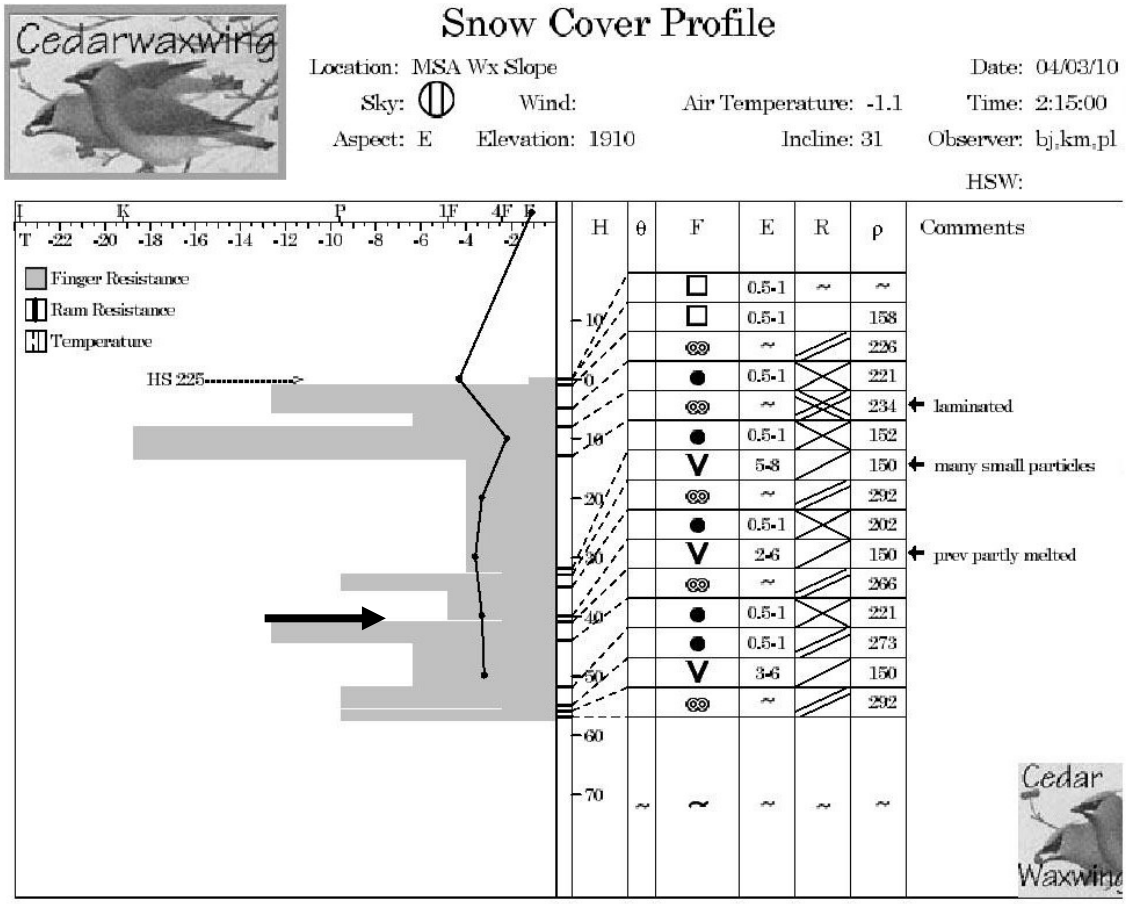

Figure B.21 – Manual snow profile for the rutschblock test array performed at Mount St. Anne near Blue River on 2004-03-10. The primary failure plane is indicated.

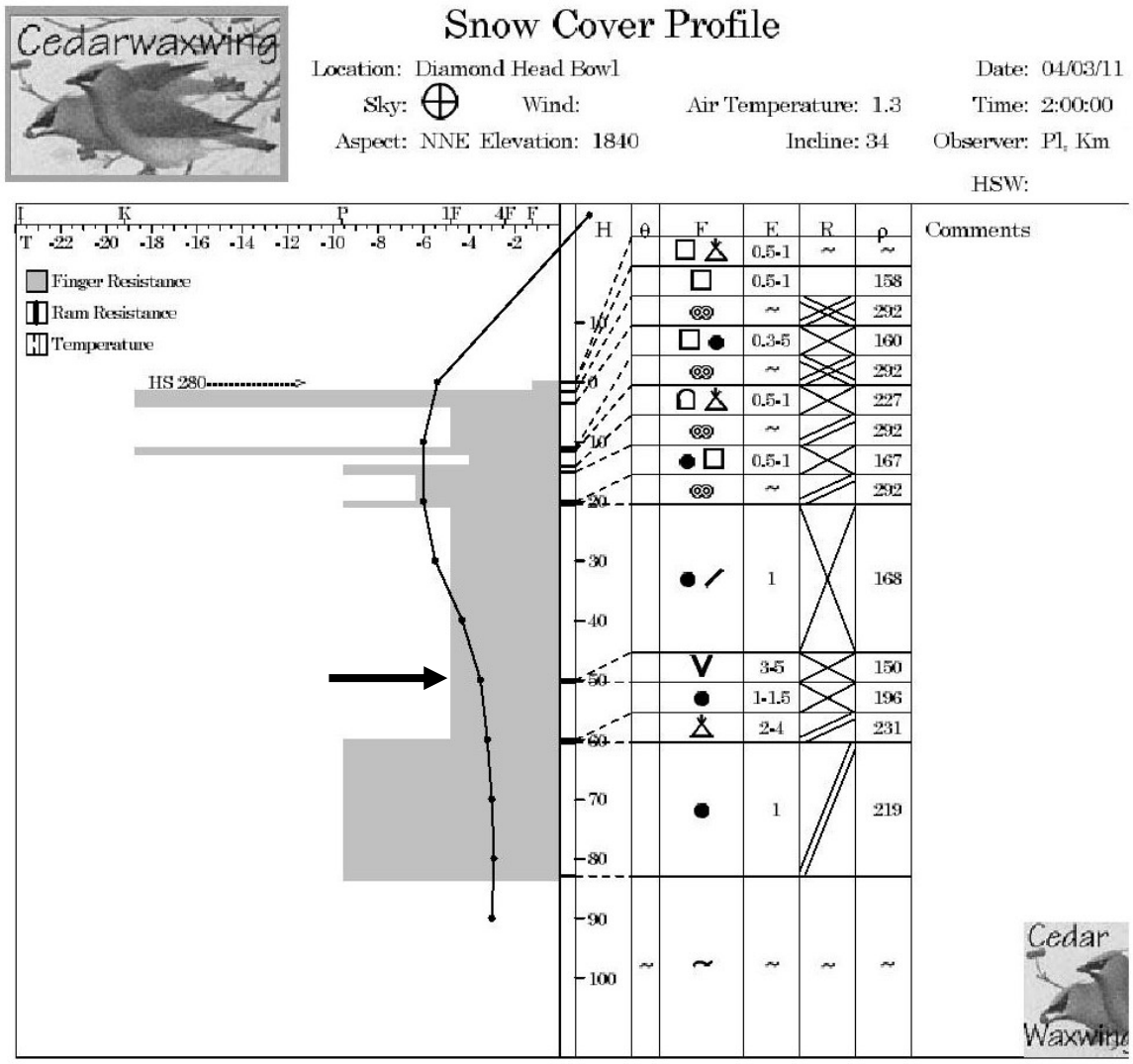

Figure B.22 – Manual snow profile for the rutschblock test arrays (a and b) performed at Bear's Den near Blue River on 2004-03-11. The primary failure plane is indicated.

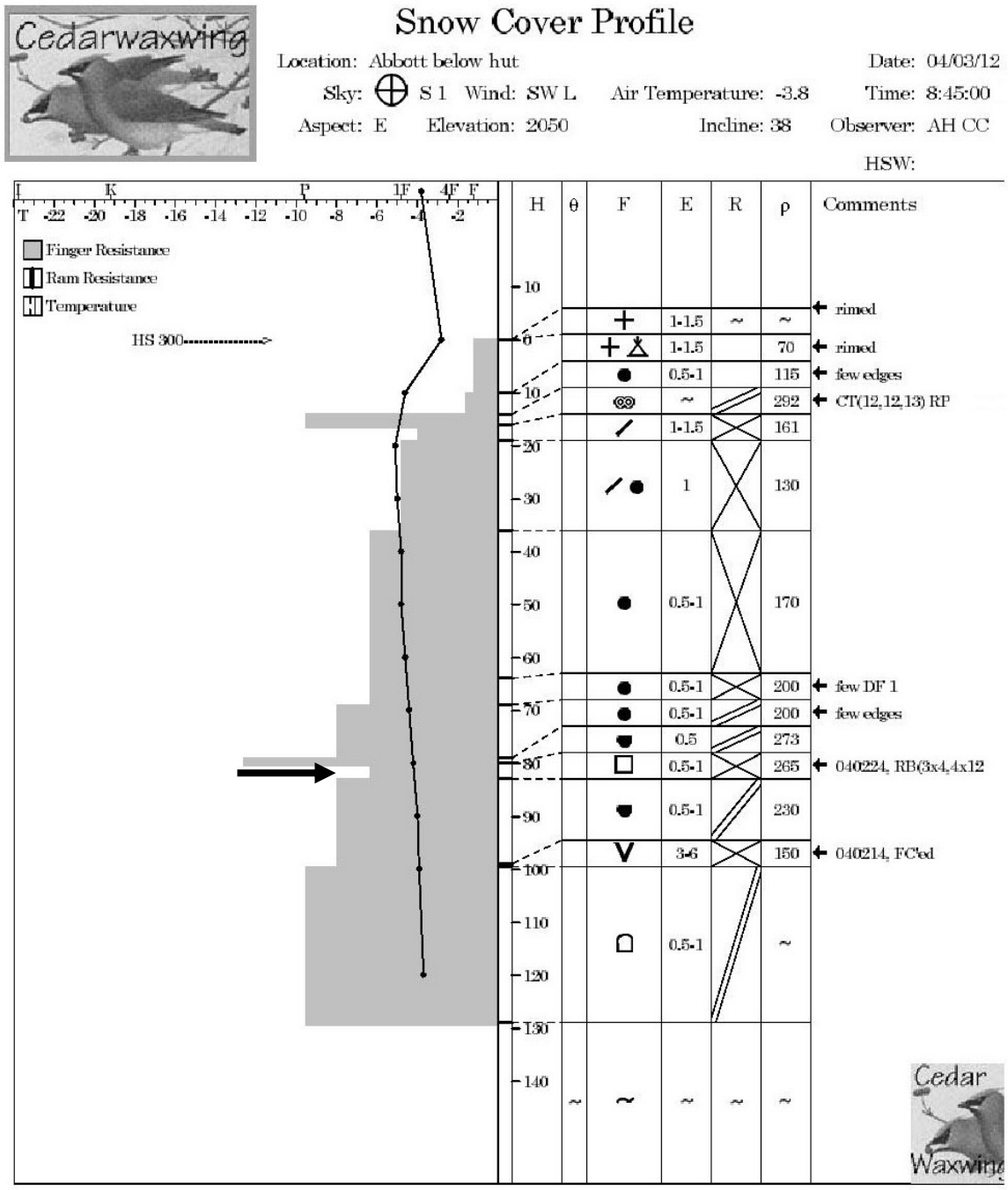

Figure B.23 – Manual snow profile for the rutschblock test array performed on Mount Abbott near Rogers Pass on 2004-03-11/12. The primary failure plane is indicated.

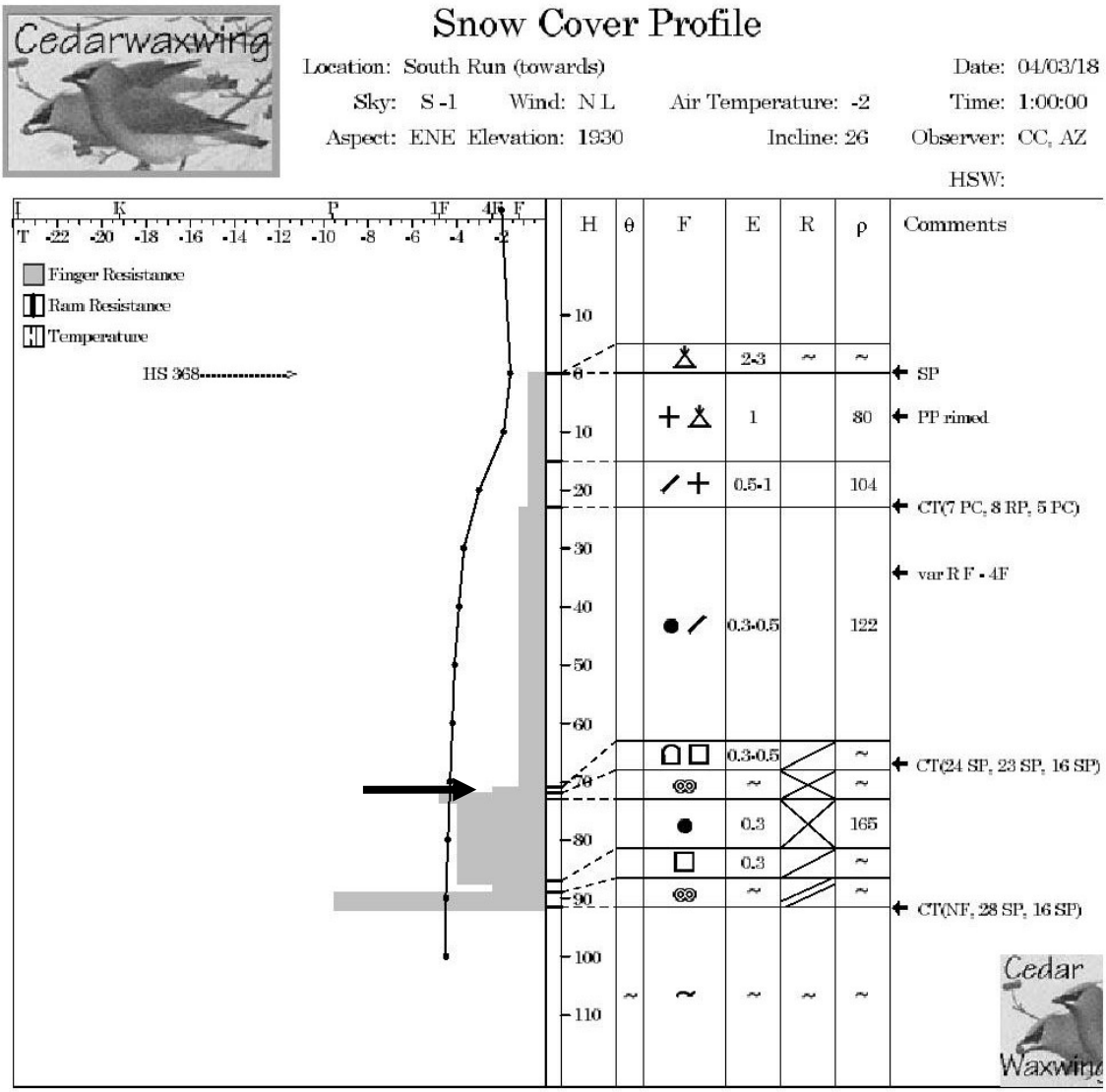

Figure B.24 – Manual snow profile for the rutschblock test array performed at South Run on Fidelity Mountain near Rogers Pass on 2004-03-18. The primary failure plane is indicated.

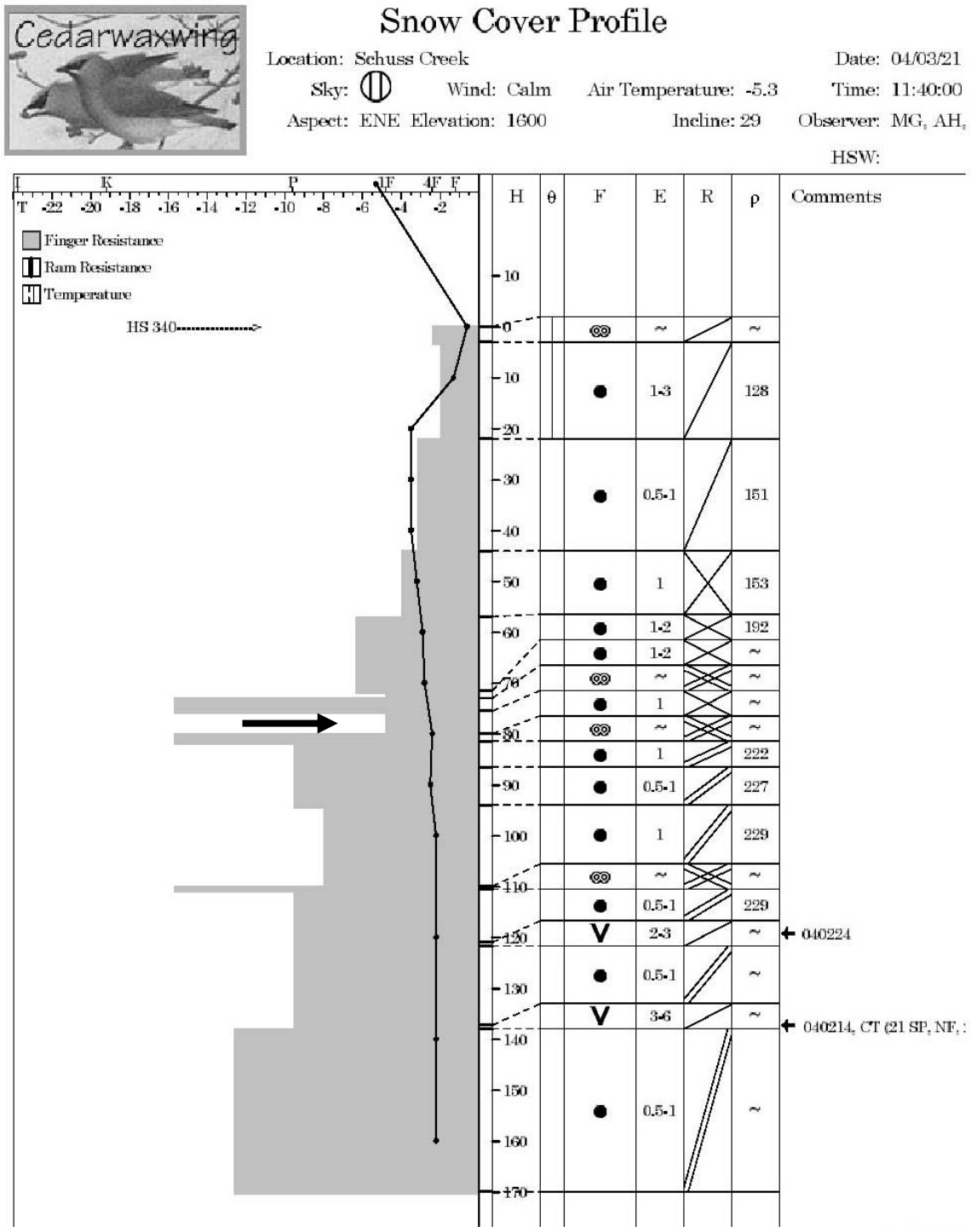

Figure B.25 – Manual snow profile for the rutschblock test arrays (a and b) performed in the Schuss Cr. drainage on Fidelity Mountain near Rogers Pass on 2004-03-21. The primary failure plane is indicated.

B.3 Propagation test arrays

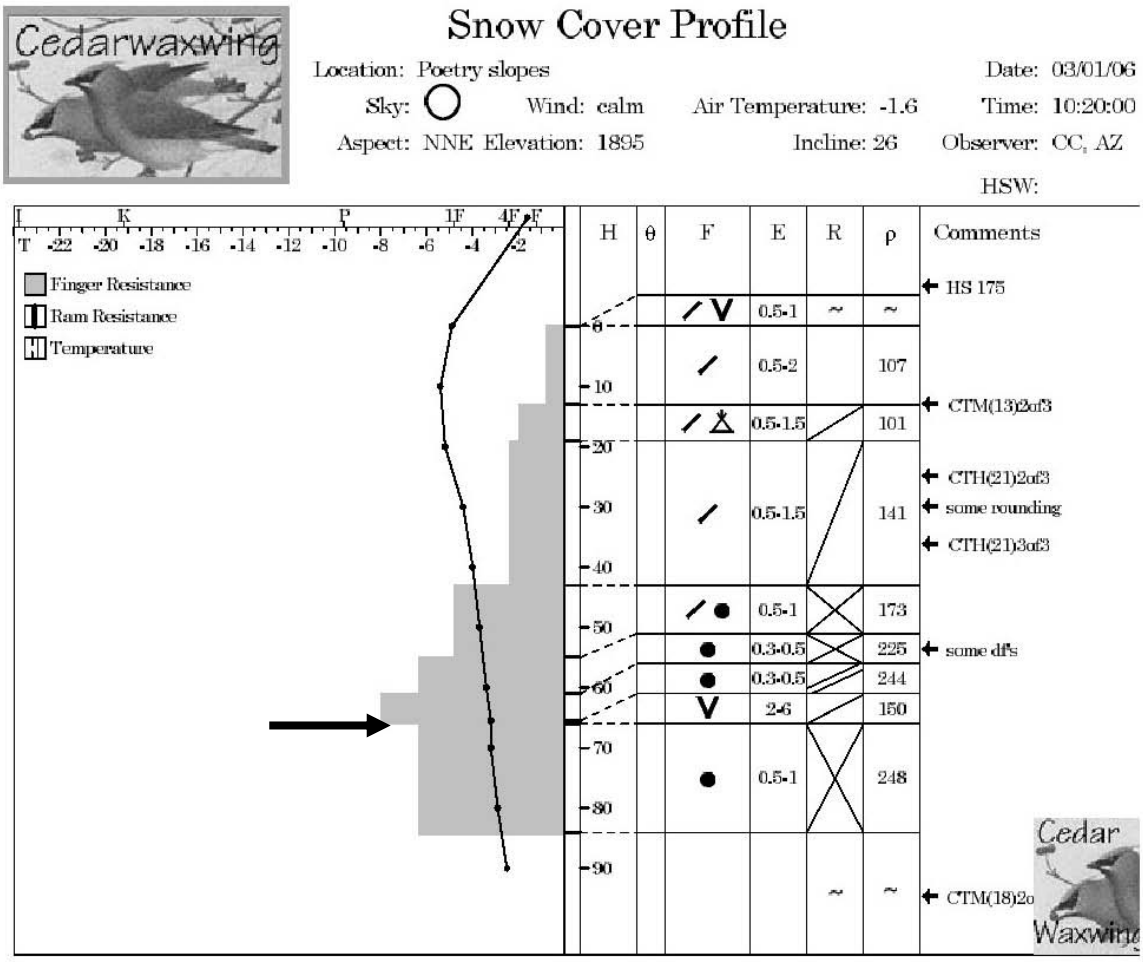

Figure B.26 – Manual snow profile for the propagation test array performed at the Poetry Slopes on Fidelity Mountain near Rogers Pass on 2003-01-06. The test layer is indicated.

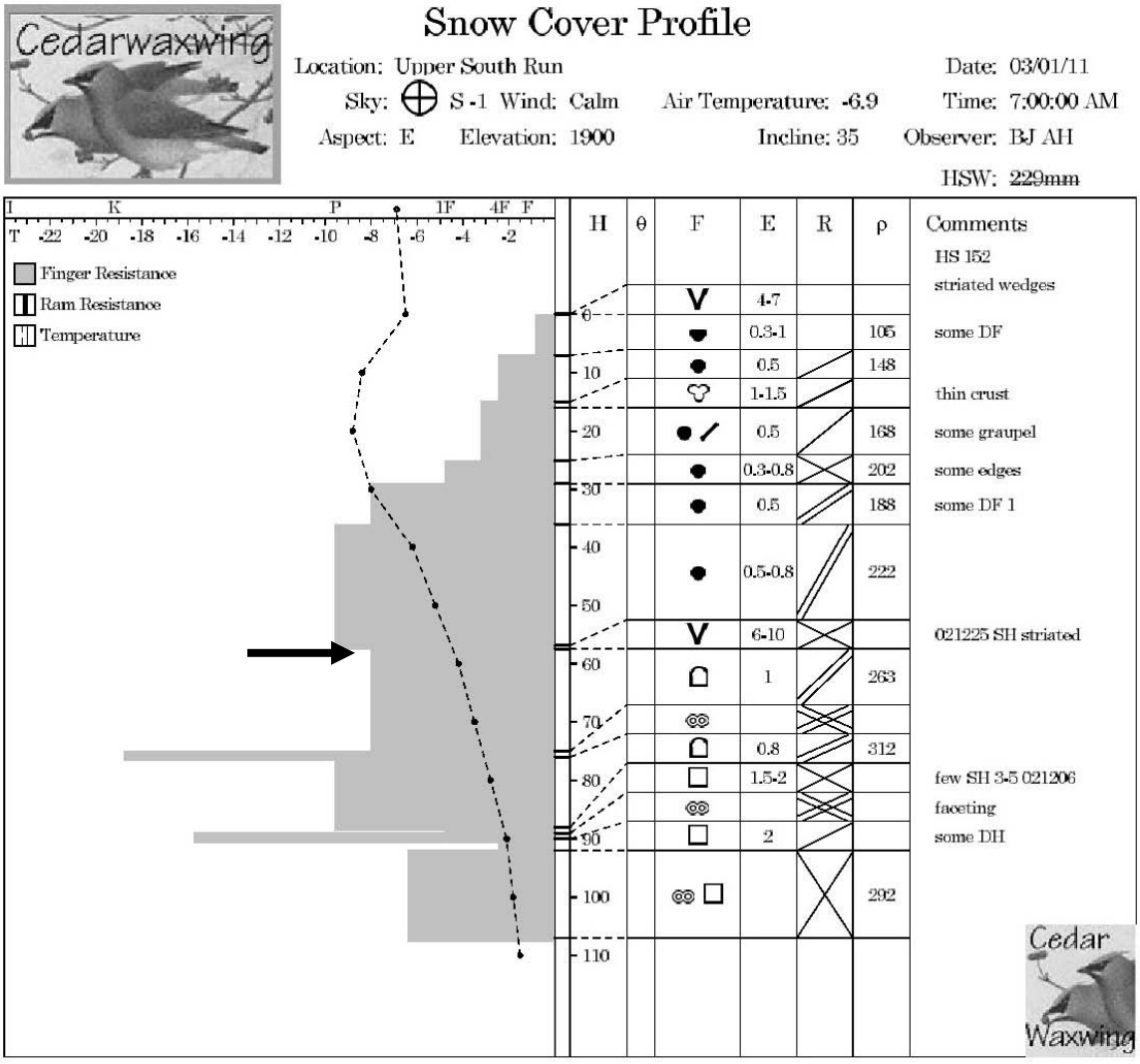

Figure B.27 – Manual snow profile for the propagation test array performed at South Run on Fidelity Mountain near Rogers Pass on 2003-01-11. The test layer is indicated.

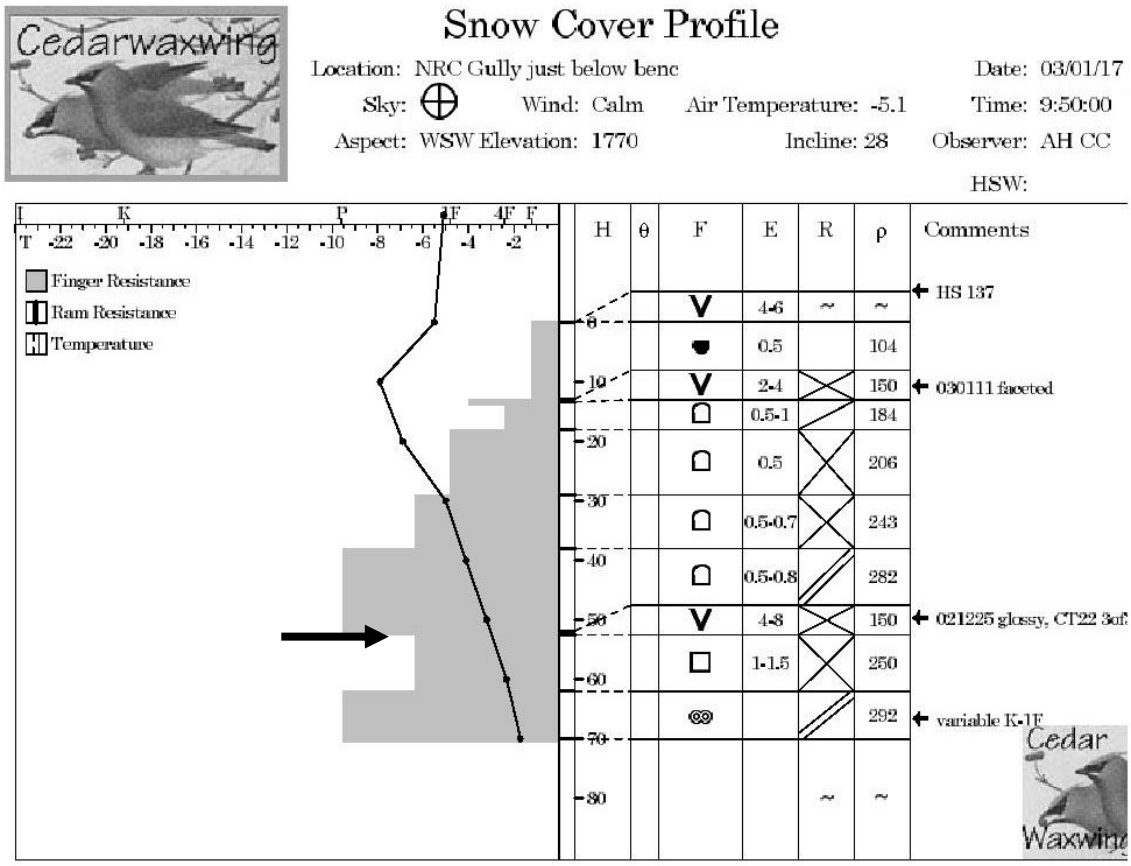

Figure B.28 – Manual snow profile for the propagation test array (a) performed on the WSW aspect of NRC Gully near Rogers Pass on 2003-01-17. The test layer is indicated.

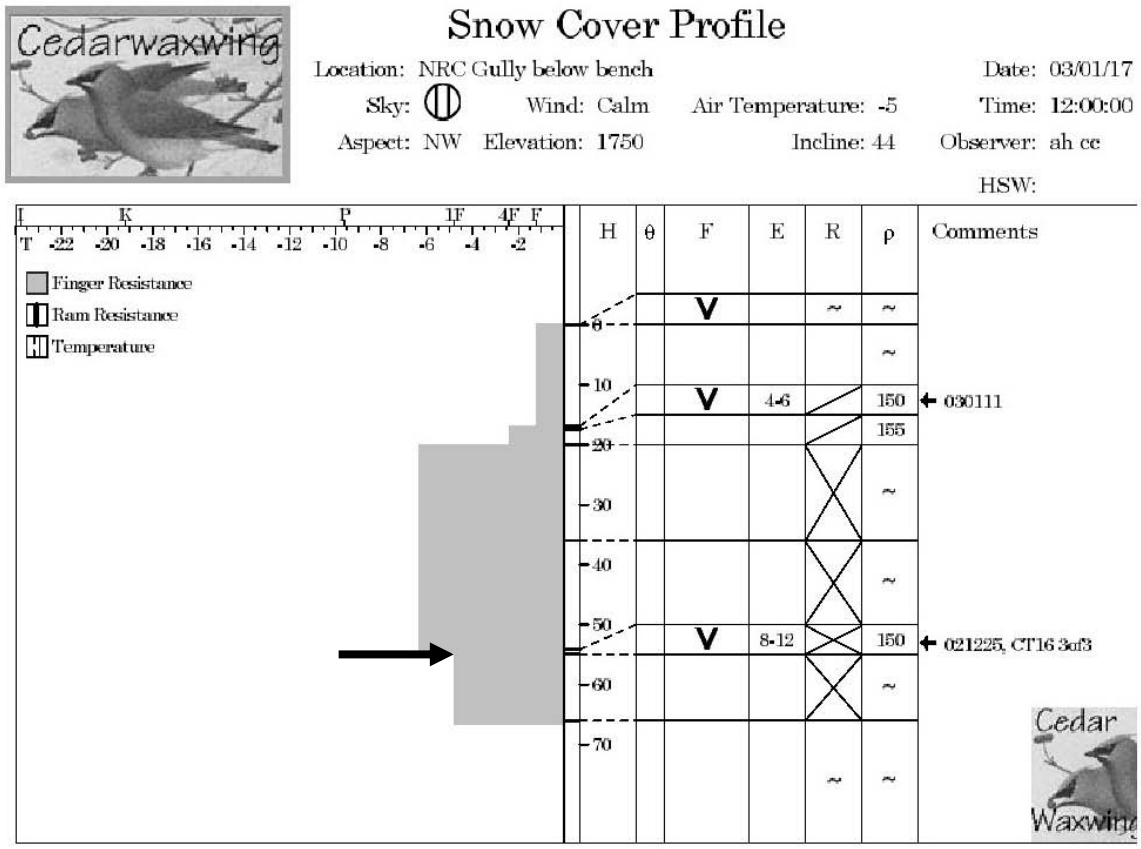

Figure B.29 – Manual snow profile for the propagation test array (b) performed on the NW aspect of NRC Gully near Rogers Pass on 2003-01-17. The test layer is indicated.

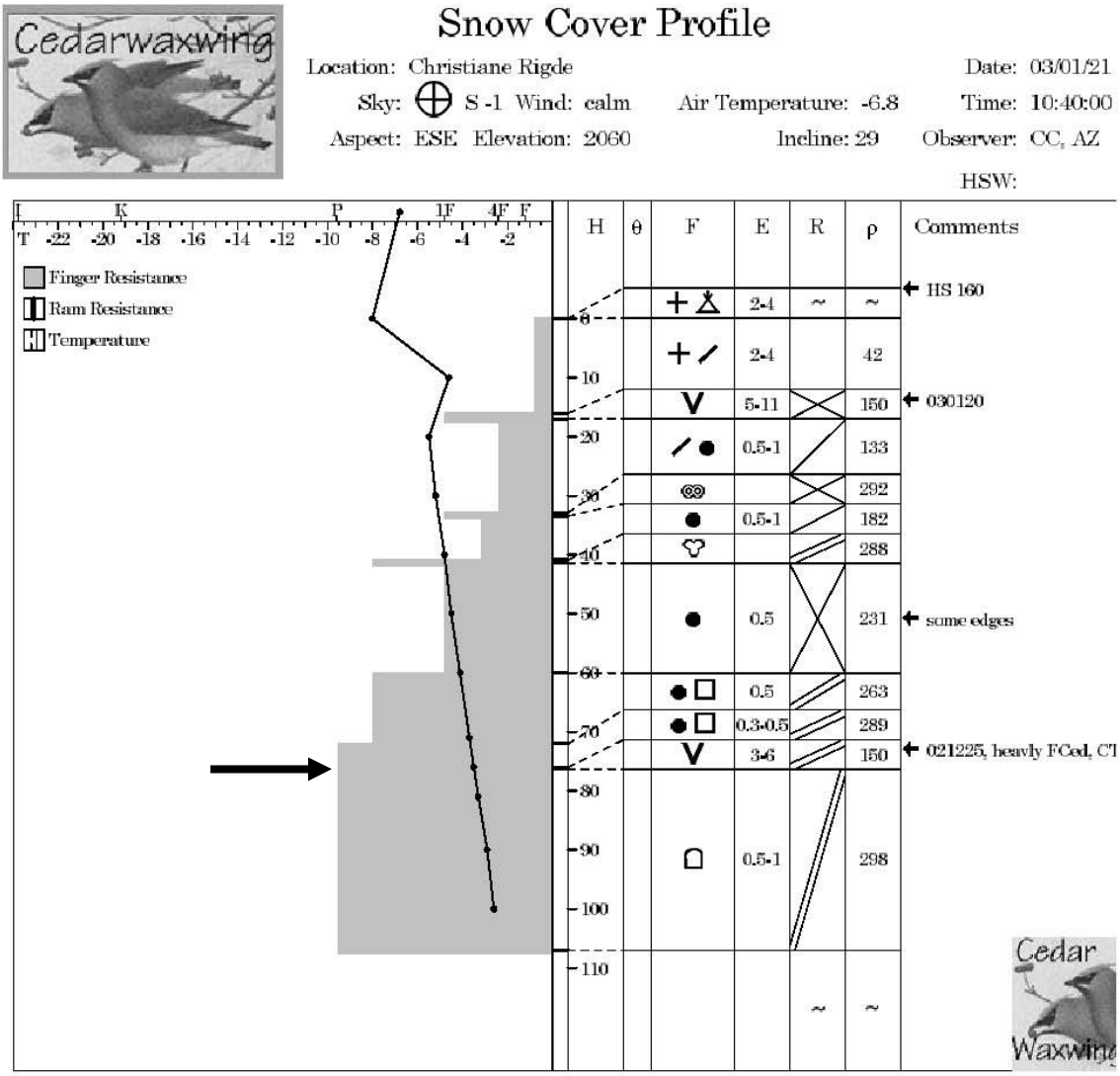

Figure B.30 – Manual snow profile for the propagation test array performed on Christiania Ridge on Fidelity Mountain near Rogers Pass on 2003-01-21. The test layer is indicated.

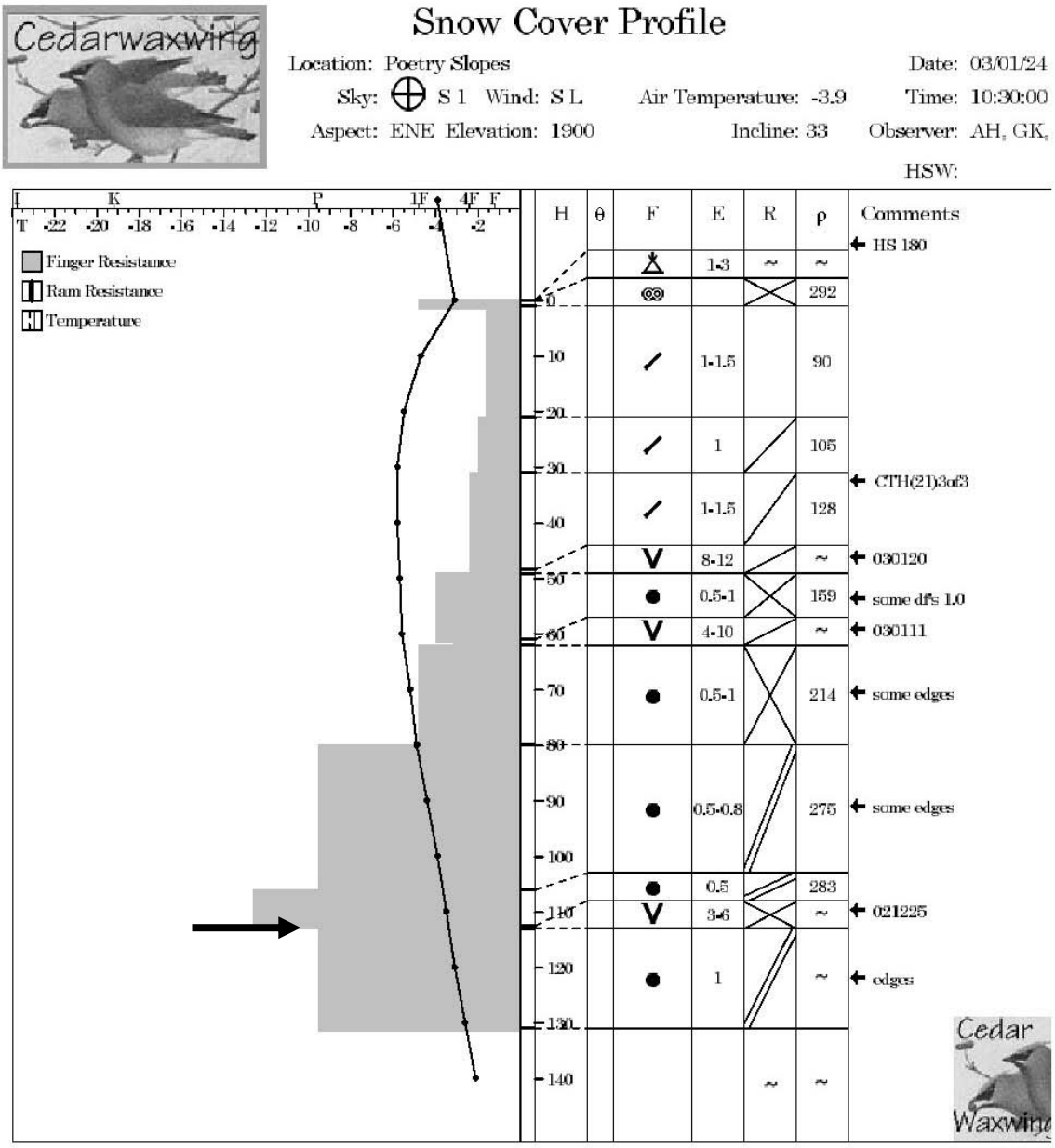

Figure B.31 – Manual snow profile for the propagation test array performed at the Poetry Slopes on Fidelity Mountain near Rogers Pass on 2003-01-24. The test layer is indicated.

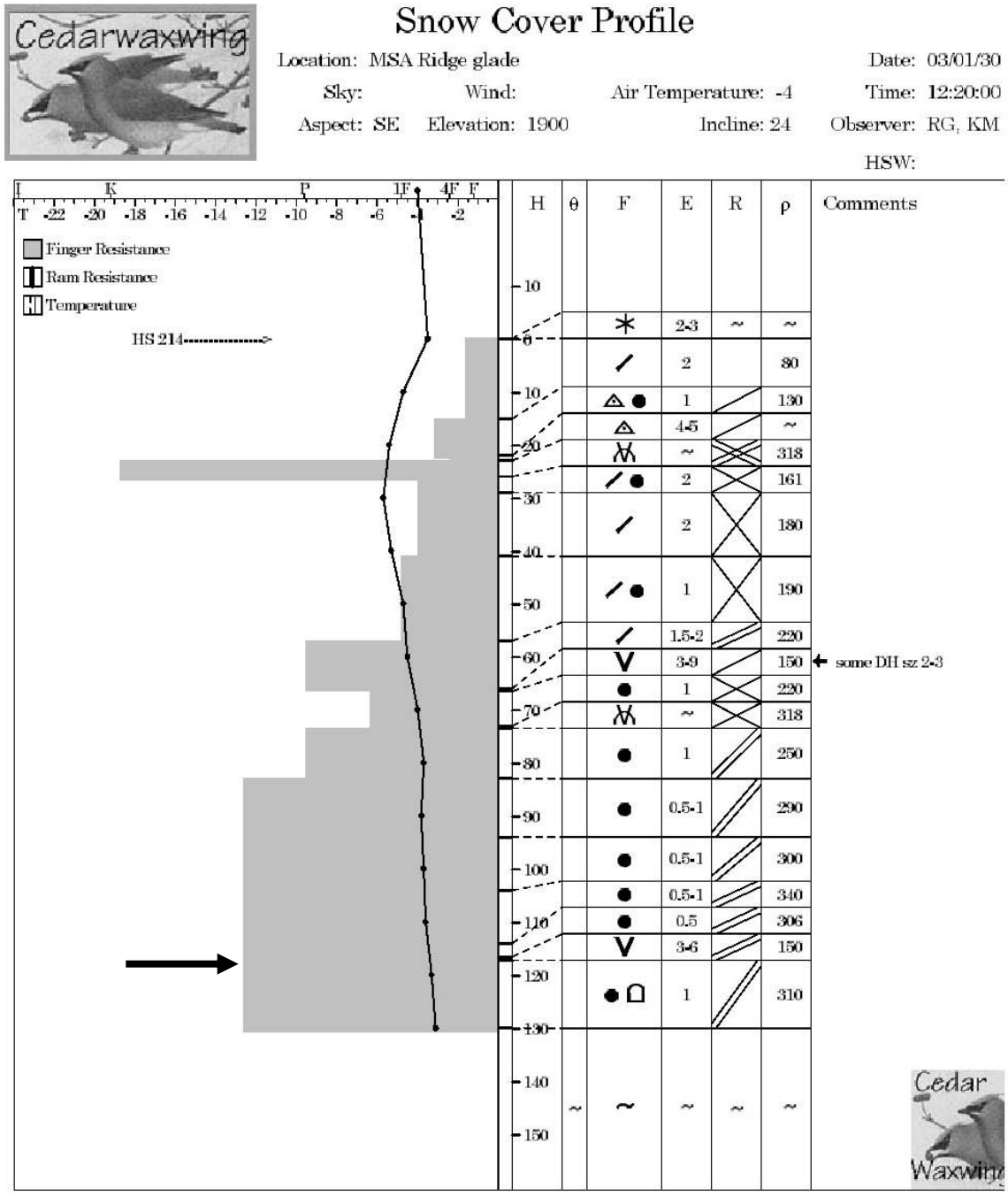

Figure B.32 – Manual snow profile for the propagation test array performed on Mount St. Anne near Blue River on 2003-01-30. The test layer is indicated.

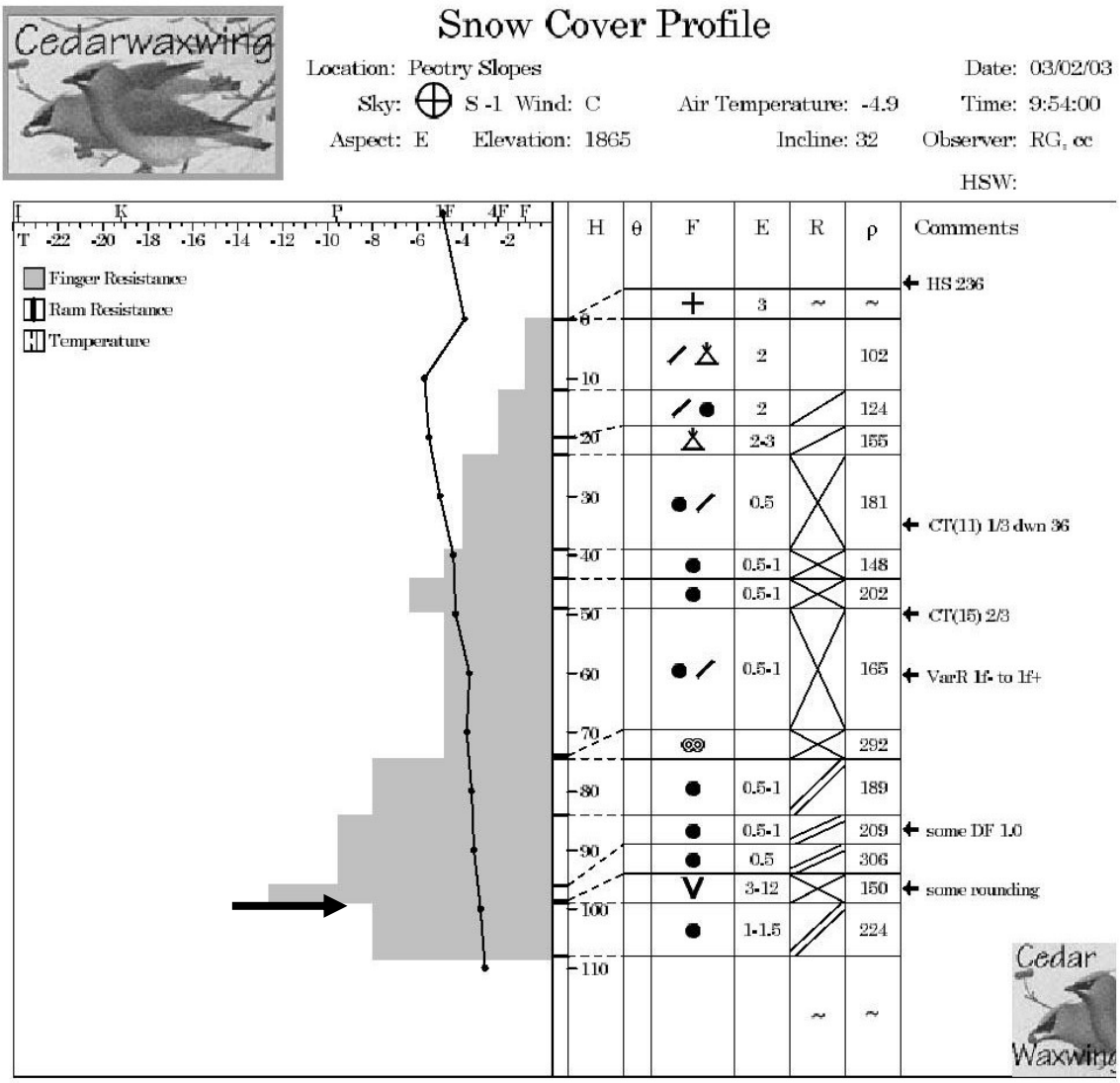

Figure B.33 – Manual snow profile for the propagation test array performed at the Poetry Slopes on Fidelity Mountain near Rogers Pass on 2003-02-03. The test layer is indicated.

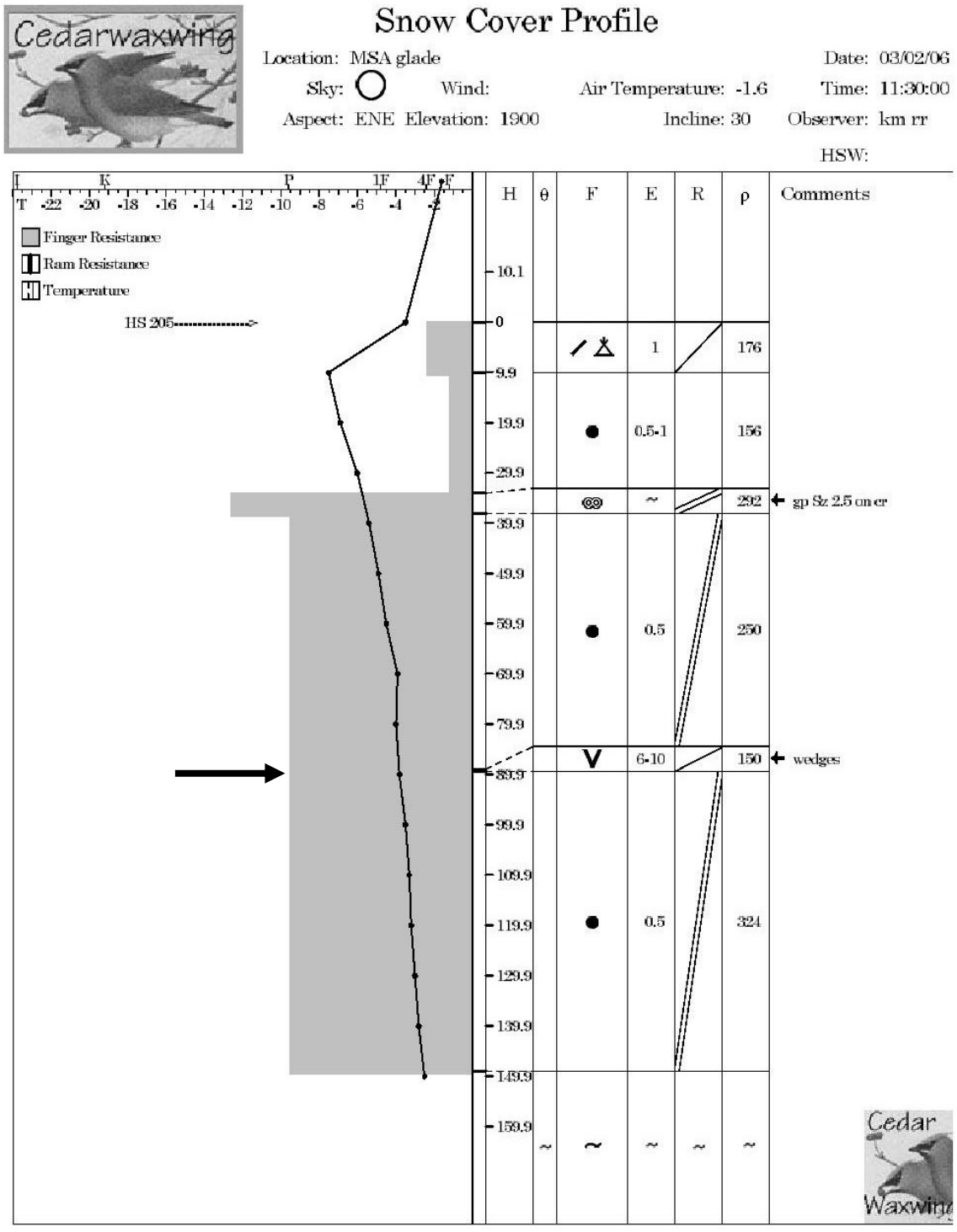

Figure B.34 – Manual snow profile for the propagation test array performed on Mount St. Anne near Blue River on 2003-02-06. The test layer is indicated.

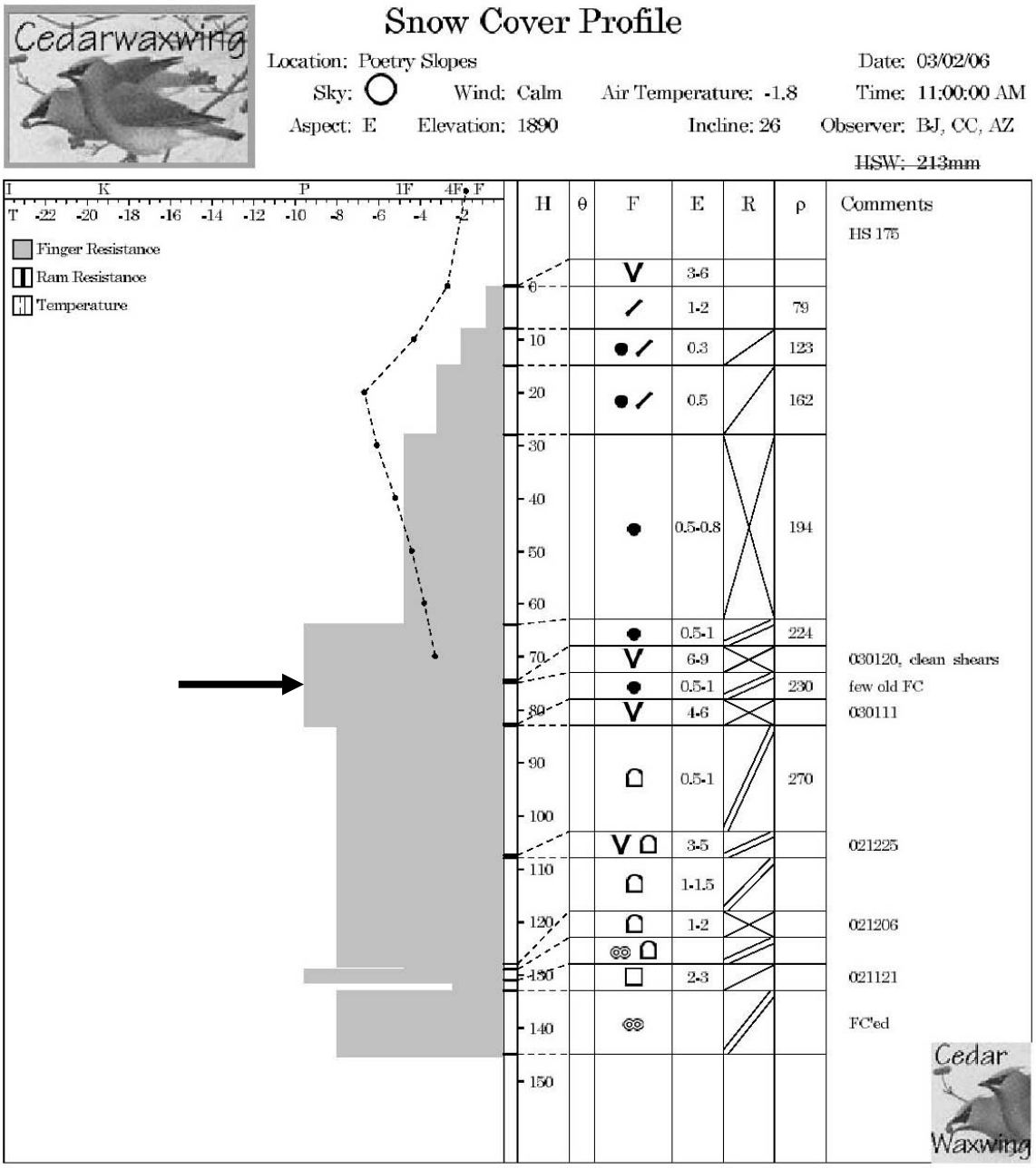

Figure B.35 – Manual snow profile for the propagation test array performed at the Poetry Slopes on Fidelity Mountain near Rogers Pass on 2003-02-06. The test layer is indicated.

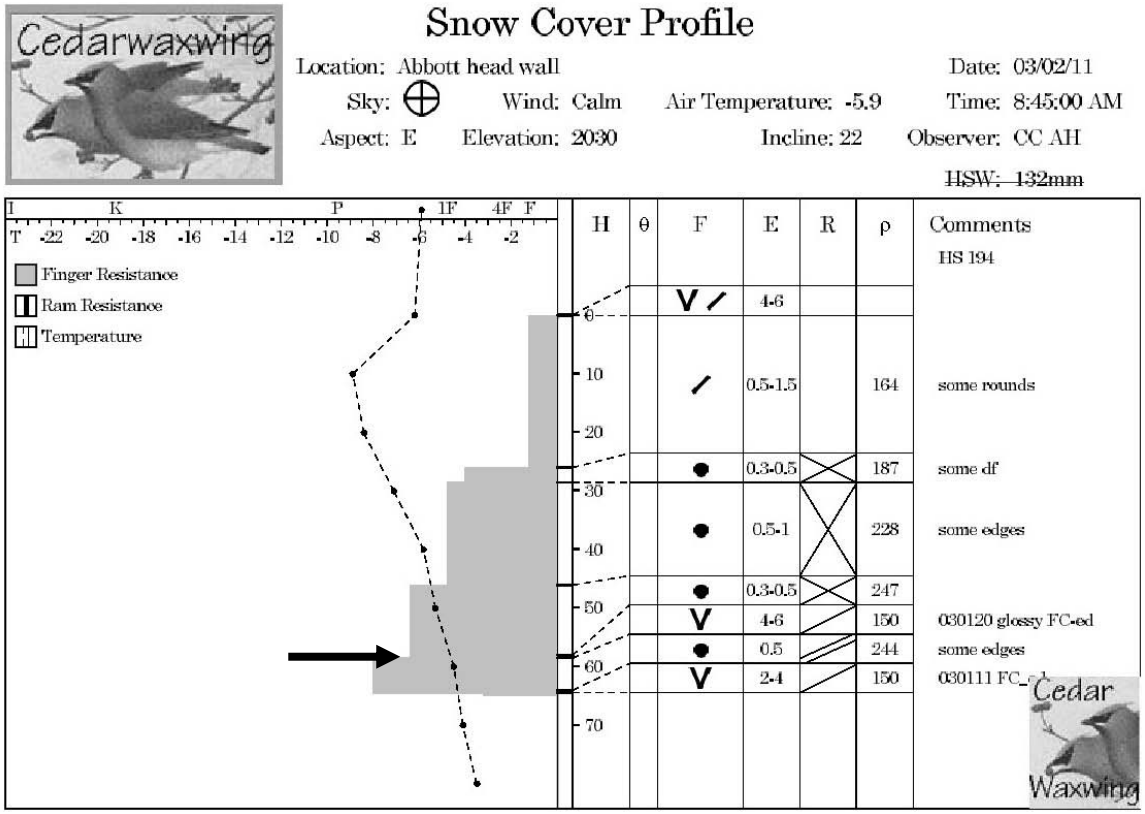

Figure B.36 – Manual snow profile for the propagation test array performed on the Abbott Headwall near Rogers Pass on 2003-02-10/11. The test layer is indicated.

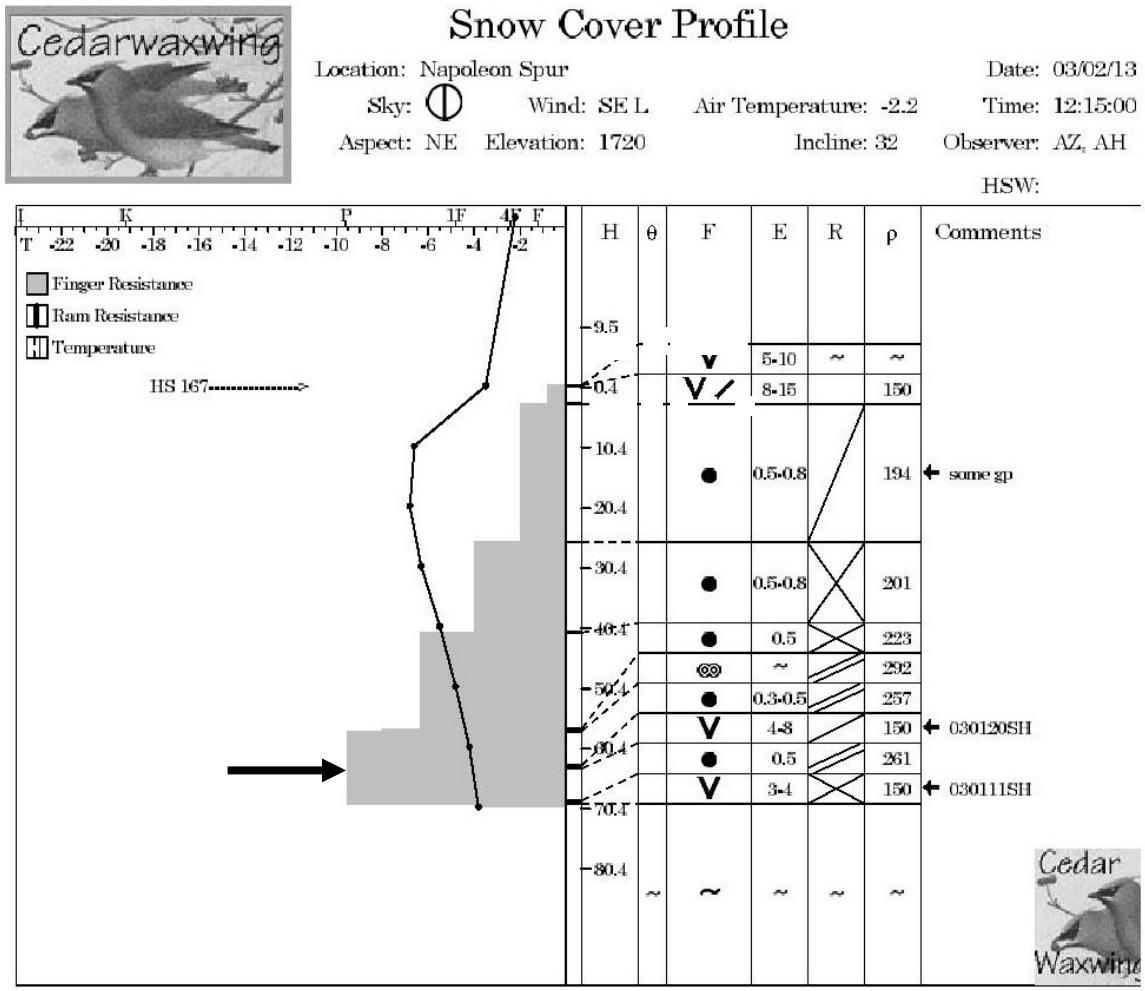

Figure B.37 – Manual snow profile for the propagation test array performed on Mount Cheops near Rogers Pass on 2003-02-13. The test layer is indicated.

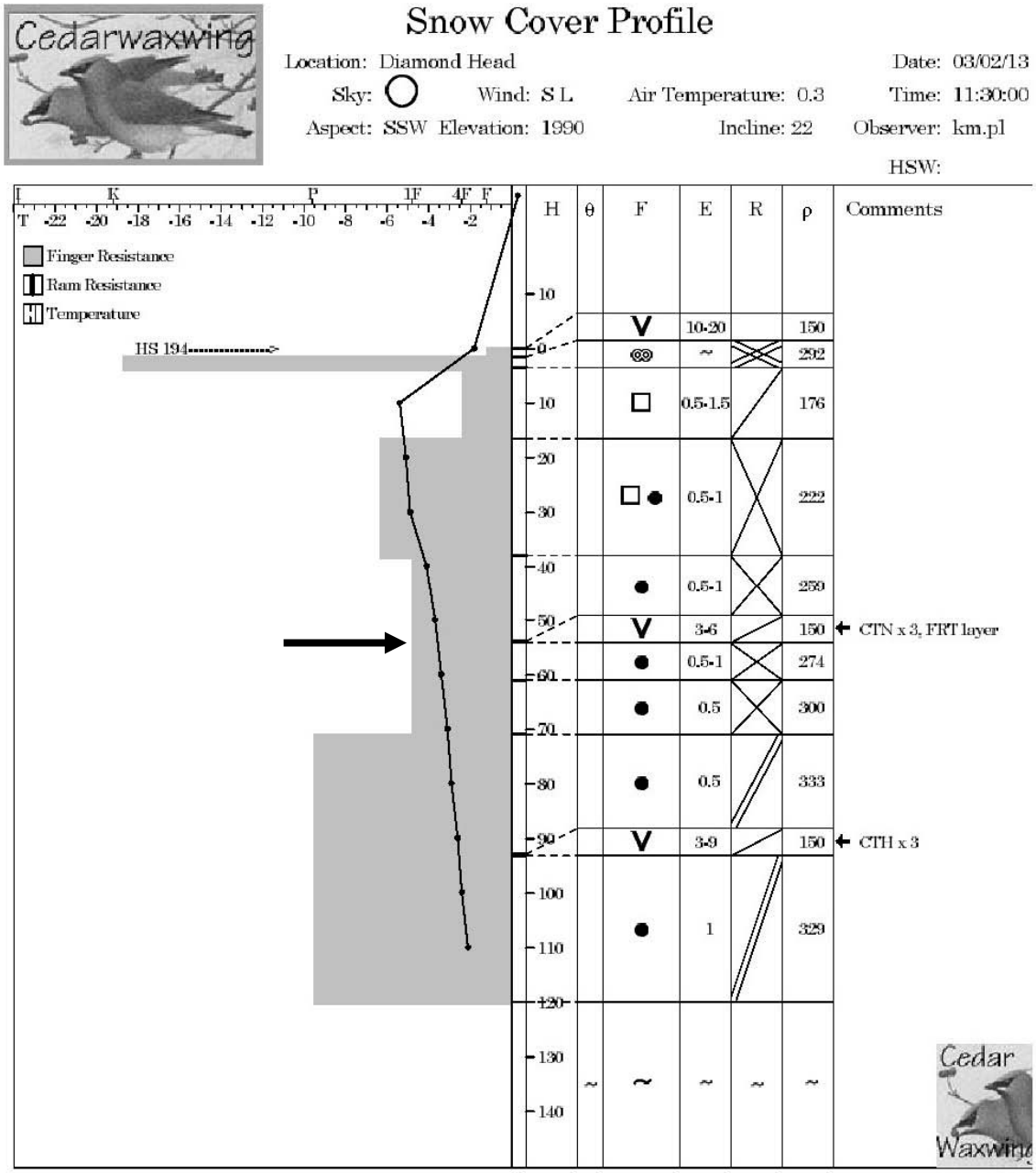

Figure B.38 – Manual snow profile for the propagation test array performed at Diamond Head near Blue River on 2003-02-13. The test layer is indicated.

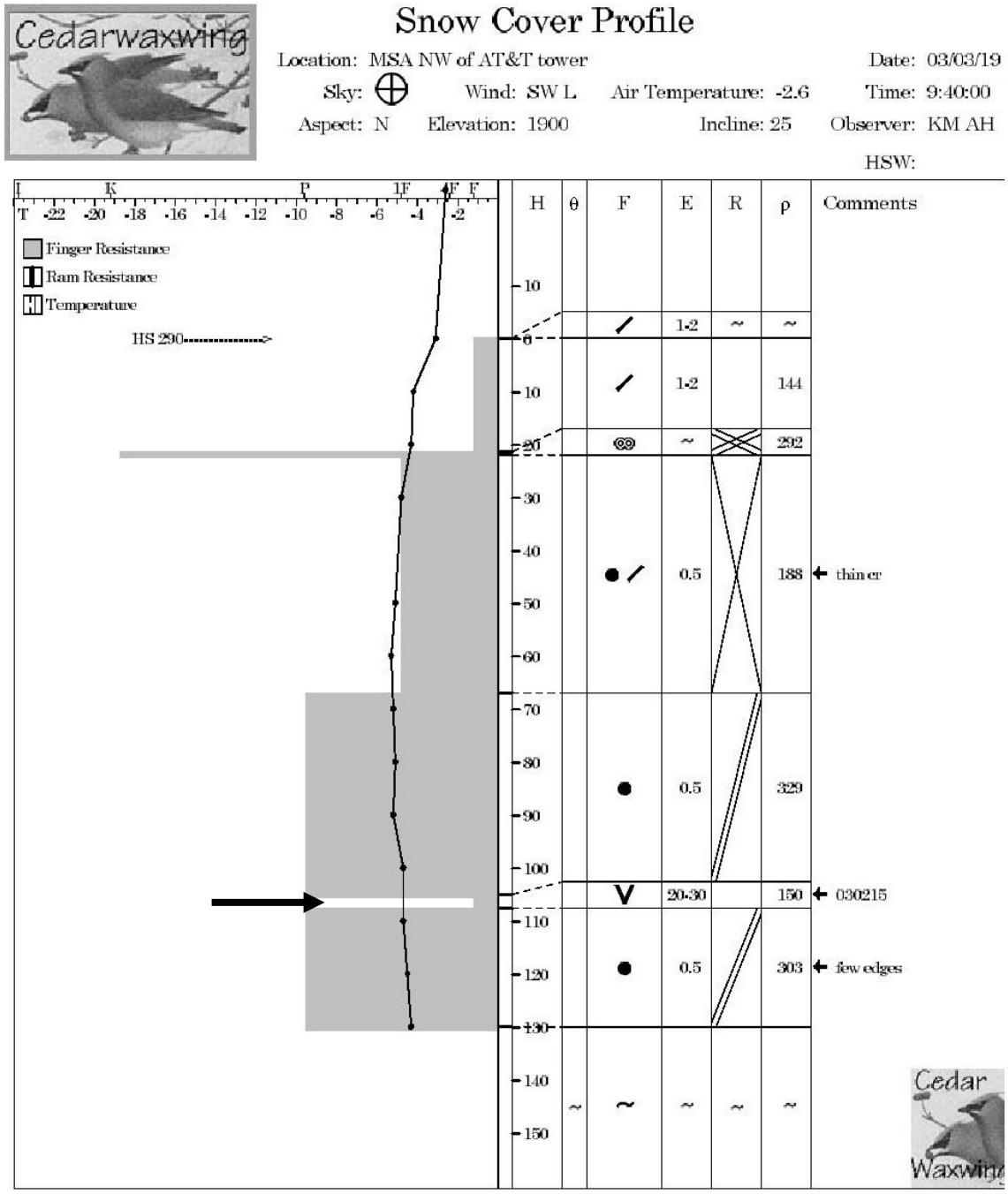

Figure B.39 – Manual snow profile for the propagation test array performed at Mount St. Anne near Blue River on 2003-03-19. The test layer is indicated.

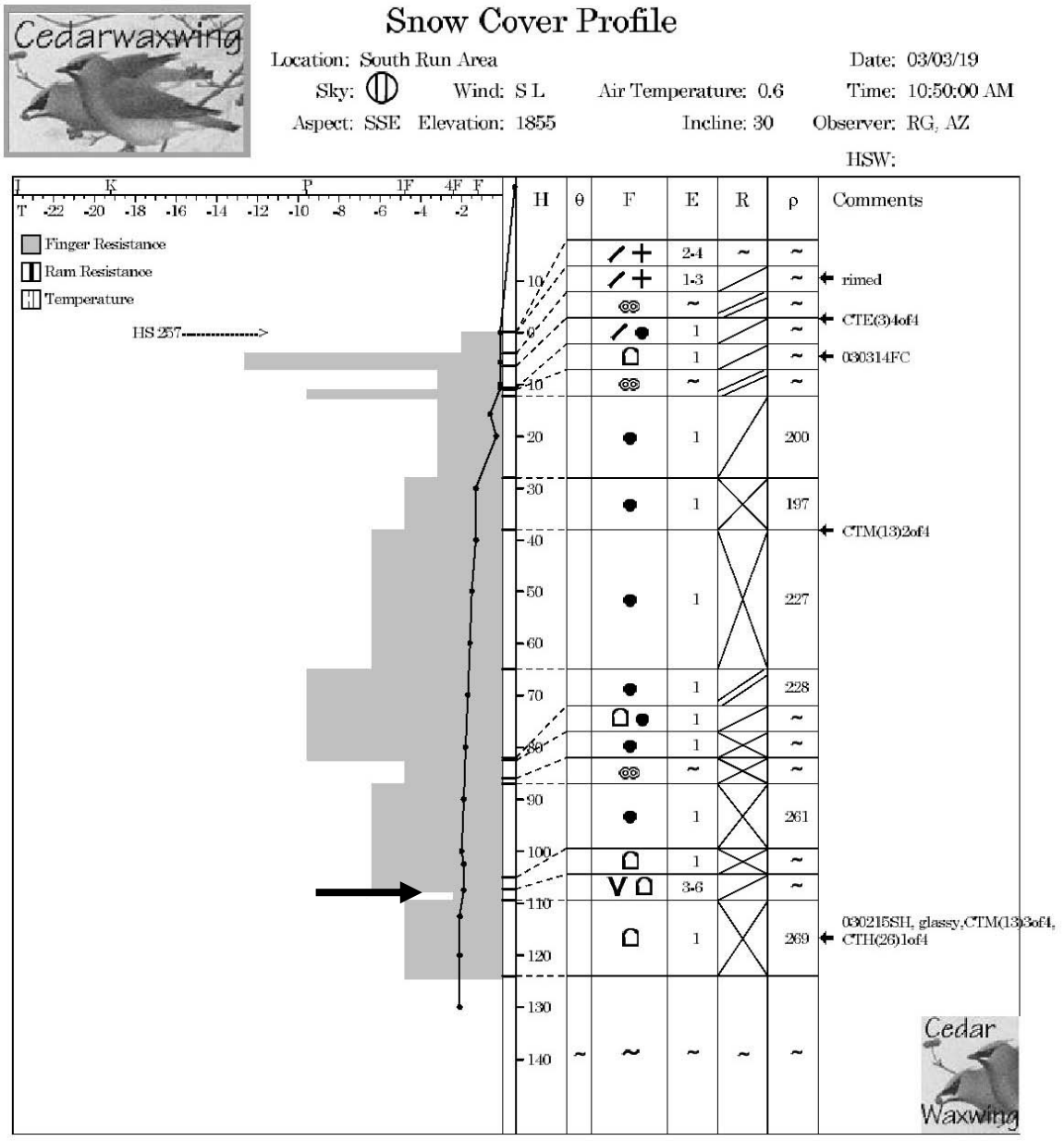

Figure B.40 – Manual snow profile for the propagation test array performed at South Run on Fidelity Mountain near Rogers Pass on 2003-03-19. The test layer is indicated.

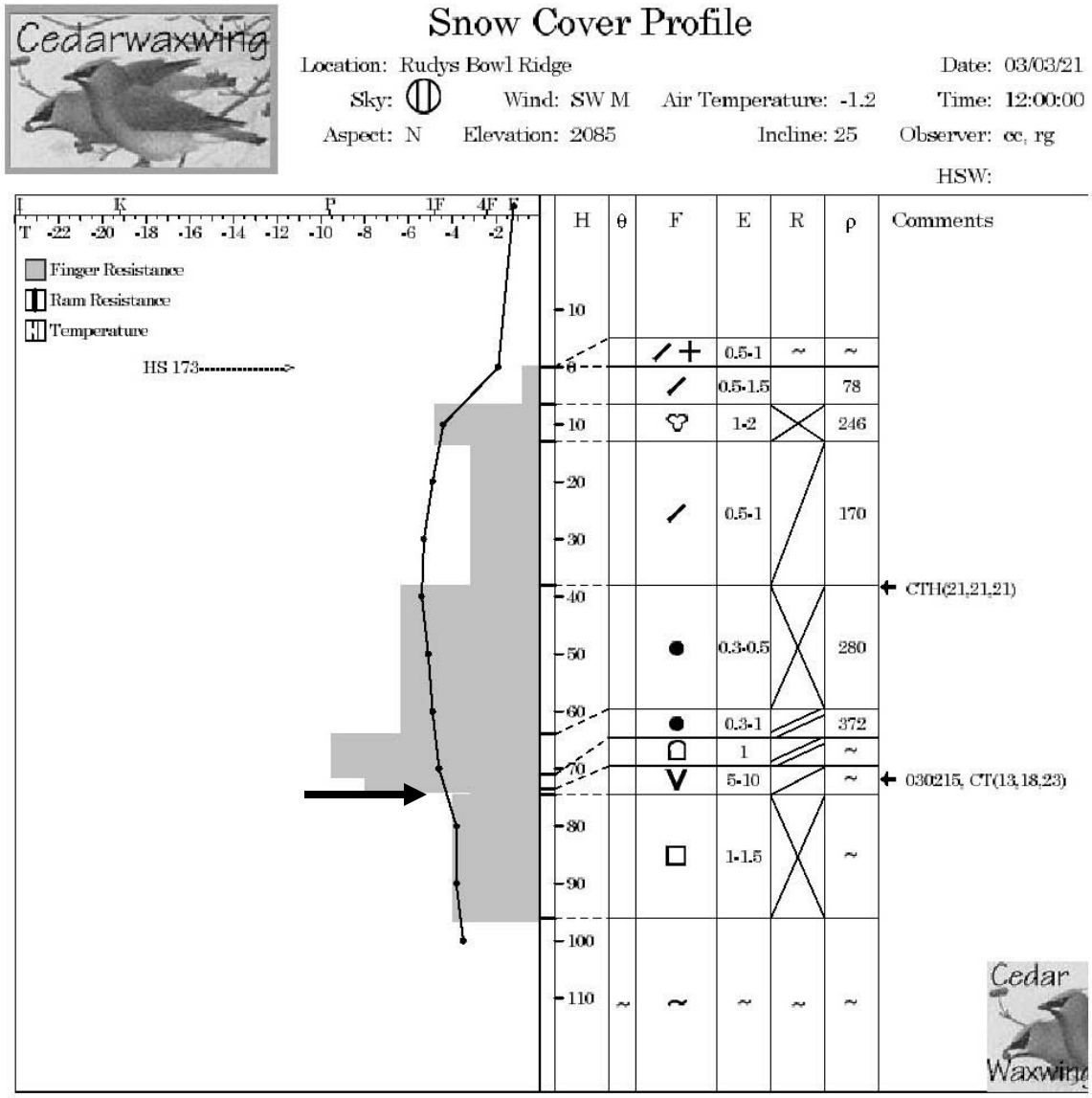

Figure B.41 – Manual snow profile for the propagation test array performed in Rudy's Bowl near Kicking Horse Mountain Resort on 2003-03-21. The test layer is indicated.

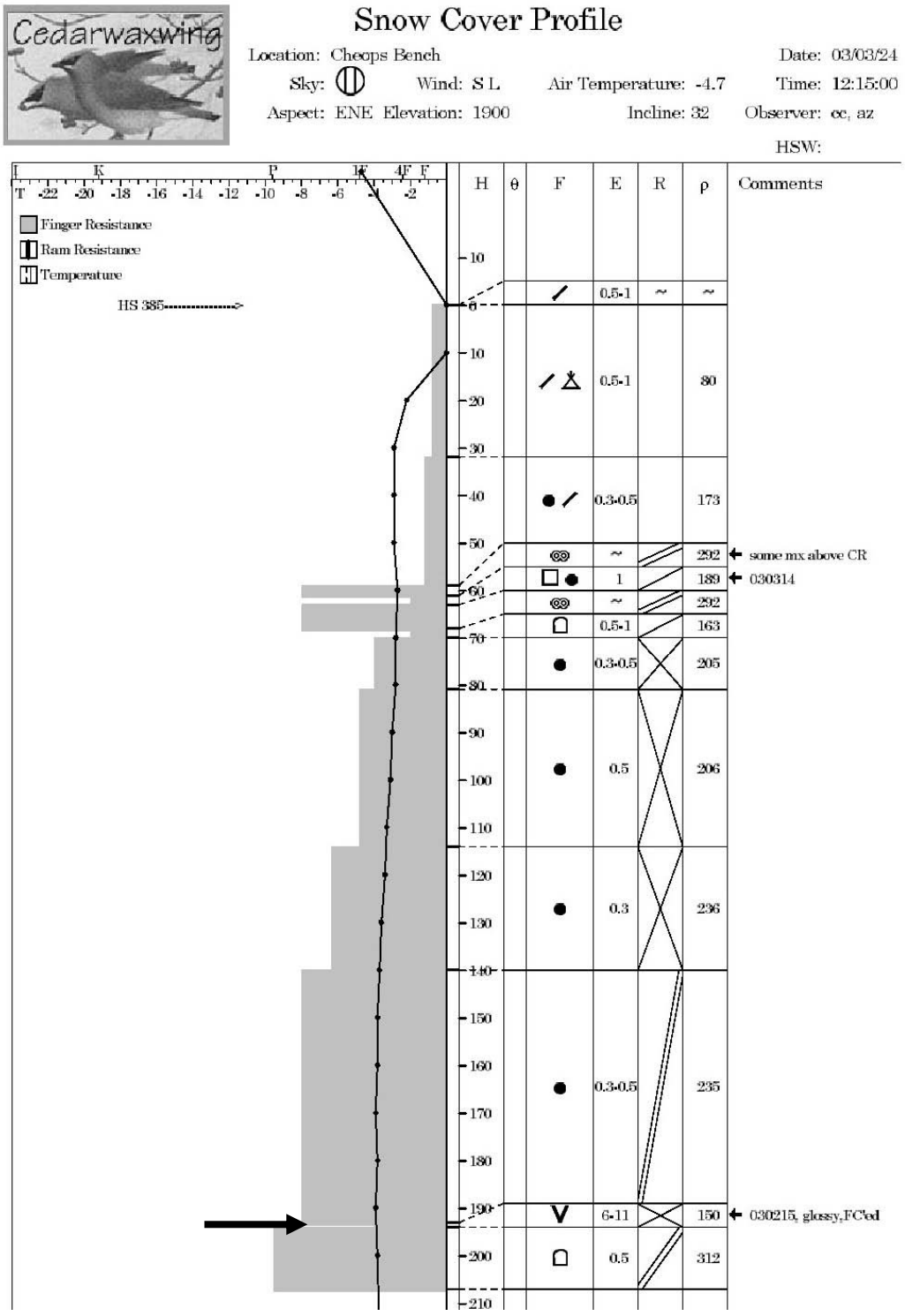

Figure B.42 – Manual snow profile for the propagation test array performed on Cheops Bench near Rogers Pass on 2003-03-24. The test layer is indicated.

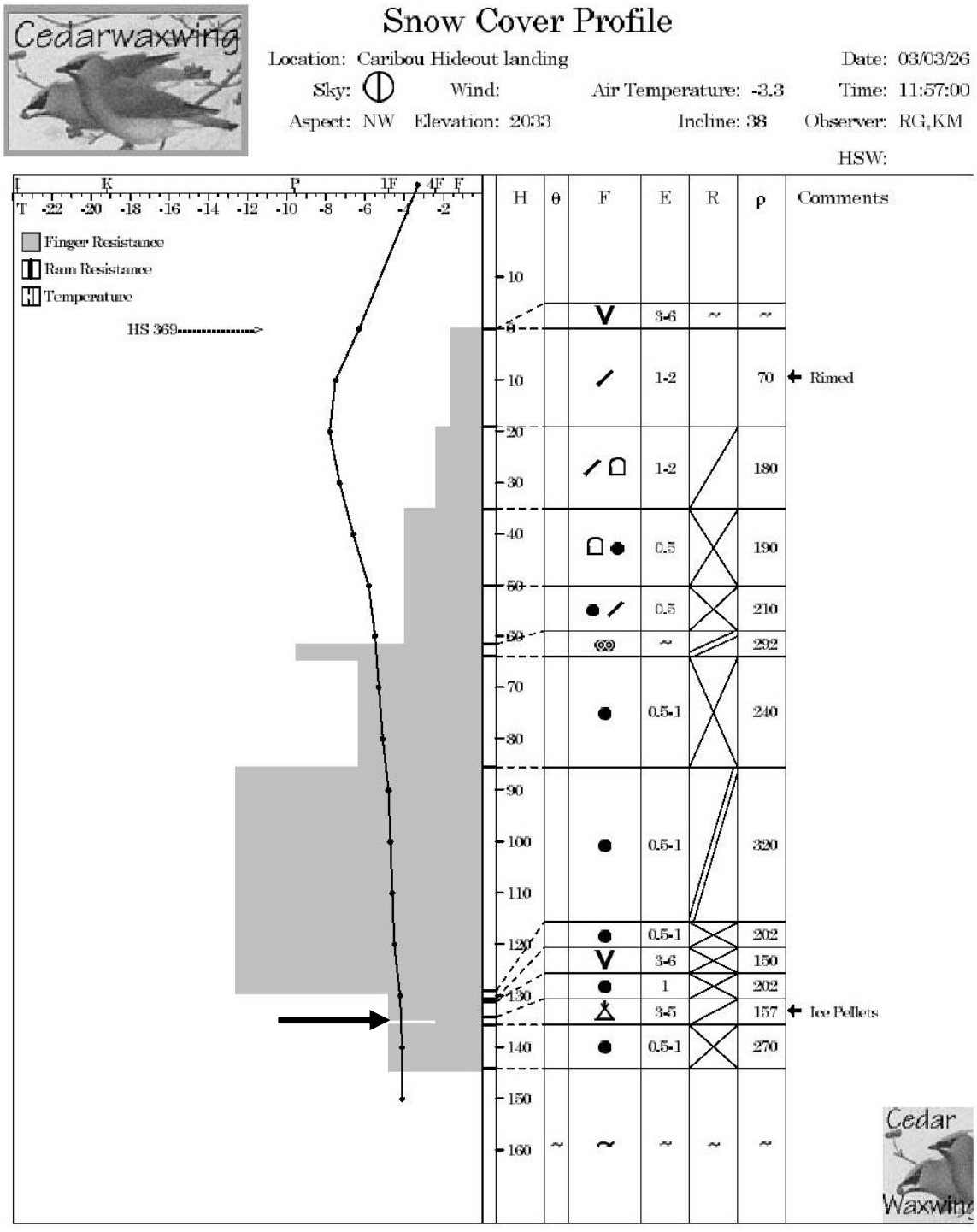

Figure B.43 – Manual snow profile for the propagation test array performed at Caribou Hideout near Blue River on 2003-03-26. The test layer is indicated.

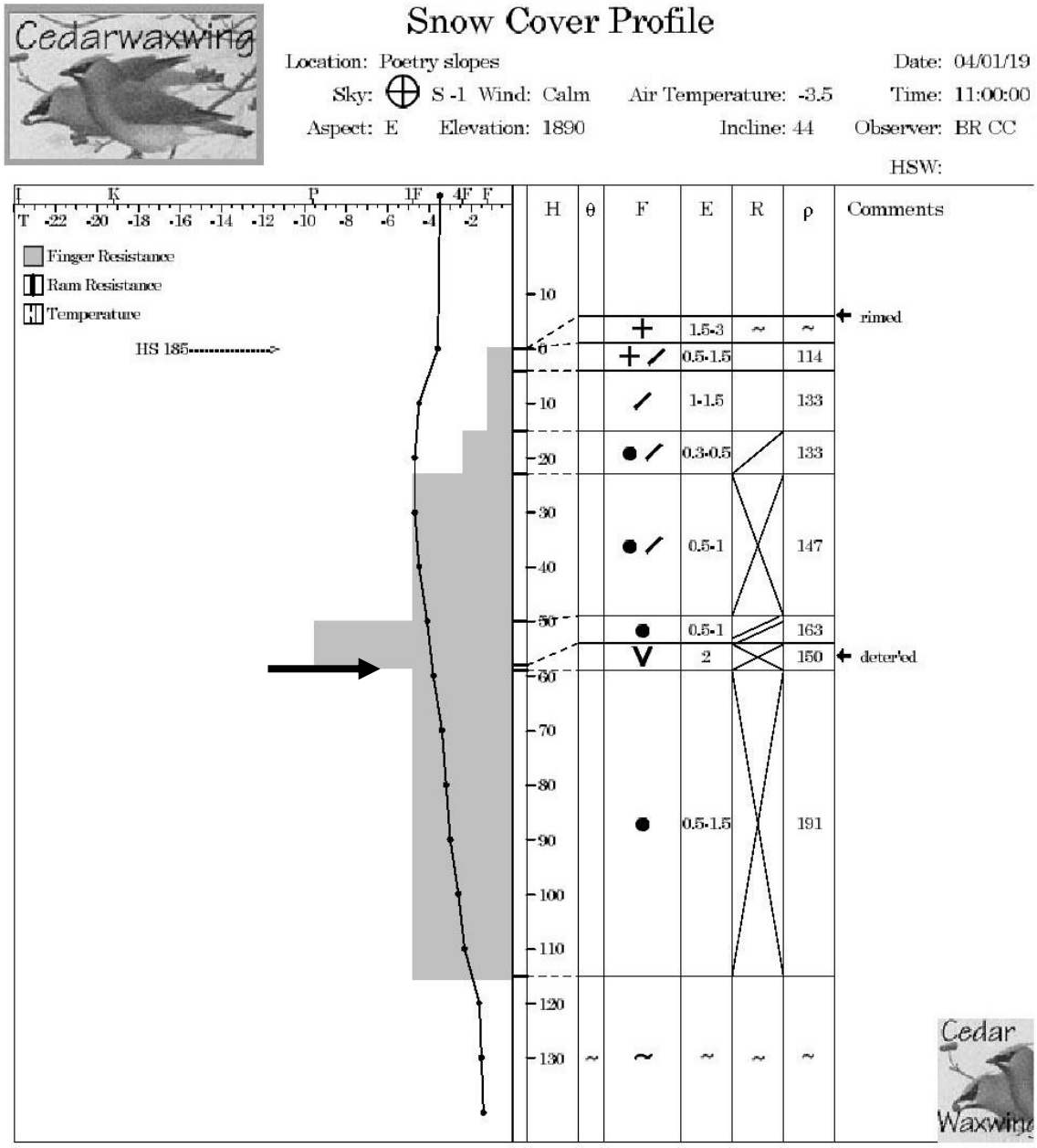

Figure B.44 – Manual snow profile for the propagation test array performed at the Poetry Slopes on Fidelity Mountain near Rogers Pass on 2004-01-19. The test layer is indicated.

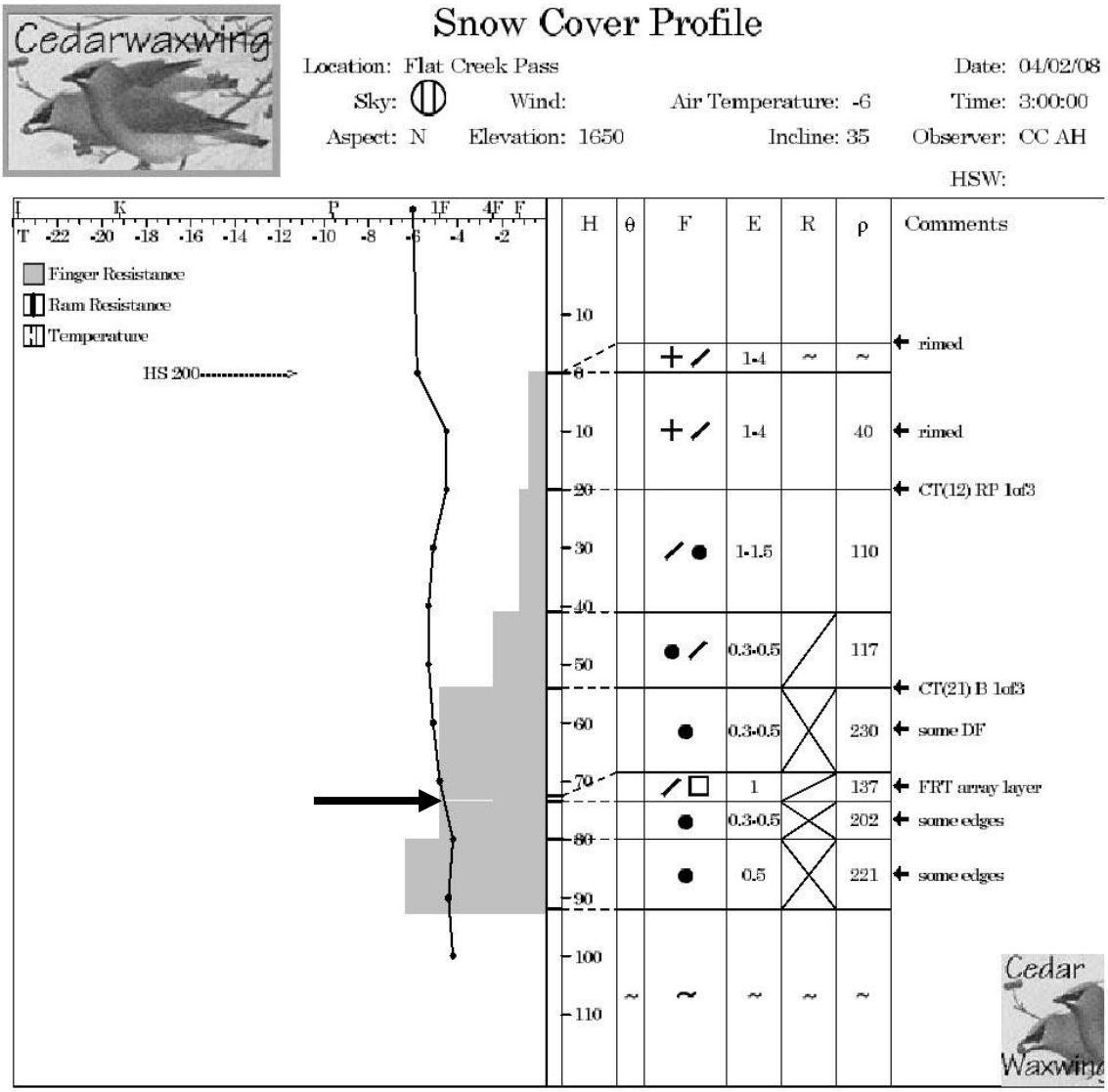

Figure B.45 – Manual snow profile for the propagation test array performed at Mount Fortitude near Rogers Pass on 2004-02-08. The test layer is indicated.

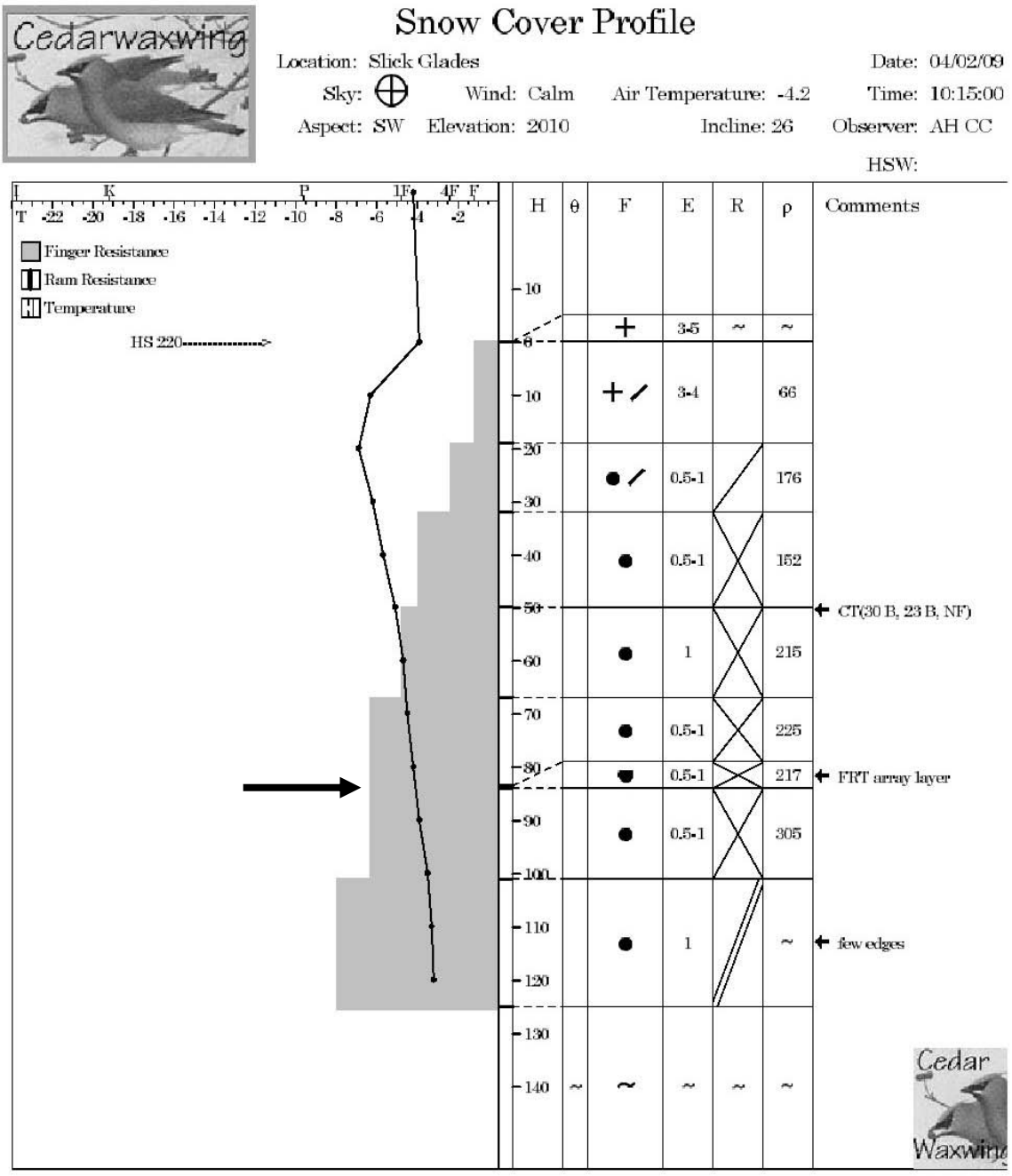

Figure B.46 – Manual snow profile for the propagation test array performed In Slick Glades near Rogers Pass on 2004-02-09. The test layer is indicated.

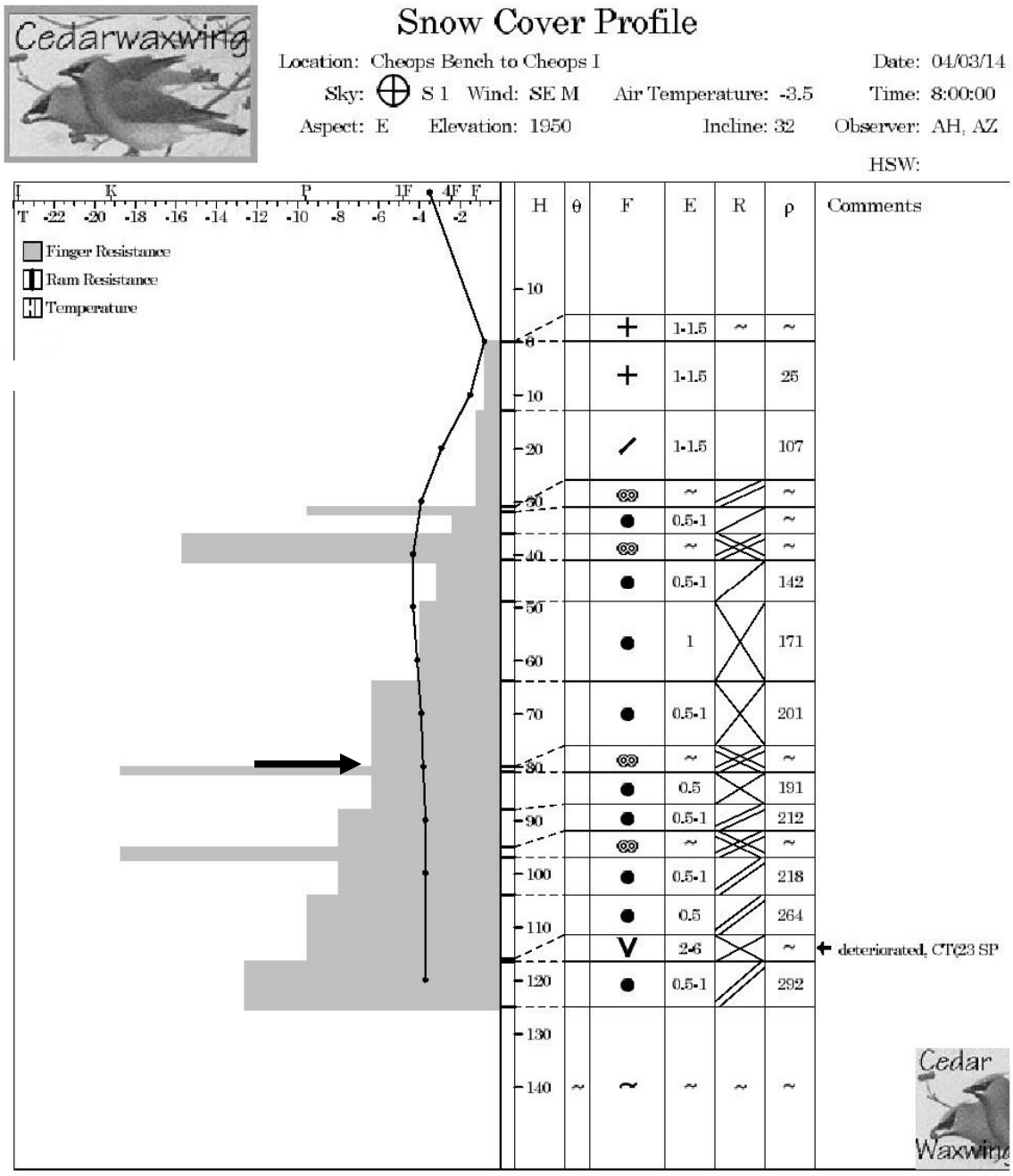

Figure B.47 – Manual snow profile for the propagation test array performed on Cheops Bench near Rogers Pass on 2004-03-14. The test layer is indicated.

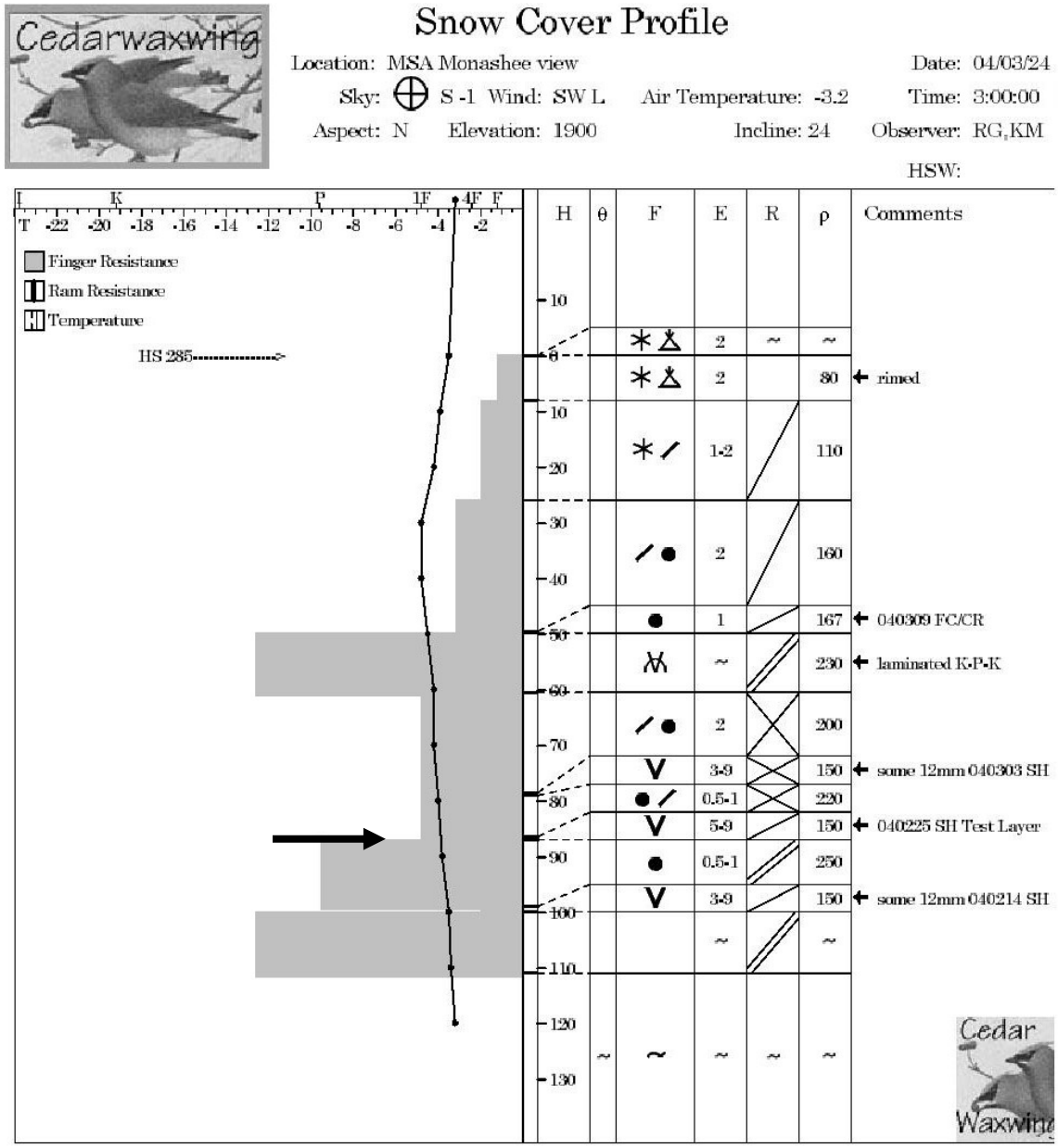

Figure B.48 – Manual snow profile for the propagation test array performed at Monashee View on Mount St. Anne near Blue River on 2004-03-24. The test layer is indicated.

Appendix C – Normality testing

C.1 Individual rutschblock test arrays

Table C.1 - Maximum Kolmogorov-Smirnov test statistics and p-values as well as Lilliefors p-values for the rutschblock test array performed at South Run on 2002-12-17.

	N	max D	K-S *p*	Lilliefors *p*
HS	16	0.24	> 0.20	**< 0.05**
Slope	16	0.19	> 0.20	< 0.15
RB	16	0.25	> 0.20	**< 0.05**
Depth	16	0.26	< 0.20	**< 0.01**
$Slope_{Trend}$	16	0.06	> 0.20	> 0.20
$Slope_{Res}$	16	0.12	> 0.20	> 0.20
$Depth_{Trend}$	16	0.07	> 0.20	> 0.20
$Depth_{Res}$	16	0.15	> 0.20	> 0.20
RB_{Trend}	16	0.10	> 0.20	> 0.20
RB_{Res}	16	0.25	> 0.20	**< 0.05**

Table C.2 – Maximum Kolmogorov-Smirnov test statistics and p-values as well as Lilliefors p-values for the rutschblock test array performed at Bears Den on 2003-01-03.

	N	max D	K-S *p*	Lilliefors *p*
Slope	21	0.25	< 0.10	**< 0.01**
RB	21	0.30	**< 0.05**	**< 0.01**
Depth	21	0.11	> 0.20	> 0.20
RB_{Trend}	21	0.06	> 0.20	> 0.20
RB_{Res}	21	0.11	> 0.20	> 0.20

Table C.3 – Maximum Kolmogorov-Smirnov test statistics and p-values as well as Lilliefors p-values for the rutschblock test array performed at South Run on 2003-01-03.

	N	**max D**	**K-S *p***	**Lilliefors *p***
HS	24	0.15	> 0.20	< 0.15
Slope	24	0.13	> 0.20	> 0.20
RB	22	0.39	**< 0.01**	**< 0.01**
Depth	23	0.20	> 0.20	**< 0.05**
RB_{Trend}	22	0.22	< 0.20	**< 0.01**
RB_{Res}	22	0.19	> 0.20	**< 0.05**

Table C.4 – Maximum Kolmogorov-Smirnov test statistics and p-values as well as Lilliefors p-values for the rutschblock test array performed at Poetry Slopes on 2003-01-07.

	N	**max D**	**K-S *p***	**Lilliefors *p***
HS	22	0.17	> 0.20	< 0.10
Slope	22	0.25	< 0.10	**< 0.01**
RB	22	0.38	**< 0.01**	**< 0.01**
Depth	22	0.23	< 0.15	**< 0.01**
Asp	10	0.26	> 0.20	**< 0.05**
RB_{Trend}	22	0.06	> 0.20	> 0.20
RB_{Res}	22	0.14	> 0.20	> 0.20

Table C.5 – Maximum Kolmogorov-Smirnov test statistics and p-values as well as Lilliefors p-values for the rutschblock test array performed at Robson View on 2003-01-16.

	N	**max D**	**K-S *p***	**Lilliefors *p***
HS	11	0.22	> 0.20	< 0.15
Slope	11	0.22	> 0.20	< 0.15
RB	11	0.48	**< 0.01**	**< 0.01**
RB_{Trend}	11	0.09	> 0.20	> 0.20
RB_{Res}	11	0.23	> 0.20	< 0.15

Table C.6 Maximum Kolmogorov-Smirnov test statistics and p-values as well as Lilliefors p-values for the rutschblock test array performed at Cheops Bench on 2003-01-20.

	N	max D	K-S *p*	Lilliefors *p*
HS	20	0.17	> 0.20	< 0.15
Slope	20	0.25	< 0.15	**< 0.01**
RB	20	0.21	> 0.20	**< 0.05**
Depth	20	0.13	> 0.20	> 0.20
RB_{Trend}	20	0.05	> 0.20	> 0.20
RB_{Res}	20	0.14	> 0.20	> 0.20

Table C.7 – Maximum Kolmogorov-Smirnov test statistics and p-values as well as Lilliefors p-values for the rutschblock test array performed at South Run on 2003-01-30.

	N	max D	K-S *p*	Lilliefors *p*
HS	15	0.16	> 0.20	> 0.20
Slope	15	0.18	> 0.20	< 0.20
RB	14	0.37	**< 0.05**	**< 0.01**
Depth	15	0.20	> 0.20	< 0.10
RB_{Trend}	14	0.11	> 0.20	> 0.20
RB_{Res}	14	0.19	> 0.20	< 0.20

Table C.8 Maximum Kolmogorov-Smirnov test statistics and p-values as well as Lilliefors p-values for the rutschblock test array performed at Fidelity on 2003-02-21.

	N	max D	K-S *p*	Lilliefors *p*
HS	20	0.13	> 0.20	> 0.20
Slope	20	0.18	> 0.20	< 0.10
RB	20	0.44	**< 0.01**	**< 0.01**
Depth	20	0.20	> 0.20	**< 0.05**
$Slope_{Trend}$	20	0.12	> 0.20	> 0.20
$Slope_{Res}$	20	0.15	> 0.20	> 0.20
RB_{Trend}	20	0.14	> 0.20	> 0.20
RB_{Res}	20	0.11	> 0.20	> 0.20

Table C.9 – Maximum Kolmogorov-Smirnov test statistics and p-values as well as Lilliefors p-values for the rutschblock test array performed at Grizzly Shoulder on 2003-02-25.

	N	max D	K-S *p*	Lilliefors *p*
HS	12	0.18	> 0.20	> 0.20
Slope	12	0.16	> 0.20	> 0.20
RB	12	0.46	**< 0.01**	**< 0.01**
Depth	12	0.26	> 0.20	**< 0.05**
$Slope_{Trend}$	12	0.09	> 0.20	> 0.20
$Slope_{Res}$	12	0.15	> 0.20	> 0.20
RB_{Trend}	12	0.11	> 0.20	> 0.20
RB_{Res}	12	0.10	> 0.20	> 0.20

Table C.10 – Maximum Kolmogorov-Smirnov test statistics and p-values as well as Lilliefors p-values for the rutschblock test array performed at Abbott Headwall on 2003-02-27/28.

	N	max D	K-S *p*	Lilliefors *p*
HS	64	0.10	> 0.20	< 0.15
Slope	46	0.11	> 0.20	< 0.20
RB	63	0.21	**< 0.01**	**< 0.01**
Depth	63	0.10	> 0.20	< 0.20
RB_{Trend}	63	0.04	> 0.20	> 0.20
RB_{Res}	63	0.13	> 0.20	**< 0.05**

Table C.11 – Maximum Kolmogorov-Smirnov test statistics and p-values as well as Lilliefors p-values for the rutschblock test array performed at Poetry Slopes on 2003-03-05a.

	N	max D	K-S *p*	Lilliefors *p*
HS	8	0.24	> 0.20	< 0.20
Slope	8	0.19	> 0.20	> 0.20
RB	8	0.28	> 0.20	< 0.10
Depth	8	0.21	> 0.20	> 0.20
RB_{Trend}	8	0.15	> 0.20	> 0.20
RB_{Res}	8	0.14	> 0.20	> 0.20

Table C.12 – Maximum Kolmogorov-Smirnov test statistics and p-values as well as Lilliefors p-values for the rutschblock test array performed at Poetry Slopes on 2003-03-05b.

	N	max D	K-S *p*	Lilliefors *p*
HS	9	0.26	> 0.20	< 0.10
Slope	9	0.17	> 0.20	> 0.20
RB	9	0.52	**< 0.01**	**< 0.01**
Depth	9	0.35	< 0.20	**< 0.01**
RB_{Trend}	9	0.18	> 0.20	> 0.20
RB_{Res}	9	0.23	> 0.20	< 0.20

Table C.13 – Maximum Kolmogorov-Smirnov test statistics and p-values as well as Lilliefors p-values for the rutschblock test array performed at Robson View on 2003-03-05.

	N	max D	K-S *p*	Lilliefors *p*
HS	29	0.24	< 0.10	**< 0.01**
Slope	29	0.12	> 0.20	> 0.20
RB	29	0.32	**< 0.01**	**< 0.01**
Depth	29	0.20	< 0.20	**< 0.01**
RB_{Trend}	29	0.08	> 0.20	> 0.20
RB_{Res}	29	0.11	> 0.20	> 0.20

Table C.14 – Maximum Kolmogorov-Smirnov test statistics and p-values as well as Lilliefors p-values for the rutschblock test array performed at Waikiki on 2003-03-12.

	N	max D	K-S *p*	Lilliefors *p*
HS	18	0.25	< 0.20	**< 0.01**
Slope	18	0.20	> 0.20	**< 0.05**
RB	18	0.30	< 0.10	**< 0.01**
Depth	18	0.21	> 0.20	**< 0.05**
RB_{Trend}	18	0.07	> 0.20	> 0.20
RB_{Res}	18	0.24	> 0.20	**< 0.05**

Table C.15 – Maximum Kolmogorov-Smirnov test statistics and p-values as well as Lilliefors p-values for the rutschblock test array performed at Toilet Bowl on 2004-01-17.

	N	max D	K-S *p*	Lilliefors *p*
HS	18	0.28	< 0.10	**< 0.01**
Slope	18	0.19	> 0.20	< 0.10
RB	18	0.28	< 0.10	**< 0.01**
Depth	18	0.26	< 0.15	**< 0.01**
HS_{Trend}	18	0.08	> 0.20	> 0.20
HS_{Res}	18	0.19	> 0.20	< 0.10
$Slope_{Trend}$	18	0.08	> 0.20	> 0.20
$Slope_{Res}$	18	0.12	> 0.20	> 0.20
RB_{Trend}	18	0.11	> 0.20	> 0.20
RB_{Res}	18	0.15	> 0.20	> 0.20
$Depth_{Trend}$	18	0.08	> 0.20	> 0.20
$Depth_{Res}$	18	0.16	> 0.20	> 0.20

Table C.16 – Maximum Kolmogorov-Smirnov test statistics and p-values as well as Lilliefors p-values for the rutschblock test array performed at Poetry Slopes on 2004-02-02.

	N	max D	K-S *p*	Lilliefors *p*
HS	14	0.21	> 0.20	< 0.10
Slope	14	0.12	> 0.20	> 0.20
RB	13	0.25	> 0.20	**< 0.05**
Depth	13	0.18	> 0.20	> 0.20
HS_{Trend}	14	0.09	> 0.20	> 0.20
HS_{Res}	14	0.14	> 0.20	> 0.20
$Depth_{Trend}$	14	0.06	> 0.20	> 0.20
$Depth_{Res}$	14	0.14	> 0.20	> 0.20
RB_{Trend}	13	0.09	> 0.20	> 0.20
RB_{Res}	13	0.16	> 0.20	> 0.20

Table C.17 – Maximum Kolmogorov-Smirnov test statistics and p-values as well as Lilliefors p-values for the rutschblock test array performed at Langevin Cutblock on 2004-02-12.

	N	max D	K-S *p*	Lilliefors *p*
HS	34	0.12	> 0.20	> 0.20
Slope	34	0.28	**< 0.01**	**< 0.01**
RB	34	0.32	**< 0.01**	**< 0.01**
Depth	34	0.15	> 0.20	< 0.10
HS_{Trend}	36	0.09	> 0.20	> 0.20
HS_{Res}:	36	0.13	> 0.20	< 0.15
$Depth_{Trend}$:	36	0.04	> 0.20	> 0.20
$Depth_{Res}$:	36	0.13	> 0.20	< 0.20
RB_{Trend}:	34	0.08	> 0.20	> 0.20
RB_{Res}:	34	0.16	> 0.20	**< 0.05**

Table C.18 – Maximum Kolmogorov-Smirnov test statistics and p-values as well as Lilliefors p-values for the rutschblock test array performed at Robson View on 2004-02-25.

	N	max D	K-S *p*	Lilliefors *p*
HS	43	0.11	> 0.20	> 0.20
Slope	43	0.15	> 0.20	**< 0.05**
RB	43	0.30	**< 0.01**	**< 0.01**
Depth	43	0.16	> 0.20	**< 0.01**
Asp	43	0.09	> 0.20	> 0.20
Asp_{Trend}	43	0.09	> 0.20	> 0.20
Asp_{Res}	43	0.14	> 0.20	**< 0.05**
RB_{Trend}	43	0.06	> 0.20	> 0.20
RB_{Res}	43	0.23	**< 0.05**	**< 0.01**

Table C.19 – Maximum Kolmogorov-Smirnov test statistics and p-values as well as Lilliefors p-values for the rutschblock test array performed at Monashee View on 2004-02-27.

	N	max D	K-S *p*	Lilliefors *p*
HS	65	0.08	> 0.20	> 0.20
Slope	65	0.14	< 0.20	**< 0.01**
RB	65	0.43	**< 0.01**	**< 0.01**
Depth	65	0.18	**< 0.05**	**< 0.01**
Asp	65	0.18	**< 0.05**	**< 0.01**
Emin	62	0.28	**< 0.01**	**< 0.01**
Emax	62	0.17	< 0.10	**< 0.01**
$Slope_{Trend}$	65	0.04	> 0.20	> 0.20
$Slope_{Res}$	65	0.08	> 0.20	> 0.20
Asp_{Trend}	65	0.05	> 0.20	> 0.20
Asp_{Res}	65	0.06	> 0.20	> 0.20
$Emin_{Trend}$	65	0.05	> 0.20	> 0.20
$Emin_{Res}$	65	0.06	> 0.20	> 0.20
$Emax_{Trend}$	65	0.05	> 0.20	> 0.20
$Emax_{Res}$	65	0.10	> 0.20	< 0.10
RB_{Trend}	65	0.05	> 0.20	> 0.20
RB_{Res}	65	0.23	**< 0.01**	**< 0.01**

Table C.20 – Maximum Kolmogorov-Smirnov test statistics and p-values as well as Lilliefors p-values for the rutschblock test array performed at Poetry Slopes on 2004-02-28.

	N	max D	K-S *p*	Lilliefors *p*
HS	30	0.13	> 0.20	< 0.20
Slope	30	0.24	**< 0.05**	**< 0.01**
RB	30	0.35	**< 0.01**	**< 0.01**
Depth	30	0.12	> 0.20	> 0.20
HS_{Trend}	30	0.08	> 0.20	> 0.20
HS_{Res}	30	0.14	> 0.20	< 0.15
$Slope_{Trend}$	30	0.04	> 0.20	> 0.20
$Slope_{Res}$	30	0.08	> 0.20	> 0.20
RB_{Trend}	30	0.05	> 0.20	> 0.20
RB_{Res}	30	0.12	> 0.20	> 0.20
$Depth_{Trend}$	30	0.13	> 0.20	< 0.20
$Depth_{Res}$	30	0.15	> 0.20	< 0.10

Table C.21 – Maximum Kolmogorov-Smirnov test statistics and p-values as well as Lilliefors p-values for the rutschblock test array performed at Squirrel Slope on 2004-03-03.

	N	**max D**	**K-S *p***	**Lilliefors *p***
HS	24	0.13	> 0.20	> 0.20
Slope	24	0.12	> 0.20	> 0.20
RB	24	0.26	< 0.10	**< 0.01**
Depth	24	0.15	> 0.20	< 0.15
Asp	24	0.21	< 0.20	**< 0.01**
Thick	24	0.18	> 0.20	**< 0.05**
$Slope_{Trend}$	24	0.08	> 0.20	> 0.20
$Slope_{Res}$	24	0.15	> 0.20	< 0.20
RB_{Trend}	24	0.19	> 0.20	**< 0.05**
RB_{Res}	24	0.29	**< 0.05**	**< 0.01**
$Depth_{Trend}$	24	0.05	> 0.20	> 0.20
$Depth_{Res}$	24	0.14	> 0.20	> 0.20

Table C.22 – Maximum Kolmogorov-Smirnov test statistics and p-values as well as Lilliefors p-values for the rutschblock test array performed at Abbott Headwall on 2004-03-06/07.

	N	**max D**	**K-S *p***	**Lilliefors *p***
HS	62	0.06	> 0.20	> 0.20
Slope	64	0.11	> 0.20	**< 0.05**
RB	64	0.24	**< 0.01**	**< 0.01**
Depth	62	0.24	**< 0.01**	**< 0.01**
Thick	62	0.20	**< 0.05**	**< 0.01**
Emin	62	0.26	**< 0.01**	**< 0.01**
Emax	63	0.19	**< 0.05**	**< 0.01**
HS_{Trend}	64	0.06	> 0.20	> 0.20
HS_{Res}	64	0.08	> 0.20	> 0.20
$Slope_{Trend}$	64	0.03	> 0.20	> 0.20
$Slope_{Res}$	64	0.06	> 0.20	> 0.20
RB_{Trend}	64	0.06	> 0.20	> 0.20
RB_{Res}	64	0.11	> 0.20	< 0.10
$Depth_{Trend}$	63	0.14	< 0.20	**< 0.01**
$Depth_{Res}$	63	0.11	> 0.20	**< 0.05**
$Thick_{Trend}$	64	0.06	> 0.20	> 0.20
$Thick_{Res}$	64	0.10	> 0.20	< 0.15
$Emax_{Trend}$	64	0.03	> 0.20	> 0.20
$Emax_{Res}$	64	0.11	> 0.20	**< 0.05**

Table C.23 – Maximum Kolmogorov-Smirnov test statistics and p-values as well as Lilliefors p-values for the rutschblock test array performed at Mt. St. Anne on 2004-03-10.

	N	**max D**	**K-S *p***	**Lilliefors *p***
HS	33	0.16	> 0.20	**< 0.05**
Slope	33	0.15	> 0.20	< 0.10
RB	33	0.37	**< 0.01**	**< 0.01**
Depth	33	0.20	< 0.15	**< 0.01**
Emin	33	0.42	**< 0.01**	**< 0.01**
Emax	33	0.42	**< 0.01**	**< 0.01**
$Slope_{Trend}$	37	0.08	> 0.20	> 0.20
$Slope_{Res}$	37	0.10	> 0.20	> 0.20
RB_{Trend}	37	0.08	> 0.20	> 0.20
RB_{Res}	37	0.11	> 0.20	> 0.20
$Depth_{Trend}$	37	0.10	> 0.20	> 0.20
$Depth_{Res}$	37	0.11	> 0.20	> 0.20

Table C.24 – Maximum Kolmogorov-Smirnov test statistics and p-values as well as Lilliefors p-values for the rutschblock test array performed at Bears Den on 2004-03-11a.

	N	**max D**	**K-S *p***	**Lilliefors *p***
HS	6	0.25	> 0.20	> 0.20
Slope	6	0.25	> 0.20	> 0.20
RB	6	0.31	> 0.20	< 0.10
Depth	6	0.26	> 0.20	> 0.20
Asp	5	0.22	> 0.20	> 0.20
Emin	5	0.30	> 0.20	< 0.15
Emax	5	0.27	> 0.20	> 0.20
RB_{Trend}	6	0.18	> 0.20	> 0.20
RB_{Res}	6	0.23	> 0.20	> 0.20

Table C.25 – Maximum Kolmogorov-Smirnov test statistics and p-values as well as Lilliefors p-values for the rutschblock test array performed at Bears Den on 2004-03-11 b.

	N	max D	K-S *p*	Lilliefors *p*
HS	8	0.15	> 0.20	> 0.20
Slope	8	0.21	> 0.20	> 0.20
RB	9	0.41	< 0.10	**< 0.01**
Depth	9	0.19	> 0.20	> 0.20
Asp	8	0.23	> 0.20	> 0.20
RB_{Trend}	9	0.16	> 0.20	> 0.20
RB_{Res}	9	0.15	> 0.20	> 0.20

Table C.26 – Maximum Kolmogorov-Smirnov test statistics and p-values as well as Lilliefors p-values for the rutschblock test array performed at Abbott on 2004-03-11/12.

	N	max D	K-S *p*	Lilliefors *p*
HS	26	0.15	> 0.20	< 0.10
Slope	26	0.20	< 0.15	**< 0.01**
RB	26	0.31	**< 0.01**	**< 0.01**
Depth	26	0.12	> 0.20	> 0.20
Emin	26	0.36	**< 0.01**	**< 0.01**
Emax	26	0.51	**< 0.01**	**< 0.01**
HS_{Trend}	27	0.11	> 0.20	> 0.20
HS_{Res}	27	0.09	> 0.20	> 0.20
$Slope_{Trend}$	27	0.21	< 0.15	**< 0.01**
$Slope_{Res}$	27	0.11	> 0.20	> 0.20
$Depth_{Trend}$	27	0.18	> 0.20	**< 0.05**
$Depth_{Res}$	27	0.15	> 0.20	< 0.10
$Emax_{Trend}$	27	0.10	> 0.20	> 0.20
$Emax_{Res}$	27	0.10	> 0.20	> 0.20
RB_{Trend}	27	0.20	< 0.15	**< 0.01**
RB_{Res}	27	0.27	**< 0.05**	**< 0.01**

Table C.27 – Maximum Kolmogorov-Smirnov test statistics and p-values as well as Lilliefors p-values for the rutschblock test array performed at South Run on 2004-03-18.

	N	max D	K-S *p*	Lilliefors *p*
HS	23	0.12	> 0.20	> 0.20
Slope	23	0.15	> 0.20	> 0.20
RB	23	0.25	< 0.10	**< 0.01**
Depth	23	0.13	> 0.20	> 0.20
Asp	23	0.11	> 0.20	> 0.20
$Depth_{Trend}$	23	0.06	> 0.20	> 0.20
$Depth_{Res}$	23	0.19	> 0.20	**< 0.05**
Asp_{Trend}	23	0.07	> 0.20	> 0.20
Asp_{Res}	23	0.13	> 0.20	> 0.20
RB_{Trend}	23	0.08	> 0.20	> 0.20
RB_{Res}	23	0.14	> 0.20	> 0.20

Table C.28 – Maximum Kolmogorov-Smirnov test statistics and p-values as well as Lilliefors p-values for the rutschblock test array (a) performed at Schuss Cr. on 2004-03-21.

	N	max D	K-S *p*	Lilliefors *p*
HS	13	0.15	> 0.20	> 0.20
Slope	13	0.23	> 0.20	< 0.10
RB	13	0.32	< 0.15	**< 0.01**
Depth	13	0.29	< 0.20	**< 0.01**
Asp	13	0.12	> 0.20	> 0.20
Emin	13	0.43	**< 0.05**	**< 0.01**
Emax	13	1.00	**< 0.01**	**< 0.01**
Asp_{Trend}	13	0.09	> 0.20	> 0.20
Asp_{Res}	13	0.19	> 0.20	> 0.20
$Emin_{Trend}$	13	0.10	> 0.20	> 0.20
$Emin_{Res}$	13	0.11	> 0.20	> 0.20
RB_{Trend}	13	0.16	> 0.20	> 0.20
RB_{Res}	13	0.15	> 0.20	> 0.20

Table C.29 – Maximum Kolmogorov-Smirnov test statistics and p-values as well as Lilliefors p-values for the rutschblock test array (b) performed at Schuss Cr. on 2004-03-21.

	N	max D	K-S *p*	Lilliefors *p*
HS	19	0.14	> 0.20	> 0.20
Slope	19	0.15	> 0.20	> 0.20
RB	19	0.21	> 0.20	**< 0.05**
Depth	19	0.24	< 0.20	**< 0.01**
Asp	19	1.00	**< 0.01**	**< 0.01**
Emin	19	1.00	**< 0.01**	**< 0.01**
Emax	19	0.40	**< 0.01**	**< 0.01**
HS_{Trend}	19	0.18	> 0.20	< 0.10
HS_{Res}	19	0.09	> 0.20	> 0.20
RB_{Trend}	19	0.10	> 0.20	> 0.20
RB_{Res}	19	0.09	> 0.20	> 0.20

C.2 Rutschblack test array medians

Table C.30 – Maximum Kolmogorov-Smirnov test statistics and p-values as well as Lilliefors p-values for the rutschblock test array medians.

	N	max D	K-S *p*	Lilliefors *p*
Med RB	29	0.20	< 0.20	**< 0.01**
RB IQR	29	0.26	**< 0.05**	**< 0.01**
RB QCV	29	0.13	> 0.20	> 0.20
RB SIQR	29	0.25	**< 0.05**	**< 0.01**
Med HS	28	0.15	> 0.20	< 0.10
Med Slope	29	0.09	> 0.20	> 0.20
Med Depth	29	0.08	> 0.20	> 0.20

C.3 Normalized rutschblock test array data

Table C.31 – Maximum Kolmogorov-Smirnov test statistics and p-values as well as Lilliefors p-values for the normalized and combined rutschblock test array data.

	N	max D	K-S *p*	Lilliefors *p*
$Slope_{Norm}$	517	0.09	**< 0.01**	**< 0.01**
RB_{Norm}	705	0.25	**< 0.01**	**< 0.01**
$Depth_{Norm}$	534	0.10	**< 0.01**	**< 0.01**
HS_{Norm}	512	0.05	**< 0.05**	**< 0.01**

C.4 Individual fracture propagation test arrays

Table C.32 – Maximum Kolmogorov-Smirnov test statistics and p-values as well as Lilliefors p-values for the propagation test array performed at Poetry Slopes on 2003-01-06.

	N	max D	K-S *p*	Lilliefors *p*
Thick	56	0.21	**< 0.05**	**< 0.01**
DH	56	0.38	**< 0.01**	**< 0.01**
Depth	56	0.11	> 0.20	< 0.10
HS	56	0.09	> 0.20	> 0.20
Slope	56	0.10	> 0.20	> 0.20
Asp	11	0.28	> 0.20	**< 0.05**
DHE	56	0.36	**< 0.01**	**< 0.01**
DHE_{Trend}	56	0.07	> 0.20	> 0.20
DHE_{Res}	56	0.28	**< 0.01**	**< 0.01**

Table C.33 – Maximum Kolmogorov-Smirnov test statistics and p-values as well as Lilliefors p-values for the propagation test array performed at South Run on 2003-01-11.

	N	**max D**	**K-S *p***	**Lilliefors *p***
Depth	43	0.12	> 0.20	< 0.15
HS	43	0.11	> 0.20	> 0.20
Slope	43	0.11	> 0.20	> 0.20
EMin	43	0.29	**< 0.01**	**< 0.01**
EMax	43	0.20	< 0.10	**< 0.01**
DHE	43	0.19	< 0.10	**< 0.01**
DHE_{Trend}	43	0.07	> 0.20	> 0.20
DHE_{Res}	43	0.11	> 0.20	> 0.20

Table C.34 – Maximum Kolmogorov-Smirnov test statistics and p-values as well as Lilliefors p-values for the propagation test array (a) performed at NRC Gully on 2003-01-17.

	N	**max D**	**K-S *p***	**Lilliefors *p***
Thick	19	0.25	< 0.20	**< 0.01**
DH	19	0.24	< 0.20	**< 0.01**
Depth	19	0.10	> 0.20	> 0.20
HS	19	0.08	> 0.20	> 0.20
Slope	19	0.14	> 0.20	> 0.20
Asp	19	1.00	**< 0.01**	**< 0.01**
DHE	19	0.21	> 0.20	**< 0.05**
DHE_{Trend}	19	0.08	> 0.20	> 0.20
DHE_{Res}	19	0.11	> 0.20	> 0.20
$Thick_{Trend}$	19	0.12	> 0.20	> 0.20
$Thick_{Res}$	19	0.12	> 0.20	> 0.20
$Slope_{Trend}$	19	0.11	> 0.20	> 0.20
$Slope_{Res}$	19	0.20	> 0.20	**< 0.05**

Table C.35 – Maximum Kolmogorov-Smirnov test statistics and p-values as well as Lilliefors p-values for the propagation test array (b) performed at NRC Gully on 2003-01-17.

	N	max D	K-S *p*	Lilliefors *p*
Thick	24	0.18	> 0.20	< 0.10
DH	24	0.34	**< 0.01**	**< 0.01**
Depth	24	0.09	> 0.20	> 0.20
HS	24	0.10	> 0.20	> 0.20
Slope	24	0.13	> 0.20	> 0.20
Asp	24	1.00	**< 0.01**	**< 0.01**
DHE	24	0.24	< 0.15	**< 0.01**
DHE_{Trend}	24	0.17	> 0.20	< 0.10
DHE_{Res}	24	0.11	> 0.20	> 0.20

Table C.36 – Maximum Kolmogorov-Smirnov test statistics and p-values as well as Lilliefors p-values for the propagation test array performed at Christiania Ridge on 2003-01-21.

	N	max D	K-S *p*	Lilliefors *p*
Thick	16	0.35	**< 0.05**	**< 0.01**
DH	29	0.20	< 0.15	**< 0.01**
Depth	29	0.16	> 0.20	**< 0.05**
HS	29	0.15	> 0.20	< 0.10
Slope	29	0.21	< 0.15	**< 0.01**
DHE	29	0.10	> 0.20	> 0.20
DHE_{Trend}	29	0.07	> 0.20	> 0.20
DHE_{Res}	29	0.16	> 0.20	**< 0.05**

Table C.37 – Maximum Kolmogorov-Smirnov test statistics and p-values as well as Lilliefors p-values for the propagation test array performed at Poetry Slopes on 2003-01-24.

	N	max D	K-S *p*	Lilliefors *p*
Thick	39	0.26	**< 0.05**	**< 0.01**
DH	39	0.10	> 0.20	> 0.20
Depth	39	0.15	> 0.20	**< 0.05**
HS	39	0.10	> 0.20	> 0.20
Slope	39	0.17	< 0.20	**< 0.01**
DHE	39	0.09	> 0.20	> 0.20
DHE_{Trend}	39	0.07	> 0.20	> 0.20
DHE_{Res}	39	0.10	> 0.20	> 0.20
$Thick_{Trend}$	39	0.04	> 0.20	> 0.20
$Thick_{Res}$	39	0.09	> 0.20	> 0.20
$Depth_{Trend}$	39	0.17	> 0.20	**< 0.01**
$Depth_{Res}$	39	0.08	> 0.20	> 0.20
HS_{Trend}	39	0.07	> 0.20	> 0.20
HS_{Res}	39	0.13	> 0.20	< 0.10

Table C.38 – Maximum Kolmogorov-Smirnov test statistics and p-values as well as Lilliefors p-values for the propagation test array performed at Mt. St. Anne on 2003-01-30.

	N	max D	K-S *p*	Lilliefors *p*
Thick	19	1.00	**< 0.01**	**< 0.01**
DH	19	0.21	> 0.20	**< 0.05**
HS	19	0.17	> 0.20	< 0.20
Slope	19	0.43	**< 0.01**	**< 0.01**
DS	19	0.24	< 0.20	**< 0.01**
DHE	19	0.16	> 0.20	> 0.20
DHE_{Trend}	19	0.08	> 0.20	> 0.20
DHE_{Res}	19	0.14	> 0.20	> 0.20

Table C.39 – Maximum Kolmogorov-Smirnov test statistics and p-values as well as Lilliefors p-values for the propagation test array performed at Poetry Slopes on 2003-02-03.

	N	max D	K-S *p*	Lilliefors *p*
Thick	52	0.23	**< 0.01**	**< 0.01**
DH	52	0.12	> 0.20	< 0.10
Depth	52	0.09	> 0.20	> 0.20
HS	52	0.10	> 0.20	> 0.20
Slope	52	0.12	> 0.20	< 0.10
DHE	52	0.09	> 0.20	> 0.20
DHE_{Trend}	52	0.03	> 0.20	> 0.20
DHE_{Res}	52	0.09	> 0.20	> 0.20

Table C.40 – Maximum Kolmogorov-Smirnov test statistics and p-values as well as Lilliefors p-values for the propagation test array performed at Mt. St. Anne on 2003-02-06.

	N	max D	K-S *p*	Lilliefors *p*
Thick	13	1.00	**< 0.01**	**< 0.01**
DH	13	0.26	> 0.20	**< 0.05**
HS	13	0.25	> 0.20	**< 0.05**
Slope	13	0.21	> 0.20	< 0.15
DS	13	0.32	< 0.15	**< 0.01**
DHE	13	0.17	> 0.20	> 0.20
DHE_{Trend}	13	0.10	> 0.20	> 0.20
DHE_{Res}	13	0.14	> 0.20	> 0.20

Table C.41 – Maximum Kolmogorov-Smirnov test statistics and p-values as well as Lilliefors p-values for the propagation test array performed at Poetry Slopes on 2003-02-06.

	N	max D	K-S *p*	Lilliefors *p*
Thick	43	0.22	**< 0.05**	**< 0.01**
DH	41	0.37	**< 0.01**	**< 0.01**
Depth	43	0.19	< 0.15	**< 0.01**
HS	43	0.08	> 0.20	> 0.20
Slope	42	0.14	> 0.20	**< 0.05**
DHE	41	0.31	**< 0.01**	**< 0.01**
DHE_{Trend}	41	0.04	> 0.20	> 0.20
DHE_{Res}	41	0.21	< 0.10	**< 0.01**

Table C.42 – Maximum Kolmogorov-Smirnov test statistics and p-values as well as Lilliefors p-values for the propagation test array performed at Abbott Headwall on 2003-02-10/11.

	N	max D	K-S *p*	Lilliefors *p*
Thick	132	0.53	**< 0.01**	**< 0.01**
DH	131	0.16	**< 0.01**	**< 0.01**
Depth	132	0.10	< 0.20	**< 0.01**
HS	132	0.06	> 0.20	> 0.20
Slope	131	0.17	**< 0.01**	**< 0.01**
DHE	131	0.14	**< 0.05**	**< 0.01**
DHE_{Trend}	131	0.04	> 0.20	> 0.20
DHE_{Res}	131	0.10	< 0.15	**< 0.01**
$Depth_{Trend}$	132	0.05	> 0.20	> 0.20
$Depth_{Res}$	132	0.08	> 0.20	< 0.10
$Thick_{Trend}$	132	0.06	> 0.20	> 0.20
$Thick_{Res}$	132	0.22	**< 0.01**	**< 0.01**
HS_{Trend}	132	0.04	> 0.20	> 0.20
HS_{Res}	132	0.07	> 0.20	< 0.15
$Slope_{Trend}$	132	0.04	> 0.20	> 0.20
$Slope_{Res}$	132	0.07	> 0.20	< 0.20

Table C.43 – Maximum Kolmogorov-Smirnov test statistics and p-values as well as Lilliefors p-values for the propagation test array performed at Cheops on 2003-02-13.

	N	**max D**	**K-S *p***	**Lilliefors *p***
Thick	35	1.00	**< 0.01**	**< 0.01**
DH	35	0.14	> 0.20	< 0.10
Depth	35	0.11	> 0.20	> 0.20
HS	35	0.11	> 0.20	> 0.20
Slope	35	0.12	> 0.20	> 0.20
DHE	35	0.13	> 0.20	< 0.15
DHE_{Trend}	35	0.07	> 0.20	> 0.20
DHE_{Res}	35	0.15	> 0.20	**< 0.05**

Table C.44 – Maximum Kolmogorov-Smirnov test statistics and p-values as well as Lilliefors p-values for the propagation test array performed at Diamond Head on 2003-02-13.

	N	**max D**	**K-S *p***	**Lilliefors *p***
DH	28	0.23	< 0.10	**< 0.01**
HS	31	0.14	> 0.20	< 0.15
Slope	30	0.23	< 0.10	**< 0.01**
Asp	31	0.12	> 0.20	> 0.20
EMin	28	0.45	**< 0.01**	**< 0.01**
EMax	28	0.46	**< 0.01**	**< 0.01**
DHE	28	0.19	< 0.20	**< 0.01**
DHE_{Trend}	28	0.10	> 0.20	> 0.20
DHE_{Res}	28	0.12	> 0.20	> 0.20

Table C.45 – Maximum Kolmogorov-Smirnov test statistics and p-values as well as Lilliefors p-values for the propagation test array performed at Mt. St. Anne on 2003-03-19.

	N	max D	K-S *p*	Lilliefors *p*
Thick	41	1.00	**< 0.01**	**< 0.01**
DH	39	0.15	> 0.20	**< 0.05**
Depth	39	0.16	> 0.20	**< 0.05**
HS	39	0.16	> 0.20	**< 0.05**
Slope	39	0.22	< 0.10	**< 0.01**
Asp	39	0.24	**< 0.05**	**< 0.01**
DHE	39	0.11	> 0.20	> 0.20
DHE_{Trend}	39	0.08	> 0.20	> 0.20
DHE_{Res}	39	0.10	> 0.20	> 0.20
$Depth_{Trend}$	39	0.08	> 0.20	> 0.20
$Depth_{Res}$	39	0.15	> 0.20	**< 0.05**
HS_{Trend}	39	0.08	> 0.20	> 0.20
HS_{Res}	39	0.07	> 0.20	> 0.20
$Slope_{Trend}$	39	0.08	> 0.20	> 0.20
$Slope_{Res}$	39	0.11	> 0.20	> 0.20

Table C.46 – Maximum Kolmogorov-Smirnov test statistics and p-values as well as Lilliefors p-values for the propagation test array performed at South Run on 2003-03-19.

	N	max D	K-S *p*	Lilliefors *p*
Thick	44	0.14	> 0.20	**< 0.05**
DH	43	0.17	< 0.20	**< 0.01**
Depth	44	0.13	> 0.20	< 0.10
HS	44	0.07	> 0.20	> 0.20
Slope	44	0.14	> 0.20	**< 0.05**
DHE	43	0.13	> 0.20	< 0.10
DHE_{Trend}	43	0.12	> 0.20	< 0.20
DHE_{Res}	43	0.12	> 0.20	< 0.10

Table C.47 – Maximum Kolmogorov-Smirnov test statistics and p-values as well as Lilliefors p-values for the propagation test array performed at Rudy's Bowl on 2003-03-21.

	N	**max D**	**K-S *p***	**Lilliefors *p***
Thick	28	0.28	**< 0.05**	**< 0.01**
DH	29	0.23	< 0.10	**< 0.01**
Depth	29	0.18	> 0.20	**< 0.05**
HS	29	0.12	> 0.20	> 0.20
Slope	29	0.18	> 0.20	**< 0.05**
Asp	4	0.31	> 0.20	< 0.20
DHE	28	0.25	**< 0.05**	**< 0.01**
DHE_{Trend}	28	0.06	> 0.20	> 0.20
DHE_{Res}	28	0.24	< 0.10	**< 0.01**

Table C.48 – Maximum Kolmogorov-Smirnov test statistics and p-values as well as Lilliefors p-values for the propagation test array performed at Cheops Bench on 2003-03-24.

	N	**max D**	**K-S *p***	**Lilliefors *p***
Thick	10	0.30	> 0.20	**< 0.01**
DH	8	0.17	> 0.20	> 0.20
Depth	8	0.22	> 0.20	> 0.20
HS	8	0.24	> 0.20	< 0.20
Slope	8	0.32	> 0.20	**< 0.05**
DHE	8	0.14	> 0.20	> 0.20
DHE_{Trend}	8	0.16	> 0.20	> 0.20
DHE_{Res}	8	0.15	> 0.20	> 0.20

Table C.49 – Maximum Kolmogorov-Smirnov test statistics and p-values as well as Lilliefors p-values for the propagation test array performed at Caribou Hideout on 2003-03-26.

	N	max D	K-S *p*	Lilliefors *p*
Thick	34	0.25	**< 0.05**	**< 0.01**
DH	35	0.23	< 0.10	**< 0.01**
Depth	35	0.11	> 0.20	> 0.20
HS	35	0.06	> 0.20	> 0.20
Slope	35	0.19	< 0.15	**< 0.01**
EMin	35	0.29	**< 0.01**	**< 0.01**
EMax	35	0.19	< 0.15	**< 0.01**
DHE	35	0.17	> 0.20	**< 0.05**
DHE_{Trend}	35	0.14	> 0.20	< 0.10
DHE_{Res}	35	0.19	< 0.15	**< 0.01**
$Thick_{Trend}$	34	0.12	> 0.20	> 0.20
$Thick_{Res}$	34	0.07	> 0.20	> 0.20
$Depth_{Trend}$	35	0.07	> 0.20	> 0.20
$Depth_{Res}$	35	0.12	> 0.20	> 0.20
HS_{Trend}	35	0.04	> 0.20	> 0.20
HS_{Res}	35	0.23	**< 0.05**	**< 0.01**
$Slope_{Trend}$	35	0.04	> 0.20	> 0.20
$Slope_{Res}$	35	0.07	> 0.20	> 0.20

Table C.50 – Maximum Kolmogorov-Smirnov test statistics and p-values as well as Lilliefors p-values for the propagation test array performed at Poetry Slopes on 2004-01-19.

	N	max D	K-S *p*	Lilliefors *p*
DH	56	0.21	**< 0.05**	**< 0.01**
Depth	56	0.17	< 0.10	**< 0.01**
HS	56	0.09	> 0.20	> 0.20
Slope	56	0.19	**< 0.05**	**< 0.01**
DHE	56	0.22	**< 0.01**	**< 0.01**
DHE_{Trend}	56	0.06	> 0.20	> 0.20
DHE_{Res}	56	0.21	**< 0.05**	**< 0.01**
HS_{Trend}	56	0.06	> 0.20	> 0.20
HS_{Res}	56	0.07	> 0.20	> 0.20
$Slope_{Trend}$	56	0.17	< 0.10	**< 0.01**
$Slope_{Res}$	56	0.11	> 0.20	< 0.10

Table C.51 – Maximum Kolmogorov-Smirnov test statistics and p-values as well as Lilliefors p-values for the propagation test array performed at Fortitude on 2004-02-08.

	N	**max D**	**K-S *p***	**Lilliefors *p***
DH	45	0.22	**< 0.05**	**< 0.01**
Depth	45	0.12	> 0.20	< 0.10
HS	45	0.14	> 0.20	**< 0.05**
Slope	45	0.54	**< 0.01**	**< 0.01**
DHE	45	0.22	**< 0.05**	**< 0.01**
DHE_{Trend}	45	0.05	> 0.20	> 0.20
DHE_{Res}	45	0.12	> 0.20	< 0.15

Table C.52 – Maximum Kolmogorov-Smirnov test statistics and p-values as well as Lilliefors p-values for the propagation test array performed at Slick Glades on 2004-02-09.

	N	**max D**	**K-S *p***	**Lilliefors *p***
DH	27	0.26	**< 0.05**	**< 0.01**
Depth	27	0.19	> 0.20	**< 0.01**
HS	27	0.18	> 0.20	**< 0.05**
Asp	8	0.18	> 0.20	> 0.20
DHE	27	0.26	**< 0.05**	**< 0.01**
DHE_{Trend}	27	0.10	> 0.20	> 0.20
DHE_{Res}	27	0.16	> 0.20	**< 0.05**

Table C.53 – Maximum Kolmogorov-Smirnov test statistics and p-values as well as Lilliefors p-values for the propagation test array performed at Cheops Bench on 2004-03-14.

	N	**max D**	**K-S *p***	**Lilliefors *p***
DH	33	0.16	> 0.20	**< 0.05**
Depth	34	0.10	> 0.20	> 0.20
HS	33	0.16	> 0.20	**< 0.05**
Slope	33	0.18	> 0.20	**< 0.05**
Emin	33	0.26	**< 0.05**	**< 0.01**
Emax	33	0.53	**< 0.01**	**< 0.01**
DHE	33	0.16	> 0.20	**< 0.05**
DHE_{Trend}	33	0.05	> 0.20	> 0.20
DHE_{Res}	33	0.13	> 0.20	< 0.20
HS_{Trend}	33	0.08	> 0.20	> 0.20
HS_{Res}	33	0.12	> 0.20	> 0.20
$Slope_{Trend}$	33	0.15	> 0.20	< 0.10
$Slope_{Res}$	33	0.15	> 0.20	< 0.10

Table C.54 – Maximum Kolmogorov-Smirnov test statistics and p-values as well as Lilliefors p-values for the propagation test array performed at Monashee View on 2004-03-24.

	N	**max D**	**K-S *p***	**Lilliefors *p***
DH	87	0.24	**< 0.01**	**< 0.01**
Depth	91	0.08	> 0.20	< 0.20
HS	88	0.06	> 0.20	> 0.20
Slope	92	0.36	**< 0.01**	**< 0.01**
DHE	87	0.24	**< 0.01**	**< 0.01**
DHE_{Trend}	92	0.05	> 0.20	> 0.20
DHE_{Res}	92	0.21	**< 0.01**	**< 0.01**

C.5 Propagation test array medians

Table C.55 – Maximum Kolmogorov-Smirnov test statistics and p-values as well as Lilliefors p-values for the propagation test array medians.

	N	max D	K-S *p*	Lilliefors *p*
MedThick	16	0.32	< 0.10	**< 0.01**
MedDepth	20	0.21	> 0.20	**< 0.05**
MedHS	23	0.09	> 0.20	> 0.20
MedSlope	23	0.17	> 0.20	< 0.10
MedDHE	23	0.14	> 0.20	> 0.20
QCV	23	0.12	> 0.20	> 0.20
SIQR	23	0.22	< 0.15	**< 0.01**

C.6 Normalized propagation test array data

Table C.56 – Maximum Kolmogorov-Smirnov test statistics and p-values as well as Lilliefors p-values for the normalized and combined propagation test array data.

	N	max D	K-S *p*	Lilliefors *p*
$Thick_{Norm}$	357	0.13	**< 0.01**	**< 0.01**
$Depth_{Norm}$	883	0.08	**< 0.01**	**< 0.01**
HS_{Norm}	939	0.03	> 0.20	**< 0.05**
$Slope_{Norm}$	764	0.08	**< 0.01**	**< 0.01**
DHE_{Norm}	930	0.13	**< 0.01**	**< 0.01**